Aqueous Alteration of Martian Crust: Constraints from Terrestrial Analogue Sites and Martian Meteorites

A thesis submitted in partial fulfillment ofthe

requirements for the degree of

Doctor of Philosophy

By

Aditya Das

(Roll No.20330019)

Under the guidance of

Dr. Dwijesh Ray

Associate Professor

Planetary Sciences Division

Physical Research Laboratory, Ahmedabad, India

DEPARTMENT OF EARTH SCIENCES

INDIAN INSTITUTE OF TECHNOLOGY

GANDHINAGAR, INDIA

2025

Declaration

I declare that this written submission represents my ideas in my own words, and where others' ideas or words have been included, I have adequately cited and referenced the original sources. I also declare that I have adhered to all principles of academic honesty and integrity and have not misrepresented, fabricated, or falsified any idea/data/fact/source in my submission. I understand that any violation of the above will be cause for disciplinary action by the Institute and may also resultin penal action from the sources that have not been properly cited or from whom proper permission has not been obtained when necessary.

(Name: Aditya Das)

Certificate

It is certified that the work contained in the thesis entitled **"Aqueous Alteration of Martian Crust: Constraints from Terrestrial Analogue Sites and Martian Meteorites"** submitted by **Aditya Das** (Roll no: 20330019), to Indian Institute of Technology, Gandhinagar, has been carried out under my supervision at the Planetary Sciences Division, Physical Research Laboratory, Ahmedabad, and that this work has not been submitted elsewhere for any degree or diploma.

Dr. Dwijesh Ray

(Thesis Supervisor)
Associate Professor,
Planetary Sciences Division
Physical Research Laboratory
Ahmedabad, India

THESIS APPROVAL

Certified that the thesis titled

"Aqueous Alteration of Martian Crust: Constraints from Terrestrial Analogue Sites and Martian Meteorites",

submitted by **Aditya Das** (IITGN Roll No. **20330019**) to the **Indian Institute of Technology Gandhinagar,** is approved for the degree of *Doctor of Philosophy.*

Date: **April 27, 2026**

Place: Gujarat, India

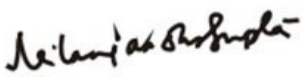

Prof. Nilanjan Dasgupta
External Examiner,
Presidency University, Kolkata

Prof. Achyut Misra
FDC Member,
IIT Gandhinagar

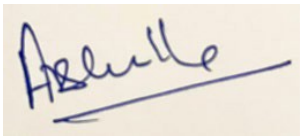

Prof. Anil D Shukla
DSC and FDC Member,
HNBGU, Srinagar

Prof. Amit Basu Sarbadhikari
DSC and FDC Member,
PRL Ahmedabad

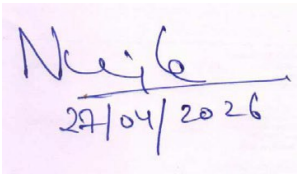

Dr. Neeraj Srivastava
DSC and FDC Member,
PRL Ahmedabad

Dr. Dwijesh Ray
PhD Supervisor and FDC member,
PRL Ahmedabad

Acknowledgement

I sincerely thank my PhD supervisor, Dr. Dwijesh Ray, for his guidance, support, and mentorship throughout my PhD. Under his supervision, I gained strong hands-on experience with several analytical techniques, including XRF, XRD, EPMA, SEM, Raman spectroscopy, and polarizing microscopy, despite having limited experience with most of these methods prior to joining PRL. He introduced me to the fascinating world of meteorites and planetary geology, which, as a geology student, has been an extremely exciting field for me. His experience in terrestrial analogue studies led to multiple field campaigns in the Deccan region, where we collected samples that closely mimic the alteration behavior observed in Martian meteorites. This work significantly strengthened my thesis. He consistently encouraged me to step out of my comfort zone, learn new techniques from scratch, and give oral presentations at conferences, which helped me overcome my stage fright and improve my confidence in scientific communication. His timely support in arranging resources, including the difficult procurement of Martian meteorites, and his constant motivation during challenging phases played a key role in the successful completion of this thesis. I am also grateful to my DSC members, Prof. Anil D. Shukla, Prof. Amit Basu Sarbhadikari, and Dr. Neeraj Srivastava, for their valuable time and thoughtful input at every stage of my PhD. The long and often demanding DSC meetings were intellectually challenging, and the pointed questions and constructive criticism I received during these discussions helped sharpen my scientific arguments and improve the clarity of this thesis. Their guidance consistently encouraged me to think more critically and played a crucial role in enhancing the overall quality of my research.

I would like to thank my PhD colleagues and friends (including seniors, juniors as well as batch-mates: especially **Dr. Trinesh Sana** for his immense help**)**, for their support and companionship throughout my PhD tenure. The discussions, shared experiences, and mutual encouragement within these groups (PRL family, PRL- 2020 Batch) created a supportive research environment and helped me navigate both academic challenges and day-to-day research life. These guys have made the mundane PhD life somewhat entertaining.

I also want to thank my parents (**Mrs. Sangeeta Das and Dr. Amabasu Das**) for their endless and thankless contributions and sacrifices they have done for me their entire life.

Abstract

Understanding the nature and extent of aqueous alteration in the Martian crust is essential for reconstructing the planet's paleoclimate and evaluating the conditions under which liquid water once interacted with basaltic rocks. This thesis investigates low-temperature aqueous alteration processes on Mars by combining detailed petrographic, mineralogical, and geochemical analyses of nakhlite Martian meteorites with complementary studies of terrestrial basaltic analogues from the Deccan Volcanic Province, India.

Petrographic observations, supported by mineral chemical data, show that alteration in the nakhlite meteorites is highly localized and predominantly controlled by fractures within olivine grains. The surrounding primary phases, such as clinopyroxene and plagioclase, remain largely unaltered, indicating that fluid–rock interaction was spatially restricted rather than pervasive. The secondary mineral assemblages identified within these fractures are dominated by Fe–Mg–rich smectitic clays and iron oxide phases. In the Lafayette meteorite, additional alteration is observed within the mesostasis, where carbonate minerals occur in close association with phyllosilicate clays, pointing to a more complex alteration history involving changes in fluid chemistry. X-ray elemental mapping provides further insight into the chemical processes operating during alteration. These maps reveal systematic redistribution of major cations, where magnesium and iron are leached from the host olivine grains and subsequently incorporated into the fracture-hosted alteration products. At the same time, aluminium and calcium are enriched within the altered zones, indicating contributions from adjacent mineral phases or interaction with chemically distinct external fluids. This element mobility highlights the coupled nature of dissolution and precipitation during low-temperature aqueous alteration. Geochemical indices of alteration and ternary compositional plots demonstrate that Yam-593, MIL 03346, and Nakhla experienced relatively low-degree and chemically constrained alteration, characterized by limited variability in alteration products. In contrast, Lafayette exhibits greater chemical scatter and multiple compositional trends, suggesting that it underwent more than one episode of alteration or interacted with fluids of differing composition. These differences point to variability in fluid availability, chemistry, and possibly timing across the nakhlite sequence.

A key component of this thesis is the use of terrestrial basaltic rocks from the Deccan Volcanic Province as analogues to better constrain the aqueous alteration processes recorded in the nakhlite meteorites. The choice of the Deccan basalts is based on their basaltic composition, mineralogy, and textural similarity to Martian basalts, as well as their wide compositional range, which includes both Mg-rich picritic basalts and more Fe-rich tholeiitic varieties. This compositional diversity allows systematic evaluation of how differences in olivine chemistry influence alteration pathways under comparable environmental conditions. Detailed petrographic analysis of the Deccan basalts reveals alteration features that closely resemble those observed in the nakhlites, particularly the localization of secondary minerals within fractures of olivine grains. As in the Martian samples, alteration in the Deccan basalts is limited in extent and does not involve widespread replacement of primary minerals. Instead, secondary phases occur as narrow, fracture-hosted assemblages, indicating interaction with small volumes of fluid and low water–rock ratios. These similarities support the interpretationthat the nakhlite alteration formed under similarly restricted conditions. Mineral chemical data and X-ray elemental maps from the Deccan basalts further reinforce theirsuitability as analogues. The redistribution of major elements during alteration follows patterns comparable to those observed in the nakhlites, with magnesium and iron beingmobilized from olivine and incorporated into secondary clay minerals, while aluminium and calcium are introduced from adjacent phases. The preservation of largely unaltered primary mineral interiors in both terrestrial and Martian samples indicates that alteration was brief and spatially confined, rather than long-lived or pervasive. The terrestrial analogue approach also provides an important advantage in constraining geochemical conditions that cannot be directly measured for Mars. Unlike Martian meteorites, the Deccan basalts allow direct assessment of alteration under known geological settings, including temperature ranges, host-rock composition, and fluid chemistry derived from regional hydrothermal systems. These constraints were used to inform geochemical modeling, enabling realistic simulation of water–rock interaction under low-temperature and limited-fluid conditions relevant to the Amazonian period on Mars. Overall, the comparison between Deccan basalts and nakhlite meteorites demonstrates that similar alteration styles can develop in basaltic crusts on different planets when fluid availability is limited and interaction is fracture-controlled. The terrestrial analogue framework therefore plays a central role in this thesis by bridging natural observations and modeling results, and by providing a

physically grounded basis for interpreting the aqueous alteration history of the Martian crust.

Geochemical modeling further supports these observations by showing that short-lived, low-temperature aqueous interactions operating in chemically restricted systems are capable of reproducing the observed secondary mineral assemblages and alteration trends seen in the nakhlites. Taken together, the results of this thesis indicate that aqueous alteration within the Martian crust during the Amazonian period was episodic, localized, and dominated by limited fluid availability rather than long-lived, large-scale hydrothermal systems. By combining observations from Martian meteorites, terrestrial analogues, and geochemical modeling, this work provides a coherent framework for understanding late-stage water–rock interaction on Mars and places new constraints on the nature of aqueous processes operating under water-limited conditions.

List of Publications

Included in this thesis

- Das, A., Sarkar, S., Ray, D., & Sirvi, R. (2025). The Columnar Jointing in the Deccan Continental Flood Basalt, India: Implications as a Martian Analogue. *Earth and Planetary Science*, 4(1), 26-38. https://doi.org/10.36956/eps.v4i1.1652
- Das, A., Ray, D., Astha, B., & Bose, A. (2026). Contrasting olivine alteration scenario in the Deccan continental flood basalt, India: Implications for Mars. Journal of Geophysical Research: Planets, 131, e2025JE009278. https://doi.org/10.1029/2025JE009278
- Das, A., Mukherjee, A., Bose, A., Majumdar, A., & Dwijesh Ray, D. The olivine alteration on Earth and Mars: Lessons from terrestrial analogue and Martian meteorite studies. *Geochemistry*, (Under revision).
- Das, A., Sinha, R., Bose, A., & Ray, D. Reconstructing Martian Subsurface Alteration Conditions Through Nakhlite Geochemistry. (in preparation)

Not included in this Thesis

- Ray, D., Sarkar, S., **Das, A**., Arora, G., Shukla, A. D., & Bhardwaj, A. (2025). The Kopargaon LL5 chondrite: A new fall of monomict breccia from India. Journal of Earth System Science, 134(1), 37. https://doi.org/10.1007/s12040-024-02497-8
- Ray, D., **Das, A**., Sarkar, S., Bhattacharya, S., & Nayak, C. (2025). Natrojarosite formed in the Matanomadh Formation, Kutch, India; a Na analog of jarosite on Mars. American Mineralogist. https://doi.org/10.2138/am-2024-9360
- Srivastava, Y., Basu Sarbadhikari, A., Nair, V. M., Kumar, A., Kadlag, Y., Mahajan, R. R., Srivastava, N., Panwar, N., **Das, A**., & Bhardwaj, A. (2025). Petrogenesis of the Rantila meteorite fall and implications for the origin of aubrites. Meteoritics & Planetary Science. https://doi.org/10.1111/maps.14357
- **Das, A**., Sivaraman, B., Ray, D., Marhas, K. K., Shukla, A. D., & Bhardwaj, A. (2025). A New Meteorite Fall from Khalwat-Limgaon Village of Wadwani Taluka in Beed District, Maharashtra. *Journal of the Geological Society of India*, *101*(10), 1578-1580. https://doi.org/10.17491/jgsi/2025/174277
- Ray, D., Annadata, H. V., Sarkar, S., Ray, A., **Das, A**., Bhattacharya, S., & Ghosh, B. (2025). Mineralogy, VNIR (Visible Near-Infrared), and Fe XAS (X-ray Absorption) Spectroscopy of Terrestrial Hematite Analogs: Implications for Iron Speciation on Mars. *ACS Earth and Space Chemistry*. https://doi.org/10.1021/acsearthspacechem.5c00160

Table of Contents

List of Figures

List of Tables

Chapter 1: Introduction

This chapter establishes the scientific context for understanding aqueous alteration in the Martian crust through the study of nakhlite meteorites and their terrestrial basalt analogues. It begins by outlining how water was delivered to Mars, how it evolved isotopically, and how it influenced the planet's geological and climatic development. The major stages of Martian surface evolution are summarized to show how changing environmental conditions shaped the formation and preservation of phyllosilicates. Particular attention is given to the mineralogy and spatial distribution of Martian clay minerals, as these phases record the physicochemical conditions of ancient water–rock interaction. The chapter then introduces Martian meteorites, focusing on the nakhlites, which preserve clear evidence of low-temperature fluid alteration in the shallow crust. Their secondary mineral assemblages provide essential constraints on the chemistry and pathways of alteration. To support interpretation of these features, the Deccan Volcanic Province is presented as a terrestrial analogue whose basaltic compositions, spectral characteristics, and hydrothermal alteration textures closely resemble Martian basalts

1.1 The Presence and Role of Water on Mars

The existence and influence of water on Mars have long been central to understanding its geological evolution, climatic changes, and potential for sustaining life. Both Earth and Mars originated from similar materials within the early Solar System, shaped by processes such as planetary accretion, internal differentiation, and intense bombardment during the first few hundred million years. Yet, the fate of water—and the geological imprints it left behind—differs greatly between the two planets. On Mars, water is not only a chemical component but also a key agent that governs habitability. It has affected the retention of the atmosphere, altered minerals on the surface, and influenced crustal development. Therefore, tracing the history of Martian water requires an integrated understanding of its delivery, long-term preservation, and subsequent geological interactions.

The role of water in shaping planetary habitability has always been one of the most compelling topics in planetary science. Because water enables chemical reactions essential for life, the conditions under which it was supplied and retained on planetary bodies must be clearly understood. Over the last few decades, significant progress has been achieved through the study of meteorites, isotopic compositions, and dynamical simulations of planetary migration. These studies have revealed that water within the inner Solar System likely originated from multiple sources rather than a single reservoir (Alexander et al., 2018; Meech & Raymond, 2020). This suggests that both endogenous and exogenous processes contributed to the acquisition of water on the terrestrial planets, including Mars.

1.1.1 The Grand Tack and Water Delivery

The movement of giant planets in the early Solar System, particularly Jupiter and Saturn, played a decisive role in redistributing material within the protoplanetary disk.

Early dynamical models of planetary migration, including scenarios such as the Grand Tack, suggest that the movement of giant planets played a major role in redistributing volatile-rich material into the inner Solar System(Fig. 1.1). The gaseous giants then moved outward together, finally stabilizingnear their current orbits (Brien et al., 2014; Morbidelli et al., 2010).

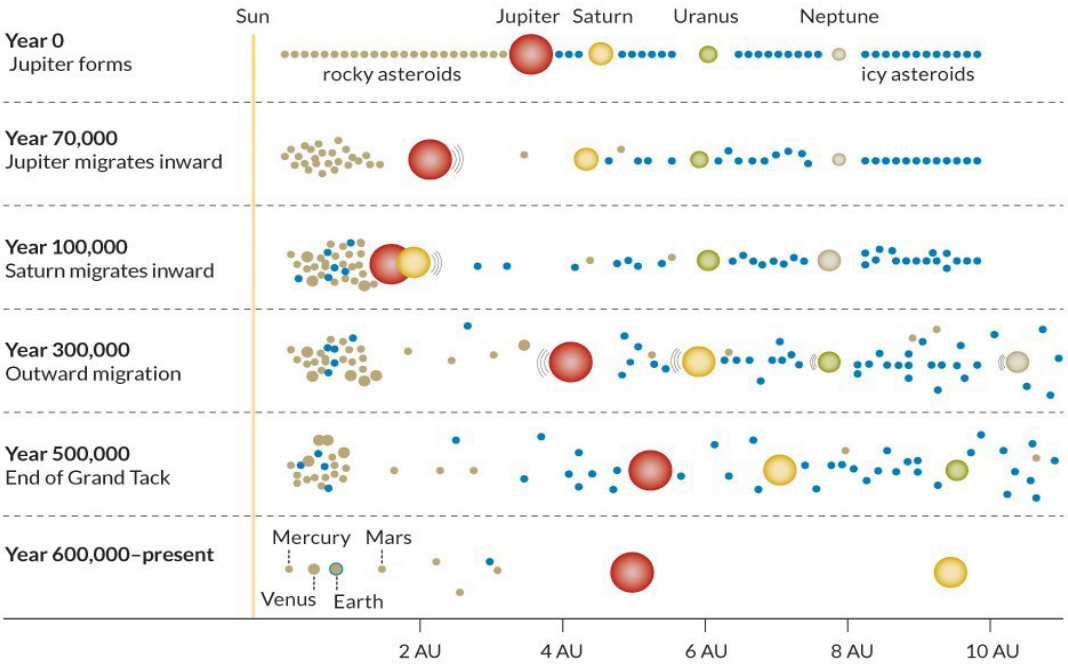

Fig. 1.1. Schematic depiction of the Grand Tack and Nice model frameworks, adapted from Tsiganis et al. (2005) and Walsh et al. (2011). In this representation, the blue bodies denote ice-rich, volatile-bearing objects, whereas the red bodies indicate denser.

This large-scale planetary migration had a profound impact on the inner Solar System. During its inward migration, Jupiter scattered volatile-poor planetesimals from the region near the Sun. As it later reversed course, it simultaneously drove volatile-rich bodies—such as C-type asteroids—from beyond 8 AU toward the inner regions. Many of these bodies were rich in water, containing up to 10% water by mass (Kerridge, 1985; Raymond & Izidoro, 2017). Mars, which formed approximately 1.5 AU from the Sun, was located precisely within this dynamic zone. Consequently, its relatively small size and volatile inventory have been linked to Jupiter's sweeping removal and later redistribution of material in the inner Solar System. Mars' water supply is thus thought

to have been enhanced by impacts and accretion of C-type asteroids and possibly cometary bodies that were driven inward during this planetary migration (Walsh et al., 2011; Tait & Day, 2018).

1.1.2 The Role of Isotopes: D/H Ratios

Although planetary migration models outline possible routes through which water could have been delivered to Mars, isotopic analyses offer more direct evidence about its actual source. Among these, the deuterium-to-hydrogen (D/H) ratio has been regarded as one of the most informative tools for tracing the history of planetary water. Deuterium, being a heavier isotope of hydrogen, tends to remain in the atmosphere or surface reservoirs when the lighter hydrogen atoms escape into space. Over extended periods, this selective loss leads to the enrichment of deuterium within the remaining water (Owen et al., 1988; Krasnopolsky et al., 1997).

On Earth, the D/H ratio of ocean water is defined by a standard known as Vienna Standard Mean Ocean Water (VSMOW). In comparison, the D/H ratio in the Martian atmosphere has been measured to be nearly five times higher than that of Earth's oceans, a difference that is widely attributed to the continuous escape of hydrogen over billions of years. This process has left behind a deuterium-enriched Martian atmosphere, indicating significant water loss throughout the planet's history (Owen et al., 1988; Krasnopolsky et al., 1997).

Additional insights have been derived from the isotopic study of Martian meteorites, which preserve signatures of both surface and subsurface water reservoirs. Hydrous secondary minerals identified in these meteorites are believed to record valuable information about variations in the isotopic composition of Martian crustal water over time. However, comprehensive data regarding their D/H ratios remains limited. Earlier bulk analyses performed by Leshin et al. (1996) and Eiler et al. (2002a),

along with high-resolution SIMS and NanoSIMS studies by Gillet et al. (2002), Sugiura and Hoshino (2000), Hallis et al. (2012a), Lee et al. (2018), and more recently by Ruggiu et al. (2025), have contributed to understanding these variations.

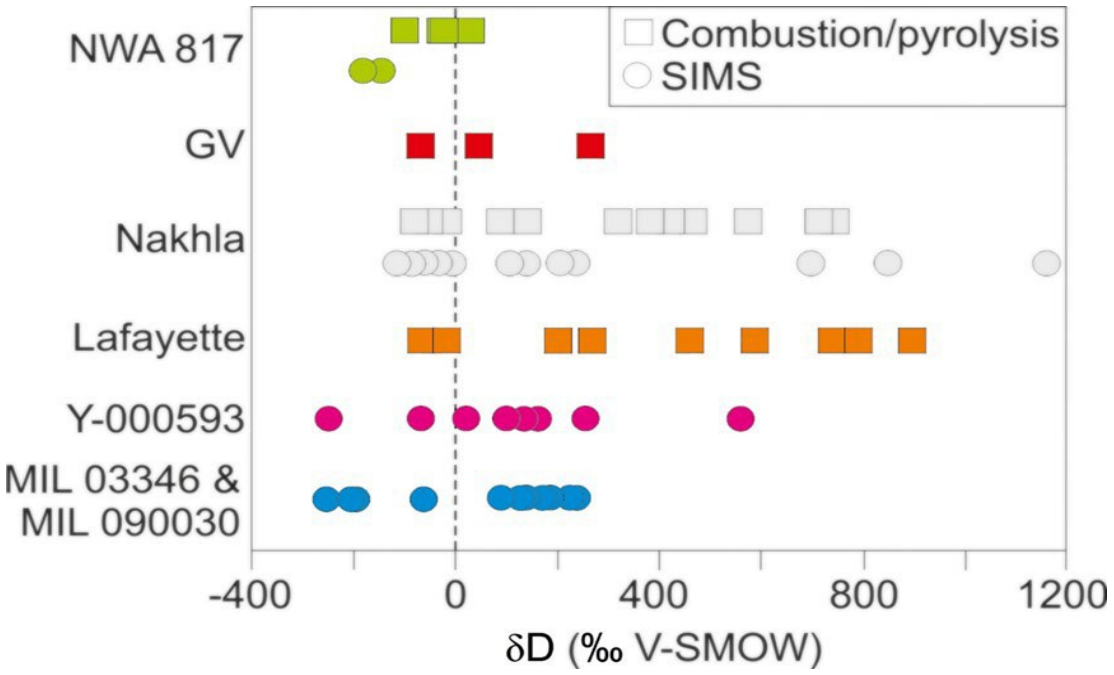

Fig. 1.2: *Hydrogen isotopic composition of the altered phase (Iddingsites) within the Nakhlite group of Martian meteorites. (Lee et al., 2018)*

The Martian atmospheric δD value has been estimated to be around 4200‰ (Bjoraker et al., 1989). Among the nakhlites (Fig. 1.2), the Nakhla meteorite—an observed fall—shows a δD value of approximately 1165 ± 116‰ (Hallis et al., 2012a). In contrast, extremely low δD values recorded in the NWA 817 meteorite, reaching as low as 30‰, suggest that its alteration minerals, such as iddingsite, may have formed from fluids derived directly from the Martian mantle. Similarly, iddingsite found in the paired Antarctic nakhlites MIL 03346 and MIL 090030 displays δD values ranging from –110‰ to 237‰ (Hallis et al., 2012a).

Although certain low D/H ratios might reflect the effects of terrestrial contamination, which could artificially reduce isotopic values (Gillet et al., 2002; Lee et al., 2018), the overall isotopic pattern remains consistent. The Martian atmosphere is

characterized by an enrichment in deuterium due to extensive hydrogen loss, while less fractionated, more primitive water signatures appear to be retained within the crust and mantle (Bjoraker et al., 1989; Robert et al., 2000). This isotopic distribution implies that Mars once possessed a considerable volume of water, much of which was gradually lost into space over geological time. As this loss continued, the remaining water reservoirs became increasingly enriched in deuterium, preserving a record of the planet's long-term atmospheric and hydrological evolution.

1.1.3 Linking D/H and Planetary Histories

By correlating isotopic data with dynamical models such as the Grand Tack, a more comprehensive narrative of Martian water evolution emerges. It has been proposed that Mars acquired much of its early water through the inward migration of volatile-rich C-type asteroids and possibly comets during the early stages of Solar System development (Morbidelli, 2018; Tait & Day, 2018). Once this water was delivered, it was stored not only on the surface but also within the planet's interior. Petrological models suggest that the early Martian mantle may have contained a larger proportion of hydrous minerals compared to Earth's, potentially exceeding 9% by volume, whereas Earth's mantle typically contains about 4% (Wade et al., 2017).

Over time, as surface water was exposed to space, the lighter hydrogen atoms escaped more readily than the heavier deuterium. This selective atmospheric loss progressively increased the D/H ratio in both the Martian atmospheric and near-surface water reservoirs. Consequently, the elevated D/H ratio observed today acts as a geochemical fingerprint of extensive water loss and long-term climatic evolution. Moreover, the variation of D/H values recorded in different Martian meteorites provides evidence for multiple water reservoirs and distinct alteration events throughout Martian history (Krasnopolsky et al., 1997; Hallis et al., 2012a).

Together, these isotopic and dynamical insights present a coherent story: water on Mars was delivered from beyond the snowline, stored within both surface and subsurface reservoirs, and gradually fractionated through atmospheric escape. What remains today is not merely a trace of ancient oceans but a record of Mars' planetary evolution, encoded in the isotopic composition of its rocks and atmosphere.

1.2 Geological History and Surface Evolution of Mars

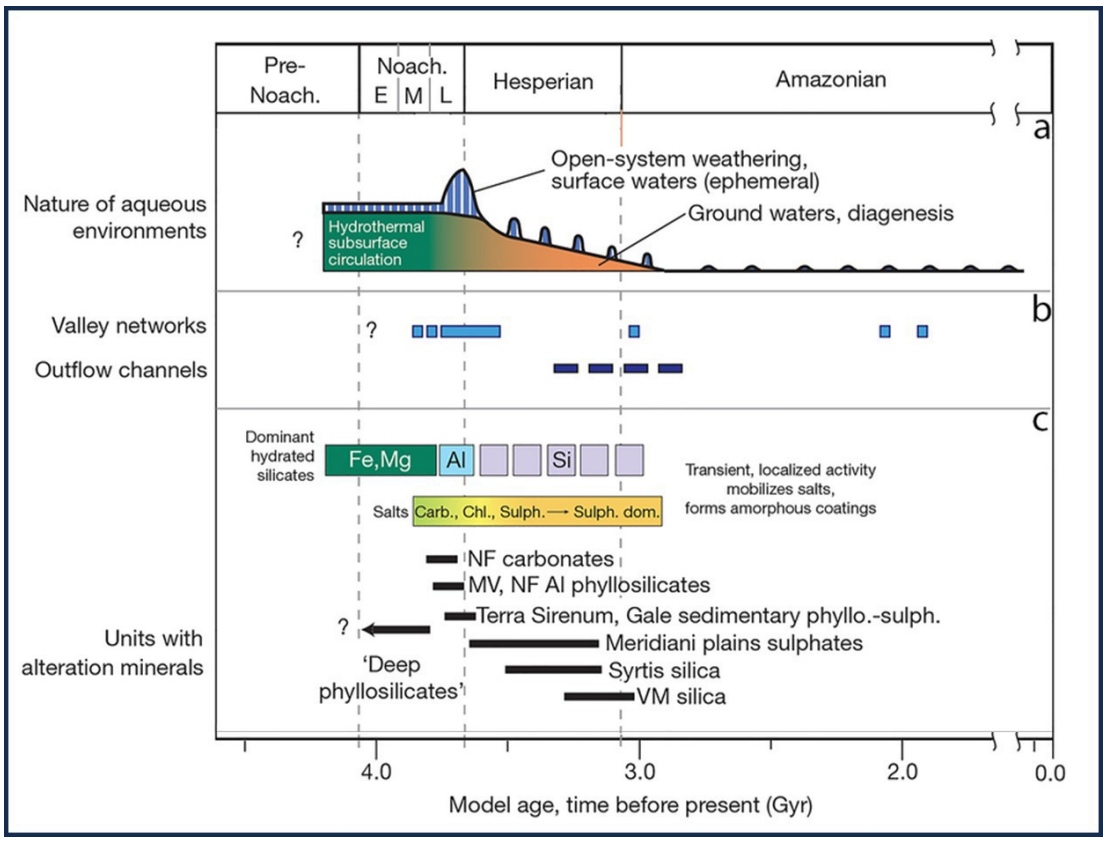

Fig. 1.3:*Martian geological timescale from the pre-Noachian to the Amazonian, illustrating the evolution of aqueous environments, surface water activity, and major hydrated mineral assemblages (modified from Hughes et al., 2023).*

Mars, as a planet, has a long and complex history, shaped by many of the same processes that have influenced Earth, such as large impacts, volcanism, flowing water, and atmospheric change (Mitchell & Wilson, 2003; Catling, 2014). One of the most striking features of the Martian surface is its global crustal dichotomy, which remains a mystery in planetary science (Nimmo & Tanaka, 2005). This boundary divides the

high-standing southern hemisphere from the lower northern plains. The southern hemisphere is dominated by ancient highlands, heavily cratered and standing several kilometers above the northern lowlands. These terrains preserve some of the oldest surfaces on the planet, including enormous basins such as Hellas and Argyre. In contrast, the northern hemisphere is lower in elevation and geologically younger, dominated by volcanic and sedimentary plains. This region also hosts the Tharsis rise, one of the largest volcanic provinces in the Solar System, and the Valles Marineris canyon system, which stretches over 4,000 km and cuts deeply into the crust. Along the boundary between the two hemispheres, landforms shaped by volcanic eruptions, river valleys, ancient lakes, glaciers, and even wind-driven processes provide evidence for a rich and varied geological past (Nimmo & Tanaka, 2005).

To understand this history, a geological timescale has been developed for Mars (Fig. 1.3) (Hartmann, 2005; Tanaka et al., 2014; Werner & Tanaka, 2011). The ages of surfaces are generally estimated using the density of impact craters, while major periods are defined by representative rock ages and the dominant geological processes. Two main schemes exist. Mars is divided into three periods: the Noachian (~4.5–3.7 Ga), the Hesperian (3.7–3.1 Ga), and theAmazonian (3.1 Ga to the present). Another scheme, which is more detailed and adopted in this study, adds an earlier pre-Noachian stage (4.5–4.1 Ga) to capture the events that occurred soon after the planet's formation (Catling, 2014).

1.2.1 Pre-Noachian Period (4.5–4.1 Ga)

The pre-Noachian represents the earliest and least well-preserved stage of Martian history. During this time, Mars was subjected to an intense bombardment of asteroids, comets, and planetesimals, which repeatedly struck its surface (Marinova et al., 2008; Abramov & Mojzsis, 2016). These collisions not only reshaped the crust but also affected the deep interior, causing large-scale melting and recrystallization. The Hellas,

Isidis, and Argyre basins—among the largest on the planet—were formed towards the end of this period, around 4.1–3.9 Ga, marking the transition into the Noachian (Carr & Head, 2010; Robbins et al., 2013; Werner, 2009).

Climatic conditions during the pre-Noachian era are thought to have been significantly different from those of today. Outgassing from widespread volcanism and repeated impacts likely supplied greenhouse gases, building a thicker atmosphere. At the same time, late impacts from comets and chondritic bodies may have delivered water. Together, these processes could have created a warm and wet climate, allowing precipitation, surface runoff, and the first lakes and sediments to form (Catling, 2014). Unfortunately, much of this evidence has been lost because the early record was erased by continued bombardment in the Noachian and further resurfacing during the Hesperian (Werner, 2009; Bottke & Andrews-Hanna, 2017).

1.2.2 Noachian Period (4.1–3.7 Ga)

The Noachian is considered the most active and transformative period in Martian history. Intense bombardment, strong erosion, volcanism, and widespread chemical weathering left their mark across the planet. One of the clearest signatures of this time is the formation of phyllosilicates (clay minerals), which are found globally and indicate prolonged water–rock interaction (Carr & Head, 2010; Ehlmann et al., 2016). Minerals such as olivine are abundant in Noachian-aged rocks. Since olivine easily alters into phyllosilicates in the presence of water, its widespread occurrence together with clays suggests a humid environment with periods of warmth (Ramirez et al., 2014; Wordsworth et al., 2017). Spectral studies of regions such as Nili Fossae and MawrthVallis confirm the presence of clay minerals, including smectite, kaolinite, and illite,which strengthens the case for abundant aqueous alteration (Ehlmann et al., 2011;Bristow et al., 2018).

Repeated impacts during this time fractured the crust, creating a thick megaregolith composed of breccias and ejecta (Ivanov, 2001). These impacts also stripped away magnetized crust, reducing the strength of the global magnetic field by more than half and eventually contributing to the collapse of Mars' dynamo (Langlais& Thébault, 2011; Mittelholz et al., 2018). With the weakening of the magnetic shield, the atmosphere became increasingly vulnerable to solar wind stripping. At the same time, basins created by large impacts acted as natural catchments for water, forming crater lakes, deltas, and fans. More than 200 such lakes have been identified, some comparable in size to Earth's largest lakes, such as Lake Baikal (Fassett & Head, 2008).

Clues from meteorites also shed light on this period. The famous ALH 84001 meteorite, dated to the Noachian, contains magnetite, carbonates, and talc-like minerals that formed through processes such as serpentinization and carbonation (Steele et al., 2022). On Earth, such reactions occur in hydrothermal systems, providing energy for microbial life, which suggests that early Mars may have hosted similar habitable environments (Kelley et al., 2001; McCollom & Seewald, 2013). Serpentinization would also have removed carbon dioxide from the atmosphere, altering its composition and influencing the crust's chemistry (Tomkinson et al., 2013; Edwards & Ehlmann, 2015). Importantly, this period coincides with the Hadean and early Archean on Earth, when life is thought to have first emerged in hydrothermal settings (Mojzsis et al., 1996). Craters on Mars that preserve water-related and sedimentary deposits, such as Jezero Crater—landing site of NASA's Perseverance rover—are therefore considered promising targets in the search for ancient biosignatures (Abramov & Kring, 2004; McMahon et al., 2018; Beaty et al., 2019).

1.2.3 Hesperian Period (3.7–3.0 Ga)

The Hesperian represents a transitional phase in Martian history, during which surface conditions underwent dramatic shifts. Impact rates decreased, but volcanic and tectonic processes remained strong. Massive volcanic outpourings created extensive flood basalts and built enormous edifices such as Olympus Mons. At the same time, tectonic activity fractured the crust and cryosphere, releasing large volumes of groundwater. This caused catastrophic floods that carved giant outflow channels across the surface.

Volcanic gases, particularly sulfur compounds, were released into the atmosphere, altering the surface chemistry. These emissions are believed to have contributed to the transition from clay-rich to sulfate-rich deposits worldwide (Carr & Head, 2010; Gourronc et al., 2014). Glacial activity has also been detected in this period, with evidence of ice accumulation and movement preserved in equatorial regions such as Valles Marineris (De Blasio, 2011; Mitrofanov et al., 2022). By the end of the Hesperian, Mars had largely shifted into the cold, arid state that it maintains today (Mittelholz et al., 2018).

1.2.4 Amazonian Period (3.0 Ga to present)

The Amazonian is the longest and most recent period in Martian history. It is characterized by low rates of impact cratering, diminished volcanism, and limited glacial activity (Golombek et al., 2006). Volcanism was mainly restricted to the Tharsis and Elysium regions, producing lava flows of basaltic composition. Occasional detections of more evolved rocks, such as dacite, have also been reported (Christensen et al., 2005). Some volcanic deposits date back to just 25–40 million years ago, raising the possibility that Mars may still be experiencing some volcanic activity (Basilevsky et al., 2006).

Water activity during the Amazonian has been minimal, though not absent. Features such as gullies and recurring slope lineae indicate that liquid water, likely in the form of salty brines, may still flow intermittently under present-day conditions (Ojha et al., 2015). Currently, the bulk of Martian water is locked up as ice in the polar caps, which are several kilometers thick. Additional subglacial reservoirs of liquid water have also been detected beneath the polar ice sheet (Tanaka et al., 2005; Carr & Head, 2010).

1.3 Martian Clays

Orbital spectroscopy studies have revealed the mineralogical evolution of Mars, particularly the transition from phyllosilicate-rich to sulfate-rich environments, reflecting major changes in water activity and surface conditions over time(Bibring et al., 2006). Most of these are hydrous in nature, implying that their formation required the involvement of liquid water and occurred under specific chemical and physical conditions, such as temperature, pH, redox potential, pressure, and water activity (Downs & Team, 2015). Since these minerals record environmental parameters at the time of their formation, their chemical composition and spatial distribution provide crucial information about Mars' past climatic and surface conditions, and by extension, its potential habitability (Bibring et al., 2006; Chevrier et al., 2007; Carter et al., 2010).

Among these minerals, clays are of particular importance. Their presence serves as direct evidence of historical liquid water activity, while their structural and compositional diversity offers insights into the range of geological settings that once existed on Mars. Furthermore, clay minerals are believed to have played a role in prebiotic chemical reactions and are known for their ability to preserve organic matter and biosignatures (Poulet et al., 2005; Ehlmann et al., 2008, 2011b; Gainey et al., 2017; Bristow et al., 2018). Numerous varieties of clay minerals have been detected on Mars

to date, including smectites (nontronite, saponite, and montmorillonite), chlorite, kaolinite, serpentine, vermiculite, illite, muscovite, and allophane (Bishop et al., 2008; Ehlmann & Edwards, 2014). Despite these findings, the full understanding of their mineralogy, structure, and formation pathways continues to evolve as exploration advances.

1.3.1 Nature and Structure of Martian Clay Minerals

Clay minerals, along with amorphous hydrated silicates such as silica impact glasses, are widely distributed across the Martian surface. They are not confined to fluvial or lacustrine settings but are particularly abundant in the heavily cratered Noachian highlands. Based on remote-sensing data, Ehlmann & Edwards, 2014 categorized Martian clays into three primary types: (1) clay-bearing strata formed through in situ alteration, (2) clays associated with impact craters and their ejecta, and (3) clay-rich sedimentary basin deposits.Recent studies also highlight the development of weathering profiles on Mars, where alteration progresses from primary basaltic minerals to clay-rich assemblages under limited fluid conditions, often preserving chemical gradients (Bultel et al., 2019)

Because clays can form under a wide range of physical and chemical environments (Wimpenny, 2018), identifying their exact origins is a complex challenge. Even advanced analytical techniques on Earth often fail to unambiguously determine the precise conditions of their formation (Tardy et al., 1987). For this reason, Noachian clay assemblages continue to be the subject of significant research interest, as their mineral compositions and spatial patterns reveal important clues about the geological and climatic evolution of Mars (Ehlmann & Edwards, 2014; Bibring et al., 2006;Mustard et al., 2008; Ehlmann et al., 2009; Poulet et al., 2005). According to Hazen et al., (2013), the formation of clay minerals reflects a planet's tectonic,

geochemical, and potentially biological processes. On Mars, these minerals preserve vital records of suchprocesses, offering a window into the planet's long-term geological development. Structurally, clay minerals belong to the phyllosilicate group, characterized by interconnected tetrahedra of silicon and oxygen (SiO_4^{4-}) that form extended sheets of $Si_2O_5^{2-}$. Most phyllosilicates also contain hydroxyl ions (OH^-) positioned between the silicate layers, along with octahedrally coordinated cations such as Fe^{2+}, Mg^{2+}, and Al^{3+}.Smectite clays, one of the most significant clay groups on Mars, exhibit a strong capacity for cation exchange and occur as a continuous compositional spectrum rather than as discrete mineral species. These minerals also respond dynamically to the presence of water, with H_2O molecules entering between the tetrahedral and octahedrallayers, binding to exchangeable cations or directly to the clay sheets, which leads to structural expansion or swelling (Brown & Brindley, 1980).

An important but still poorly understood component of smectite clays is the presence of hydroxy-interlayered material, which forms during the weathering of metal oxides and existing clays (Barnhisel, 1977; Georgiadis et al., 2019). Determining the structure and formation conditions of these materials remains difficult due to their complex chemistry and variable stability. Data obtained from the Mars Science Laboratory's CheMin and SAM instruments indicate that the Martian surface hosts trioctahedral Fe-rich smectite (saponite) containing partial metal-hydroxy intercalation. These clays are interpreted to have originated from pedogenic or lacustrine environments (Bristow et al., 2015). As noted by Tardy et al., (1987), even apparently uniform smectites may actually represent aggregates of microscopically variable particles, each reflecting slightly different environmental conditions and geochemical histories.

1.3.2 Spatial Distribution of Clay Minerals on Mars

Orbital observations have shown that clay minerals are widely distributed throughout the Martian crust, especially within terrains dating back to the Noachian and earlyHesperian periods (Fig. 1.4) (approximately 4.1–3.5 Ga) (Bibring et al., 2005; Mustard et al., 2008; Fairén et al., 2010; Marzo et al., 2010; Ehlmann et al., 2011b; Carter et al., 2013; Ehlmann & Edwards, 2014; Vaniman et al., 2014; Sun & Milliken, 2015). Their spatial distribution reflects the strong geological dichotomy between the ancient southern highlands and the younger northern lowlands.

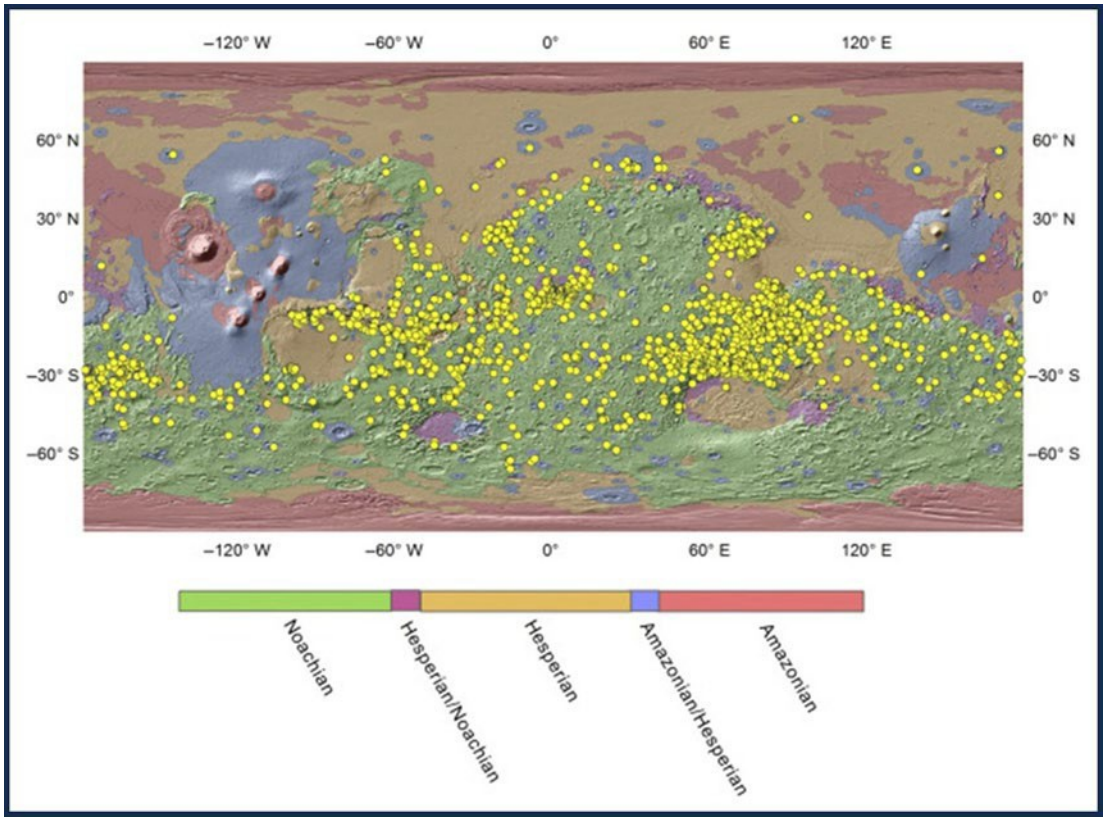

Fig. 1.4: *Spatial distribution of hydrated minerals on Mars, with detection points marking occurrences of clays (phyllosilicates and sulfates). These detections are shown on a MOLA shaded-relief basemap overlain by geologic units color-coded by age (Mustard et al., 2019).*

In the southern highlands, clays are commonly observed in light-toned outcrops, crater rims, and central peaks, with the densest occurrences recorded in regions such as Mawrth Vallis, Nili Fossae, and Valles Marineris (Poulet et al., 2005; Mustard et al., 2008; McKeown et al., 2009). In contrast, the northern plains show weaker alteration

signatures—primarily amorphous coatings and weathering rinds on volcanic glass and allophane—indicating short-lived interactions with small quantities of liquid water (Horgan & Bell, 2012; Rampe et al., 2012; Ehlmann & Edwards, 2014).

Crystalline clays are mostly restricted to Noachian terrains or large impact craters (20–200 km across), where deep crustal material has been exposed (Carter et al., 2010;Bishop et al., 2018; Pan et al., 2017). These occurrences suggest that clay-bearing layers may extend several kilometers below the Martian surface (Sun & Milliken, 2015). Some clays identified in younger terrains, such as the Hesperian and Amazonian, appearto have formed from impact-related hydrothermal processes (Sun & Milliken, 2014), although evidence for significant new clay formation after the Noachian remainslimited (Bishop et al., 2018).

Among all identified clay types, Fe/Mg-rich smectites—mainly nontronite and saponite—are the most abundant, representing over three-quarters of hydrous silicate detections (Ehlmann et al., 2013). Because these minerals exhibit similar spectral characteristics, they are often grouped together as "Fe/Mg smectites." Mixed-layered clays, including chlorite–smectite combinations, have also been reported based on overlapping spectral features (Milliken & Bish, 2010).

A consistent vertical pattern is often observed in stratigraphic sequences, where Fe/Mg smectites form the lower layers and are overlain by Al-rich clays (Bishop & Rampe, 2016; Carter et al., 2015; Ye & Michalski, 2022). This stratigraphy has been documented across numerous regions, including Noachis Terra, Mawrth Vallis, Nili Fossae, western Arabia Terra, Valles Marineris, Gale Crater, Eridania Basin, and Thaumasia Planum (Noe Dobrea et al., 2010; Murchie et al., 2009; Bristow et al., 2018; Ye & Michalski, 2021). In some cases, allophane and imogolite are detected above this

layer, representing the latest stages of weathering (Bishop & Rampe, 2016; Ye & Michalski, 2021).

Apart from the clays observed on a regional scale via landers and orbiters, clay minerals/ phyllosilicates have also been reported to be found in Martian meteorites. These meteorites can be used for numerous in-situ analyses, which will aid in understanding the paleoclimatic and geochemical conditions that prevailed during early Mars.

1.4 Martian meteorites

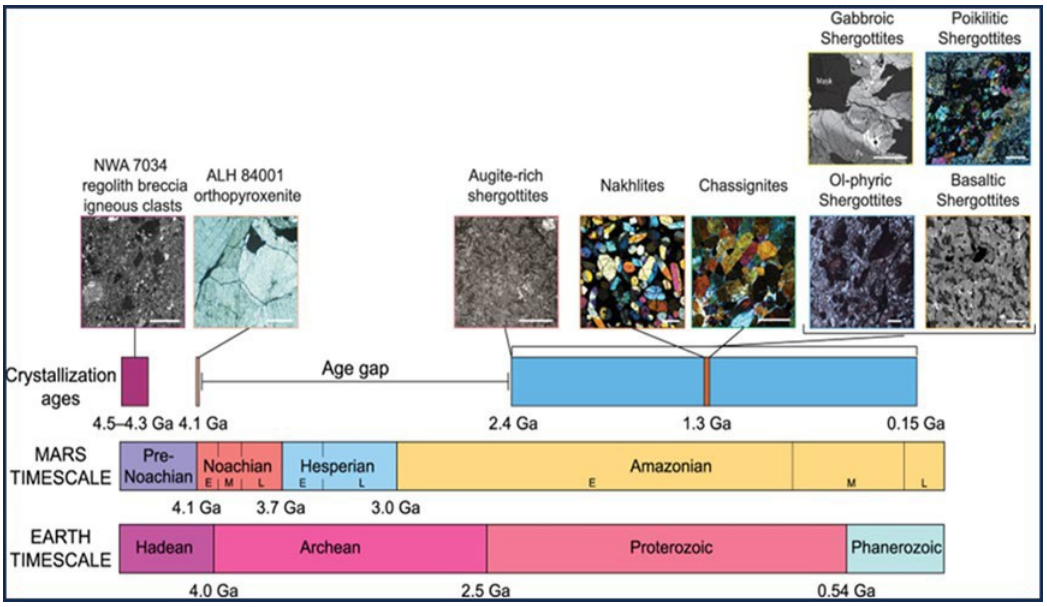

Fig. 1.5: Schematic representation of the crystallization ages of Martian meteorites relative to the Martian geological timescale. The diagram highlights a pronounced age gap between ~4.1 Ga and ~2.4 Ga, with most SNC meteorites crystallizing during the Amazonian epoch. Earlier Noachian samples include NWA 7034 and ALH 84001. (Udry et al., 2025)

Martian meteorites have provided one of the most direct windows into the geology and evolution of Mars. Their origin was confirmed when the chemical and isotopic signatures of trapped noble gases inside these rocks were found to match thosemeasured in the Martian atmosphere by the Viking landers (McSween, 1984; Treiman et al., 2000). This discovery offered strong evidence that these meteorites were launched from Mars by large impact events and later fell to Earth. Because they

preserve records of volcanic activity, atmospheric components, and water-driven alteration, these samples demonstrate that Mars once hosted volcanism, an atmosphere, and an active hydrological cycle. Except for Earth, no other planetary body in the Solar System records all three processes together, which makes the Martian meteorites uniquely important.

Most Martian meteorites are grouped into the SNC suite — Shergottites, Nakhlites, and Chassignites — which represent igneous rocks of volcanic or cumulate origin. These meteorites are mostly formed during the recent ages of Martian geological history, i.e., the Amazonian period (Fig. 1.5). In addition, there are a few meteorites that represent the Noachian Mars, which do not belong to the SNC class of meteorites; these include the ancient orthopyroxenite ALH 84001 and the regolithic breccia NWA 7034, along with its paired stones (Fig. 1 .5) (Agee et al., 2013; Wittmann et al., 2015). Each of these samples contributes distinct insights into Mars' mantle composition, magmatic processes, alteration history, and even the potential for habitability. Their value is especially high because Mars, unlike Earth, has not undergone plate tectonics that would recycle and erase its oldest crust. As a result, Martian meteorites preserve signatures of ancient processes that are no longer visible in Earth's oldest rocks (Mojzsis et al., 1996).

1.4.1 Shergottites

The Shergottites are the most abundant group of Martian meteorites, first recognized after the fall of the Shergotty meteorite in India in 1865. They make up nearly 90% of all Martian meteorites by number and are compositionally diverse (Udry et al., 2020). Compared with Earth's basalts, Martian shergottites generally show higher Fe/(Fe+Mg) ratios and lower Al_2O_3 contents, reflecting differences in mantle chemistry between the two planets (Nyquist et al., 2001).

Shergottites are often classified by their enrichment or depletion in incompatible trace elements (ITE). These variations are believed to reflect both the early differentiation of Mars during the crystallization of a global magma ocean and later processes, such as partial melting, mantle metasomatism, or the assimilation of crustal material (Borg & Draper, 2003; Lapen et al., 2017; Day et al., 2018). The loss of volatiles during eruption or magma ascent is recorded in the volatile-depleted nature of some shergottites, suggesting that their parental magmas once contained significant water that degassed during emplacement (McCubbin et al., 2012; Herd et al., 2017). Texturally, shergottites exhibit a wide variation, reflecting differences in their crystallization environments. Five main subgroups are recognized:

- Basaltic shergottites (Fig. 1.6a) consist largely of clinopyroxene and plagioclase, and their fine-grained, sometimes diabasic textures indicate near-surface crystallization in dikes or flows (Jambon et al., 2002).
- Olivine-phyric shergottites (Fig. 1.6b) contain abundant olivine phenocrysts within a porphyritic groundmass, pointing to crystallization in ascending magmas (Goodrich, 2002).
- Poikilitic (or lherzolitic) shergottites (Fig. 1.6c) are coarse-grained and olivine-rich, with large pyroxene crystals enclosing earlier olivine grains; they resemble cumulates crystallized deeper within the crust (Treiman et al., 1986).
- Gabbroic shergottites (Fig. 1.6d) are defined by cumulate textures dominated by large plagioclase or pyroxene crystals, consistent with slow crystallization in magmatic reservoirs (Hewins et al., 2019).
- Augite-rich shergottites (Fig. 1.6e) (such as NWA 8159 and NWA 7635) are rare and unusual, with distinctive mineral and isotopic signatures pointing to a separate, relatively oxidized mantle source (Herd et al., 2017; Udry et al., 2020).

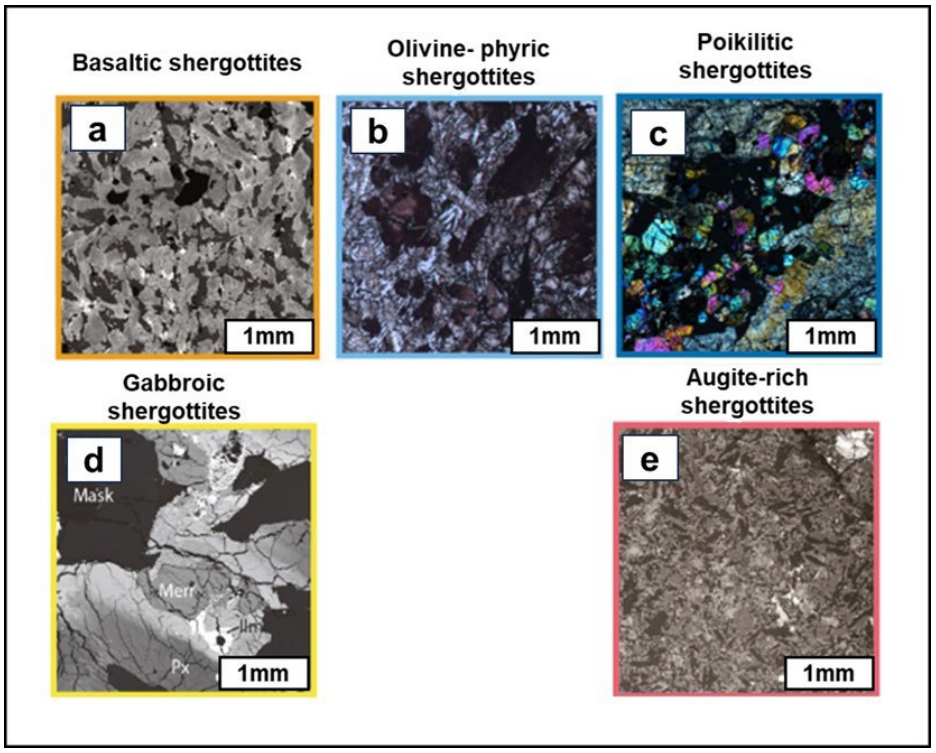

Fig. 1.6: Petrographic diversity within the shergottite meteorite suite illustrated through representative examples: (a, top left) basaltic shergottites, showing fine-grained intergrowths of clinopyroxene and plagioclase typical of near-surface crystallization;; (b, top middle) olivine-phyric shergottites, characterized by prominent olivine phenocrysts set within a porphyritic groundmass; (c, top right) poikilitic (lherzolitic) shergottites, where coarse pyroxene oikocrysts enclose earlier-formed olivine, reflecting deeper crustal cumulate processes; (d, bottom left) gabbroic shergottites, displaying slowly cooled cumulate textures dominated by large plagioclase and pyroxene crystals; and (e, bottom right) augite-rich shergottites, a rare subgroup distinguished by their unusual mineral assemblages and isotopic signatures that suggest derivation from a distinct, comparatively oxidized mantle source. (modified after Udry et al., 2025)

Chronologically, shergottites were long thought to be the youngest Martian meteorites, with crystallization ages ranging from ~575 to 150 million years ago (Ma) (Nyquist et al., 2001). However, new analyses of some augite-rich specimens suggest crystallization ages as old as ~2.4 Ga, indicating that magmatism persisted in different mantle reservoirs over billions of years (Herd et al., 2017; Bellucci et al., 2020). Their cosmic-ray exposure ages range widely (0.5–19 Ma), indicating that multiple impact events were likely responsible for ejecting them into space. The Zunil and Mojave craters have been suggested as possible sources, but uncertainties remain because

exposure ages do not align with a single event (McEwen et al., 2005; Werner et al., 2014).

1.4.2 Nakhlites

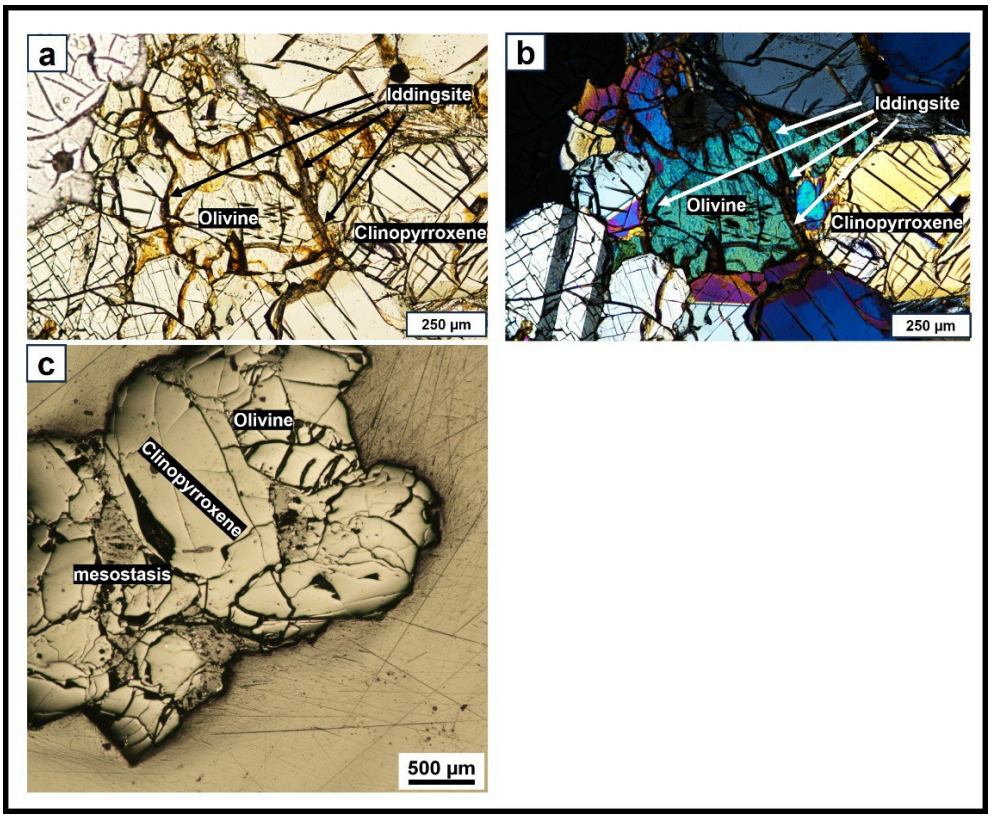

Fig. 1.7: *Petrographic images of the nakhlite Yam-593 obtained in plane-polarized light (a), cross-polarized light (b), and reflected light (c). The sample displays the typical cumulate texture of nakhlites, which is clinopyroxene-rich. In both transmitted-light views (a, b), clay-rich alteration products identified as iddingsite are visible along fractures of olivine grains.*

The Nakhlites are named after the Nakhla meteorite, which fell in Egypt in 1911. They are clinopyroxene-rich cumulates (Fig. 1.7) dominated by augite (~80%) with lesser olivine (~10–15%) and a mesostasis of feldspar, sulfides, and accessory minerals (Treiman & Gooding, 1991; Bridges et al., 2001). Their crystallization ages average around 1.35 Ga, suggesting that they formed in long-lived volcanic systems during the Middle Amazonian (Treiman, 2005). High-precision dating indicates that they were produced during several discrete eruptions between ~1416 and 1322 Ma (Cohen et al., 2017). Their ejection from Mars occurred much more recently, around

3.9–12 Ma, and they arrived on Earth within the past 10,000 years (Nyquist et al., 2001; Eugster et al., 2002).

Nakhlites preserve strong evidence of interaction with Martian fluids. Olivine and glass within them were partly altered to iddingsite, smectite, Fe-oxides, gypsum, and halite, pointing to low-temperature aqueous alteration in the shallow crust or surface (Bridges et al., 2001; Hallis et al., 2012a; Lee et al., 2015a). These phases indicate transient episodes of liquid water, which are consistent with localized weathering under limited hydrological conditions.

Texturally, nakhlites differ from one another, implying variable emplacement and cooling settings. Some samples (e.g., MIL and Yamato) exhibit quench textures consistent with shallow emplacement, while others (e.g., Lafayette and Nakhla) crystallized more slowly at depth (Treiman, 2005). They also record impact-related shock features, such as melt veins and inclusions, which provide pressure estimates of less than 45 GPa for their ejection (Fritz et al., 2005). Terrestrial weathering has affected most nakhlites, although Nakhla and Lafayette show minimal contamination due to early recovery (Treiman, 2005; O'Brien et al., 2022).

1.4.3 Chassignites

The Chassignites are the rarest of the SNC suite, named after the Chassigny fall in France in 1815. Only three examples are known: NWA 8694, Chassigny, and NWA 2737 ("Diderot") (Fig. 1.8). These meteorites are cumulate dunites, composed primarily of olivine (~90%) with minor amounts of pyroxene, feldspar, chromite, and accessory phases (Johnson et al., 1991; Hewins et al., 2020). Their noble gas signatures are distinct from those of nakhlites and shergottites and are thought to record mantle compositions unique to Mars (Johnson et al., 1991).

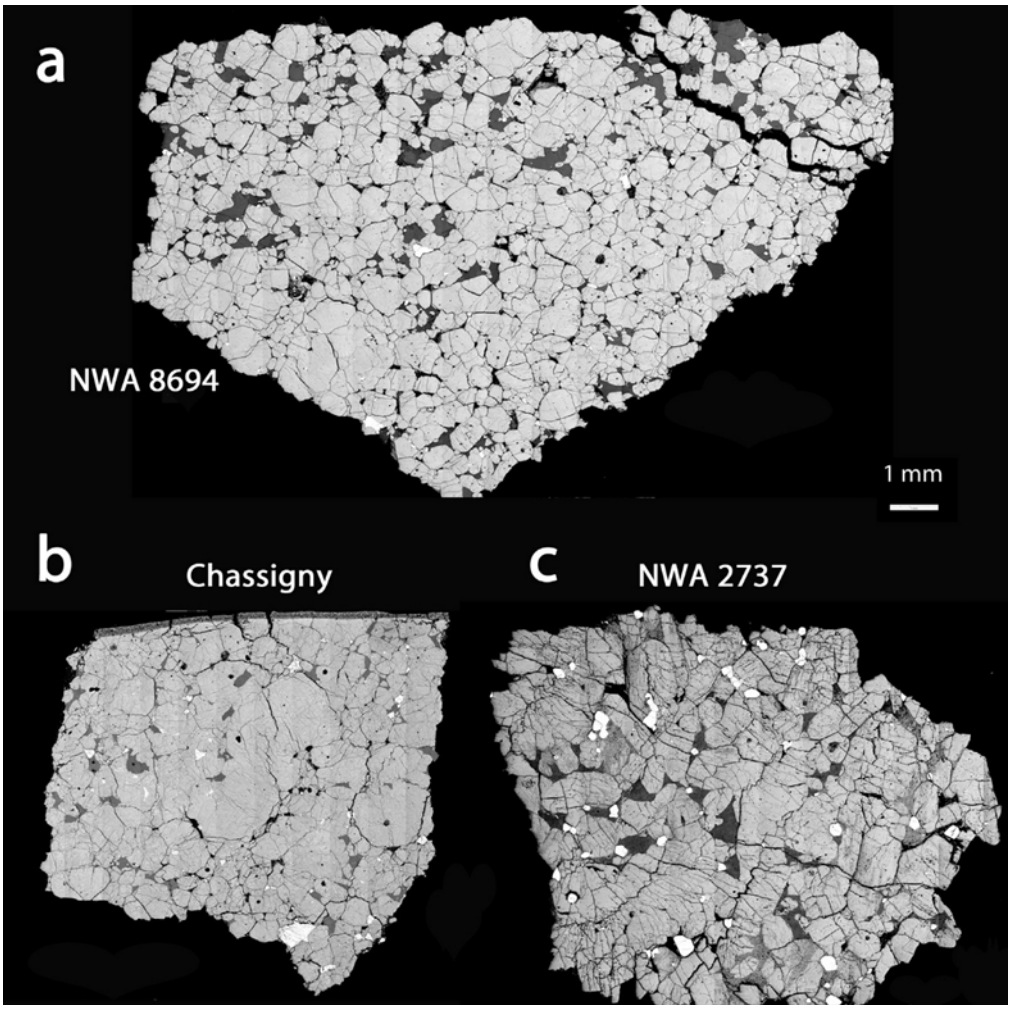

Fig. 1.8: *Backscattered electron (BSE) images of the chassignite meteorites NWA 8694 (top),Chassigny (bottom left), and NWA 2737 (bottom right) (Hewins et al., 2020)*

Geochemically, chassignites are depleted in rare-earth elements (REEs) compared with nakhlites. Their mineral textures, such as exsolved pyroxenes and Ca-zoned olivines, suggest crystallization under high-temperature conditions (~900–1,230 °C) from fractionated magmas (Mikouchi et al., 2005; Treiman et al., 2007). Unlike nakhlites, they exhibit little to no evidence of Martian aqueous alteration, and the minor changes that do exist are attributed to terrestrial weathering after their fall (Misawa et al., 2005; McCubbin et al., 2013). Shock features indicate that they experienced at least two impact events before ejection, and cosmic-ray exposure ages of ~10–12 Ma are consistent with those impacts (Treiman et al., 2007; McCubbin et al., 2013).

1.5 Deccan Volcanic Province (DVP)

The Deccan Traps, formed during the Late Cretaceous to Paleocene (~65 Ma), represent one of the largest volcanic provinces on Earth. This continental flood basalt province extends across approximately 500,000 km² of western and central India and is composed mainly of extensive tholeiitic lava flows, dyke swarms, and associated plutonic complexes. The original eruptive volume of these basalts has been estimated at ~1.6 × 10^6 km^3 (Jay & Widdowson, 2008), with significant additional magmatic activity recorded offshore in the Arabian Sea and the Seychelles region (Calvès et al., 2011; Pande et al., 2017; Shellnutt et al., 2017; Fainstein et al., 2019). They are classified as Continental Flood Basalts (CFBs) that erupted around the Cretaceous–Paleogene boundary and are widely regarded as potential terrestrial analogues for Martian basalts (Self et al., 2022). Their origin has been explained by two main competing hypotheses. The plume hypothesis proposes that the basalts were generated by partial melting of a deep mantle plume that rose beneath the Indian plate as it migrated over the present-day Réunion hotspot (Duncan & Richards, 1991; Mahoney et al., 2002). In contrast, the non-plume hypothesis suggests that magma generation occurred due to decompression melting of the shallow mantle or subcontinental lithosphere, without the involvement of a deep mantle plume (Sheth, 2005; Hawkesworth et al., 2000). The Deccan flood basalts are well exposed along the Western Ghats escarpment, where the lava pile reaches a thickness of ~1.6 km and a stratigraphic thickness of up to ~3.5 km. In contrast, lava sequences in the eastern and northeastern parts of the province are considerably thinner, typically ranging from 10 to 100 m. While tholeiitic basalts and basaltic andesite flows dominate the eastern and southeastern regions, the western and northwestern parts of the province—particularly along the rifted continental margins of Saurashtra and Kutch in Gujarat—contain

several volcano-plutonic complexes and display significant compositional diversity. These regions include picrite and ankaramite, lamprophyres, diorite, trachyte, granophyre, and rhyolite (Sheth et al., 2012; Zellmer et al., 2012; Kshirsagar et al., 2012; Cucciniello et al., 2022). The immense areal extent of the lava flows, coupled with limited evidence of sedimentation between successive flows, suggests that the Deccan Volcanic Province was susceptible to weathering either soon after emplacement or during pauses in eruptive activity (Mitra et al., 2018).

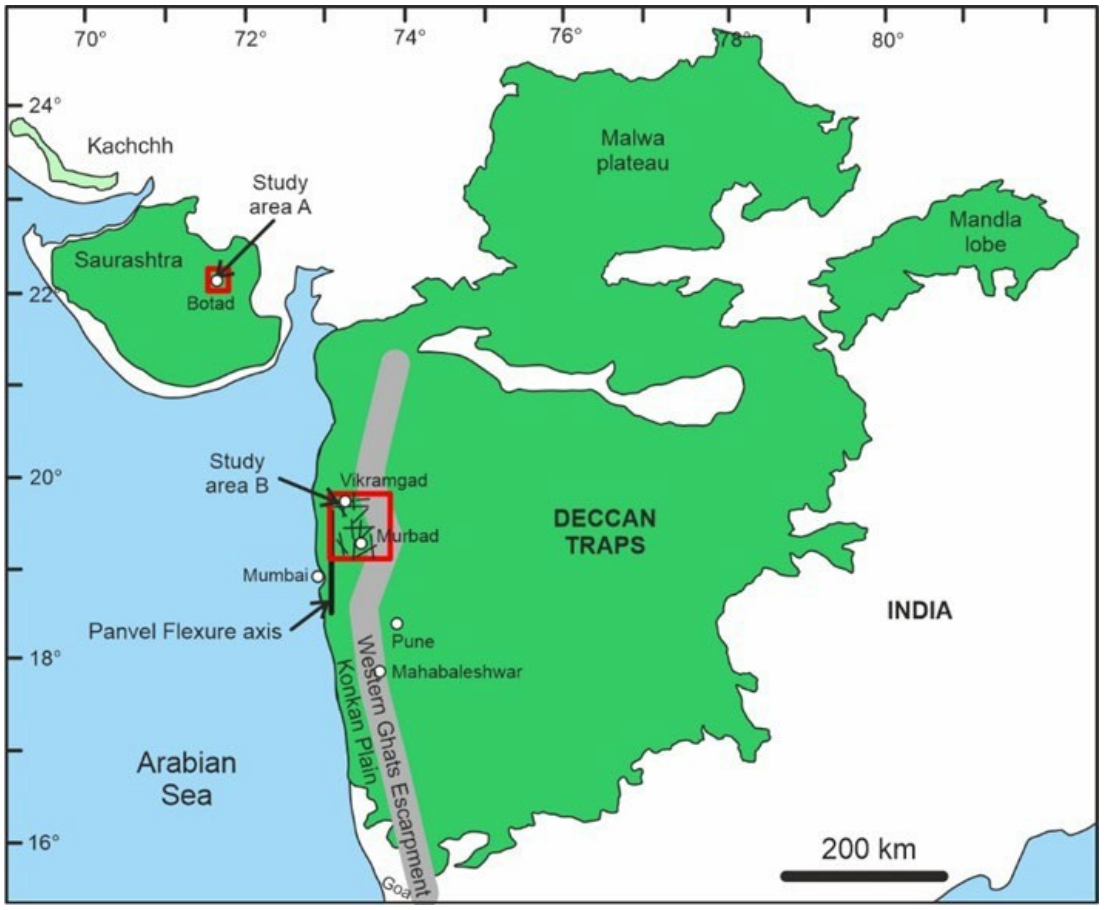

Fig.1.9: presents a simplified map of western India, where the main distribution areas of the Deccan Volcanic Province (DVP) are shown (modified after Krishnamurthy et al., 2020). The DVP, recognized as one of the largest continental flood basalt provinces, is estimated to cover an area of approximately 500,000 square kilometres. It is primarily divided into the Main Deccan Province, Malwa Plateau, Mandla Lobe, and Saurashtra regions. In this study, the locations from which the Deccan basalt samples were collected are highlighted in blue on map.

In the present study, picritic lava flows from Botad, Gujarat, and tholeiitic dykes from the Konkan Plain were selected for detailed analysis. These samples were investigated to examine olivine textures and to constrain the nature and extent of alteration processes operating within contrasting basaltic lithologies.

1.5.1 Terrestrial analogy of the Deccan to the Martian crust

The Deccan Traps stand out as one of the best natural examples on Earth for exploring processes that may also have influenced the Martian crust. Their significance as an analogue becomes clearer when the effects of meteorite impacts, hydrothermal alteration, and volcanic cooling features are examined more closely. Spectral analysis provides an effective approach for linking Martian surface compositions with suitable terrestrial analogues. Mid-Infrared (MIR) data obtained from the Mars Global Surveyor Thermal Emission Spectrometer (MGS-TES) confirmed that much of the Martian crust is basaltic in composition and shows a strong correspondence with Deccan basalts (Christenson et al., 2000).

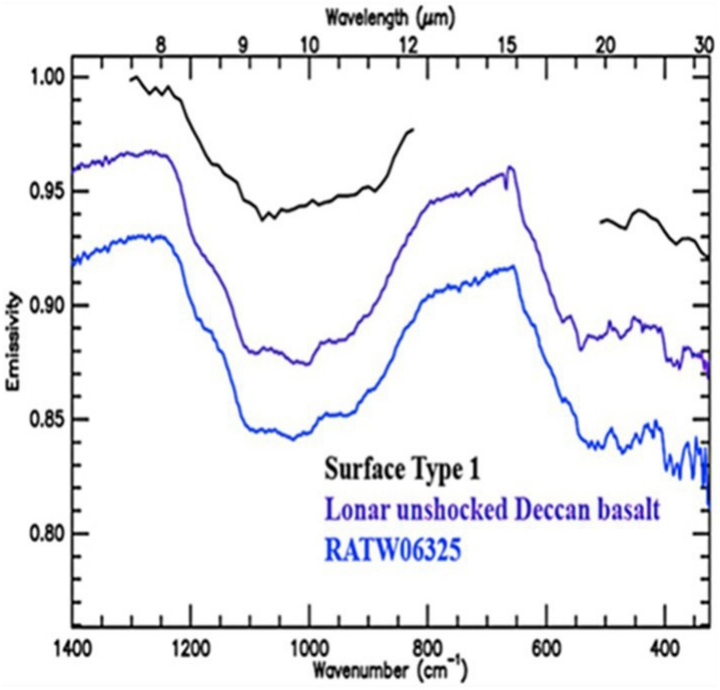

Fig. 1.10: Thermal emission spectra showing the close match between Deccan basalt from Lonar (sample RATW06325) and Martian Surface Type 1 terrains (Christenson et al., 2003)The strong overlap in spectral features provides clear support for using Deccan basalt as a reliable analogue for basaltic regions on Mars

A close similarity has been observed between the spectral features of Martian Surface Type 1 and those of Deccan basalt samples (Fig. 1.10). In particular, spectra from the Lonar unshocked basalt (sample RATW06325) exhibit a strong match with basaltic terrains on Mars. These comparisons highlight that the Deccan Volcanic Province is not only chemically comparable to Martian basalts but also reproduces theirspectral behavior. As a result, Deccan basalts provide a valuable analogue for exploringMartian mineralogy, understanding alteration processes, and conducting experiments under Mars-like conditions (Wright et al., 2011; Christenson et al., 2000).

The unusual chemistry of the Deccan basalts lends further weight to their value as a Mars analog. With higher Fe and lower Al abundances, the Deccan basalts closely resemble the composition of Martian basalts and differ from most other terrestrial examples (Haggerty & Newsom, 2001). The AFM ternary plot (Fig 1.11) also shows that the Deccan basalt falls in the same tholeiitic field as the Martian crustal basalts (Das et al., 2025)

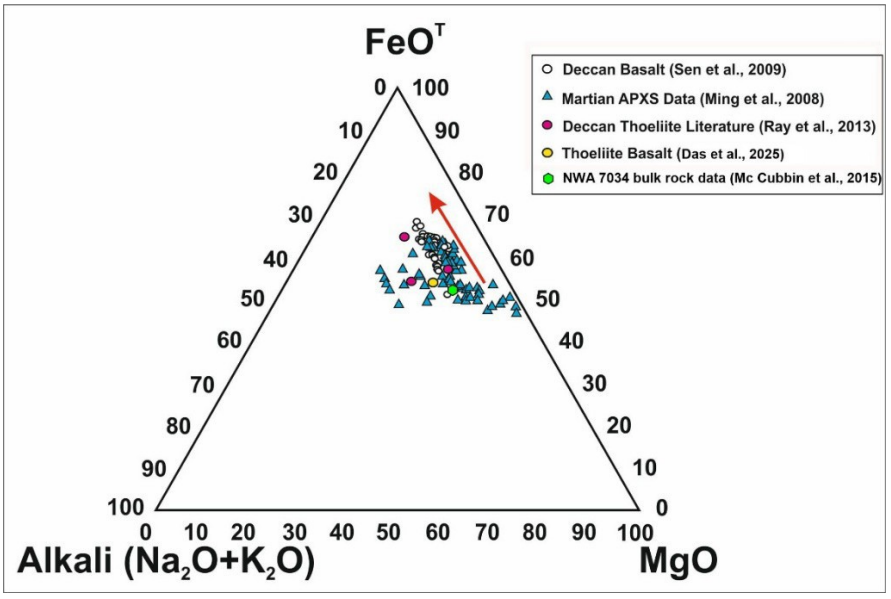

Fig 1.11: In addition to their bulk composition, hydrothermal alteration at Lonar (Deccanbasalt) provides evidence of how water interacted with basalt following the impact. Theheat generated by crater formation enabled groundwater to circulate through thefractured rocks, leading to the development of secondary clay minerals, such assaponite and celadonite, at moderate temperatures of approximately 130–200 °C (Hagerty & Newsom, 2003). These clays bear a close resemblance to alteration

products observed on the Martian surface by orbiters and rovers. Together, the chemical and alteration features of the Deccan reinforce its importance as a natural laboratory for understanding how basaltic terrains on Mars may have been shaped by water and impact activity.

Alongside impact-related processes, the Deccan basalts also display volcanic structures that echo those identified on Mars. One of the most distinctive is columnar jointing, where cooling and contraction of lava flows produced long, hexagonal columns extending several meters in height. These columns developed as lava cooled relatively quickly under conditions that allowed fractures to spread in regular, geometric patterns. Recent work suggests that water present during cooling may have contributed to their formation, either by increasing cooling rates or by influencing stress within the solidifying lava (Millazo et al., 2009; Das et al., 2025). On Mars, widespread basaltic lava flows with columnar jointing have also been reported, strongly implying that comparable cooling processes occurred there. The comparison between Deccan and Martian columnar basalts, therefore, strengthens the idea that water played an active role in the cooling and shaping of Martian lava flows.

Taken together, the shock effects from impacts, post-impact hydrothermal alteration, and volcanic cooling features of the Deccan Traps provide a rich analogue for Martian environments. These examples reveal that the Deccan is not only

chemically similar to Martian basalts but also preserves the same types of processes that were likely active on Mars. Studying these features in the Deccan allows researchers to draw valuable conclusions about how Martian basalts were modified by water, heat, and impact activity. This perspective is especially relevant for interpreting aqueous alteration in nakhlite meteorites, which represent one of the clearest records of late-stage water–rock interaction preserved in the Martian crust.

1.6 Research Gaps & Motivation

The aqueous alteration preserved in nakhlite meteorites remains only partially understood, as several limitations hinder a complete reconstruction of the alteration sequence. One of the main challenges is the small number of Martian meteorite samples available for study. Another is the lack of precise knowledge about the chemistry of the fluids responsible for alteration. Due to these restrictions, the processes that control fluid–rock interactions in nakhlites remain difficult to interpret. Parameters such as water-to-rock ratios, fluid compositions, reaction pathways, and the order in which minerals were transformed are still debated and not clearly defined.

Evidence for past water activity on Mars also comes from geomorphological features such as Fresh Shallow Valleys (FSVs), which are common in the mid-latitude regions and formed during the Amazonian period. These valleys are believed to have developed during short-lived episodes of stable liquid water flow, possibly lasting less than a year (Hobley et al., 2014). While such events confirm that transient surface water existed, it remains unclear whether they left any detectable imprint in the deeper crust. Specifically, it remains uncertain whether the mineralogical and geochemical changes observed in nakhlites are related to these fleeting hydrological episodes. Linking short-term surface processes to longer-term subsurface alteration is, therefore, an important but unresolved question.

To address these uncertainties, terrestrial analogue studies have become highly valuable. Basaltic terrains on Earth, particularly those that developed under semi-arid or cold climatic conditions, can replicate alteration features similar to those observed in Martian meteorites. By investigating such sites, important information can be obtained about mineral transformations, fluid circulation, and geochemical gradients. When combined with data from Martian meteorites, rover-based observations, and orbital measurements, these analogue studies can significantly improve our understanding of the aqueous geochemistry of Mars' basaltic crust.

1.7 Thesis Objectives

The aim of this thesis is to explore how water influenced the alteration of the Martian basaltic crust, with a particular focus on nakhlite meteorites. This is being carried out using in situ analytical techniques that provide micro-scale evidence of fluid–rock interaction. Methods such as microstructural examination, mineralogical characterization, and chemical analysis of minerals are being applied to capture the textural and compositional details preserved in these meteorites. These techniques are essential for reconstructing the history of low-temperature aqueous alteration under Martian conditions, as they retain the spatial context of secondary minerals within their host phases.

Alongside meteorite studies, this thesis also aims to test the reliability of terrestrial analogs in replicating Martian-style alteration processes. Selected basaltic terrains, particularly from the Deccan Traps, are being evaluated to see how closely they match Martian meteorites in terms of water-to-rock ratios, fluid chemistry, mineral assemblages, and alteration mechanisms. By comparing these analogs with nakhlites, the research aims to enhance the understanding of fluid–rock interactions on Mars and refine the application of analog-based models.

This dual approach—integrating detailed meteorite analyses with terrestrial analog investigations—is expected to provide new insights into the geochemical and environmental conditions that shaped Mars' basaltic crust. It will also help identify diagnostic geochemical fingerprints that can be used to trace past fluid activity and assess whether these settings could have supported habitable conditions. Ultimately, this study contributes to a broader understanding of aqueous environments on Mars by reconstructing their composition, temperature, and duration. Such findings are crucial for assessing the planet's past habitability and for informing the interpretation of data from current and future Mars exploration missions.

1.8 Work done & Thesis organisation

Chapter 1 – Introduction

This chapter provides the geological and scientific background necessary for the thesis. It introduces Mars as a basalt-dominated planet, outlines its geological evolution with emphasis on aqueous activity, and discusses the global distribution of Martian clay minerals. The role of Martian meteorites and terrestrial analogues is introduced, followed by the objectives and scope of the study.

Chapter 2 – Samples, Instrumentation, and Methodology

This chapter details the analytical and modelling approaches adopted in the thesis. It describes petrographic analysis, Raman spectroscopy, electron probe microanalysis, X-ray elemental mapping, and geochemical modelling techniques. The criteria for sample selection, analytical conditions, data processing, and limitations of each method are also clearly explained.

Chapter 3 – Nakhlite meteorites: petrography, mineral chemistry, and aqueous alteration

This chapter provides a detailed investigation of Martian nakhlite meteorites, focusing on their petrography, mineral chemistry, and alteration features. The textures and modal abundances of primary minerals are described for each nakhlite, with particular emphasis on olivine grains and their fracture-controlled alteration. Mineral chemistry data are used to assess compositional homogeneity and cation behaviour, while x-ray elemental maps reveal patterns of elemental mobility during alteration. Alteration indices and compositional plots are employed to compare the degree and style of alteration among different nakhlites. The chapter highlights both common alteration characteristics and sample-specific differences, especially the complex alteration history recorded by Lafayette, thereby providing direct constraints on the nature of aqueous processes that affected the Martian crust during the Amazonian period.

While this chapter has focused on documenting the nature of aqueous alteration recorded within nakhlite meteorites, an important next step is to place these Martian observations into a broader geological context. The alteration features described here—such as fracture-controlled clay formation in olivine, limited degrees of chemical modification, and variations in alteration style among different nakhlites—raise the question of whether similar processes can be reproduced in basaltic rocks on Earth under comparable conditions. Addressing this requires a terrestrial system that is basaltic in composition, olivine-bearing, and capable of preserving low-temperature, water-limited alteration features analogous to those observed in Martian meteorites. The upcoming chapter takes up this task by examining olivine alteration in Deccan Continental Flood Basalts and directly comparing these terrestrial samples with the nakhlites. This Earth–Mars comparison enables the alteration processes inferred from nakhlites to be tested against a well-constrained terrestrial analogue, thereby helping to assess whether the alteration signatures observed in Martian meteorites reflect conditions unique to Mars or more general basalt–water interactions under low water-

to-rock ratios. In this way, the next chapter builds directly on the findings presented here and provides a critical link between observations of Martian meteorites and terrestrial geological processes

Chapter 4 – Comparison between Martian nakhlites and terrestrial Deccan basalts

This chapter establishes a direct comparison between Martian nakhlite meteorites and terrestrial Deccan basalts to evaluate whether similar alteration processes operated on Earth and Mars. Petrographic textures, fracture-controlled alteration features, mineral chemistry, and elemental redistribution patterns are systematically compared. Particular attention is given to similarities in olivine alteration behaviour despite differences in bulk composition and planetary setting. The chapter demonstrates that many features observed in Martian samples can be reproduced in terrestrial basalts altered under limited water availability. This comparison supports the use of Deccan basalts as suitable terrestrial analogues and strengthens the interpretation that nakhlite alteration reflects localized, low water–rock ratio processes rather than extensive aqueous alteration. The next chapter builds directly on this need by examining how olivine alters within two chemically contrasting Deccan basalts—one picritic and rich in magnesium, the other tholeiitic and more iron-rich. By comparing these two terrestrial systems in detail, the chapter develops a clearer baseline for understanding how variations in olivine composition affect alteration textures, clay mineralogy, and the extent of reaction under restricted water availability. These insights deepen the contextual framework required for interpreting Martian meteorites. In this way, the work in the next chapter acts as a bridge between the natural observations presented here and the geochemical modelling that follows later, strengthening the foundation for reconstructing past fluid–rock interactions on both Earth and Mars.

Chapter 5 – Aqueous alteration in Deccan basalts under controlled conditions

This chapter focuses exclusively on terrestrial Deccan basalts and examines how different basalt types respond to aqueous alteration. Picritic and tholeiitic basalts are studied to assess the influence of olivine composition on alteration behaviour. Petrographic observations are combined with mineral chemistry and alteration indices to document fracture-controlled alteration and limited secondary mineral formation. The chapter further explores how variations in water–rock ratio and temperature affect the nature and extent of alteration. By isolating these parameters in a terrestrial setting, this chapter provides a controlled framework that helps interpret the Martian alteration record and clarifies which features are primarily controlled by composition versus fluid availability.

Chapter 6 – Geochemical modelling of low water–rock ratio alteration

This chapter presents geochemical modelling designed to quantitatively constrain the physicochemical conditions responsible for the observed alteration features. Models are run for Mg-rich and Fe-rich basalt compositions over a range of low to moderate temperatures and restricted water–rock ratios. The modelling results are compared directly with petrographic and geochemical observations from both terrestrial basalts and Martian nakhlites. This chapter demonstrates that limited alteration and smectite formation can be reproduced under water-starved conditions, even when temperatures are moderately elevated. The modelling results provide quantitative bounds on water availability, temperature, and reaction progress, reinforcing the interpretation that nakhlite alteration occurred during short-lived, localized aqueous or hydrothermal events on Mars.

Chapter 7 – Summary, Conclusions, and Future Scope

This chapter summarizes the major findings of the thesis and presents the key scientific conclusions. It highlights the significance of localized, fracture-controlled alteration under limited water availability and discusses the broader implications for the evolution of the Martian crust. The chapter concludes by outlining realistic future research directions, including the development of improved constraints on fluid chemistry, and comparison with rover and orbital datasets and many more.

.

Chapter 2: Samples, Instrumentation and Methodology

In this study, a variety of analytical techniques were used to investigate the Martian nakhlite meteorites along with their terrestrial basalt analogues. These techniques were chosen because they provide important information about the samples, allowing both microscopic details and overall chemical patterns to be studied in a systematic way. The use of such a combined approach was important for understanding not only the original mineralogy but also the secondary alteration products that formed through fluid-rock interaction. This integrated approach provided a strong framework for identifying the pathways of aqueous alteration on Mars and for drawing meaningful comparisons with similar processes observed in terrestrial basalts.

2.1. Fieldwork Area

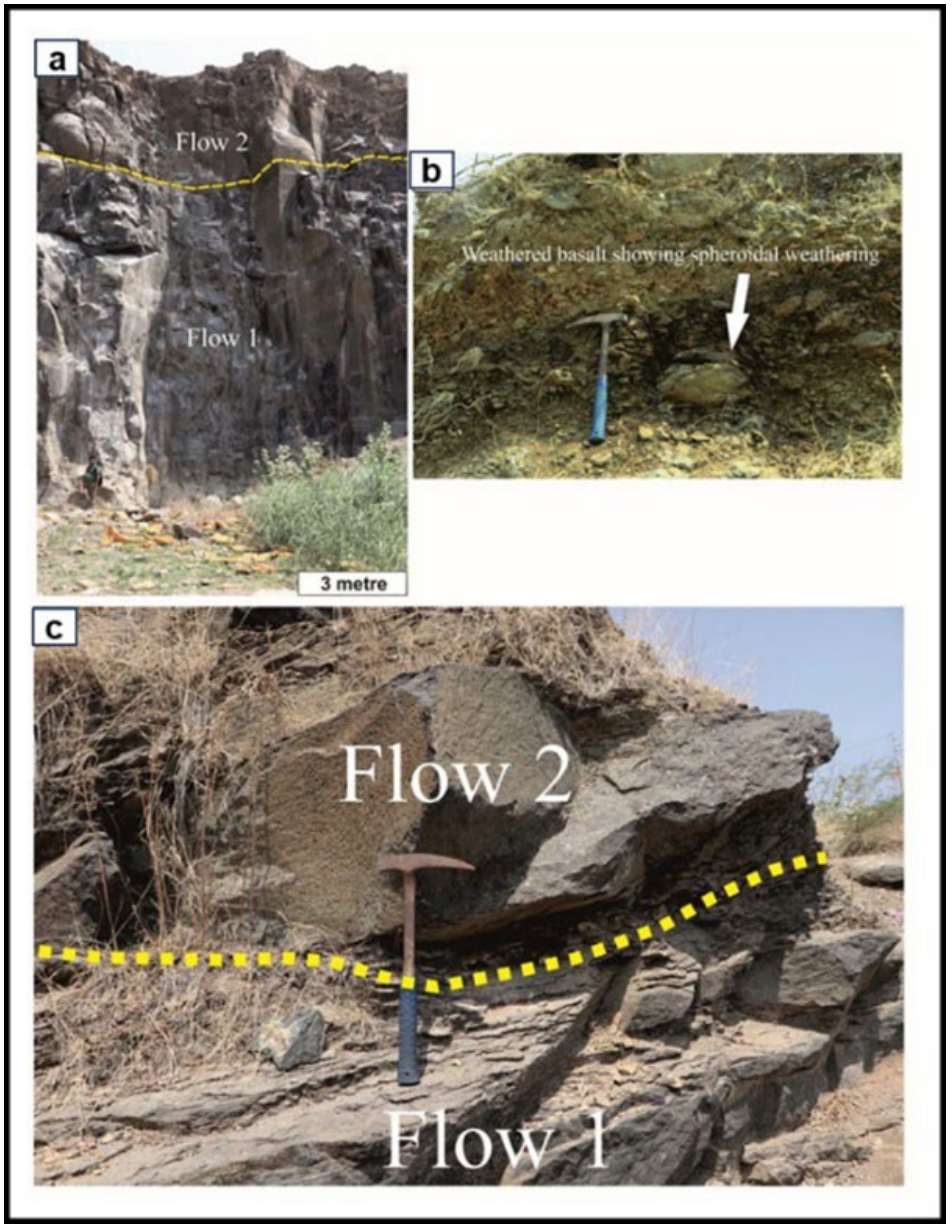

Fig. 2.1: Field photograph of the stone quarry comprising compact picritic basalts. Fig (a) shows the exposure of lava flows, where the average width of the flow for the lower flow and the upper flow is 9.5 m and 4 m, respectively. Fig (b) depicts the top part of the flow shows evidence of weathering resulting in spheroidally weathered basalts. Fig (c) shows a close-up view showing a distinct boundary between the two lava flows

Fieldwork for this study was carried out in two regions within the western part of the Deccan Volcanic Province (DVP), India, which forms part of the western Indian volcanic rifted margin. This region is characterized by extensive basaltic lava flows and widespread mafic intrusions such as dykes. The general geological framework of the DVP has been discussed in Chapter 1 and is not repeated here. The first study area is located near Botad town in Gujarat

(22°10′19.2″N, 71°41′16.8″E), where picritic basalts were examined in a stone quarry. The region is dominated by thick basalt flows, while the surrounding areas mainly consist of Quaternary sediments. The exposed section shows two overlapping lava flows, with the lower flow having an average thickness of ~9.5 m and the upper flow ~4 m. These basalts are mostly compact and fresh, with only minor visible alteration, except near the top of the upper flow where spheroidal weathering is observed. High-Mg basalts (MgO 8–12 wt%) and picrites (MgO 12–18 wt%) are common in the Deccan province (Le Bas, 2000). Some picrites from Gujarat contain high-forsterite olivine ($Fo_{88–92}$) and are interpreted as near-primary melts, while others reflect olivine accumulation processes (Krishnamurthy & Cox, 1977; Melluso et al., 1995; Krishnamurthy et al., 2000; Sheth & Melluso, 2008; Chatterjee, 2024).

Fig. 2.2: *exhibits field photographs of the sample locations. Fig a represents the picrite basalt samples (very high forsterite content) from a stone quarry near the Botad town in Gujarat. Fig. 1a shows a field photograph of a stone quarry composed of compact picritic basalts, where two distinct lava flowscan be clearly observed. The lower flow is measured to have an average thickness of approximately 9.5 meters, while the upper flow has an average thickness of around 4 meters. Fig.s (b, c, d) represent field photographs of tholeiitic dykes from Konkan Plain. (Fig. 1b) Dyke BA22/23 exposed in a streambed near*

Tansa Lake. The dyke with margins well exposed is 3 m wide and columnar-jointed. (Fig. 5.1c) Dyke BA22/02 near Khand dam is ~13 m wide, columnar-jointed, and forms a hillock, with compound pāhoehoe lava flows on either side. (Fig. 5.1d) N-S trending dyke BA22/37, dipping 75°E,is exposed near Vehloli, and shows columnar joints

,The second study area is located in the Konkan Plain region, around Vikramgad, Shahapur, and Murbad, where tholeiitic basaltic dykes were studied. This region lies between the Panvel flexure zone and the Western Ghats escarpment and provides well-exposed sections of dyke intrusions. The Panvel flexure extends for ~150 km and shows seaward dips of 15–20° towards the Arabian Sea (Dessai & Bertrand, 1995). The dykes intrude compound pāhoehoe lava flows that preserve features such as ropy flow tops, tumuli, pipe vesicles, and squeeze-up structures, indicating low-viscosity eruptive conditions (Sheth et al., 2024). These dykes are basaltic to doleritic in composition and are less affected by weathering compared to the host lava flows, often forming prominent linear ridges. Cooling-related jointing patterns are well developed within the dykes (Fig. 2.2). Many dykes show columnar joints oriented perpendicular to their margins, while thicker dykes display blocky or cuboidal joint patterns due to slower cooling. Most dykes are vertically oriented, although some show steep dips (~75°), suggesting structural control on their emplacement (Yatheesh, 2020). Together, these two field areas provide access to both olivine-rich picritic basalts and tholeiitic basaltic systems, allowing investigation of alteration processes across a range of compositions relevant to Martian basaltic crust.

The samples used in this study include Martian meteorites (nakhlites) and terrestrial basaltic rocks from the Deccan Volcanic Province, India. The nakhlites represent basaltic rocks from the Martian crust and preserve evidence of aqueous alteration, while the Deccan basalts serve as well-constrained terrestrial analogues for comparison. Field-based samples include picritic basalts from Botad (Gujarat) and tholeiitic basalts from the Konkan Plain, selected to represent variations in olivine

composition and texture.All samples were prepared as thin sections for petrographic observations and as polished mounts for detailed microanalytical work. A range of analytical techniques was used to characterize the samples, including polarizing microscopy for textural studies, electron microscopy for high-resolution imaging, electron probe microanalysis for mineral chemistry, Raman spectroscopy for phase identification, and X-ray fluorescence for bulk chemical composition. In addition, geochemical modelling was carried out using the derived mineral and bulk compositions to understand water–rock interaction processes.A summary of the samples, their source locations, preparation methods, and analytical techniques used in this study is presented in Table 2.1.

Table 2.1: Summary of samples used in this study, including their source/location, sample preparation methods, and analytical techniques applied to both Martian meteorites and terrestrial Deccan basalt analogs.

Sample Type and name	Source / Field Location	Sample Preparation	Analytical Techniques Used
Martian meteorite: Yam-593 (Nakhlite)	Yamato Glacier; find (Antarctica)	Thin section preparation; polished mounts for microanalysis	Polarizing Microscopy, SEM, EPMA, Raman Spectroscopy, X-ray Elemental Mapping, Geochemical Modelling
Martian meteorite: MIL 03346 (Nakhlite)	Miller Ranges; find (Antarctica)	Thin section; polished section	SEM (BSE imaging), EPMA, Elemental Mapping
Martian meteorite: Nakhla (Nakhlite)	Nakhla; fall (Egypt)	Thin section; polished mounts	Polarizing Microscopy, SEM, EPMA
Martian meteorite: Lafayette (Nakhlite)	Lafayette; find (USA)	Thin section; polished mounts	SEM (BSE imaging), EPMA, Elemental Mapping, Raman Spectroscopy
Terrestrial Basalt: Picritic Basalt	Botad, Gujarat, India	Hand specimen collection; thin sections; polished mounts	Polarizing Microscopy, SEM, EPMA, Raman Spectroscopy, XRF, Geochemical Modelling
Terrestrial Basalt: Tholeiitic Basalt	Konkan Plain, India	Hand specimen collection; thin sections; polished mounts	Polarizing Microscopy, SEM, EPMA, Raman Spectroscopy, XRF,

			Geochemical Modelling

2.2. Sample preparation

Rock samples selected for this study were prepared as epoxy-mounted thick sections to enable high-quality petrographic, electron microscopy, and Raman spectroscopic analyses. Initially, hand specimens were broken into small chips using a rock hammer. Chips with relatively flat surfaces were preferentially selected to facilitate efficient exposure during subsequent grinding and polishing steps. The selected rock chips were placed into cylindrical moulds with an internal diameter of 1 inch and a height of approximately 1 cm. The chips were positioned such that their flattest surface faced downward, ensuring optimal orientation for later surface exposure. A low-viscosity epoxy resin (Buehler Epothin 2) was prepared by mixing the epoxy resin and hardener in a 2:1 weight ratio. The epoxy mixture was then carefully poured into the moulds to fully encapsulate the rock chips, ensuring the absence of air bubbles. The filled moulds were left undisturbed at room temperature for approximately 9–12 hours to allow the epoxy to cure completely. After curing, the hardened epoxy mounts were removed from the moulds and immediately subjected to surface preparation. Initial material removal was carried out by sanding the mounts on a series of abrasive and silicon carbide papers, progressing from coarse to finer grit sizes. This step was performed to gradually remove the epoxy overburden and to expose a fresh, flat surface of the embedded rock chip. Once the rock surface was adequately exposed, final polishing was carried out using a rotating polishing machine operated at a constant speed of 500 rpm. Polishing was performed in successive stages using alumina abrasive powders of decreasing particle size, starting from 1 μm, followed by 0.3 μm, and finally 0.05 μm. Each polishing stage was conducted for approximately one hour, with lapping oil used as a lubricant to minimize surface damage and ensure uniform polishing. Between each polishing step,

the epoxy mounts were thoroughly cleaned in an ultrasonic bath to remove residual abrasive particles and polishing debris. This systematic grinding and polishing procedure yielded an exceptionally flat, smooth, and scratch-free surface with minimal topographic relief. The high-quality surface finish achieved through this preparation protocol is critical for minimizing analytical artefacts and ensuring reliable data acquisition during electron microscopy, Raman spectroscopy, and other surface-sensitive analytical techniques employed in this study.

2.3. Polarising Microscope

The polarising (petrological) microscope is a fundamental tool in optical mineralogy and petrography, designed to study minerals based on their interaction with polarised light. The working principle of this microscope is based on the fact that most rock forming minerals are optically anisotropic, meaning that their optical behaviour varies with crystallographic direction. When light passes through such minerals, its velocity and vibration direction are modified depending on the internal crystal structure and orientation of the mineral grains. In a polarising microscope, illumination is provided by an internal light source, and the emitted white light initially vibrates in all possible directions perpendicular to its direction of travel. This unpolarised light first encounters the polariser, which is positioned below the microscope stage. The polariser restricts the light vibrations to a single plane, producing plane-polarised light. This step is critical, as the optical properties of minerals—such as colour, pleochroism, relief, and cleavage—can be observed only when minerals interact with plane-polarised light. After passing through the polariser, the plane-polarised light enters the mineral thin section mounted on the microscope stage. If the mineral is isotropic, such as glass or certain cubic minerals, the light passes through without being modified. However, most silicate minerals are anisotropic and split the incoming plane-polarised light into two rays that vibrate in mutually perpendicular directions and travel at different velocities

within the crystal. This phenomenon produces a phase difference between the two rays, which leads to birefringence and other diagnostic optical effects. As the stage is rotated, the orientation of the mineral relative to the vibration direction of the incoming light changes. This causes systematic variations in brightness, colour, and extinction behaviour, which are used to determine mineral identity and crystallographic orientation. Under plane-polarised light, properties such as mineral colour, transparency, relief, grain boundaries, and fractures are examined, providing essential information on mineral texture and alteration features.

Fig. 2.3: *Polarising microscope installed at the PRL, Thaltej campus*

When the analyser is inserted into the optical path above the objective lenses, the microscope operates under crossed-polarised light conditions. The analyser is oriented perpendicular to the polariser and allows only light that has been modified by the mineral to reach the eyepiece. In this configuration, isotropic materials appear dark throughout rotation, while anisotropic minerals display interference colours that depend on their birefringence and thickness. The appearance and change of these colours During stage rotation are used to identify minerals and assess deformation or alteration

effects.The polarising microscope also allows observations under convergent light when the condenser and Bertrand lens are inserted. Under this mode, interference figures are produced, which provide information about optical symmetry, optic sign, and crystallographic orientation. Although convergent light observations are not always required for routine petrography, they are essential for detailed mineral identification and optical characterization. In this study, petrographic observations were performed using a Nikon LV100 polarising microscope (Fig. 2.3), which enables systematic examination of thin sections under plane-polarised light, crossed polars, and convergent light conditions. These observations provided the first level of mineralogical and textural information and formed the basis for subsequent microanalytical and geochemical investigations.

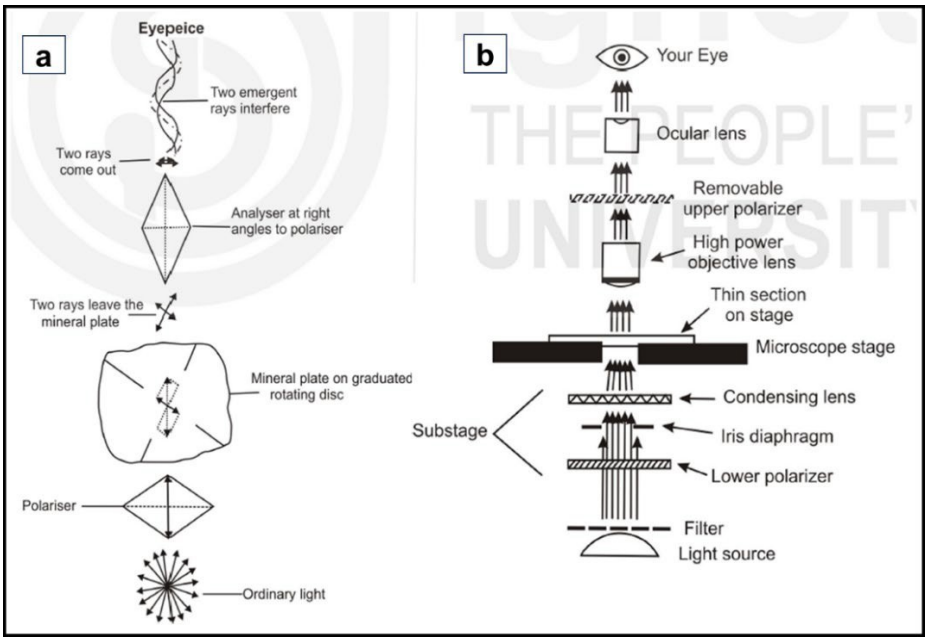

Fig. 2.4: *Schematic illustration of the working principle and optical layout of a polarising (petrological) microscope.* ***(a)*** *Diagram showing the interaction of plane-polarised light with an anisotropic mineral, including splitting into two vibration directions within the crystal, recombination at the analyser, and formation of interference effects during stage rotation.* ***(b)*** *Simplified optical path of a polarising microscope, showing the arrangement of the light source, lower polariser, condenser, rotating stage with thin section, objective lens, analyser, ocular lens, and observer's eye.*

2.1.1. Components of the Polarising Microscope

The main components of a polarising microscope and their functions are described below. A schematic representation of the optical layout and major parts is shown in Fig. 2.4.

- **Light Source**: The light source provides illumination for the microscope. In modern instruments, including the Nikon LV100, an in-built electric lamp is used. Tungsten or halogen bulbs are commonly employed. Because these bulbs produce light with a yellowish tone, a blue filter is placed above the light sourceto modify the illumination and approximate natural daylight conditions. This improves colour perception during mineral identification.

- **Polariser**: The polariser is positioned below the microscope stage. Its functionis to convert ordinary, unpolarised light into plane-polarised light by allowing vibrations only in a single direction. This step is essential, as most optical properties observed in petrography depend on the interaction of minerals with plane-polarised light.

- **Condenser (Condensing Lens):** The condenser is located below the stage andfocuses light onto the thin section. It ensures uniform illumination and improvesimage clarity, particularly at higher magnifications. The condenser can be raisedor lowered to optimise illumination conditions. It is especially important duringconvergent-light observations, where it is used in conjunction with the Bertrand lens.

- **Substage Diaphragm**: One or more diaphragms are present below the stage toregulate the amount and area of light entering the thin section. By adjusting thediaphragm, image contrast and resolution can be improved. The diaphragm is also adjusted during specialized optical observations, such as interference figureanalysis.

- **Graduated Rotating Stage**: The rotating stage is placed between the polarizer and analyzer and holds the thin section. It can be rotated through 360° and is marked with

a graduated scale, often with a vernier, allowing accurate angular measurements. This rotation is crucial for observing extinction positions and formeasuring optical angles. The thin section is held in place using spring clips.

- **Objective Lenses**: Objective lenses are mounted on a rotating nosepiece below the stage. They are responsible for forming the primary image of the specimen.Objectives of low, medium, and high magnification are commonly used in petrographic studies. Image quality depends on factors such as magnification, numerical aperture, and correction of optical aberrations. Accessory plates canbe inserted above the objective lenses when required.

    - **Microscope Tube and Focusing System**: The microscope tube houses the optical components above the stage. Focusing is achieved using coarse and fineadjustment knobs, which move either the stage or the optical tube vertically. Fine focusing is particularly important during high-magnification observations to resolve fine textures and alteration features.

    - **Accessory Slot**: An accessory slot is located below the analyser and allows optical plates, such as quartz wedges or gypsum plates, to be inserted into the light path. These plates are introduced at a fixed orientation, typically 45° to thecross-wires, and are used to determine optical properties such as birefringence sign and optic orientation.

    - **Analyser**: The analyser is the second polarising element and is positioned abovethe objective lenses within the microscope tube. It can be inserted into or removed from the optical path. When inserted, it is oriented perpendicular to the polariser, producing crossed-polarised light conditions. Under crossed polars, anisotropic minerals display interference colours, while isotropic materials appear dark. When

The analyzer is removed, and observations are made under plane-polarised light.

- **Eyepiece (Ocular):** The eyepiece is located at the top of the microscope tube and magnifies the image formed by the objective lens. It commonly contains cross-wires that can be focused independently and are used for alignment and measurement. Binocular eyepieces are typically used in advanced petrographic microscopes for comfortable observation.

- **Bertrand Lens**: The Bertrand lens is used for convergent light observations and is essential for studying interference figures. When inserted into the optical pathand used together with the condenser, it allows interference figures to fill the field of view. These figures are used to determine optic sign and symmetry of minerals.

2.4. Electron Microscopy and Microanalysis

Electron microscopy is a widely used non-destructive technique in which a finely focused beam of high-energy electrons (typically 5–30 keV, with a spot size as small as~1 nm) is directed onto the polished surface of a solid sample. The interaction between this primary electron beam and the sample occurs over a depth ranging from about 1 µm to 0.1 nm, producing a variety of signals, the most important being secondary electrons (SE), backscattered electrons (BSE), and characteristic X-rays (Fig. 2.5).

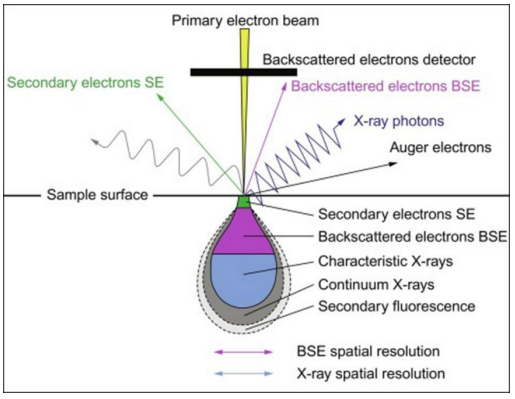

Fig. 2.5: Schematic of electron beam–sample interaction showing multiple signals, withbackscattered electrons, secondary electrons, and characteristic X-rays utilized in this study (Sharma & Bhardwaj, 2019)

Each of these signals provides complementary information about the sample. Secondary electrons, generated through inelastic scattering, are highly sensitive to surface morphology and are useful for documenting fine-scale topography (Loretto, 1984). Backscattered electrons, produced by elastic scattering, provide compositional contrast because regions enriched in heavy elements such as Fe or Ti appear brighter than those dominated by lighter elements like Si or Al. Characteristic X-rays arise when inner-shell electrons are displaced and replaced by outer-shell electrons, releasing energy specific to the element. These X-rays are detected either by energy dispersive spectrometry (EDS), which allows rapid elemental identification, or by wavelength dispersive spectrometry (WDS), which provides higher spectral resolution and is preferred for precise quantitative analyses. By analyzing the emitted and scattered signals in this way, both the textural features and chemical composition of the sample can be systematically examined

Scanning Electron Microscopy (SEM)

Scanning Electron Microscopy was performed using the JEOL IT300 SEM equipped with Oxford EDS at the Physical Research Laboratory (PRL), Ahmedabad (Fig. 2.6).

Fig. 2.6: *Scanning Electron Microscope (SEM) installed at the Physical Research Laboratory(PRL), Ahmedabad, India.*

In this technique, a rastered electron beam is scanned across the sample surface, and the emitted signals are collected to form high-resolution images. SE imaging was used for documenting surface textures, while BSE imaging was extensively applied to distinguish between mineral phases based on compositional contrast. In BSE images, heavier elements appear brighter because of their greater scattering efficiency, whereas lighter elements appear darker. This property enabled the direct visualization of mineralogical differences in grayscale images, facilitating the petrographic examination of Martian meteorites and terrestrial basalts. SEM was also used to perform EDS analyses for quick elemental characterization, as well as to generate elemental maps that highlighted the distribution of major phases before undertaking detailed EPMA work.

2.3.2 Electron Probe Microanalysis (EPMA)

Quantitative chemical analyses were carried out using the JEOL JXA-8530F Field Emission Electron Probe Microanalyzer (FE-EPMA) at PRL, Ahmedabad. In this method, the primary electron beam excites inner-shell electrons in atoms, producing characteristic X-rays that are measured using WDS and EDS detectors. WDS is preferred for quantitative work due to its higher spectral resolution and lower detection limits compared to EDS, which can suffer from overlapping peaks. WDS operates according to Bragg's law,

$$n\lambda = 2d \sin\theta$$

where crystals diffract X-rays of specific wavelengths onto detectors.

The JEOL 8530F EPMA at PRL (Fig. 2.7) is equipped with five multi-crystal WDS spectrometers containing pseudo-crystals such as LDE1, thallium acid phthalate (TAP), pentaerythritol (PET), and lithium fluoride (LIF), along with their large-crystal counterparts (TAPL, PETL, LIFL). These crystals are chosen depending on the elements to be analyzed; for example, TAP is commonly used for Si, Al, and Mg, PET for Ca, Ti, and K, and LIF for Fe, Mn, Cr, and Ni. Because a single crystal cannot cover the full range of X-ray wavelengths, multiple crystals must be employed sequentially to analyze different elements effectively.

Fig. 2.7: *Image of the Field Emission Electron Probe Microanalyzer (FE-EPMA) facility at the Physical Research Laboratory (PRL), Ahmedabad, India*

Calibration was performed routinely against a set of natural and synthetic standards. Reference materials such as diopside (Si, Ca), olivine (Mg), plagioclase (Al), rutile (Ti), sanidine (K), magnetite (Fe), rhodonite (Mn), Cr-oxide (Cr), jadeite (Na), and Ni-metal (Ni) were used to convert X-ray counts into accurate element concentrations. Standard measurements were repeated periodically during analytical sessions to monitor instrumental stability and ensure precision.

In this study, EPMA was employed to determine the major and minor element compositions of mineral phases in Martian meteorites and terrestrial basalt samples. In addition to spot analyses, line profiles were acquired across grains to study compositional zoning, while X-ray maps were generated to visualize the distribution of multiple elements over selected regions of interest

2.4 Raman Spectroscopy

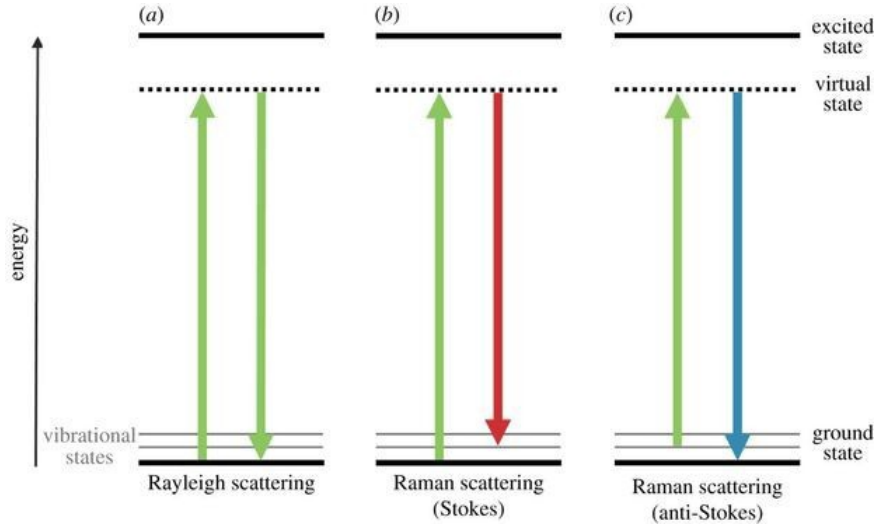

Fig. 2.8: *Schematic illustration of elastic (Rayleigh) and inelastic (Raman) scattering shownon an energy level diagram. Raman scattering arises from the interaction of incident photons with molecular vibrational modes, resulting in either a gain of energy (anti-Stokes) or a loss ofenergy (Stokes) relative to the vibrational state (Moura et al., 2016).*

Raman spectroscopy is a vibrational technique that relies on the Raman Effect, where a small portion of light scattered from a sample differs in frequency from the incident monochromatic radiation. In practice, a focused laser beam is directed onto the sample, and most of the scattered light retains the same frequency as the incident beam, a process known as Rayleigh scattering (Fig. 2.8). However, a minor fraction undergoes an exchange of energy with the vibrating molecules of the sample, producing inelastic scattering that gives rise to Raman spectra. These energy differences, referred to as Raman shifts, can appear as either Stokes or anti-Stokes lines depending on whether the scattered photons loss or gain energy relative to the incident photons (Fig. 2.8).

The spectral features that result provide a distinct fingerprint of the mineral, offering insights into its molecular vibrations, crystallinity, and structural characteristics, while also allowing phases with similar chemical compositions to be distinguished (Ember et al., 2017). Since the method is non-destructive and requires minimal sample preparation, it is particularly advantageous in meteorite studies, where the preservation of rare and fragile material is essential.

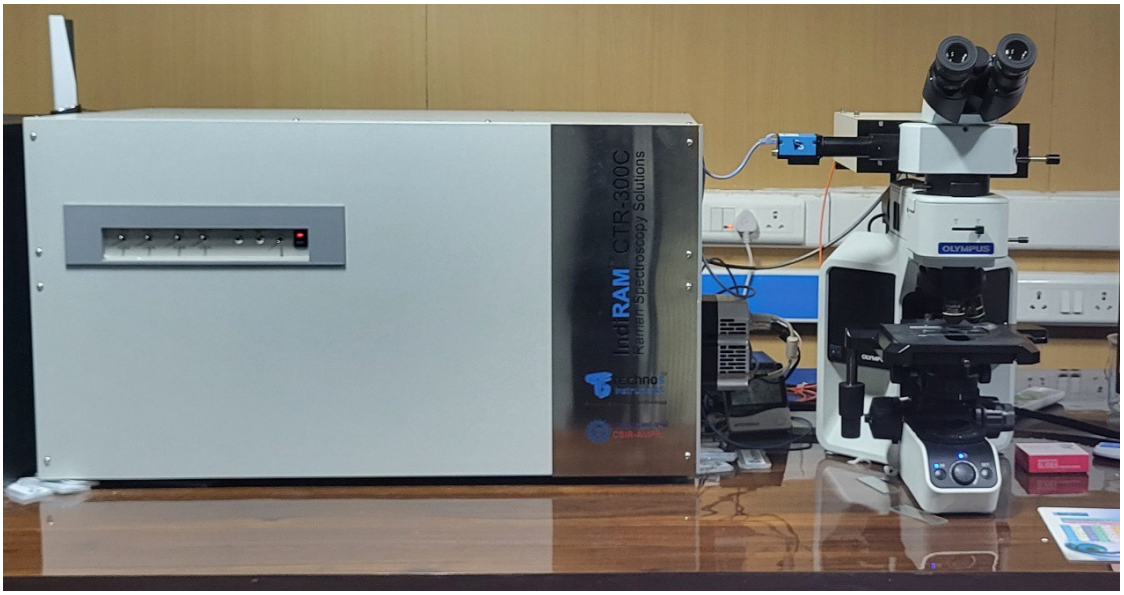

Fig. 2.9: *IndiRam CTR 300C micro-Raman spectrometer coupled with an Olympus BXM-53Mmicroscope at the Physical Research Laboratory (PRL), Ahmedabad, India*

Raman spectroscopic analyses were performed at the Physical Research Laboratory (PRL), India, using an IndiRam CTR 300C confocal micro-Raman spectrometer coupled with an Olympus BXM-53 M microscope (Fig. 2.9). Excitation was provided by a 532 nm diode green laser (class 1), and spectra were collected over polished sections within the range of 150–1200 cm^{-1}. Instrument calibration was carried out using a reference silicon wafer with a characteristic Raman shift at 520.7 ± 0.5 cm^{-1}. A diffraction grating with 2400 lines/mm was employed, yielding a spectral resolution of approximately 2 cm^{-1}. Signal detection was facilitated by a back-illuminated CCD detector cooled to −65 °C through a Peltier module to minimize noise.

The incident laser power on the sample surface was carefully regulated to avoid heating or degradation of the sample. For primary phases such as olivine, the laser was operated at full intensity (25 mW), ensuring well-defined spectra with adequate signal strength. In contrast, secondary alteration products were analyzed at a reduced power setting of 25% of 25 mW to minimize potential thermal damage and suppress fluorescence. Each measurement was conducted with a fixed spot size of 2 μm, an exposure time of 5 seconds, and averaged over 10 successive acquisitions to improve the signal-to-noise ratio.

2.5 X-ray Fluorescence (XRF)

X-ray fluorescence spectrometry (XRF) is a widely applied technique for determining the chemical composition of materials that may occur in different forms, such as solids, powders, liquids, or filtered residues. It is an established atomic method used for both qualitative and quantitative analyses, and it is suitable for samples with diverse matrices and a wide range of elements, extending from boron (B) to uranium (U) in the periodic table (Margui et al., 2022). A major advantage of XRF lies in its ability to provide rapid, non-destructive, and multi-elemental results, making it particularly useful in geochemical investigations.

The method works on the principle that when a material is excited by an external X-ray source, it emits secondary or 'fluorescent' X-rays. These emissions are unique to each element and allow its identification and quantification. Two types of detection systems are commonly used to measure these X-rays: wavelength-dispersive XRF (WDXRF) and energy-dispersive XRF (EDXRF). In WDXRF, the emitted X-rays are passed through diffracting crystals or multilayer optics that select a narrow range of wavelengths corresponding to the characteristic emission of a particular element. This approach provides high elemental specificity and excellent sensitivity because of its

high signal-to-background ratio. EDXRF, on the other hand, detects a wide range of elements simultaneously. In this system, resolution depends on the detector's ability to separate X-rays of different energies and on its counting efficiency. While WDXRF is preferred for precise measurements of specific elements, EDXRF is advantageous when rapid multi-element detection is required.

The XRF technique differs from electron-based microanalysis, such as that performed in scanning electron microscopy (SEM). In XRF, the excitation is provided by X-ray tubes, while in SEM, excitation is caused by electrons. The difference in excitation sources also affects the penetration depth within the sample. X-ray tubes typically penetrate microns to millimeters into the material, providing information about bulk composition, whereas electron excitation in SEM is limited to a few microns, making SEM more surface-sensitive (Settle et al., 1997). This distinction makes XRF especially well-suited for determining whole-rock or bulk sample compositions.

For this study, major element concentrations were measured using a Philips AXIOS automated X-ray spectrometer equipped with a rhodium (Rh) X-ray tube. The instrument was operated at 30 kV and 120 mA, with a maximum power of 4 kW, and is housed at the Physical Research Laboratory (PRL), Ahmedabad (Fig. 2.10). The analyses were carried out on pressed pellets prepared from finely powdered samples. Calibration of the instrument was achieved using a set of internationally recognized USGS rock standards, including BCR-2, and BHVO-2. Care was taken to select appropriate standards that matched the matrix of the samples being analyzed, thereby minimizing errors due to interferences and absorption effects. For example, igneous rocks were calibrated against igneous standards to ensure consistency and reliability of the results. The accuracy and precision of the analyses were carefully monitored.

At the 2σ level, the precision for major oxides was found to be better than 5%, based onrepeated analyses of both samples and standards (Table 2.2).

Table 2.2: Major oxide compositions (wt.%) of BHVO-2 and BCR-2 reference standards analyzed as unknowns by XRF, compared with recommended standard values.

Sample name	**BHVO-2 (std)**	**BHVO-2 (Measured)**	**BCR-2 (std)**	**BCR-2 (Measured)**
SiO_2	49.90	49.48	54.10	53.43
TiO_2	2.73	2.60	2.26	2.27
Al_2O_3	13.50	12.53	13.50	12.82
$Fe_2O_3{}^T$	12.30	12.14	13.80	13.91
MnO	0.17	0.16	0.19	0.20
MgO	7.23	6.46	3.59	3.53
CaO	11.40	11.26	7.12	6.81
Na_2O	2.22	1.98	3.16	2.84
K_2O	0.52	0.56	1.78	1.97
P_2O_5	0.27	0.21	0.35	0.38
Total	**100.24**	**97.38**	**99.85**	**98.17**

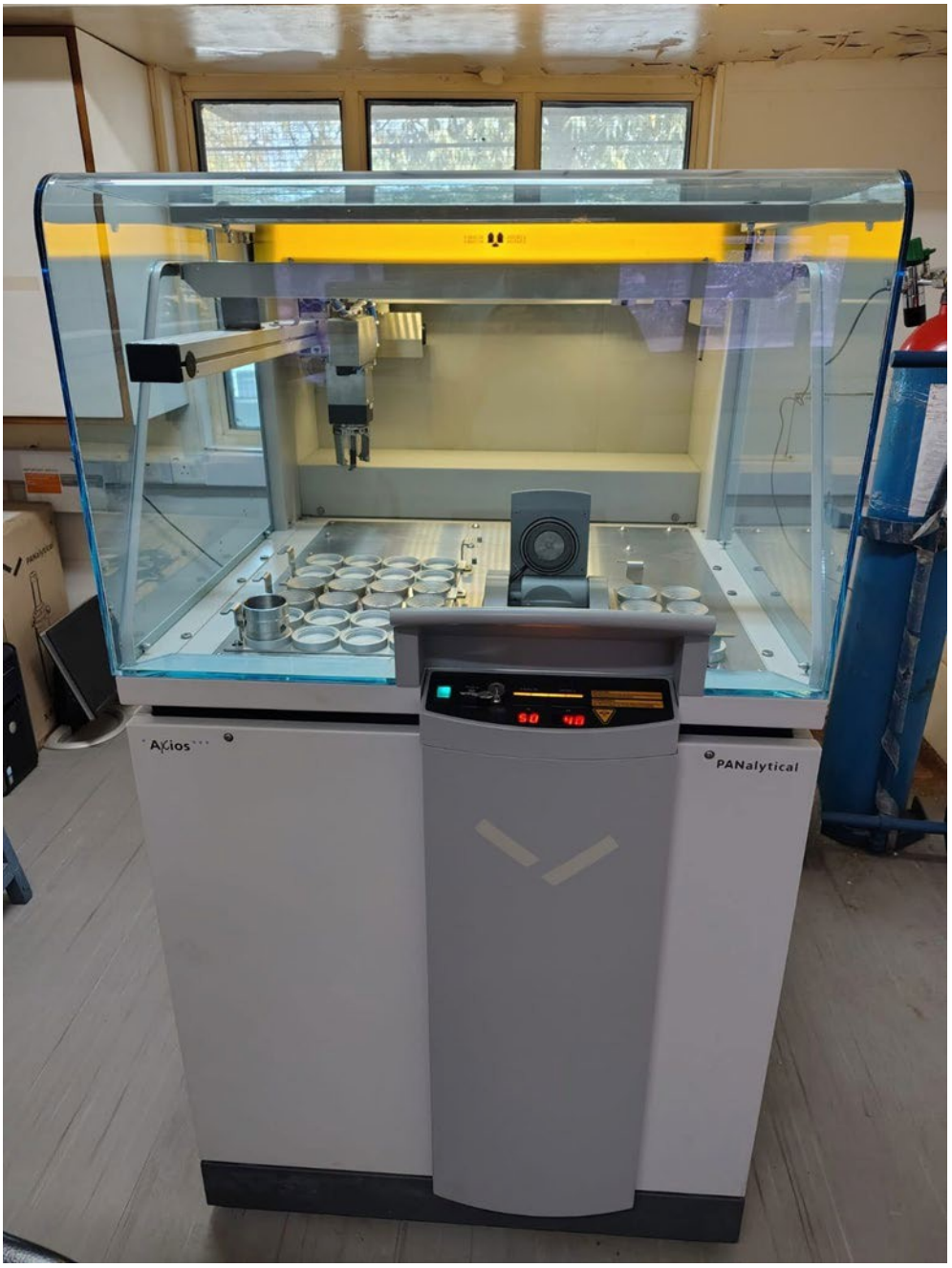

Fig. 2.10: Image of the Philips AXIOS X-ray fluorescence (XRF) spectrometer with a rhodium (Rh)X-ray tube, housed at the Physical Research Laboratory (PRL), Ahmedabad

.Sample preparation involved mixing 2.0 g of finely powdered sample with 0.5 g of waxbinder to achieve a homogeneous mixture. The mixture was ground thoroughly in an agate mortar and then placed in 37 mm standard aluminum cups. Using a hydraulic press, a pressure of 150 kN was applied for about one minute to form solid pellets. The pressure was released gradually to prevent cracking, and the intact pellets were recovered for analysis. This procedure yielded pellets with consistent density and surface smoothness, both of which are crucial for accurate XRF measurements.

2.6 Geochemist Workbench (GWB)

The modeling framework of Geochemist's Workbench (GWB) is grounded in classical chemical thermodynamics, where the stability of chemical species is determined by minimizing Gibbs free energy while satisfying mass conservation. Calculations are supported by comprehensive thermodynamic datasets, such as the V8 R6+ database maintained by the Lawrence Livermore National Laboratory, which provides standard Gibbs free energies and equilibrium constants for minerals, aqueous complexes, and gases across a wide range of pressures and temperatures. This well-established dataset ensures the reliability of input parameters used in the present work (Bethke, 2007). These values allow the law of mass action to be applied, where each equilibrium constant (K_i) is related to the activities of the participating species through the general relation

$$KK_{ii} = \prod_{jj} jj^{vv_{iiii}}$$

where a are activities of species (normalized concentrations) and $\nu_{(ij)}$ are stoichiometric coefficients. At equilibrium, the activities of all species simultaneously satisfy these mass-action equations, driving the system toward chemical stability.

Mineral stability is expressed through the saturation index (SI), which compares the ion activity product (Q) with the equilibrium constant (K)

$$SSSS = llllgg_{10}\left(\frac{QQ}{KK}\right)$$

$$-\log_{10}(\gamma\gamma_{ii}) = \frac{AA\, zz^2 \sqrt{(SS)}}{1 + BB_{ii}\sqrt{(SS)}} + (bb\ SS)$$

An SI value of zero indicates equilibrium between mineral and fluid, SI > 0 reflects supersaturation and a tendency for precipitation, while SI < 0 implies undersaturation

and a tendency for dissolution. To calculate activities, GWB applies activity coefficient models, most commonly the extended Debye–Hückel (B-dot) equation, which provides reliable results for solutions of moderate ionic strength.

The program solves mass-balance equations, which conserve the total amount of each element, together with mass-action equations, which enforce equilibrium relationships. This combined solution ensures a self-consistent distribution of species, though in some cases multiple mathematical solutions are possible, requiring expert evaluation to identify geochemically meaningful outcomes. Reactions between fluids and rocks are examined using the React module through a process called reaction-path modeling. In this approach, water is progressively equilibrated with a chosen set of minerals, and at each step, the fluid composition is recalculated and the stability of secondary minerals reassessed. Equilibrium models assume complete reaction progress, whereas kinetic models use rate laws derived from transition-state theory to simulate time-dependent dissolution and precipitation. These kinetic rate laws depend on variables such as saturation state (Q/K), pH, and temperature, and often draw on experimental datasets (Palandri & Kharaka, 2004).

Although GWB assumes local equilibrium and is limited by the completeness of its databases, it remains a powerful modeling tool. In this study, it has been applied to reconstruct aqueous alteration conditions on Mars. By combining the bulk chemistry of Martian meteorites such as nakhlites with terrestrial analogues like Deccan basalts, the software can simulate water–rock interactions under Mars-like conditions of

temperature and water-to-rock ratios. Such models provide important insights into secondary mineral formation pathways and help to constrain the paleoclimatic conditions that shaped the planet's geological history.

In this chapter, the analytical approach adopted for this study has been described in detail. Techniques ranging from optical petrography and electron microscopy to mineral chemistry, Raman spectroscopy, and X-ray elemental mapping were outlined to explain how textural and chemical information was obtained from both Martian and terrestrial samples. In addition to laboratory-based analyses, geochemical modelling using Geochemist's Workbench (GWB) was introduced to simulate water–rock interaction under controlled conditions. This modelling framework enables the examination of the effects of temperature, fluid composition, and water–rock ratio in a systematic manner. The next chapter focuses on the nakhlite Martian meteorites, presenting detailed petrographic, mineralogical, and geochemical results. These observations provide the first direct constraints on the nature and extent of aqueous alteration in the Martian crust, forming the basis for later comparison with terrestrial analogue systems and geochemical simulations.

Chapter 3: Petrography & Mineral Chemistry of Nakhlites

This chapter focuses on understanding aqueous alteration on Mars through a detailed study of nakhlite meteorites. Nakhlites are particularly important because they preserve clear evidence of interaction between Martian basaltic rocks and liquid water, while still retaining their original igneous textures. By studying these meteorites at the microscopic and chemical scale, it becomes possible to directly examine how water interacted with the Martian crust during the Amazonian period, when liquid water was limited and short-lived. Four nakhlite meteorites—Yam-593, MIL 03346, Nakhla, and Lafayette—were selected for this study because they represent different positions within the nakhlite sequence and show varying degrees of alteration. Together, they provide a useful framework to investigate how alteration intensity, chemistry, and style change across the nakhlite suite. This chapter combines petrography, Raman spectroscopy, mineral chemistry, X-ray elemental mapping, and geochemical indices to characterize both the primary minerals and the secondary alteration products. Special emphasis is placed on olivine, as alteration is consistently localized within fractures cutting these grains. The chapter documents how these fracture-hosted alteration products vary in texture, chemistry, and homogeneity among the nakhlites. Lafayette, in particular, shows additional alteration features not observed in the other meteorites, including carbonate formation within the mesostasis, pointing toward more complex fluid–rock interactions.

3.1 Introduction

Evidence for water–rock interaction on Mars has been built over time from lander measurements, orbital spectroscopy, and rover analyses, which collectively showed widespread phyllosilicates, sulfates, and other alteration products formed at the surface and near surface (Bandfield, 2002; Bibring et al., 2005; Poulet et al., 2005; Klingelhöfer et al., 2004; Squyres et al., 2004; Ming et al., 2006; Murchie et al., 2009). These minerals record a transition from wetter Noachian settings to increasingly evaporitic Hesperian conditions, with younger Amazonian deposits indicating that liquid water was locally available even during an overall cold, arid climate (Ehlmann et al., 2008, 2009; McEwen et al., 2011). Meteorites that arrived from Mars provide a way to examine such alteration in detail, because some secondary phases predate Earth's arrival and can be studied at microscopic scales (Gooding et al., 1991; Treiman et al., 1993).

Among the SNC (Shergottites-Nakhlites-Chassignites) group of Martian meteorites, the Nakhlites exhibit a significant amount of aqueous alteration, making them an excellent source for understanding the nature of water-rock interactions on Mars. These augite-rich cumulates crystallized ~1.42–1.32 Ga and were ejected ~10.7 Ma ago, yet many contain secondary phases that cut primary igneous textures and fusion crusts, showing that fluid–rock interaction occurred on Mars (Cohen et al., 2017; Treiman, 2005; Gooding et al., 1991; Treiman et al., 1993). A common assemblage is referred to as "iddingsite," which includes Fe/Mg-rich clays and associated oxides, carbonates, or sulfates in veins and patches within olivine, pyroxene, and mesostasis (Bridges & Grady, 2000; Bridges et al., 2001; Changela & Bridges, 2010; Hicks et al., 2014; Tomkinson et al., 2013; Lee et al., 2015a; Piercy et al., 2022). Chronology and fluid fingerprints have been used to test a Martian origin for these phases. Rb–Sr leachates from Lafayette and Yam 000593 yielded ages near 650–675 Ma, implying

late Amazonian alteration, although the two-point nature of the isochrons and potential fractionation during leaching limit their robustness (Shih et al., 1998; Misawa et al., 2005; Borg & Drake, 2005). However, a recent $^{40}Ar/^{39}Ar$ radiometric dating of the altered products within the Lafayette meteorite suggested that the alteration might have occurred at a relatively early age of 742 ± 15 Ma (Trembley et al., 2024).

Independent constraints come from D/H measurements that distinguish Martian fluids from terrestrial waters and have confirmed Martian signatures in several iddingsite-like veins (Leshin et al., 1996). Additionally, comparative studies of nakhlites with different weathering histories further support this approach; for example, Nakhla provides a minimally contaminated end-member, whereas Antarctic finds such as MIL 03346 and MIL 090030 retain Martian-style alteration despite variable terrestrial exposure (Anand et al., 2005; Stopar et al., 2005; Hallis & Taylor, 2011; Changela & Bridges, 2010).

An active debate concerns whether the aqueous alteration in the nakhlites formed by low-temperature aqueous processes or whether some formed by high-temperature, tardi-magmatic (deuteric) alteration during cooling of the host magma (Viennet, 2020; 2021). Classical terrestrial studies and recent Martian work have shown that both pathways can yield similar Fe/Mg-rich phyllosilicates, making discrimination challenging without sub-micrometre analyses (Baker& Haggerty, 1967; Eggleton, 1984;). Reports of clay minerals formed in late-magmatic contexts and alteration of melt inclusions in several Martian samples support the plausibility of deuteric processes, while other nakhlites preserve clear aqueous textures and isotopic signals (McCubbin et al., 2009; Viennet et al., 2020, 2021; Kuebler, 2013; Kizovski et al., 2020). Variability among nakhlites, such as the abundant but carbonate-poor veins and distinct D/H values in NWA 817, further indicates that alteration conditions were not

uniform across flows or stratigraphic positions (Gillet et al., 2002; Lee et al., 2018; Jambon et al., 2016; Udry & Day, 2018; Ruggiu et al., 2025).

In this study, four nakhlite meteorites —polished thin-section and thick-section samples of the nakhlite meteorites Miller Range 03346 (MIL-3346), Yamato 000593 (Yam-593), Nakhla (Nakh), and Lafayette (Laf) were examined to investigate the alteration products and understand the water-rock interaction that occurred on the Martian crust (Fig. 3.1). These samples are considered to have been emplaced at varying stratigraphic depths within the nakhlite pile (Mikouchi et al., 2012; Changela & Bridges, 2010). These meteorites from different emplacement depths thus provide a comprehensive framework to examine the extent and progression of aqueous alteration across the nakhlite depth sequence.

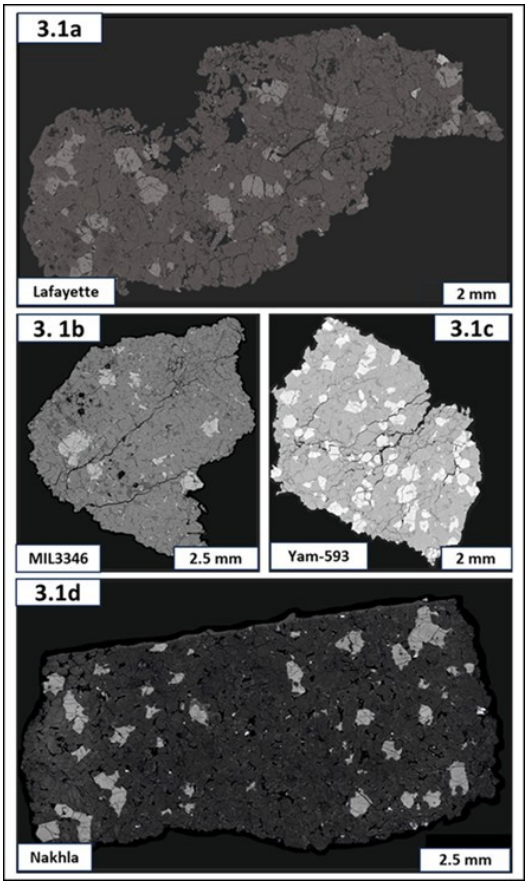

Fig. 3.1: Backscattered Electron (BSE) mosaic images of nakhlite meteorites: (a) Lafayette, (b) MIL 03346, (c) Yam-593, and (d) Nakhla. The images exhibit the typical cumulate igneous texture of nakhlites, characterized by large prismatic clinopyroxene (augite) crystals and some olivine cumulates. In between the cumulates, we find the occurrence of fine-grained mesostasis. (Das et al., under preparation)

3.2 Results

3.2.1. Petrography

The nakhlite meteorites examined in this study—MIL-3346, Nakhla, Yam-593, and Lafayette—are all clinopyroxene-dominated cumulate rocks that crystallized from basaltic magmas on Mars. Although they share a broadly similar igneous framework, careful petrographic examination reveals important differences in modal mineralogy, olivine composition, fracture development, and the nature of fracture-hosted alteration products. In all samples, secondary alteration is strictly confined to olivine grains and does not affect the surrounding clinopyroxene or mesostasis. This section describes the petrography of each nakhlite individually, followed by a detailed comparison of olivine forsterite content and alteration characteristics.

3.2.1.1. Yam-593

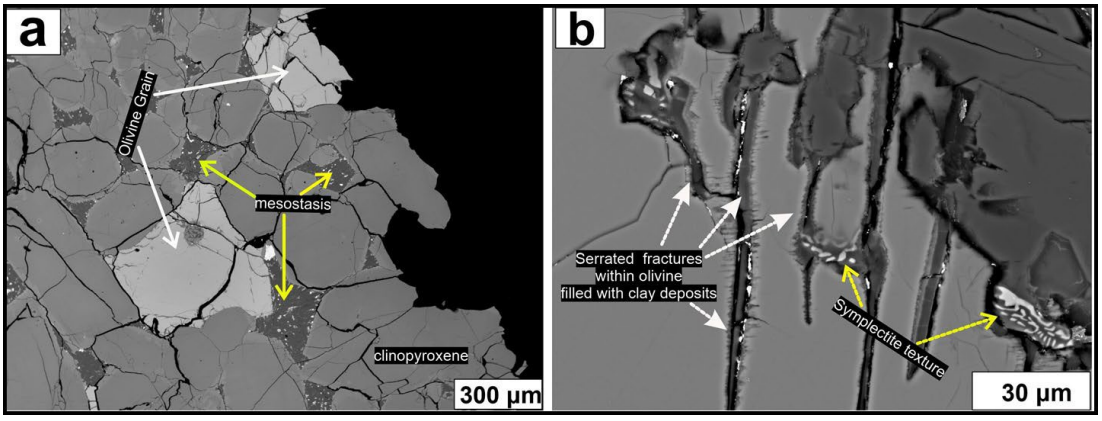

Fig. 3.2: Backscattered electron (BSE) images of the Yam-593 nakhlite showing fractured Fe-rich olivine grains enclosed within a clinopyroxene-dominated cumulate framework. (a) Overview image showing an olivine grain enclosed within surrounding clinopyroxene. The olivine grain is fractured. Mesostasis is also observed in the surrounding regions. (b) High-magnification view of the fractured olivine grain showing serrated fractures filled with clay-rich alteration products

.The BSE image of Yam-593 exhibits a fine-to medium-grained nakhlite characterized by a well-developed cumulate texture dominated by clinopyroxene, with few olivine and interstitial mesostasis (Fig. 3.2a–b). Modal mineralogical analysis shows that augite is the most abundant phase, comprising approximately 73 vol.%, followed by

olivine (~20 vol.%) and fine-grained mesostasis (~7 vol.%), which is made up of mostly plagioclase. Olivine occurs as subhedral to anhedral grains enclosed within a framework of augite crystals, consistent with the classic nakhlitic cumulate texture.. These olivines are pervasively fractured, displaying irregular, serrated fracturemargins that cut across the grains (Fig. 3.2a). At higher magnification, these fractures are seen to be partially to completely filled with fine-grained secondary material interpreted as clay-rich alteration products (Fig. 3.2b). The alteration is strictly confinedto the fracture networks, while the interiors of the olivine grains remain largely intact. The surrounding clinopyroxene grains appear comparatively fresh, with sharp grain boundaries and minimal evidence of alteration. The mesostasis in Yam-593 occurs as interstitial patches between clinopyroxene and olivine grains, which are rich in plagioclase. It shows a fine-grained, heterogeneous texture but does not display pervasive alteration.

3.2.1.2. MIL 03346

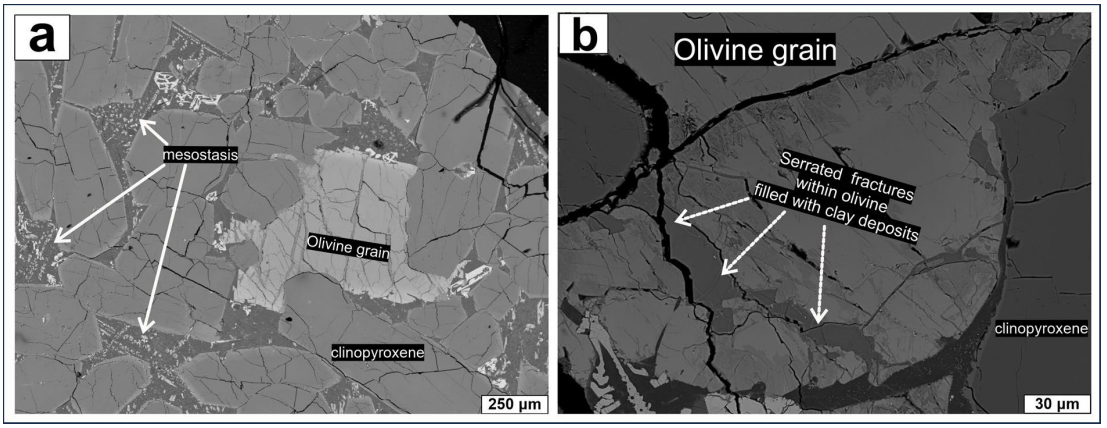

Fig. 3.3: Backscattered electron (BSE) images of MIL 03346 illustrating its cumulate texture with abundant clinopyroxene, minor olivine, and relatively abundant interstitial mesostasis. (a) Overview image showing the cumulate texture dominated by clinopyroxene crystals, with minor olivine grains and interstitial mesostasis distributed between the mineral phases. (b) High-magnification image of an olivine grain showing serrated fractures filled with clay-rich alteration products. The surrounding clinopyroxene remains largely unaltered, indicating that alteration is localized within the olivine.

MIL 03346 is a relatively coarse-grained nakhlite with a cumulate texture similar to that of Yam-593, but with subtle differences in modal mineralogy and textural organization (Fig. 3 .3a–b). Augite is the dominant phase, comprising approximately

78% of the volume, while olivine accounts for about 5.5% of the volume. Notably, the mesostasis, which is majorly composed of plagioclase, constitutes roughly 15.8 vol.%, representing the highest mesostasis abundance among all the nakhlite meteorites investigated in this study. Minor titanomagnetite (~0.7 vol.%) is present as small, bright grains in backscattered electron images. Olivine grains in MIL 03346 are fewer in number and generally smaller than those observed in Yam-593. Despite their lower abundance, olivine grains exhibit well-developed fracture networks similar to those seen in other nakhlites (Fig. 3.3b). The fractures exhibit serrated margins and are filled with altered products (clay minerals). The alteration in MIL 03346 is again highly localized, restricted to fractureswithin olivine grains. The tonal contrast of the fracture fillings appears relatively uniform, suggesting a compositionally homogeneous alteration product. The mesostasisis more abundant in this meteorite compared to Yam-593 and occurs as irregular interstitial domains, but it does not show extensive secondary mineralization. Clinopyroxene grains remain largely unaltered, preserving primary igneous textures

3.2.1.3. Nakhla

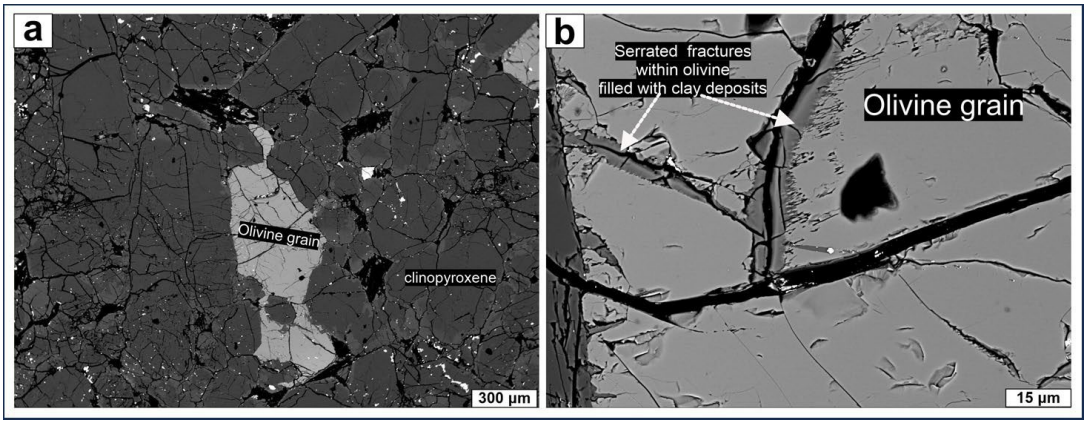

Fig 3.4: *Backscattered electron (BSE) images illustrating the petrographic characteristics and alteration features of the Nakhla meteorite. (a) Overview image showing the cumulate texture dominated by clinopyroxene with minor olivine grains. The olivine occurs as distinct grains within the clinopyroxene framework, and overall alteration appears limited in extent. (b) High-magnification image of an olivine grain showing serrated fractures filled with clay-rich alteration products. The alteration is confined within fractures, while the interior of the olivine grain remains largely unaltered.*

Nakhla displays a classic nakhlite texture with well-developed cumulate features and

relatively coarse grain sizes (Fig. 3.4a–b). Modal mineralogical data indicate that augite is the dominant phase (~79.5 vol.%), followed by mesostasis (~11.5 vol.%) and olivine (~8.8 vol.%). Minor titanomagnetite (~0.2 vol.%) is present. Olivine grains in Nakhla are Fe-rich, with forsterite contents centred around Fo_{29}. Olivine grains from Nakhla, like their counterparts in previous studies, commonly exhibit extensive fracturing, with irregular and serrated fractures (Fig. 3.4b). As observed in the other nakhlites, these fractures are filled with fine-grained secondary material interpreted as clay-rich alteration products. The alteration is sharply confined to fracture zones, with no evidence for pervasive replacement of the olivine grain interiors. The mesostasis in Nakhla is moderately abundant and occurs as interstitial material between augite grains. While it shows textural heterogeneity, it does not display prominent carbonate mineralization. The overall petrographic appearance of Nakhla suggests a single-stage, localized alteration event affecting olivine along fracture pathways.

3.2.1.4. Lafayette

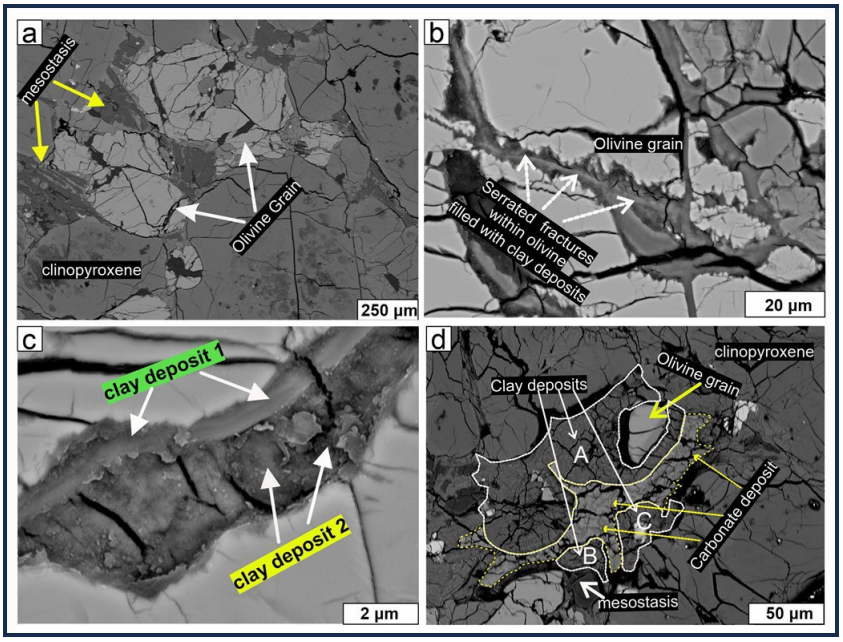

Fig. 3.5: *(a) Backscattered electron (BSE) images of the Lafayette nakhlite showing fractured olivine grains enclosed within clinopyroxene. Alteration products are mainly present along the fractures within olivine, while surrounding minerals remain largely unaltered. with (b) High-magnification view of an olivine grain showing serrated fractures filled with clay- rich alteration products. The alteration is restricted to fracture zones. (c)tonal variation within the fracture-hosted alteration products, indicating the presence of different clay-rich phases within the same fracture.*

(d)Additional alteration features are observed within the mesostasis region, including carbonate domains surrounded by phyllosilicate material alteration features are observed within the mesostasis region, including carbonate domains surrounded by phyllosilicate material

Backscattered electron (BSE) images of the Lafayette meteorite reveal large, fractured olivine grains embedded within a fine-grained groundmass (Fig. 3.5a). The olivine grains are subhedral to anhedral and display an extensive network of fractures that vary in width and continuity. Modal mineralogy shows that augite remains the dominant phase (~74.7 vol.%), with olivine (~10.5 vol.%), mesostasis (~14.5 vol.%), and minor titanomagnetite (~0.2 vol.%). Olivine grains in Lafayette have forsterite contents of around $Fo_{31–32}$, similar to those of Yam-593 but lower than those of MIL 03346. At higher magnification, the fractures are observed to be filled with fine-grained secondary material that appears darker than the surrounding olivine in BSE contrast (Fig. 3.5b–c). The infilling material within individual fractures shows clear tonal variability, with alternating lighter and darker domains occurring along the same fracture plane. In some cases, this variability appears layered, while in others it is patchy, suggesting internal heterogeneity within the fracture-fill material. The fracture walls themselves are uneven, and the altered material conforms closely to the serrated geometry of the fractures (Fig. 3.5c). Bright and dark regions occur within the same fracture, suggesting compositional heterogeneity and possibly multiple generations of mineral precipitation. An additional and unique feature of Lafayette is the presence of carbonate deposit as an additional alteration product within the mesostasis region (Fig. 3.5d). Here, the carbonate-rich domains are observed to be surrounded by phyllosilicate-rich layers that have a relatively uniform texture. This association of carbonate and phyllosilicate phases might be indicative of a more complex alteration environment compared to the other nakhlites.

3.2.2. Raman Spectroscopy

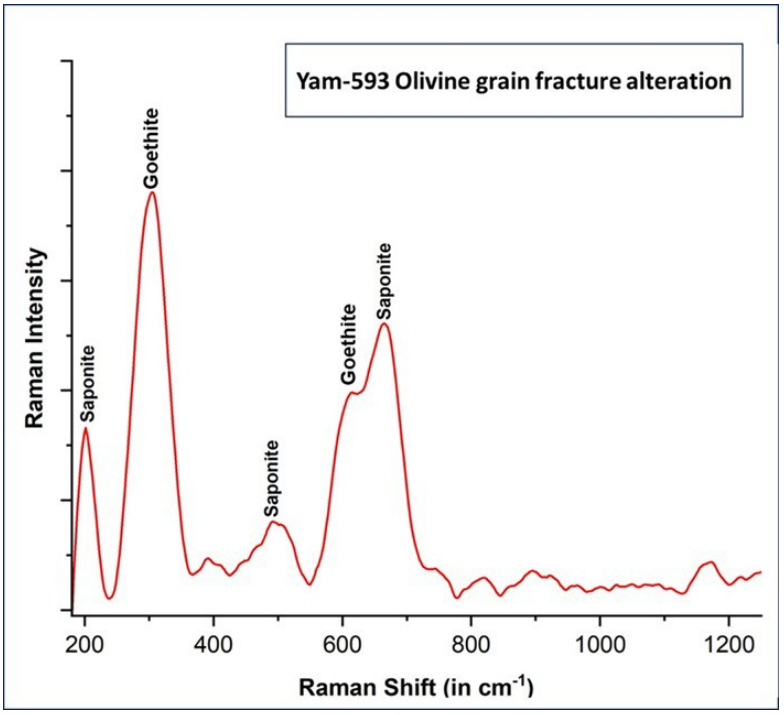

Fig. 3.6: Representative Raman spectra obtained from fracture-hosted alteration products within olivine grains of Yam-593, showing diagnostic peaks corresponding to smectite clayminerals and Fe-oxide phases

.Raman spectroscopic analyses were carried out on the Martian nakhlite meteorites to identify both the primary minerals and the alteration products present within them (Fig. 3.6). In the nakhlite Yam-593, the large cumulate olivine grains are clearly fractured, and these fractures contain visible alteration material. Raman spectra collected from these altered zones exhibit distinct peaks at approximately 198, 462, and 687 cm^{-1}, which are characteristic of saponite, a type of smectite clay mineral (Kloprogge & Ponce, 2021). Along with the smectite peaks, additional Raman bands are observed near 298 and 610 cm^{-1}. These peaks correspond to goethite and indicate the presence of iron-oxide phases within the same fracture-hosted alteration material (Fuentes-Carreón et al., 2022). The association of saponite and iron oxides within the olivine fractures suggests that the secondary material is a mixed assemblage rather than a single mineral phase. Such a combination of smectite clays and Fe-oxides is commonly referred to as iddingsite (Smith et al., 1987) and is consistent with low-temperature aqueous alteration of olivine.

Raman analyses were also attempted on the other nakhlite meteorites included in this study. In these samples, the primary minerals produced clear and well- defined Raman peaks. However, the altered clay-rich regions showed strong luminescence, which interfered with the Raman signal and prevented reliable identification of clay minerals. Because of this limitation, clear Raman signatures of clay minerals could only be obtained from Yam-593, and therefore only these results are presented in this chapter.

3.2.3. Mineral Chemistry

The mineral chemistry of the nakhlite meteorites—Yam-593, MIL 03346, Nakhla, and Lafayette—was examined in detail to characterize the compositions of olivine and the secondary phases formed during aqueous alteration. Quantitative analyses of olivine grains from all four meteorites are summarized in Table 3.1, while the compositions of alteration products developed within olivine-hosted fractures are compiled in Table 3.2. Across all four meteorites, the primary olivine grains show a high degree of chemical uniformity. Analyses of grain interiors reveal no systematic differences between core and rim compositions, with only very minor point-to-point variations observed (Table 3.1). The total cation sums for all olivine analyses are close to 3.0 atoms per formula unit(a.p.f.u.), confirming the analytical precision and stoichiometric consistency of the dataset

Table 3.1: Representative electron probe micro-analysis (EPMA) data for primary olivine grains from Yam-593, MIL 03346, Nakhla, and Lafayette

	Yam-593 Ol			**MIL-3346 Ol**			**Nakhla Ol**	**Laf Ol**			
	N=19	***N=44***	***N=49***	***N=13***	***N=12***	***N=21***	***N=26***	***N=3***	***N=7***	***N=9***	***N=10***
SiO_2	32.61	32.54	32.56	33.73	34.40	33.85	32.33	32.88	32.78	32.79	32.94
TiO_2	0.02	0.00	0.00	0.01	0.02	0.02	0.01	0.00	0.00	0.00	0.00
Al_2O_3	0.01	0.01	0.01	0.02	0.02	0.02	0.01	0.01	0.01	0.01	0.02
Cr_2O_3	0.01	0.01	0.01	0.01	0.02	0.01	0.01	0.01	0.02	0.00	0.01
FeO^T	54.11	52.82	52.83	46.38	45.60	47.03	52.97	53.49	53.37	53.64	53.40
MnO	1.09	0.90	0.91	0.90	0.90	0.95	0.99	0.00	0.02	0.02	0.01
MgO	12.80	13.11	13.08	18.00	18.97	17.63	12.43	13.70	14.03	13.82	14.19
CaO	0.32	0.38	0.37	0.53	0.53	0.50	0.18	0.00	0.00	0.00	0.00
Na_2O	0.01	0.01	0.01	0.01	0.01	0.01	0.03	0.00	0.01	0.03	0.02
K_2O	0.02	0.02	0.02	0.00	0.00	0.00	0.02	0.00	0.00	0.00	0.00
NiO	0.01	0.01	0.01	0.02	0.04	0.03	0.02	0.00	0.00	0.01	0.00
Total	**101.00**	**99.80**	**99.80**	**99.63**	**100.50**	**100.05**	**98.99**	**100.10**	**100.24**	**100.31**	**100.60**
Fo Content	**0.30**	**0.31**	**0.31**	**0.41**	**0.43**	**0.40**	**0.29**	**0.31**	**0.32**	**0.31**	**0.32**
Basis of Oxygen	**4.00**	**4.00**	**4.00**	**4.00**	**4.00**	**4.00**	**4.00**	**4.00**	**4.00**	**4.00**	**4.00**
Si	1.00	1.00	1.00	1.00	1.01	1.00	1.01	1.00	1.00	1.00	1.00
Ti	0.00	0.00	0.00	0.00	0.00	0.00	0.00	0.00	0.00	0.00	0.00
Al	0.00	0.00	0.00	0.00	0.00	0.00	0.00	0.00	0.00	0.00	0.00
Cr	0.00	0.00	0.00	0.00	0.00	0.00	0.00	0.00	0.00	0.00	0.00
Fe	1.38	1.36	1.36	1.15	1.12	1.17	1.38	1.37	1.36	1.37	1.36
Mn	0.03	0.02	0.02	0.02	0.02	0.02	0.03	0.00	0.00	0.00	0.00
Mg	0.58	0.60	0.60	0.80	0.83	0.78	0.58	0.62	0.64	0.63	0.64
Ca	0.01	0.01	0.01	0.02	0.02	0.02	0.01	0.00	0.00	0.00	0.00
Na	0.00	0.00	0.00	0.00	0.00	0.00	0.00	0.00	0.00	0.00	0.00
K	0.00	0.00	0.00	0.00	0.00	0.00	0.00	0.00	0.00	0.00	0.00
Ni	0.00	0.00	0.00	0.00	0.00	0.00	0.00	0.00	0.00	0.00	0.00
Total Cation No	**3.00**	**3.00**	**3.00**	**3.00**	**2.99**	**2.99**	**3.00**	**3.00**	**3.00**	**3.00**	**3.00**

Table 3.2: Chemical compositions of alteration products developed within fractures of olivine grains in Yam-593, MIL 03346, Nakhla, and Lafayette

	Laf Ol grain Alt								**Nakhla OI grain Alt**						**MIL-3346 Ol grain Alt**										**Yam-593 Ol grain Alt**			
	N=10	***N=4***	***N=4***	***N=6***	***N=3***	***N=3***	***N=3***	***N=42***	***N=31***	***N=13***	***N=40***	***N=47***	***N=30***	***N=65***	***N=27***	***N=4***	***N=9***	***N=3***	***N=26***	***N=17***	***N=41***	***N=15***	***N=8***	***N=8***	***N=10***	***N=9***	***N=4***	***N=7***
SiO2	41.19	38.85	31.94	32.40	28.68	41.89	47.04	36.71	40.85	38.39	41.94	42.80	43.43	40.24	43.01	41.31	41.04	44.19	44.84	45.48	40.90	44.25	41.27	41.83	34.78	31.66	26.20	28.18
TiO2	0.00	0.00	0.00	0.00	0.00	0.00	0.02	0.04	0.04	0.02	0.02	0.02	0.05	0.02	0.13	0.05	0.04	0.04	0.04	0.05	0.05	0.05	0.05	0.05	0.02	0.06	0.02	0.08
Al2 O3	6.54	4.27	2.35	11.33	11.94	1.21	3.19	8.21	0.41	0.32	0.39	0.30	0.31	0.10	0.60	0.17	0.16	0.13	0.26	0.09	0.26	0.22	0.10	0.35	0.48	0.65	0.40	0.20
Cr2 O3	0.02	0.01	0.01	0.02	0.00	0.01	0.00	0.01	0.01	0.01	0.01	0.01	0.03	0.01	0.02	0.04	0.03	0.03	0.04	0.05	0.02	0.03	0.03	0.02	0.02	0.03	0.04	0.01
FeO T	24.66	28.03	39.73	28.90	33.13	25.42	22.94	25.88	37.09	37.62	39.18	33.38	32.95	37.86	37.39	37.73	36.00	38.72	38.41	40.05	36.95	36.56	38.14	36.91	44.91	43.64	54.59	48.30
Mn O	0.03	0.00	0.00	0.02	0.02	0.02	0.03	0.52	0.49	0.56	0.51	0.54	0.42	0.49	0.62	0.68	0.71	0.76	0.72	0.66	0.69	0.54	0.65	0.61	0.97	0.56	0.58	0.79
MgO	10.11	9.66	7.92	7.62	7.13	7.54	10.95	6.82	7.22	5.01	6.59	5.64	6.41	5.32	2.74	2.13	2.19	2.56	2.60	2.58	2.50	2.89	2.45	2.44	3.89	3.51	1.64	6.57
CaO	1.22	0.09	0.17	0.12	0.15	0.16	0.08	1.09	0.38	0.44	0.10	0.18	2.18	0.38	0.69	0.06	0.05	0.05	0.09	0.18	0.12	0.08	0.17	0.15	0.30	0.40	0.34	0.26
Na2 O	0.18	0.15	0.17	0.17	0.23	0.10	0.01	0.08	0.52	0.48	0.35	0.63	0.42	0.45	0.04	0.07	0.06	0.05	0.08	0.02	0.09	0.03	0.02	0.02	0.32	0.49	0.55	0.17
K2O	0.00	0.00	0.00	0.00	0.00	0.00	0.00	0.18	0.93	0.80	0.66	1.04	0.84	0.89	0.06	0.07	0.24	0.58	0.63	0.20	0.21	0.09	0.05	0.05	0.27	0.27	0.24	0.08
NiO	0.01	0.01	0.00	0.01	0.02	0.03	0.01	0.01	0.01	0.01	0.01	0.01	0.01	0.01	0.01	0.01	0.01	0.00	0.01	0.01	0.01	0.01	0.01	0.01	0.01	0.02	0.02	0.01
SO3	0.00	0.00	0.00	0.01	0.00	0.00	0.02	0.18	0.08	0.09	0.05	0.21	0.12	0.16	0.57	0.00	0.69	0.77	0.84	1.03	1.06	0.71	0.81	0.55	0.95	1.23	1.61	1.39
Total	**83.96**	**81.07**	**82.27**	**80.60**	**81.31**	**76.37**	**84.29**	**79.72**	**88.04**	**83.75**	**89.81**	**84.75**	**87.16**	**85.95**	**85.87**	**82.31**	**81.22**	**87.89**	**88.54**	**90.41**	**82.84**	**85.46**	**83.72**	**82.99**	**86.92**	**82.52**	**86.22**	**86.05**
XMg	**0.42**	**0.41**	**0.25**	**0.32**	**0.29**	**0.35**	**0.39**	**0.31**	**0.25**	**0.19**	**0.23**	**0.23**	**0.25**	**0.20**	**0.12**	**0.09**	**0.10**	**0.11**	**0.11**	**0.10**	**0.11**	**0.12**	**0.10**	**0.11**	**0.13**	**0.12**	**0.05**	**0.19**
Fe/Si	**1.02**	**1.10**	**2.10**	**1.49**	**2.08**	**1.03**	**0.83**	**1.30**	**1.56**	**1.67**	**1.57**	**1.35**	**1.30**	**1.60**	**1.45**	**1.52**	**1.46**	**1.46**	**1.43**	**1.47**	**1.51**	**1.38**	**1.54**	**1.47**	**2.22**	**2.37**	**3.78**	**2.91**

The chemical composition of the alteration products developed within the mesostasis region of the Lafayette meteorite reveals two distinct secondary assemblages: phyllosilicate-rich domains and Fe–Ca carbonate phases (Table 3.3). The relatively uniform chemistry of these clay-rich phases suggests that they formed under chemicallysimilar conditions within the mesostasis, despite their spatial association with other alteration products. In contrast, the carbonate-bearing domains show a markedly different chemical signature (Table 3.3). These phases are strongly enriched in FeO (~49wt%) and CaO (~12 wt%), while being notably depleted in SiO_2 (~3.6 wt%), Al_2O_3 (~0.5 wt%), and MgO (~0.7 wt%). The low analytical totals (~67 wt%) are consistent with carbonate mineralogy.

Across the nakhlite suite, the olivine grains display a relatively restricted compositional range, varying between Fo20 and Fo43, which corresponds to a dominant fayalitic (Fe-rich) character. This compositional range suggests that the olivines within nakhlite meteorites are significantly enriched in iron compared to their terrestrial counterparts. Within this range, the olivine in Yam- 593, Nakhla, and Laf exhibits broadly comparable compositions, averaging between Fo29 and Fo32. The olivine crystals in these meteorites are compositionally homogeneous, showing no evidence of core-to-rim zoning, and maintain uniform Fe/Mg ratios throughout individual grains. In contrast, the olivine in MIL 03346 shows a slightly higher forsteritic component, with compositions ranging from Fo40 to Fo43, representing the most magnesian olivine among the studied samples. Across all four nakhlite meteorites studied, a consistent and striking feature is the highly localized nature of aqueous alteration. In every case, secondary minerals are restricted to fractures within olivine grains, while the surrounding clinopyroxene and most of the mesostasis remain largely unaltered. The interiors of olivine grains are generally preserved, indicating that the duration of fluid– rock interaction was

short and that fluid availability was limited. A key difference among the nakhlites lies in the tonal characteristics of the clay-filled fractures. In Yam- 593, MIL 03346, and Nakhla, the alteration material within olivine fractures appears relatively uniform in BSE contrast, implying compositionally homogeneous clay assemblages formed during a single or closely related alteration event. In contrast, Lafayette exhibits marked tonal variability within the same fracture, indicating compositional heterogeneity and possibly multiple stages of clay deposition. This distinction suggests that Lafayette experienced a more complex alteration history than the other nakhlites, even though the overall alteration remained spatially restricted.

Table 3.3: Electron probe micro-analysis (EPMA) compositions of alteration products within the mesostasis region of the Lafayette meteorite, distinguishing between phyllosilicate-rich domains and Fe–Ca carbonate phases.

	Laf Meso Clay (phyllosilicate)			**Laf Meso Carbonate**	
	N=14	***N=16***	***N=33***		***N=13***
SiO2	37.60	36.29	36.20	**SiO2**	3.63
TiO2	0.00	0.00	0.00	**TiO2**	0.00
Al2O3	8.19	9.12	7.88	**Al2O3**	0.46
Cr2O3	0.01	0.01	0.02	**Cr2O3**	0.02
FeO	28.67	29.92	29.36	**FeO**	49.23
MnO	0.02	0.03	0.02	**MnO**	0.04
MgO	10.14	10.41	9.54	**MgO**	0.66
CaO	0.19	0.15	0.13	**CaO**	12.37
Na2O	0.22	0.19	0.14	**Na2O**	0.35
K2O	0.00	0.00	0.00	**K2O**	0.00
NiO	0.01	0.01	0.01	**NiO**	0.01
Total	**85.06**	**86.14**	**83.29**	**Total**	**66.77**
XMg	**0.38**	**0.38**	**0.37**		
Fe/Si	**1.27**	**1.38**	**1.35**		

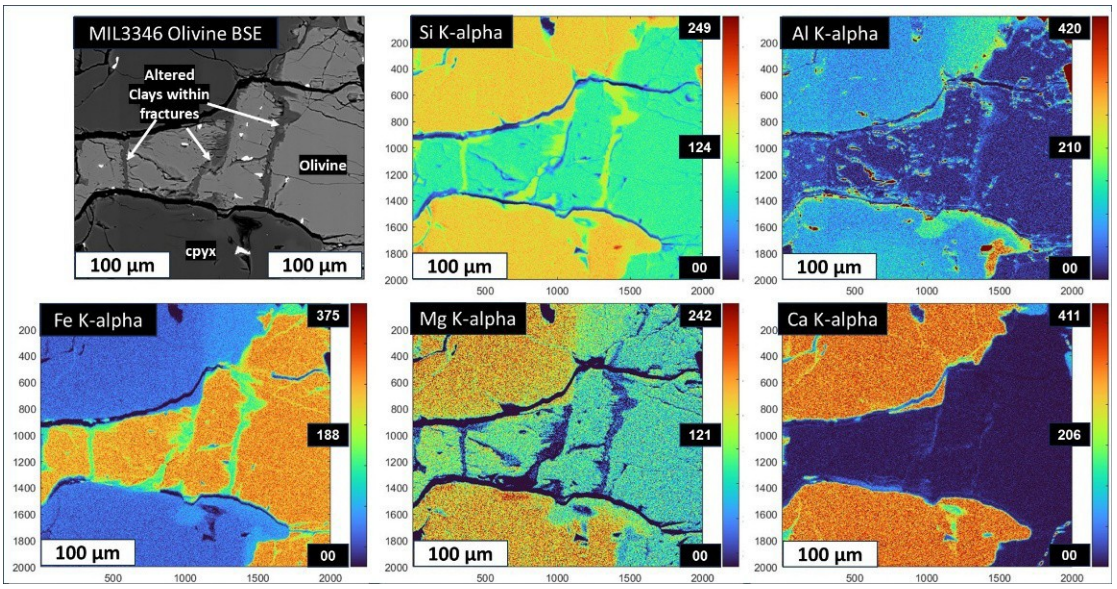

Fig. 3.7: X-ray elemental (Kα) maps of an olivine grain from MIL 03346 illustrating fracture-controlled alteration. The backscattered electron (BSE) image (top left) shows olivine grains cut by fractures that are filled with secondary clay-rich alteration products. The Si, Al, Fe, Mg, and Ca maps reveal clear chemical differences between altered and unaltered regions. The altered fracture zones show enrichment in Si, Fe, Mg, and Al, indicating the formation of secondary phases. This enrichment reflects the leaching of Fe and Mg from the host olivine grain into the alteration products, along with the input of Ca and Al from the surrounding clinopyroxene and plagioclase-rich mesostasis.

A representative example of fracture-controlled olivine alteration in the nakhlites is shown by the X-ray elemental (Kα) maps of the MIL 03346 meteorite (Fig. 3.7). The backscattered electron image highlights an olivine grain in which alteration products are restricted to narrow, well-defined zones, emphasizing that chemical modification islimited and spatially confined rather than pervasive. The elemental maps provide clearevidence for changes in chemical composition associated with these altered regions. The Si K-α map shows enhanced Si concentrations within the alteration zones relativeto the surrounding unaltered olivine, indicating silica enrichment during aqueous interaction. Similarly, the Al Kα and Ca Kα maps reveal that the altered clay-rich material contains higher Al and Ca concentrations compared to the host olivine. This contrast suggests that Al and Ca were introduced into the alteration zones during secondary mineral formation, most likely through interaction with neighbouring mineral phases and subsequent incorporation into the clay assemblage. The Fe Kα andMg Kα maps show complementary behaviour.

It is observed that the altered minerals contain both Fe and Mg, indicating that these elements were mobilized from the host olivine during alteration and redeposited locally within the fractures. Importantly, the elemental distributions within the altered material appear relatively uniform, with no clear internal zoning or localized concentration peaks. Overall, the X-ray maps demonstrate that alteration in MIL 03346 is highly localized, chemically coherent, andrestricted to discrete regions within olivine (Fig. 3.7). The consistent enrichment of Si,Al, Ca, Fe, and Mg within the altered zones, combined with their homogeneous distribution, closely matches the petrographic observations and supports a model of low-degree, fracture-controlled aqueous alteration.

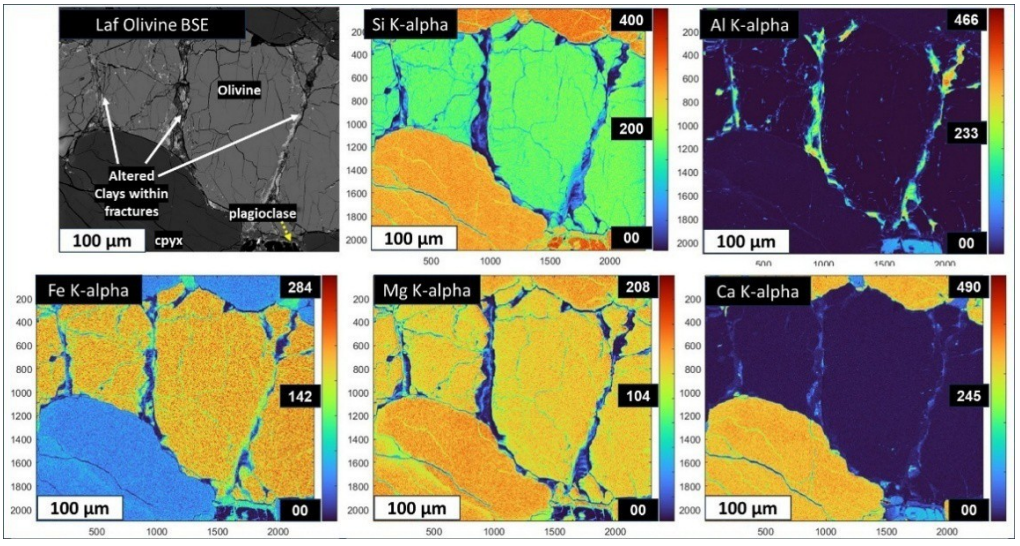

Fig. 3.8*: X-ray elemental (Kα) maps of olivine-hosted alteration in Lafayette showing fracture-localized secondary phases with pronounced aluminium enrichment relative to both host olivine and adjacent plagioclase. This shows similar behaviour as that of the MIL 3346 Olivine alteration case*

The X-ray elemental (Kα) maps of the Lafayette meteorite show that alteration associated with olivine grains is spatially restricted but chemically distinct when compared with the other nakhlites (Fig. 3.8). In the backscattered electron images, the altered material occurs primarily along serrated fractures within olivine grains, similarin geometry to those observed in Yam-593, MIL 03346, and Nakhla. Just like the otherNakhlite counterparts, the Fe Kα and Mg Kα maps further indicate

that both iron and magnesium are present within the altered material, suggesting the mobilization of these elements from the olivine host and their subsequent redistribution within the fractures. However, the elemental maps reveal that the chemical character of these fracture-hostedalteration products in Lafayette differs in detail. The Al Kα map shows clear aluminiumenrichment within the fracture fillings relative to the host unaltered olivine. The enrichment of Al is even higher than the Al-rich nearby plagioclase phase. Unlike the other nakhlites, the elemental distributions within the altered olivine fractures ofLafayette show subtle variations in intensity, suggesting minor chemical heterogeneitywithin the fracture fillings rather than a single uniform composition (Fig. 3.8).

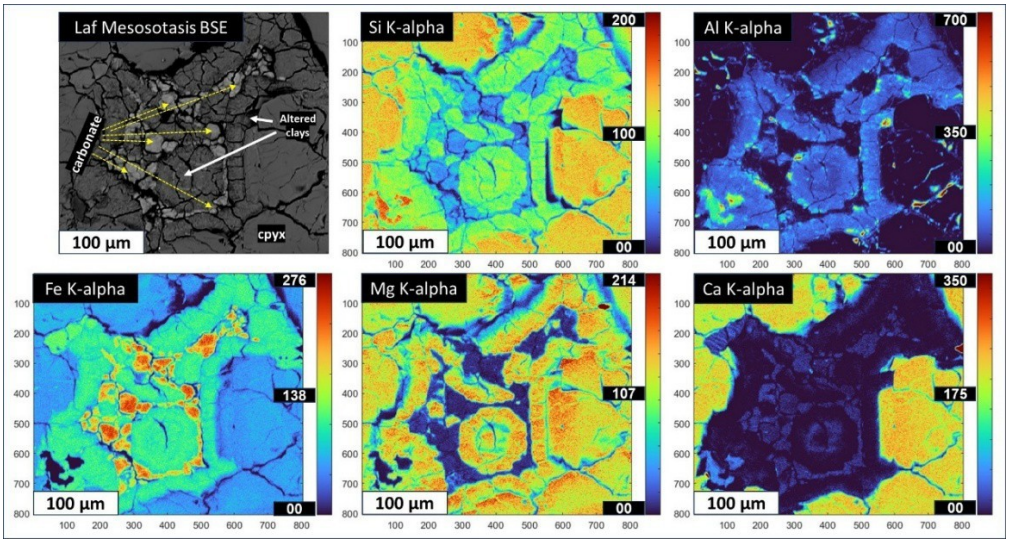

Fig. 3.9*: X-ray elemental (Kα) maps of altered mesostasis in the Lafayette meteorite showing Fe–Ca carbonate domains surrounded by phyllosilicate-rich material.*

In contrast to the other nakhlites studied, Lafayette also exhibits chemically altered regions within the mesostasis, which are clearly distinguished in the X-ray elemental maps and are described separately from the olivine-hosted alteration (Fig. 3.9). The mesostasis alteration is characterized by discrete, irregular domains that show strong enrichment in calcium and iron. The Ca Kα map highlights localized Ca-rich patches that coincide with areas identified petrographically as

-carbonate deposits, while the FeKα map shows corresponding iron enrichment within the same domains. These carbonate-bearing regions are surrounded by finer-grained phyllosilicate clays encasing the carbonate phases. The chemical distinction between the carbonate cores and the surrounding clay-rich material is reflected in the contrast observed across these maps. This mesostasis-hosted alteration is absent in Yam-593, MIL 03346, and Nakhla and represents an additional alteration feature unique to Lafayette. The coexistence of carbonate and phyllosilicate phases within the mesostasis, along with their distinct elemental signatures, highlights a more chemically diverse alteration assemblage in this meteorite compared to the fracture-controlled olivine alteration observed in the other nakhlites.

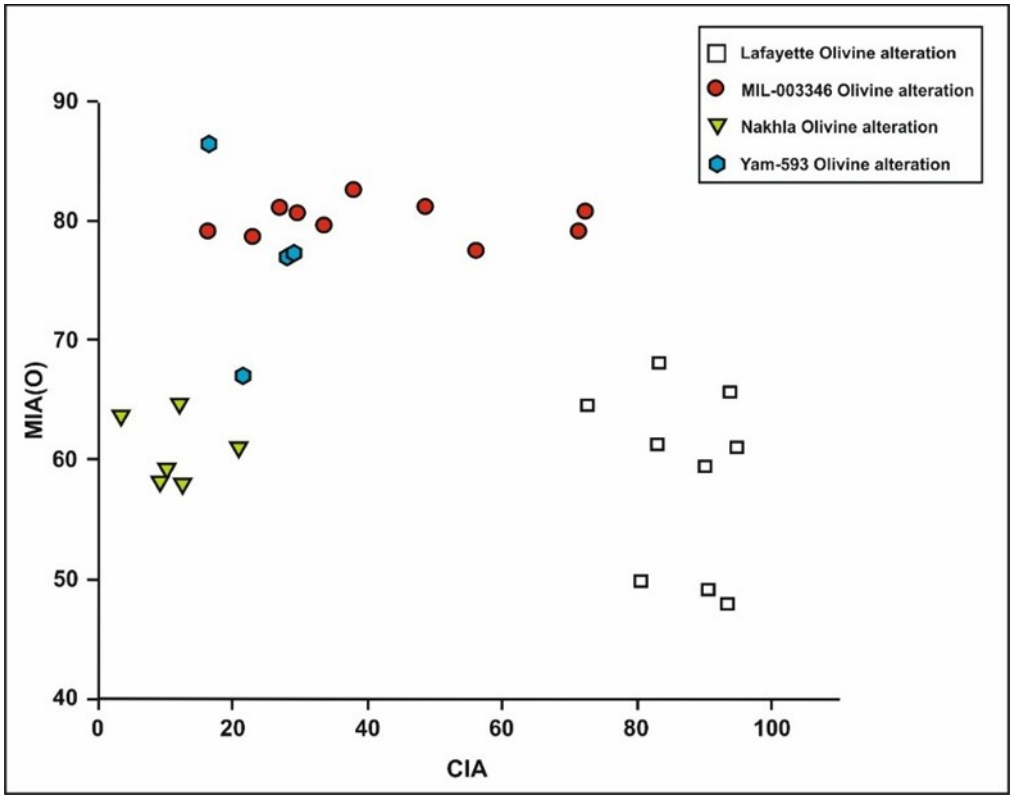

Fig. 3.10*: Bivariate plot of Mafic Index of Alteration under oxidising conditions (MIA(O)) versus Chemical Index of Alteration (CIA) for olivine-hosted alteration products in the nakhlites.*

To evaluate the chemical nature and degree of alteration affecting olivine-hosted secondary phases in the Nakhlite meteorites, the compositions of the altered products were examined using the Chemical Index of Alteration (CIA: [Al_2O_3 / (Al_2O_3 + CaO*+ Na_2O + K_2O)] × 100*) and the Mafic Index of Alteration calculated under oxidizing conditions MIA(O): [Al_2O_3 + $Fe_2O_3^T$] / (Al_2O_3 + $Fe_2O_3^T$ + MgO + CaO + Na_2O + K_2O)× 100,]). CIA provides a measure of the relative enrichment of Al with respect to mobile alkalis and alkaline earth elements, while MIA(O) tracks the redistribution of Fe^{3+} andAl during alteration of mafic minerals under oxidising conditions. Together, these indices allow comparison of alteration intensity and chemical pathways across the different Nakhlite samples. The MIA(O)–CIA bivariate plot (Fig. 3.10) reveals distinctclustering patterns for the altered clay minerals formed within olivine fractures in Yam- 593, MIL 03346, Nakhla, and Lafayette. The altered products in Yam-593 plot at moderate CIA values and relatively high MIA(O) values. These data points form a tightcluster, indicating limited compositional variability among the altered phases. This clustering suggests a chemically consistent alteration process affecting olivine in this meteorite. MIL 03346 exhibits a similar overall pattern, with CIA values comparable tothose of Yam-593, but with MIA(O) values that remain consistently high. The data points for MIL 03346 also cluster closely, reflecting a uniform alteration signature. Theproximity of the Yam-593 and MIL 03346 fields indicates that the alteration products in these two meteorites share broadly similar chemical characteristics despite differences in olivine composition. In contrast, Nakhla plots at lower CIA values and slightly lower MIA(O) values relative to Yam-593 and MIL 03346. The Nakhla data define a compact cluster, indicating chemically homogeneous alteration products, but with comparatively less aluminium enrichment. This suggests that, although alterationwas fracture-controlled and

localized, the degree of chemical modification in Nakhla was more limited. Lafayette displays a markedly different distribution on the MIA(O)– CIA plot. The altered products span a wide range of CIA values, extending to significantly higher CIA than the other Nakhlites, while MIA(O) values are comparatively lower and more scattered. This broad spread indicates substantial chemical variability within the alteration products, reflecting the presence of multiple alteration compositions.

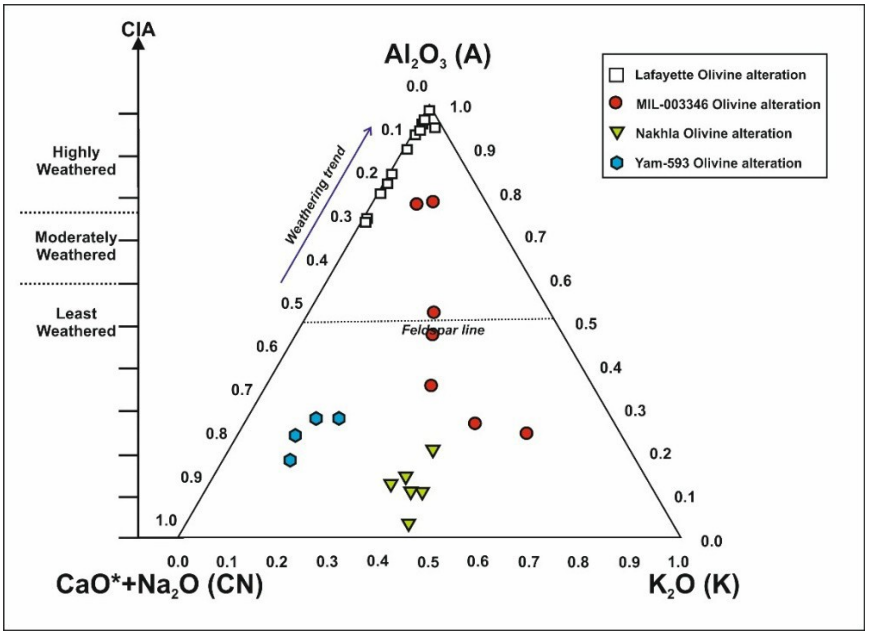

Fig. 3.11: A–CN–K ternary diagram showing the chemical characteristics of olivine-derived alteration products in the nakhlite meteorites.

The A–CN–K ternary diagram (Fig. 3.11) provides further insight into the chemical evolution of the olivine-derived alteration products. The altered products from Yam-593 and Nakhla cluster more tightly compared to MIL 03346, indicating relatively uniform alteration compositions. However, subtle but systematic differences are evident between these two meteorites. The Yam-593 data show relatively higher CaO* + Na_2O contents and lower K_2O proportions, suggesting stronger involvement of Ca–Na-bearing components during alteration. In comparison, Nakhla displays relatively higher K_2O enrichment and lower CaO* + Na_2O contents, indicating a greatercontribution of potassium during alteration.

Despite these differences, both meteorites show limited spread in Al_2O_3, consistent with chemically coherent alteration under restricted conditions. MIL 03346 shows a much broader spread across the ternary field. The altered products from this meteorite span a wide range of compositions, with variable proportions of Al_2O_3, CaO* + Na_2O, and K_2O. Instead, the data suggest variable degrees of cation mobility during alteration, with contributions from both Ca– Na–rich and K-bearing components, as well as differing levels of Al enrichment.

Lafayette again stands apart from the other meteorites. The Lafayette data plot close to the Al_2O_3 apex and along the A–CN line, indicating enrichment in Al_2O_3 relative to CaO* + Na_2O, with very limited involvement of K_2O. This distribution indicates strong aluminium enrichment and significant chemical heterogeneity within the alteration products.

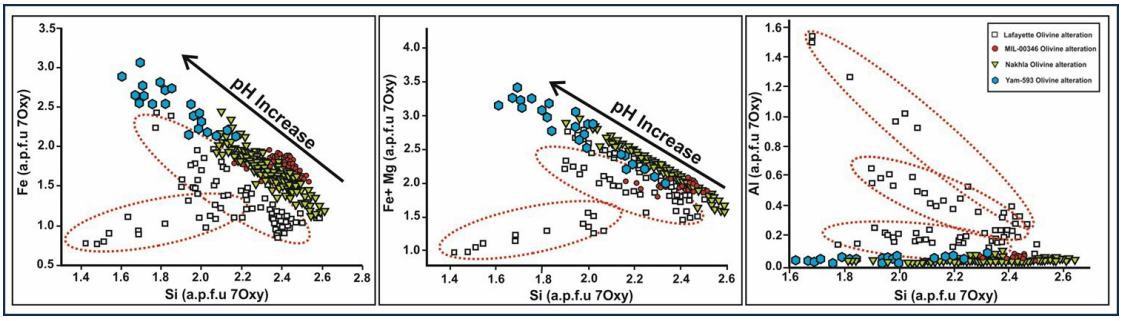

Fig. 3.12: Bi-variant plots of Fe vs. Si, Fe+Mg vs. Si, and Al vs. Si (atoms per formula unit) foraltered products from the nakhlite meteorites. Consistent trends are observed for Yam-593,MIL 03346, and Nakhla, whereas multiple trends in Lafayette indicate chemically diverse andmulti-stage alteration.

The bi-variant plots shown in Fig. 3.12 compare the chemical relationships between Si and selected major elements (Fe, Fe+ Mg, and Al) within the altered products of the Nakhlite meteorites. Together, these plots provide insight into how element mobility varied during aqueous alteration across different samples. A consistent and well-defined trend is observed for Nakhla, Yam-593, and MIL 03346 in all three bi-variant plots.In both the Fe vs. Si and Fe+ Mg vs. Si plots, an increase in Si content is systematically accompanied by a decrease in Fe or Fe+ Mg (a.p.f.u.). This inverse relationship suggests that silica enrichment in the altered material occurred alongside the progressive removal

of Fe- and Mg-bearing components from the reacting system. The similarity of this trend across these three meteorites indicates that their alteration followed comparable chemical pathways and was governed by broadly similar physicochemical conditions. The Al vs. Si plot further supports this observation. The altered products of Nakhla, Yam-593, and MIL 03346 cluster tightly along a single trend with relatively low Al contents and limited dispersion. This behaviour suggests that Al was not highly mobile during alteration and that the alteration products formedunder relatively uniform and chemically constrained conditions. In contrast, the Lafayette meteorite displays markedly different behaviour across all three plots. In theFe vs. Si and Fe+ Mg vs. Si diagrams, the Lafayette data define two distinct trends, rather than a single coherent relationship. These trends span a wider range of Fe, Fe+ Mg, and Si compositions, indicating greater variability in element redistribution duringalteration. The divergence is even more pronounced in the Al vs. Si plot, where the Lafayette data define three separate trends, reflecting substantial variability in Al content at similar Si levels. The presence of multiple trends in Lafayette, compared to the single, well-defined trends observed in the other three Nakhlites, indicates that the alteration products in Lafayette did not form under a single, uniform set of conditions.Instead, the chemical variability suggests that Lafayette experienced multiple rounds or stages of alteration, each characterized by different degrees of element mobility and fluid–rock interaction. In contrast, the coherent trends shown by Nakhla, Yam-593,and MIL 03346 point toward a more restricted and internally consistent alteration process

3.3. Discussion

The combined mineral chemistry, X-ray elemental mapping, and geochemical index results indicate that aqueous alteration in the nakhlite meteorites was spatially restricted yet chemically diverse, with clear differences in alteration style and intensity among the samples. The X-ray elemental maps confirm that alteration in Yam-593, MIL 03346,

and Nakhla is largely fracture-controlled and confined to narrow zones within olivine grains, with relatively uniform elemental distributions. This restricted geometry and chemical coherence suggest low degrees of fluid–rock interaction under conditions where fluids were limited and locally buffered by the host mineralogy. In contrast, the Lafayette meteorite records a more complex alteration history. In the Lafayette meteorite, the X-ray elemental maps reveal a pronounced enrichment of Al within the alteration-filled fractures of olivine grains. Notably, the Al concentrations within these fracture-hosted alteration products exceed those of the surrounding Al-rich plagioclase phase. This relationship suggests that aluminium was not sourced solely from adjacent primary minerals, but was instead introduced by a geochemically distinct reacting fluid that was itself enriched in Al. Such a fluid composition differs from that inferred for Yam-593, MIL 03346, and Nakhla, where Al enrichment within alteration zones canbe reasonably explained by local redistribution from neighbouring phases. The elevatedAl content in Lafayette, therefore, indicates that this meteorite experienced interactionwith a chemically distinct alteration fluid, suggesting a relatively more open and compositionally evolved alteration system compared to the other Nakhlites studied. The presence of Fe–Ca (siderite-calcite) carbonate phases within and surrounding phyllosilicate-rich material in the mesostasis region indicates a change in fluid chemistry during alteration, most plausibly reflecting a shift from relatively acidic to more alkaline conditions. Such a transition is not observed in the other nakhlites, pointing to a distinct alteration environment for Lafayette. Previous studies have proposed different sequences for carbonate and clay formation within the Lafayette meteorite. Early work suggested that siderite precipitation occurred after the formation of alteration veins (Lee et al., 2015a; Tomkinson et al., 2013). More recent interpretations, however, indicate a more complex evolution, in which Ca-rich siderite initially precipitated from the reacting fluid, followed by partial dissolution and

subsequent precipitation of clay minerals that infilled fractures and pore spaces (Piercy et al., 2022). This sequence is consistent with scenarios involving low water–rock ratio conditions, where the composition of the alteration fluid is strongly influenced by interaction with mafic host rocks. Under such conditions, dissolution of olivine-rich nakhlite material releases Fe, Mg, and Ca into the fluid, which subsequently combine with dissolved carbonate species to form carbonate minerals. The precipitation of these carbonates acts as an important buffering mechanism, modifying fluid chemistry during progressive alteration (Bridges & Schwenzer, 2012). The relative scarcity of carbonate phases in most Nakhlites further suggests that bicarbonate-bearing fluids were rapidly depleted during alteration. In the case of Lafayette, the localized occurrence of carbonate within the mesostasis implies that carbonate precipitation was restricted to specific zones where fluid availability and chemistry remained favourable, likelyduring an early stage of fluid migration through fractures (Changela & Bridges, 2010; Bridges & Schwenzer, 2012).

The A–CN–K ternary plot shows that alteration was most advanced in Lafayette, as reflected by its high Chemical Index of Alteration (CIA) values and strong displacement toward the Al_2O_3 apex. This pattern indicates substantial removal of mobile cations and pronounced aluminium enrichment, consistent with intense and chemically open alteration. MIL 03346, although generally comparable to Yam-593and Nakhla in petrography and fracture-controlled alteration geometry, displays a wide spread in A–CN–K space. This variability suggests that alteration in MIL 03346 was less uniform than might be inferred from petrography alone, highlighting additional complexity within the nakhlite alteration sequence. In contrast, the close clustering of data points for Yam-593 and Nakhla in the A–CN–K ternary diagram indicates relatively uniform alteration chemistry, consistent with a single, chemically constrained

alteration process affecting these meteorites.

The bi-variant a.p.f.u. plots provide further insight into the chemical evolution of alteration. The multiple trends defined by the Lafayette data, particularly in Fe–Si, Fe+Mg–Si, and Al–Si relationships, suggest that Lafayette likely underwent more than one pulse of alteration, each characterized by distinct degrees of element mobility and fluid composition. In comparison, the single, coherent trends observed for Yam-593,MIL 03346, and Nakhla suggest that alteration in these meteorites proceeded under more uniform physicochemical conditions. Together, these observations suggest that while fracture-controlled aqueous alteration is a common feature across the nakhlites, the intensity, chemical openness, and temporal complexity of alteration increase significantly in Lafayette, indicating a more dynamic alteration environment compared to the other meteorites studied. A key limitation in interpreting the alteration features observed in the nakhlite meteorites is the lack of direct constraints on the composition of the aqueous fluid responsible for these alterations. While petrographic, mineralogical, and geochemical evidence clearly indicates low-temperature, fracture-controlled alteration of olivine, the exact chemical nature of the reacting fluid—including its pH, redox state, and solute composition—remains uncertain. This uncertainty restricts our ability to fully reconstruct the physicochemical conditions under which alteration occurred on Mars during the Amazonian period. To address this limitation, it becomes necessary to turn to terrestrial analogue systems where fluid–rock interactions can be studied in greater detail and under better-constrained conditions.

3.4. Conclusions

- All nakhlite meteorites studied preserve primary cumulate igneous textures, with aqueous alteration strictly confined to olivine grains. Olivine alteration is consistently fracture-controlled, with secondary minerals filling narrow, serrated fractures, while olivine interiors, clinopyroxene, and most mesostasis remain largely unaltered.

- Yam-593, MIL 03346, and Nakhla show relatively uniform alteration products within olivine fractures, suggesting chemically consistent and localized alteration under restricted fluid conditions. Lafayette exhibits more complex alteration features, including tonal variability within fracture-filling clays and additional alteration within the mesostasis.

- X-ray elemental maps show that altered materials are enriched in Si, Fe, and Mg relative to unaltered olivine, while Al and Ca concentrations are higher in the alteration products than in the host olivine. In Lafayette, aluminium enrichment within olivine fracture fillings exceeds that of nearby plagioclase, indicating interaction with a chemically distinct, Al-rich fluid.

- The presence of Fe–Ca carbonate phases within the mesostasis of Lafayette, surrounded by phyllosilicate clays, indicates a change in fluid chemistry from acidic to more alkaline conditions.

- Chemical Index of Alteration (CIA) and Mafic Index of Alteration under oxidising conditions (MIA(O)) show that alteration intensity is highest in Lafayette and more limited in the other nakhlites.

- A–CN–K ternary plots indicate uniform alteration chemistry for Yam-593 and Nakhla, variable alteration for MIL 03346, and strongly Al-enriched alteration for Lafayette.

- Bi-variant plots reveal single, coherent alteration trends for Yam-593, MIL 03346, and Nakhla, but multiple trends for Lafayette, suggesting more than one alteration pulse.
- Overall, the results indicate that while all nakhlites experienced low-degree, fracture-controlled aqueous alteration, Lafayette records a more open, chemically diverse, and multi-stage alteration history compared to the other meteorites.

Chapter 4: From Deccan to Mars:How Limited Fluids Shape OlivineAlteration

This chapter investigates how olivine in basaltic rocks responds to limited water–rock interaction by comparing terrestrial picritic basalts from the Deccan Traps with the Martian nakhlite Yam-593. Through petrography, Raman spectroscopy, mineral chemistry, and X-ray elemental mapping, the chapter documents how alteration develops primarily along fractures within olivine grains, producing clay-rich secondary phases under low-temperature, low-fluid conditions. The study highlights the chemicalsignatures of cation mobility, the contrasting behavior of Mg-rich and Fe-rich olivine, and the formation pathways of alteration products. By examining these processes in both Earth and Martian samples, the chapter provides a clear framework for understanding localized aqueous alteration in basaltic crusts. The parallels observed between the Deccan analogue and Yam-593 offer insights into the nature of fluid activity on Martian surface and how such interactions may have shaped mineralogical textures preserved in Martian meteorites

4.1. Introduction

The Martian surface is predominantly covered by basaltic material, with olivine,pyroxene, and plagioclase being commonly identified (Mustard et al., 2005; Poulet et al., 2009; Viviano et al., 2019). Evidence of olivine has been detected in mafic rocks and the Martian crust through orbital observations and rover-based studies (Hoefen et al., 2003; Ody et al.,2013; Morrison et al., 2018; Beyssac et al., 2023). While olivine, a ferromagnesian mineral, is highly susceptible to aqueous alteration (Goldich, 1938; Wilson, 2004), its alteration during the Noachian and Early Hesperian epochs is believed to have resulted in widespread clay mineral formation, commonly driven bythe interactions with deuteric, hydrothermal, and surface waters (Vaniman et al., 2014). The availability of liquid water is considered essential for such alterations, and studying these processes can provide constraints on Mars' history of water. These insights are also critical for interpreting ancient environments, assessing potential habitability, and identifying possible biosignature preservation (Shen et al., 2022; Banham et al., 2024). Furthermore, the current Mars mission objectives, as well as the selection of landing sites like Gale Crater, Jezero Crater, and Oxia Planum, are closely aligned with the study of these processes (Milliken et al., 2010; Wiens et al., 2022; Ivanov et al., 2020). Over the last two decades, the idea of a "wet" Mars has been reinforced by the discoveryof extensive secondary hydrous minerals (Carter et al., 2013). These findings have primarily been obtained through orbiter data, in-situ lander and rover measurements, and studies of Martian meteorites. For instance, phyllosilicates have been identified across various Martian terrains, including highland regions, impact craters, and stratigraphic units from the Noachian (4.3–3.7 Ga) to the Amazonian (2.9 Ga) epochs (Bibring et al., 2005; Poulet et al., 2005; Bishop et al., 2008; Ehlmann & Edwards,

2014). At Gale Crater, secondary hydrous minerals have been confirmed through in situ analyses conducted by the CheMin instrument onboard the Mars Science Laboratory (MSL) Curiosity rover (Vaniman et al., 2014; Bristow et al., 2015; Rampe et al., 2018). Recently, hydrated phases have also been discovered at Jezero Crater Fan and floor bythe SHERLOC onboard Mars 2020 Perseverance rover (Phua et al., 2024). Evidence of ancient hydrological activity, such as valley networks and crater lakes, also supportsthe presence of liquid water on Mars (Wordsworth, 2016; Goudge et al., 2012; Horvath & Andrews-Hanna, 2017). These observations suggest that Mars experienced periods of weathering, hydrothermal alteration, and shifts in climate from water-dominantalkaline conditions to water-limited acidic environments (Carter et al., 2015; Deka et al., 2019). Among the SNC (Shergottite-Nakhlite-Chassignite) meteorites, the Nakhlite group is the second most abundant and has undergone significant aqueous and diagenetic alterations (Treiman, 2005; Day et al., 2006; Imae & Ikeda, 2010; Changela & Bridges, 2010; Hallis et al., 2014). However, understanding Mars' wet history is constrained by the limited number of Martian meteorite samples (~11 Nakhlites) and the capabilities of onboard instruments for detailed clay mineralogy characterization. Studies of terrestrial olivine alteration in basaltic environments could, therefore, aid inrefining alteration models and validating remote sensing data. It may further help in inferring the evolution in redox conditions during progressive olivine alteration with relevance to the Martian paleoclimate. Due to its nesosilicate structure, which lacks bridging oxygen bonds, olivine ishighly reactive and readily dissolved, often altering into iddingsite, a mixed mineral phase containing smectite, and iron oxyhydroxides (Smith, 1987). This alteration is thought to result either from deuteric processes during magma

coolingor, more commonly, from weathering. High-temperature alteration of olivine typically produces ferric iron oxides (symplectite), while low-temperature hydrothermal processes generate phyllosilicates and goethite. Laihunite, a high-temperature phase, often forms as opaque exsolution lamellae within olivine (Noguchi et al., 2009).

Despite extensive studies, the origin of iddingsite remains poorly understood to date, with many uncertainties surrounding fluid/rock ratios, fluid composition, reaction pathways, and mineral transformations. Although the discovery of alteration features and the formation mechanisms of hydrous minerals emphasise the significant role of water- rock interactions, ambiguity remains on whether these minerals formed through a singleepisode with multiple stages or distinct fluid episodes. How iddingstite formation after altering olivine controls the redox condition of the interacting fluid is also uncertain. Detailed petrographic studies, including microstructural analyses and mineralchemistry, are needed to address these gaps.

Investigations of new terrestrial analogue sites could provide critical insights into alteration histories, complement rover data, and enhance the understanding of Mars' basaltic crust aqueous geochemistry. Additionally, the study of secondary minerals on Mars offers vital clues about habitability by shedding light on the characteristics of the water involved in these processes.

4.2. Results

The study is based on olivine reaction interfaces in polished thin and thick sections of Continental Flood Basalt (CFB) samples from the Botad area in Gujarat, India, as well as the Martian meteorite Yamato 593 (Yam-593). Three thin polished sections of the picritic Deccan basalts from Botad and two thick sections (mounted on epoxy) of the Martian meteorite were used for this study.

4.2.1. Petrography

Picritic basalt samples from the Botad area were studied using thin polished sections. Under an optical microscope, the texture is akin to typical porphyritic with olivine phenocrysts (Fig. 4.1a & 2b). Large phenocrysts of olivine grains, often ranging up to ~3 mm in size, are embedded within a groundmass composed of fine-grained plagioclase and clinopyroxene. The Fe-Ti oxides occur as an accessory phase. The olivine grains were predominantly euhedral to subhedral in shape and fractured and veined. The fracturing and veining are irregular and confined exclusively within the olivine phenocrysts, with no evidence of cross-cutting into the surrounding groundmass. The fractures are filled with brown-coloured secondary minerals (clay) (Fig. 4.1b). In Back Scattered Electron (BSE) images, the fractures exhibit a serrated nature, providing further insights into the microstructural characteristics of the samples (Fig. 4.1c & 4.1d). The clay deposits within these highly serrated fractures (frequently with prominent teeth and notches) appear poorly crystalline in nature. Olivine grains are zoned with a typical Mg-rich core and Fe-rich rim. The Nakhlite represents a group of Martian meteorites that host a wide range of aqueous alteration products, collectively referred to as iddingsite, thought to originate from the same launch site on the Martian surface (Udry et al., 2020). The texture of the nakhlites resembles that of terrestrial basaltic cumulates, especially those rapidly cooled in lava flows or shallow sills (Treiman, 1986; Mikouchi et al., 2012). The Martian olivine compositionally differs from the terrestrial counterpart, where the former (olivine in nakhlite) is typically Fe-rich (Fa_{56-78}).

The typical serrated structure of secondary vein minerals is also common in Nakhlite. Subhedral olivine and euhedral pyroxenes are common, while mesostasis comprises feldspar in Yamato nakhlite (Yam-593) (Fig. 4.1d & 4.2e). Iddingsite is found to be composed of saponite in association with hematite.

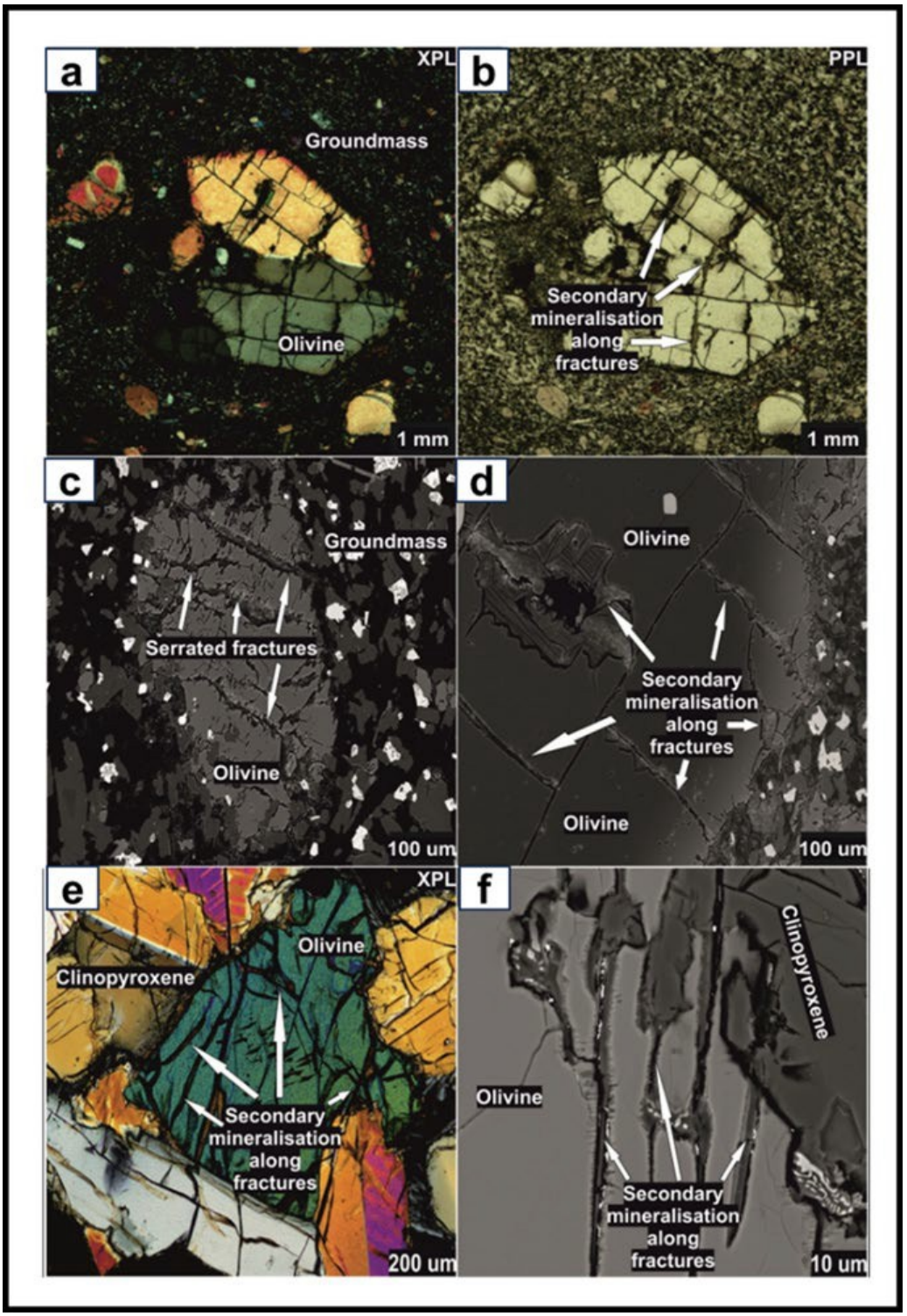

Fig. 4.1: Figs (a) and (b) shows plane-polarised (PPL) and crossed-polarised (XPL) photomicrograph of Deccan basalt showing an olivine phenocryst surrounded by a groundmass, with a typical porphyritic texture. The olivine grain is fractured, which are filledwith alteration-clay products. Figs (c) and (d) Back Scattered Electron (BSE) images showinghighly serrating fracturing in olivine phenocrysts. Fig (e) shows the XPL photomicrograph of Martian Nakhla Yam-593 exhibiting a cumulate texture. Similar to Deccan CFB, Martian olivine grains are also fractured and filled clays. In Fig (f) just like the terrestrial counterpartthere is serrated fracturing within the olivine grains of Yam-593 meteorite sample

.

4.2.2. Raman Spectroscopy

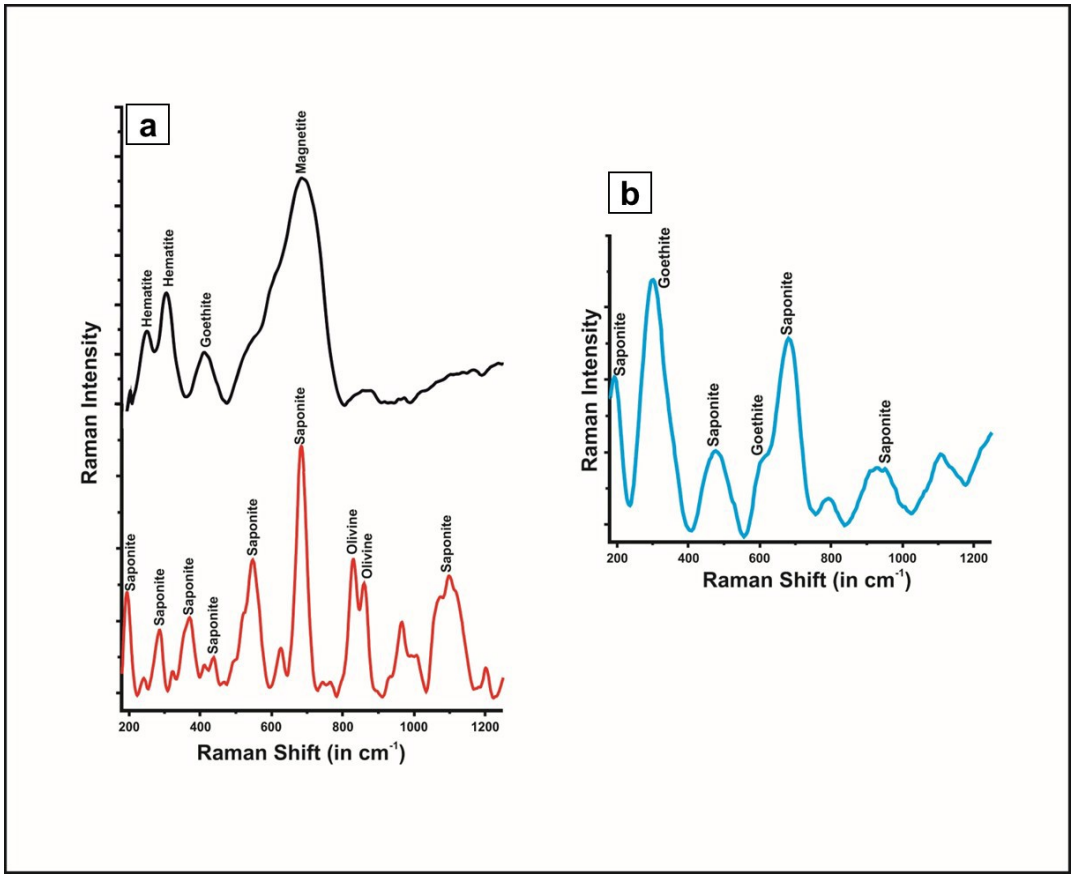

Fig 4.2: *shows the Raman signatures of the altered products in both terrestrial and Martian samples. Fig. (a) shows the Raman spectra of the clay from a terrestrial basalt sample. Saponite, a member of the smectite group, is clearly distinguished. Olivine is typically characterised by a doublet feature. Along with the smectites Raman signatures for goethite, hematite, and magnetite were also detected.* Fig. *b. Raman spectra of the iddingsite from Yam-593. Other mineralogical association includes the smectite group of clays, i.e., saponite, alongwith goethite (iron oxides)*

The Raman spectrum of forsterite grain is dominated by its signature doublet peak at 857 cm^{-1}(Fig. 4.2a). It also contains several weak peaks at 226, 304, 434, 545, 590, 608 cm^{-1}, and two medium-strong peaks at 921 and 963 cm^{-1}, respectively (Kuebler et al., 2006). The olivine grains are observed to be fractured, with secondary minerals deposited within these fractures. Raman shifts peaks at approximately 196, 288, 363, 430, 491, 552, 680, 1050, and cm^{-1} confirm that the secondary product is saponite (Kloprogge & Ponce, 2021), a type of smectite group of clays. Additionally, Fe oxides are detected in the Botad thin section sample in the form of goethite, marked by a peak

around 389 cm-1 (Almuslet et al., 2017) magnetite, with a prominent peak near 667 cm-1 (Lu & Tsai, 2014), and hematite, identified by Raman peaks at approximately 222 and 286 cm-1 (Almuslet et al., 2017) (Fig. 4.2a).

Similarly, Raman analysis has been performed on the Martian Nakhlite meteorite Yam-593 (Fig. 4.2b). In this sample, the large cumulates of olivine are also fractured, with alteration products present within these fractures. These alteration products are predominantly saponite, which exhibits Raman shift peaks at approximately 196, 464, 682, and 918 cm-1 (Kloprogge & Ponce, 2021). Fe oxides in the form of goethite are also found, represented by peaks at approximately 296 and 613 cm-1 (Fuentes-Carreón et al., 2022). The presence of a mixture of Fe oxides and saponite (smectite) within the fractures of olivine grains suggests that the alteration product is iddingsite.

Table 4.1: EPMA point analysis of the olivine grains of both Terrestrial picritic basalt from Deccan CFB (Botad) and Martian Nakhlite Yam-593

Botad Olivine Grain					Yam-593 Olivine					
	Grain 1	**Grain 2**	**Grain 3**	**Grain 4**		**Grain 1**	**Grain 2**	**Grain 3**	**Grain 4**	**Grain 5**
	N=36	**N=49**	**N=16**	**N=35**		**N=12**	**N=26**	**N=30**	**N=24**	**N=26**
SiO2	40.5	39.48	38.83	38.75	**SiO2**	31.48	32.38	32.62	32.12	31.79
TiO2	b.dl	b.dl	0	0	**TiO2**	0.04	0.03	0	0.02	0.06
Al2O3	0.06	0.03	0.11	0.02	**Al2O3**	0.03	b.dl	b.dl	b.dl	0.02
FeO	10.8	11.65	12.11	12.2	**FeO**	58.74	55.23	52.95	55.86	56.92
MgO	47.63	46.99	47.01	47.13	**MgO**	8.34	11.98	13.15	10.67	10.16
MnO	0.16	0.19	0.18	0.18	**MnO**	1.15	1.12	0.89	1.08	1.13
CaO	0.25	0.47	0.29	0.45	**CaO**	0.24	0.31	0.38	0.3	0.3
Na2O	b.dl	b.dl	b.dl	b.dl	**Na2O**	b.dl	b.dl	b.dl	b.dl	b.dl
K2O	0.02	0.02	0.01	0	**K2O**	0.03	0.02	0.02	0.02	0.02
P2O5	b.dl	b.dl	b.dl	b.dl	**P2O5**	b.dl	b.dl	b.dl	b.dl	0.1
Cr2O3	0.08	0.06	0.08	0.05	**Cr2O3**	b.dl	b.dl	b.dl	b.dl	b.dl
NiO	0.34	0.28	0.33	0.28	**NiO**	b.dl	b.dl	b.dl	b.dl	b.dl
Total	**99.86**	**99.19**	**98.96**	**99.09**	**Total**	**100.08**	**101.1**	**100.05**	**100.12**	**100.53**
Fo Content	0.9	0.88	0.87	0.87	**Fo Content**	0.2	0.28	0.31	0.25	0.24
Fa Content	0.1	0.12	0.13	0.13	**Fa Content**	0.8	0.72	0.69	0.75	0.76

***b.dl: below Detection Limit**

Table 4.2: EPMA point analysis of the alteration features within the olivine grain fractures of both Deccan CFB (Botad) and Martian Nakhlite Yam-593.

Botad Olivine Grain Alteration in fractures							**Yam-593 Olivine Grain Alteration in Fractures**				
	Grain 1	**Grain 2**	**Grain 3**	**Grain 4**	**Grain 5**	**Grain 6**		**Grain 1**	**Grain 2**	**Grain 3**	**Grain 4**
	N= 11	***N= 19***	***N= 29***	***N= 41***	***N= 45***	***N=35***		***N=10***	***N=10***	***N=28***	***N= 17***
SiO2	35.61	39.3	40.71	44.52	41.01	44.92	**SiO2**	34.78	31.66	26.2	28.18
TiO2	0.02	0.02	0.02	0.02	0.02	0.02	**TiO2**	0.02	0.06	0.02	0.08
Al2O3	5.42	5.32	2.92	6.3	5.9	3.05	**Al2O3**	0.48	0.65	0.4	0.2
FeO	19.95	15.2	13.96	15.39	14.34	10.14	**FeO**	44.91	43.64	54.59	48.3
MgO	14.94	14.6	15.2	16.3	17.3	18.42	**MgO**	3.89	3.51	1.64	6.57
MnO	0.08	0.09	0.05	0.05	0.05	0.04	**MnO**	0.97	0.56	0.58	0.79
CaO	1.47	2.11	1.57	0.95	1.35	1.06	**CaO**	0.3	0.4	0.34	0.26
Na2O	0.15	0.25	0.14	0.06	0.18	0.11	**Na2O**	0.32	0.49	0.55	0.17
K2O	0.22	0.33	0.32	0.18	0.23	0.22	**K2O**	0.27	0.27	0.24	0.08
P2O5	0	0	0	0	0	0	**P2O5**	0	0	0	0
SO3	b.dl	b.dl	b.dl	b.dl	b.dl	b.dl	**SO3**	0.95	1.23	1.61	1.39
Cr2O3	b.dl	0.04	0.05	0.06	0.06	0.08	**Cr2O3**	0.02	0.03	0.04	b.dl
NiO	0.14	0.13	0.17	0.24	0.2	0.25	**NiO**	0.01	0.02	0.02	b.dl
Total	**77.98**	**77.39**	**75.12**	**84.09**	**80.63**	**78.31**	**Total**	**86.92**	**82.52**	**86.22**	**86.05**
XMg	0.57	0.63	0.66	0.64	0.68	0.76	**XMg**	0.13	0.12	0.05	0.19
Fe/Si	0.93	0.64	0.57	0.58	0.58	0.38	**Fe/Si**	2.22	2.37	3.78	2.91

***b.dl: below Detection Limit**

4.2.3. Mineral Chemistry

In the Botad polished thin sections, the olivine grains are recognized as being predominantly forsteritic in composition (Table 4.1), with large phenocrysts often showing zoning. The core of the olivine is characterized by a very high forsterite content (~Fo_{90}), while the rim exhibits an average forsterite content of Fo_{83}. In the Fo versus NiO plot, no trend is identified within the core of the forsteritic olivine, whereas the rim data reveal an increase in NiO content as Fo increases (Fig. 4.3). In comparison, the nakhlite (Yam-593) is relatively fayalite-rich (Fo_{26}) (Table 4.1) when contrasted withthe terrestrial olivine. Furthermore, zoning is absent in the olivine grains of this Martianmeteorite. The comparison of altered olivine composition from Deccan CFB and Martian Nakhla is given in Table 4.2.

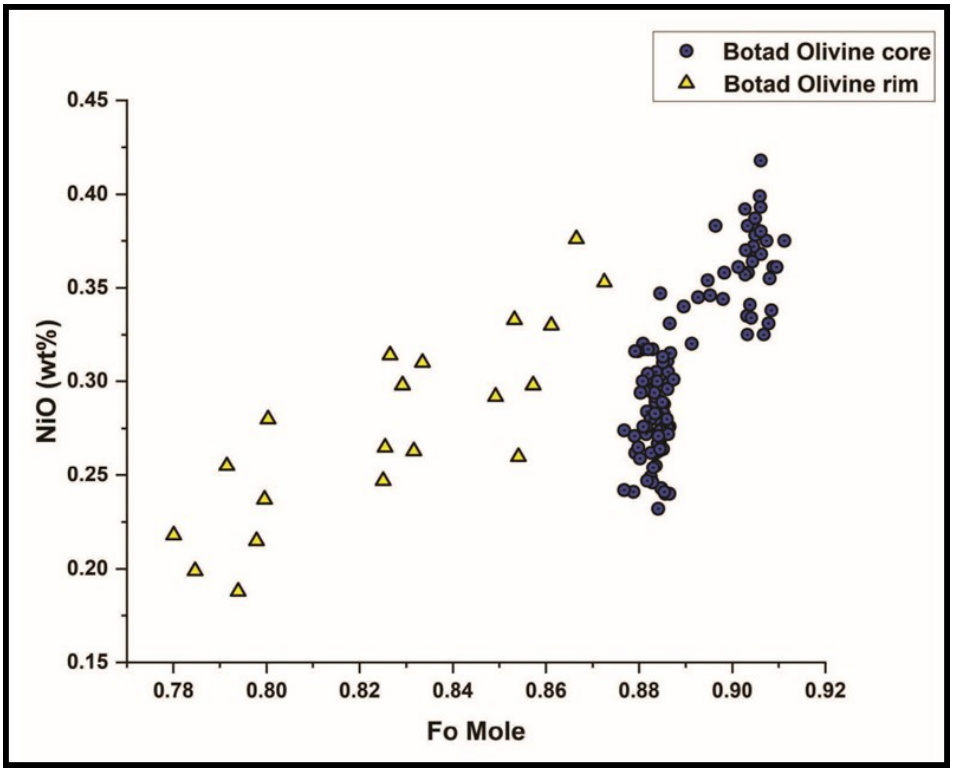

Fig. 4.3: Bivariant plot of NiO (wt%) v/s (Fo mol%) of the zoned (core as well as rim) olivine grain from terrestrial deccan basalt sample (Botad). Progressive change of NiO isnoticed as Fo increases

A clear contrast in the primary composition of the olivine for both the Yam-593 nakhlite and the terrestrial Botad sample is observed; however, similar behaviour in thealteration products within the fractures of these olivine grains is also identified. During the weathering of olivine, progressive changes in the degree of weathering indices are caused by the loss of mobile elements relative to immobile ones.

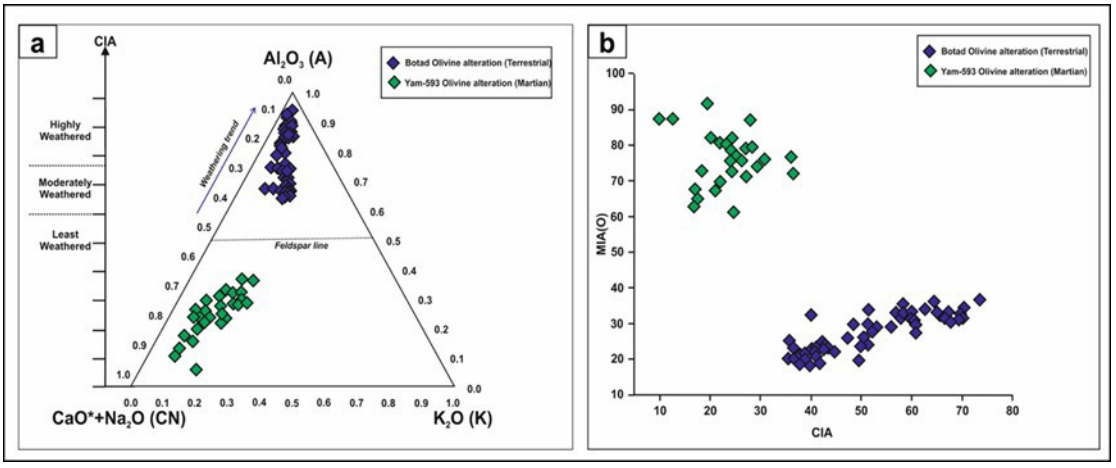

Fig. 4.4*: Fig (a) (left) Al2O3-CaO*+Na2O-K2O (A-CN-K) ternary plot of iddingsite from terrestrial Deccan basalt (Botad) and Yam-593 (Martian), respectively. The secondary mineralstypically fall along the A-CN line with increasing Al2O3 content as weathering progresses. Fig (b) (right) The bivariate plot of Mafic Index of Alteration (MIA) vs Chemical Index of Alteration(CIA). A higher CIA is noticeable for terrestrial (Deccan CFB) as compared to the Martian counterpart. A linear correlation between the MIA and CIA is diagnostic for terrestrial weathering.*

In the Al_2O_3–CaO*+Na_2O–K_2O (A-CN-K) ternary diagram (Fig. 4.4a), it is noted that while the chemical index of alteration (CIA): Al2O3/(Al2O3+CaO*+Na2O+K2O)) for secondary minerals is higher for the Botad samples compared to the Martian counterpart, both products are aligned along the Al_2O_3– CaO*+Na_2O (A-CN) line, with nakhlite secondary minerals showing a relatively lower Al_2O_3 concentration. A higher CIA is exhibited by terrestrial olivine in comparison to the Martian counterpart (Fig. 4.4b), and a linear correlation between the mafic index of alteration (MIA): [(Al2O3+Fe2O3T)/(Al2O3+Fe2O3T+MgO+CaO*+Na2O+K2O)]) and CIA is consistent among the terrestrial samples, indicating a similar bulk weathering behaviour

of Ca and Na. This correlation, however, is not well established for Martian samples, where a poorer overall correlation of secondary minerals is seen, potentially reflecting a different behaviour of Ca and Na during phyllosilicate formation in intermediate weathering.

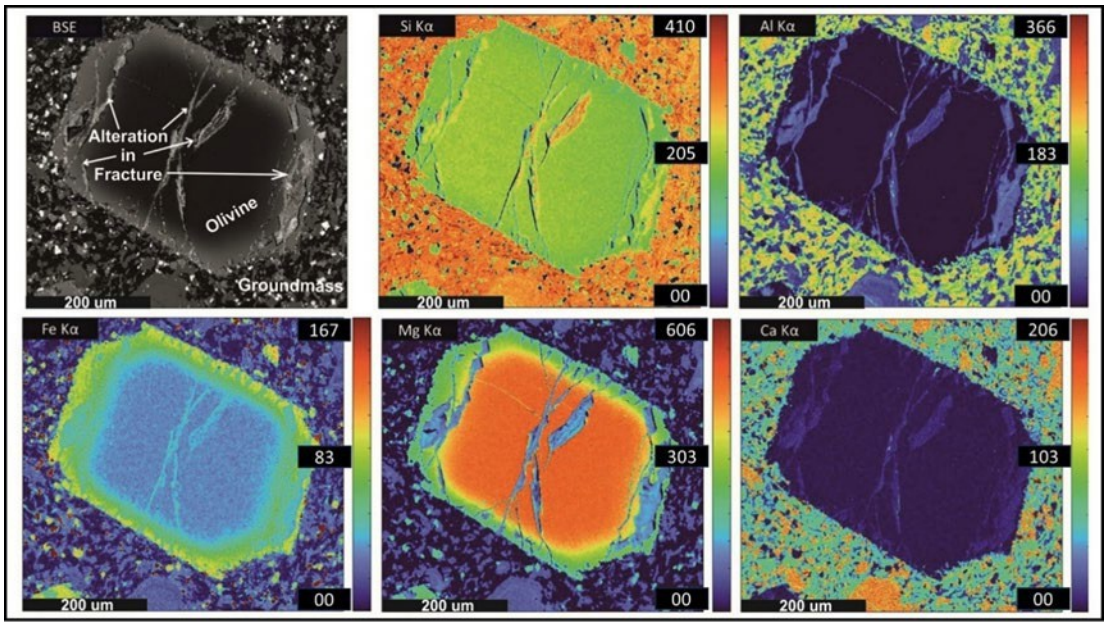

Fig. 4.5*: X-ray elemental maps of a fractured olivine grain from the terrestrial Deccan basalt (Botad) sample. Alteration is localized along fractures and is marked by enrichment in Si, Al, and Ca within the secondary material, while Mg and Fe show depletion from the olivine host and incorporation into the alteration products.*

The X-ray maps of the terrestrial picritic basalt sample from the Deccan Traps (Fig. 4.5) show that alteration is strongly localized within fractures cutting the olivine grain. These fractures contain secondary products enriched in Mg and Fe, indicating that these cations were leached from the host olivine and incorporated into the alteration assemblage. In contrast, elements such as Si, Al, and Ca appear more concentrated within the altered zones than in the surrounding olivine, suggesting that these components were supplied by neighbouring phases in the groundmass and subsequently transported into the fractures during aqueous alteration. Overall, the terrestrial picritic basalt exhibits a clear pattern of cation mobility, where Mg and Fe are removed from

the olivine structure while Si, Al, and Ca are externally sourced and incorporated into the infilling material.

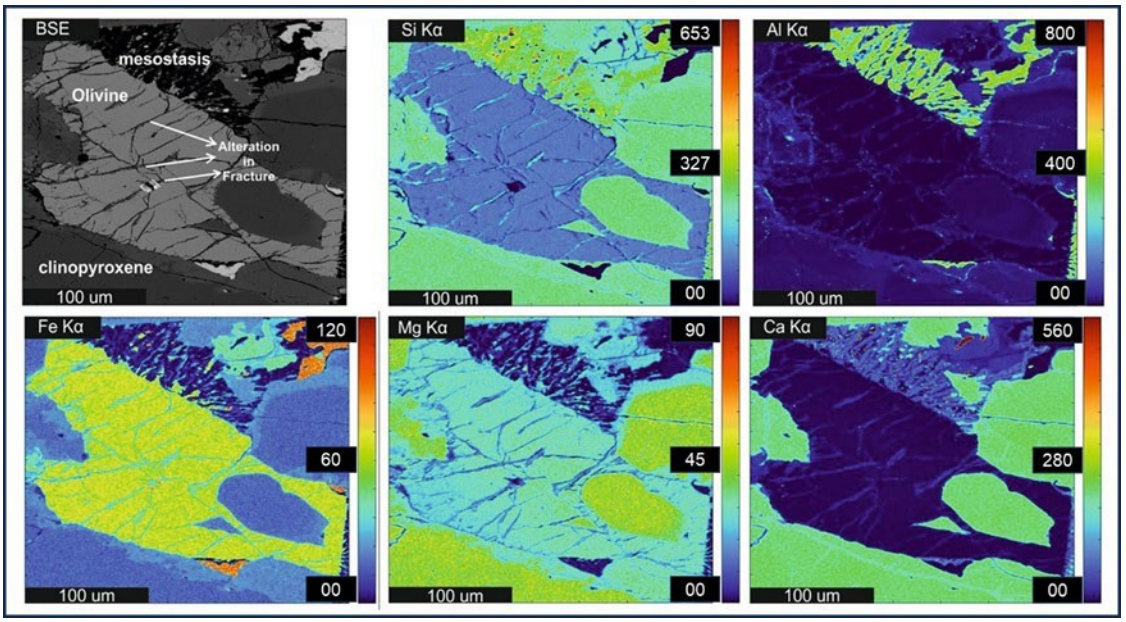

Fig. 4.6*: X-ray elemental maps of a fractured olivine grain in the Martian nakhlite Yam-593. The alteration veins show increased Si, Al, and Ca relative to the olivine, along with Mg andFe derived from leaching of the Fe-rich olivine. The elemental distributions closely parallelthose in the terrestrial sample (Fig. 4.7), indicating that both rocks experienced similar fracture-focused alteration pathways under limited-fluid conditions*

In the Martian nakhlite Yam-593 (Fig. 4.6), a comparable elemental distribution is observed, despite the olivine being significantly more Fe-rich than its terrestrial counterpart. The olivine grain is also cut by fractures that host alteration products enriched in Mg and Fe relative to the adjacent groundmass, consistent with leaching of these elements from the olivine itself. Similar to the terrestrial sample, the altered zones in Yam-593 show elevated Si, Al, and Ca, indicating incorporation of these cations from nearby phases during fluid–rock interaction. The close resemblance between the patterns seen in Fig. 4.5 and Fig. 4.6 suggests that both the terrestrial picritic basalt and the Martian nakhlite experienced fracture-controlled, low-temperature aqueous alteration following broadly comparable chemical pathways.

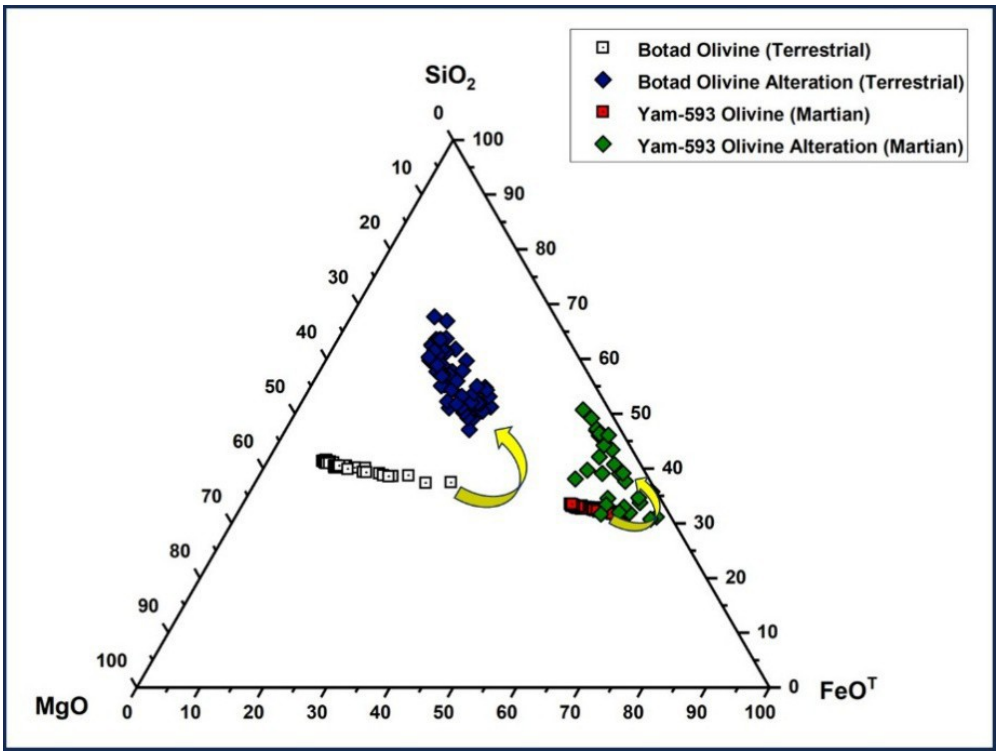

Fig. 4.7*: The SiO_2–MgO–FeO^T triangular plot showing distinct chemical composition of olivines from Mars and Earth. The Martian olivine is characteristically Fa-rich. However, as alteration progresses, the trend of alteration shows resemblance due to the leaching of MgO and FeO and the corresponding enrichment of SiO_2.*

The SiO_2–MgO–FeO^T ternary diagram (Fig. 4.7) highlights clear compositional distinctions between the terrestrial picritic olivine from Botad and the Martian olivine from Yam-593, as well as the trajectories each sample follows during alteration. The unaltered Martian olivine plots toward the FeO^T apex, reflecting its characteristically Fe-rich nature relative to the terrestrial olivine, which plots closer to the MgO-rich limb. Despite these initial compositional differences, the alteration products derived from both samples display converging geochemical trends. In each case, the secondary phases shift away from the MgO–FeO^T field toward the SiO_2 apex, indicating a progressive depletion of Mg and Fe from the olivine structure during aqueous alteration. This movement toward higher SiO_2 compositions suggests that the alteration process in both samples occurred in a relatively acidic environment. Notably, the similarity in the alteration trends—despite the contrasting Fe/Mg ratios of the original olivine grains—

demonstrates that the geochemical pathways governing olivine breakdown were broadly comparable in both terrestrial and Martian settings.

4.3. Discussion

4.3.1. Microstructural characteristics and process of iddingsite formation.

The iddingsites are a complex product of olivine alteration and do not represent a single mineral (Sun, 1957). The high and low-temperature iddingsites are known for different mineralogical assemblages. Gualtieri et al., (2003) observed the formation of hematite, magnetite, and orthopyroxene during high-temperature oxidation experiments on olivine. Additionally, several authors have earlier discussed the high-temperature iddingsite (HTI), which has a similar composition (orthopyroxene, magnetite, hematite, cristobalite, and amorphous silica), within continental and oceanic basalt flows (Goff, 1996; Caroff et al., 2000) and in gabbroic intrusions (Clément et al., 2007). Tschegg et al., (2010) observed a systematic HTI-like corrosion phenomenon of olivine phenocrysts in alkaline lavas, which is unlikely in naturally occurring iddingsite formation, corroborating high-temperature corrosion (HTC) of olivine.

The microscopic and macroscopic features of this study suggested iddingsite to be a meteoric origin. The iddingsite in Deccan forsterite appears fracture-controlled, and the microstructural features of iddingsite appear similar for Earth and Mars. Additionally, Lee et al. (2015a) classified the iddingsite in Lafayette as fine serration and coarse serration based on the textures and cross-cut relationship; nevertheless, their mineralogy remains the same. The mineral assemblages of iddingsite, irrespective of Earth and Mars, are consistent with the low-temperature alteration. On Earth, iddingsite formed either in the subsurface or during the surface weathering process after exhumation. In contrast, for Mars, the impact-induced, shorter-lived hydrothermal

alteration produced the fluids and precipitated along the fractures. This limited alteration does not seem to be part of any large impact crater; rather, it appears to be consistent with the smaller crater that experienced limited hydrous alteration. The unaltered pyroxene appears in the matrix but never surrounds the iddingsitised olivine.

4.3.2. Formation mechanism and weathering indices

Earlier studies suggested that iddingsite in Martian meteorites formed due to the replacement of olivine (Meunier et al., 2012); however, Treiman (2005) argued for a dissolution process. Later, Changela and Bridges (2010) proposed that cementation and replacement processes are the major factors. A model developed by Plümper et al. (2012) to describe the formation of serpentine veins in terrestrial olivine suggests the mechanism by which the Lafayette veins may have been widened and lengthened. They proposed that interface-coupled dissolution–precipitation on the walls of an initial fracture or etch pit produces hydrous minerals, whose volumetric expansion generates stresses at the etch pit corners. These stresses are sufficient to fracture the olivine, thus enabling aqueous solutions to penetrate further into grain interiors. The hairline cracks that are associated with the faceted inclusions beyond the tips of discontinuous veins in Nakhlite (e.g., Fig. 4.1e) are evidence that the precipitation of Fe–Mg silicate has fractured the olivine, thus increasing the surface area available for aqueous alteration. There are several pieces of evidence arguing against the impact-triggered fracture formation in the Martian Nakhlite. For example, the serrated veins are only common in the olivine but are absent in the adjoining mineral grains. This suggests some intrinsic property of olivine, like the higher reactivity of olivine, which ultimately induces the serration. The serrated structure also does not form in the natural and experimental shock experiment of olivine. The teeth and notches of serration also do not match up with either wall.

Microtextural attributes are consistent with dissolution and simultaneous precipitation. The carbonation of olivine and subsequent precipitation of saponite may often correlate with more than one episode of alteration (Lee et al., 2015a). Saponite is a trioctahedral smectite clay mineral, the octahedral layer of which is occupied by Mg cations (Grim, 1953). This mineral is mainly formed after forsterite and Mg-rich olivine grains, but is also dependent on the leaching intensity in the level of alteration. If Mg is removed, the Fe of olivine oxidizes and accumulates.

The EPMA analysis of secondary phases enables the evaluation of elemental mobility at alteration fronts and provides constraints on the chemistry of the interacting fluid. However, due to fine-scale intergrowths of mineral phases, the chemical composition often represents the mixed phases. The gradual decrease of magnesium in iddingsite, as seen in the X-ray maps (Fig. 4.7), as compared to olivine, suggests the removal of Mg relative to Fe. The relatively higher SiO_2 in the alteration phase (both fall parallel to the Fe-Si line) of terrestrial and Martian samples, as compared to olivine, is attributed to the presence of a smectite phase.

Based on the A-CN-K triangular plot (Fig. 4.4a) and the CIA vs. MIA bivariant plot (Fig. 4.4b), it can be inferred that the terrestrial alteration likely occurred in a relatively open-system environment with a higher water-to-rock ratio compared to the Martian alteration setting. This suggests that cations from nearby phases have migrated into the fractures, while Mg has been leached out of the olivine grains from these regions. A similar pattern of cation mobility is evident from the X-ray maps of the altered products within the fractures of the Yam-593 olivine grain. A correlation between the CIA and MIA suggests similar bulk weathering behaviour of Mg, Ca, and Na. The greatest strength of the CIA as a chemical weathering proxy is the utility of the

accompanying Al_2O_3-CaO*+Na_2O-K_2O (A–CN–K) diagram, which has empirically and kinetically predictable weathering vectors for various minerals and rock types (Nesbitt & Young, 1984; Nesbitt, 1992). The overall weathering vector for feldspar destruction in various parent rocks is parallel or sub-parallel to the A–CN axis. The low CIA of secondary minerals from Martian Nakhlite suggested a closed system and low water/rock ratio. Since Martian olivine is not expected to have high CIA, we interpret this as indicative of Al-mobilization into altered olivine, possibly under hydrothermal conditions. Saponite is ubiquitous in terrestrial and Martian iddingsite. Saponite, like nontronite, contains some Al3+, which replaces Si4+ in the tetrahedral layer. This Al content may be very small, but it raises the problem as to why aluminium is present in a pseudomorph formed after a mineral that originally contained no aluminium. It is very likely that the Al-content of these clays is due to hydrothermal alteration, which allows some aluminium transfer from adjacent minerals. This is seen from the X-ray map of the Deccan olivine grain, where we see that aluminium is likely enriched into the olivine fractures from the groundmass. Whereas the high CIA for the terrestrial iddingsite is suggested for a relatively open system environment. In contrast, the altered olivine in Deccan experiences greater hydration and oxidation (degradation of olivine doublet, presence of hematite and goethite), implying that the terrestrial mode of alteration took place where the availability of liquid water was relatively greater, as compared to the alteration scenario in the Martian meteorite. The Yam-593 samples are also reportedto have jarosite (Noguchi et al., 2009), consistent with the acidic environment. The presence of hematite sometimes argues in favour of deuteric alteration. However, caution needs to be taken, and it is suggested that the associated mineral be taken into account. It is reasonable that the alteration of olivine results in a mixture of phyllosilicate (saponite), hematite, and goethite (Delvigne et al., 1979; Talbi & Honnorez, 2003). According to Baker and Haggerty (1967), the association of the low-

temperature alteration products, such as goethite and phyllosilicates, is not analogous and differs substantially as compared to high-temperature alteration (Clement et al., 2007). At lower temperatures, complex assemblages containing goethite and interstratified phyllosilicates form through oxidation and hydrothermal alteration. Therefore, the Martian and the terrestrial iddingsite are more consistent and argue for low-temperature aqueous alteration.

4.4. Conclusions

The observation that olivine in both the Deccan basalts and the Martian nakhlite Yam-593 has undergone alteration through remarkably similar processes strongly suggests that comparable geological conditions operated on Earth and Mars. In both settings, olivine grains display fractures—many of which show distinctive serrated or saw-tooth edges—where secondary minerals have been deposited. These infilled fractures contain iddingsite, a mixed assemblage of smectite-group clays and iron oxides that forms through the breakdown of olivine. The development of these minerals within fracture networks indicates that alteration likely occurred in situ and under conditions where only limited amounts of fluid were available. This is consistentwith the known high reactivity of olivine, which can undergo significant modification even when exposed to very small volumes of water.

Although the olivine compositions differ—Deccan picritic basalts contain more magnesium-rich olivine, whereas the Martian nakhlite hosts iron-rich olivine—the secondary mineral products generated by alteration are strikingly similar. In both cases, the altered material is dominated by saponite and related smectite clays, along with intermixed iron oxides, which together form the mineralogical assemblage referred to as iddingsite. The terrestrial sample appears to have interacted with a slightly greater amount of water compared to the Martian specimen, yet the overall behaviour of mobile

cations such as Mg, Fe, Ca, and Si remains broadly comparable. The enrichment of SiO_2 observed in both altered products suggests that alteration progressed under acidic conditions, where silica becomes more stable relative to other dissolved species. Further support for the similarity in alteration environments comes from X-ray elemental mapping. These maps show parallel patterns of cation mobility in both samples: magnesium and iron are leached from the olivine structure and incorporated into the secondary minerals, while elements such as silicon, aluminium, and calcium become enriched within the fracture-filling clays. Such congruent geochemical signatures imply that the conditions promoting olivine alteration—limited fluid presence, low-temperature regimes, and fracture-controlled fluid pathways—were broadly alike on Earth and Mars, even though the exact water availability and redox state may not have been identical. The limited understanding of the geochemical composition of Martian subsurface liquid, along with the lack of available samples to investigate the interaction between the Martian crust and liquid water during the water-starved Amazonian era, poses significant challenges. Nevertheless, studies of terrestrial analogues, despite variations in their primary mineral composition (e.g., Fe and Mg content), exhibit alteration products and conditions closely resembling those found in Martian meteorites. Furthermore, these pH-dependent phyllosilicates can largely influence the preservation potential of biosignatures on Mars, which remains the topmost priority of the ongoing Mars mission. In this chapter, the comparison between the Deccan picritic basalt and the Martian nakhlite highlighted how similarly olivine responds to brief, limited interactionwith water on both planets. The fractured olivine grains, the formation of smectite-type clays, and the clear signatures of cation movement revealed that even short-lived or low-volume fluid activity can leave strong mineralogical and chemical imprints. Thesefindings helped establish a broader context for recognizing what early-stage aqueous alteration looks like in basaltic systems, whether on Earth or Mars. The

next chapter moves deeper into this problem by studying the Deccan basalts in greater detail. Instead of comparing Earth and Mars, the focus shifts to understanding how two chemically different basalt types—magnesium-rich picrites and more evolved tholeiites—alter under the same temperature, water–rock conditions. The next chapter explores how fracture-controlled alteration develops, why the two basalts produce slightly different clay mineral assemblages, and how olivine composition influences the pathways of alteration. This closer look at the Deccan samples provides a clearer framework for identifying the early steps of aqueous alteration and strengthens the interpretation of similar features seen in Martian meteorites. The comparative study presented in this chapter has highlighted several important parallels between the alteration behaviour of olivine in the Deccan picritic basalts and the Martian nakhlite Yam-593. Despite originating on different planets andexperiencing distinct geological histories, both rock types preserve a remarkablysimilar pattern of fracture-controlled alteration, clay-mineral formation, and cation mobility. These shared features suggest that olivine responds in a broadly comparable way when exposed to small amounts of water under low-temperature conditions. However, the observations from Mars cannot be fully understood without a clearer picture of how terrestrial basalts with different olivine compositions behave under similar fluid-limited environments. This becomes especially important because the Martian olivine in nakhlites is noticeably Fe-rich, while some Deccan olivines are strongly Mg-rich. Understanding how this compositional range influences theformation of secondary minerals, the progress of dissolution, and the stability of clay phases is necessary before we can draw stronger conclusions about Martian alteration

Chapter 5: Alteration Behaviour of High- and Low-Fo Olivine in Basalts

This chapter explores how basalt reacts with small amounts of water under low-temperature conditions, using two types of Deccan basalt as natural examples. Olivine, one of the most reactive minerals in basalt, plays a central role because it readily breaks down to form clay-rich alteration products such as iddingsite. By studying how olivine alters within picritic basalt (rich in magnesium) and tholeiitic basalt (more evolved and iron-rich), this work aims to understand how fluid–rock interaction progresses when water is scarce and confined to narrow fractures. By studying how alteration progresses within fractures of magnesium-rich (high-Fo) and iron-rich (low-Fo) olivine, this work explores how water–rock interaction begins and evolves under restricted fluid conditions. Although this study is based on terrestrial basalts from the Deccan Traps, the results are valuable for understanding similar alteration features observed in some Martian rocks and meteorites. The processes outlined here may mirror how small, short-lived amounts of water once interacted with basaltic crust on Mars, leaving behind mineralogical clues in the form of clay minerals and altered olivine.

5.1. Introduction

Olivine, a silicate mineral composed of iron and magnesium with the general formula $(Mg, Fe)_2SiO_4$, is prevalent and extensively found both on Earth and Mars (Deer et al., 2013). It constitutes approximately 3% to 5% of the basaltic crust on Earth and is one of the abundant minerals within the mantle in differentiated bodies. Notably, olivine undergoes weathering to produce the secondary phase iddingsite at a faster rate as compared to other significant rock-forming silicate minerals (Goldich, 1938; Wilson, 2004). Iddingsite is a reddish-brown mineraloid that forms from the alteration of olivine crystals, commonly observed in basaltic rocks and also identified in Martian meteorites. Due to its non-definite crystal structure, iddingsite is not an International Mineralogical Association (IMA)-recognized mineral species, but rather a collective term describing the complex assemblage of secondary phases formed during the alteration of olivine. It typically comprises a mixture of clay minerals, iron oxides, and ferrihydrites that develop through hydration and oxidation processes. The process of its formation, referred to as "iddingsitisation," denotes the alteration of olivine into this composite assemblage rather than the formation of a distinct mineral phase. Textural analyses of iddingsite and the associated clay minerals are thus useful for comprehending the interactions between minerals and water (near surface or subsurface), the degree and extent of alteration, reaction kinetics, and the pathway. Clay minerals serve as unequivocal evidence for the presence of water, while also supporting the potential for preservation of biosignatures and favorable conditions for habitability, making them key indicators of environments capable of supporting and sustaining life. The alteration of olivine induces the formation of a smectite group of phyllosilicates that has the capacity to adsorb organic matter (Murray et al., 2024). The recent detection of organic

molecules in clay minerals from Jezero Crater on Mars also indicates that clay minerals may be a potential host for planetary habitability (Sharma et al., 2023).

Olivine is equally prevalent in continental flood basalts (CFB) worldwide. TheDeccan Traps basaltic province (Cretaceous-Paleogene) in India is one of the most well- studied flood basalts globally (Krishnamurthy et al., 2020, and references therein). Both picritic and tholeiitic basalts are frequently observed at the outcrop level in different sectors of the Deccan CFB in western India (Chatterjee et al., 2024). High Fo (high MgO) olivine grains (Fo ~ 90 mol%) are typically common in picritic basalt, whereas low Fo olivine (Fo ~ 84−70 mol%) is more prevalent with tholeiites. The weathering of the basaltic profile in Deccan CFB is well exposed due to the effect of the tropical and humid climate after the emplacement of basalts at the Cretaceous-Paleogene boundary. Thus, the olivine-altered phyllosilicates/ clay minerals (also known as iddingsite) are expected to be prevalent due to water-rock interaction. This mineralogical transformation during weathering is of increasing importance for interpreting and validating the basaltic substrate alteration elsewhere. Despite comprehensive investigations, iddingsite is still inadequately characterized, with numerous uncertainties regarding fluid/rock ratios, fluid composition, reaction pathways, and mineral transformations. To bridge these gaps, detailed petrographic studies, including microstructural analyses and mineral chemistry assessments, are essential and provide a foundation for further geochemical modelling. The variety of alteration features and the mechanisms behind the formation of hydrous minerals highlight the critical influence of water-rock interactions. It remains unclear whether these minerals originated from a single extended episode with multiple stages or from separate fluid episodes. The objectives of this paper are to (1) investigate the

microstructures resulting from the interaction between chemically distinctive olivinegrains (high and low Fo) and water, (2) infer the conditions of formation of secondary minerals, and (3) employ geochemical modelling to quantify the physicochemical conditions associated with the alteration process.

Mars is largely known as a basaltic planet. In the geologic past, Mars has experienced wet and warm epochs, and liquid water is thought to have existed on Mars' surface and subsurface. The presence of a significant proportion of phyllosilicates, along with other hydrated minerals, is currently suggested as a major reservoir of wateron Mars (Wernicke & Jakosky, 2021) and holds clues into the planet's potential for past

habitability (Sleep et al., 2011). Therefore, understanding the physicochemical conditions for the formation of the olivine-altered clay minerals is important not onlyfor comprehending olivine dissolution on Earth but also for validating the data collectedby current and future rovers on Mars.

In the context of the present work, the tholeiitic dykes provide an important lithological contrast to the picritic basalt samples. The geological setting and field characteristics of the terrestrial samples have already been addressed in the previous chapters; Together, the picritic and tholeiitic samples allow for a comparative assessment of olivine alteration processes within the Deccan Volcanic Province.

5.2. Results

5.2.1. Petrography & Microstructures

A total of 6 picritic basalt lava flow samples from Botad, Gujarat, and 21 tholeiitic dykesamples from the Konkan Plain, western Deccan Traps, were collected. For the picriticbasalt flows, samples were taken from both the top and bottom portions, while in the tholeiitic dykes, samples were obtained from the central (core) zones. These samples were studied to investigate the alteration of olivine and to understand the mechanisms responsible for these transformations.

A comprehensive investigation into the formation of iddingsite within olivine grains was conducted through comparative petrographic, microstructural, and mineral chemical analyses of two distinct types of Deccan olivine. In this study, the picritic basalt samples from Botad, Gujarat, contain highly forsteritic olivine (average Fo_{88}), while the tholeiites from Konkan Plain have relatively more evolved olivine (average Fo_{40}). The iddingsites commonly found along the fractures and margins of these olivine grains were thoroughly examined to elucidate the initial geochemical conditions that led to the formation of secondary alteration. Additionally, the study aimed to investigatewhether variations in olivine composition affected the formation of iddingsite.

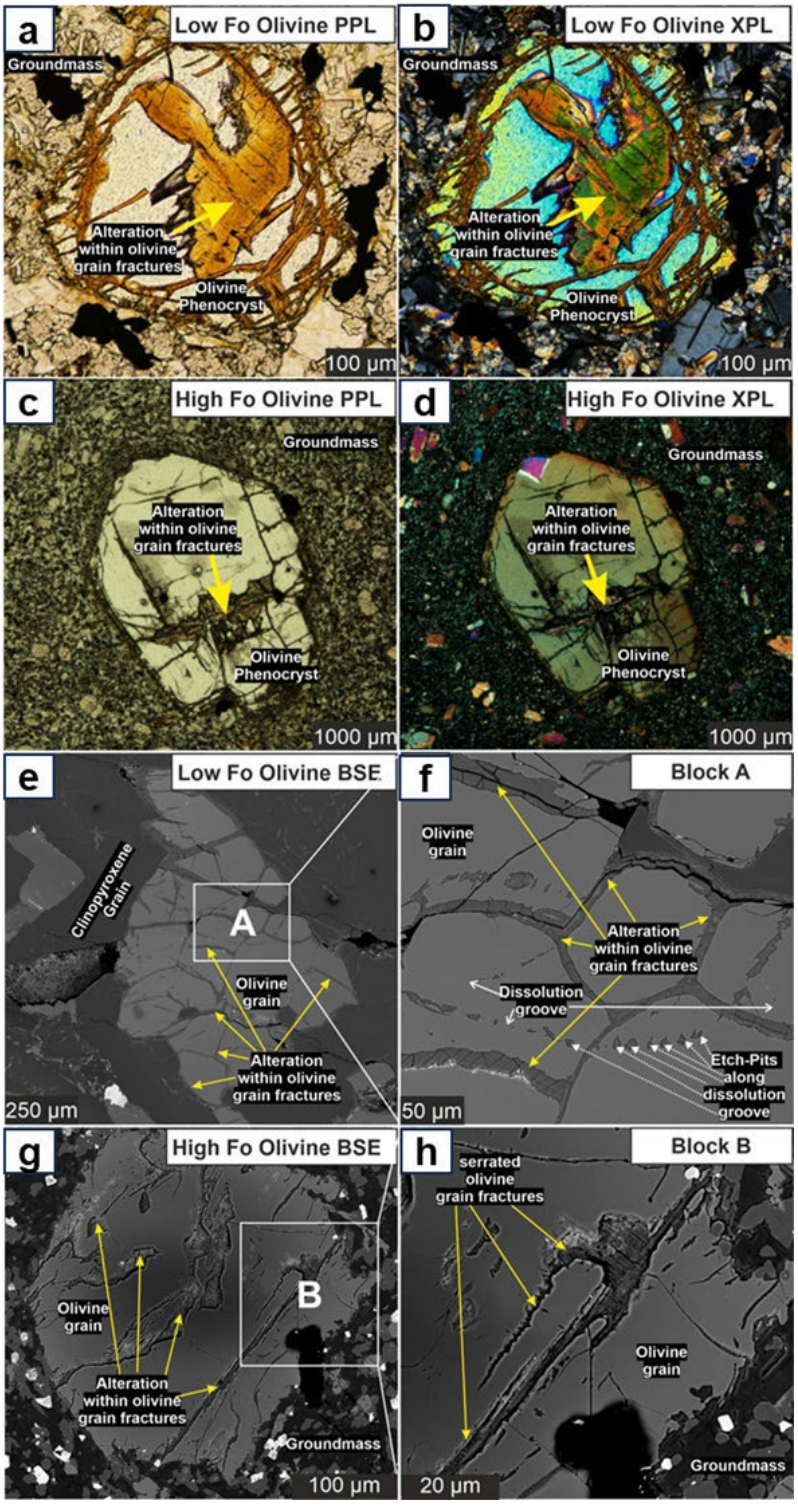

Fig. 5.1: depicts Plane Polarised Light (PPL) and Crossed Nicols (XPL) photomicrographs of tholeiitic (low Fo) and picritic (high Fo) basalt samples. In both cases, a porphyritic texture is observed, with fractured olivine phenocrysts that have deposited altered clay-like products within their fractures. Fig.s 2 (e, f, g, h) show high-magnification back-scattered electron (BSE) images for both basalt types. In Fig.s 2e and 2f, representing the low Fo basalt, the altered mineral-filled fractures within olivine appear relatively smooth, and notable features, such asetch pits and erosional grooves, can be observed. In contrast, Fig.s 3g and 3h, which correspond to the high Fo basalt, display infilled fractures with a distinct saw tooth-like morphology, clearly differing from the smoother textures observed in the low Fo sample.

Under a polarizing microscope, both Deccan basalt samples exhibit a porphyritic texture, characterised by large olivine phenocrysts set within a fine-grained groundmass. The picritic basalt samples exhibit euhedral to subhedral olivine phenocrysts of approximately 3 mm in size. The tholeiite samples have phenocrysts of lath-shaped plagioclase and subhedral olivine, which are relatively smaller (~ 0.5 mm) than those in the picritic basalt samples (Fig. 5.1a-d). The groundmass is primarily composed of plagioclase, clinopyroxene, Fe-Ti oxides, and apatite as accessory phases, and interstitial glass. Both samples exhibit fractures within the olivine phenocrysts, which are filled with brown-coloured infillings. These infillings are identified as secondary clay mineral products resulting from the aqueous alteration of the primary minerals due to chemically active fluids. Notably, the fractures in the picritic basalt samples exhibit a serrated appearance, a feature that is absent in the tholeiite. It is also noteworthy that in both samples, the fractures were confined to the olivine grains, and they did not extend into adjacent phases; the altered products were solely found within these fractures of olivine grains.

To further enhance understanding of the secondary products within the olivine grains, backscattered electron (BSE) imaging was conducted on polished thin sections. High-magnification BSE imaging revealed that the altered products within the fractures of the olivine phenocrysts in both Deccan basalt samples are poorly crystalline (Fig. 5.1e-h). The fractures of the olivine grains of picrite basalt display a pronounced serrated structure, characterised by sharp relief. The BSE imaging of the secondary clay minerals appears uniform with a darkish tone. Conversely, in the case of Deccan tholeiites, the fractures in the olivine grains are relatively smooth.

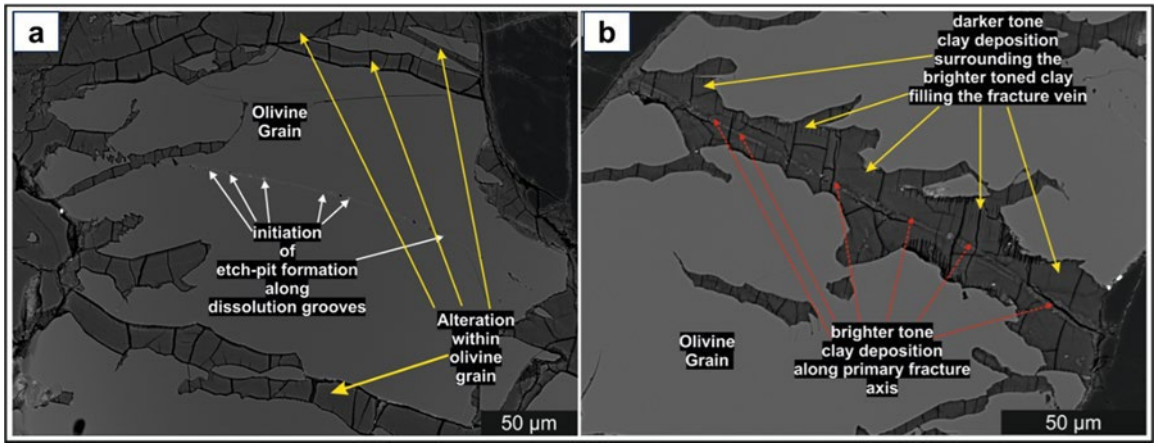

Fig. 5.2: *Backscattered electron (BSE) images of an olivine grain from a tholeiitic basalt (low-Fo olivine) showing fracture development and heterogeneous alteration. (a) Overview image of an olivine grain showing the initiation of alteration along dissolution grooves and the formation of etch pits. Fractures develop within the grain, and alteration is mainly concentrated along these zones. (b) High-magnification image showing heterogeneous filling of fractures. A brighter-toned altered product occurs along the central axis of the fracture, which is surrounded by a thicker layer of darker-toned alteration material, indicating variation in composition within the altered phases.*

A notable observation in these basalt samples is the presence of dissolution grooves throughout the olivine grains (Fig. 5.2a), along with etch-pits that are filled with clay minerals. In some fractures of these basalts, BSE imaging shows at least two distinct altered products: a thin bright layer aligned with the primary fracture axis, surrounded by a darker-toned clay mineral deposits that completely fills the fracture vein, indicating the inhomogeneity of the alteration products (Fig. 5.2b). In both tholeiite and picrite, the iddingsitisation process is exclusively fracture-controlled.

5.2.2. Raman Spectroscopy

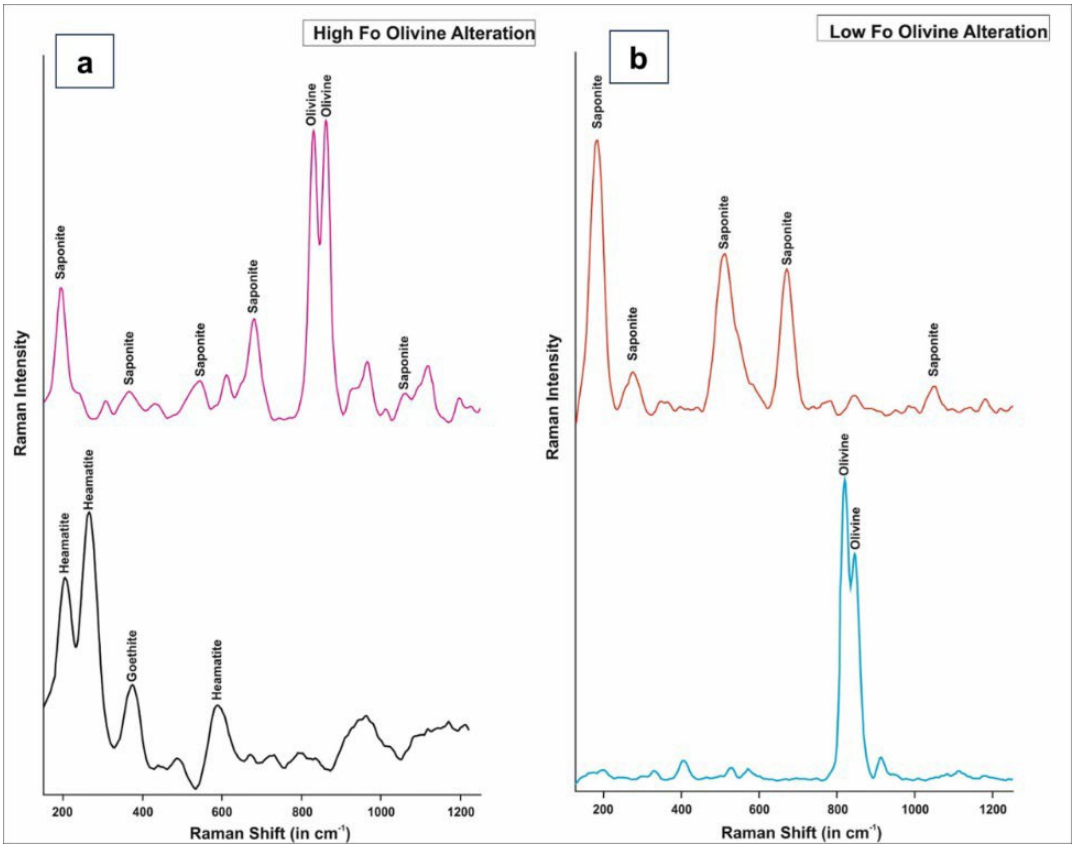

Fig. 5.3: *represents the Raman peaks for the altered product within both basalt samples. In both cases, we see that the altered products that occur within the fractures of the olivine grains mainly exhibit a Raman peak for saponite (a smectite group of minerals). Apart from smectites,the altered phase also shows peaks for Fe ioxide4s, which are mixed in homogeneously. Such a mineral assemblage is termed as iddingsite (Smith et al., 1987).*

In order to characterize the minerals as well as the altered products within the fractures, Raman analysis of the thin sections of picrite and tholeiite basalts was performed. The picritic basalt sample contains large phenocrysts of olivine, which are characterized by strong and prominent doublet peaks at approximately 821 and 852 cm^{-1}, respectively (Keubler et al., 2006) (Fig. 5.3a). Petrography revealed that these olivine grains are fractured and are filled with altered products (clay minerals). These clay minerals exhibit Raman shifts at approximately 196, 363, 552, 680, and 1050 cm^{-1} (see Fig. 5.3a, b), confirming that the clay mineral is saponite (Kloprogge & Ponce, 2021), a type of smectite within the group of minerals. Additionally, the dominant Fe oxides in the

picrite basalt sample include hematite, which is recognized by characteristic Raman peaks at 221, 292, and 611 cm^{-1}, respectively (Veneranda et al., 2019). Alongside these, we also find the presence of goethite represented by the Raman peaks at 386 cm^{-1} (Hernanz et al., 2008). These heterogeneous mixed phases of Fe-oxides, along with the saponite phyllosilicate, are termed iddingsite (Smith, 1987). Under petrography, this appears as rust-coloured secondary infilling within olivine fractures, matching the description given by Bunch and Reid (1975).

The tholeiites comprise olivine phenocrysts, which also display a characteristic Raman shift at approximately 820 and 850 cm^{-1} (Keubler et al., 2006) (Fig. 5.3b), similar to the picritic basalt. In this basalt sample, the clay minerals within the olivine exhibit Raman shifts at approximately 196, 280, 513, 680, and 1050 cm-1. This clay mineral also shows similarity with saponite (Kloprogge & Ponce, 2021).

5.2.3. Mineral Chemistry

The chemical analyses of olivine and the altered products within the fractures of olivine grains for both picritic (high Fo) and tholeiitic (low Fo) basalt samples are given in Tables 5.1 and 5.2, respectively. Characterization of the altered products via Raman spectroscopy suggests that saponite is the predominant mineral present in both Deccan basalt samples. It is imperative that we discuss the chemical behaviour of these clay minerals as well as the host primary minerals (in this case, olivine).

Table 5.1: represents olivine grain composition for both picritic (high Fo) and tholeiitic (low Fo) basalt samples

	High Fo Olivine Grain					**Low Fo Olivine Grain**			
	Grain 1	**Grain 2**	**Grain 3**	**Grain 4**		**Grain 1**	**Grain 2**	**Grain 3**	**Grain 4**
	N=36	***N=49***	***N=16***	***N=35***		***N=24***	***N=8***	***N=7***	***N=15***
SiO_2	40.5	39.48	38.83	38.75	**SiO_2**	33.63	34.18	32.87	34.26
TiO_2	b.dl	b.dl	0	0	**TiO_2**	0.05	0.03	0.05	0.02
Al_2O_3	0.06	0.03	0.11	0.02	**Al_2O_3**	0.01	0.01	0.01	0.02
FeO (T)	10.8	11.65	12.11	12.2	**FeO (T)**	50.49	47.65	54.79	43.46
MgO	47.63	46.99	47.01	47.13	**MgO**	15.8	18.34	12.77	21.03
MnO	0.16	0.19	0.18	0.18	**MnO**	0.71	0.63	0.82	0.56
CaO	0.25	0.47	0.29	0.45	**CaO**	0.26	0.28	0.2	0.28
Na_2O	b.dl	b.dl	b.dl	b.dl	**Na_2O**	b.dl	b.dl	b.dl	b.dl
K_2O	0.02	0.02	0.01	0	**K_2O**	0.02	0.02	0.02	0.02
P_2O_5	b.dl	b.dl	b.dl	b.dl	**P_2O_5**	0.06	b.dl	0.09	b.dl
Cr_2O_3	0.08	0.06	0.08	0.05	**Cr_2O_3**	b.dl	b.dl	b.dl	b.dl
NiO	0.34	0.28	0.33	0.28	**NiO**	0.04	0.04	0.02	0.07
Total	**99.86**	**99.19**	**98.96**	**99.09**	**Total**	**101.1**	**101.21**	**101.64**	**99.72**
Fo Content	**0.9**	**0.88**	**0.87**	**0.87**	**Fo Content**	**0.36**	**0.41**	**0.29**	**0.46**
Fa Content	**0.1**	**0.12**	**0.13**	**0.13**	**Fa Content**	**0.64**	**0.59**	**0.71**	**0.54**
b.dl	Below detection Limit								

Table 5.2: represents the composition of the altered products within the fractures of olivine grains for both picritic (High Fo) and tholeiitic (low Fo) basalt samples

	High Fo Olivine Grain Alteration in fractures							Low Fo Olivine Grain Alteration									
	Grain 1	**Grain 2**	**Grain 3**	**Grain 4**	**Grain 5**	**Grain 6**		**Grain 1**	**Grain 2**	**Grain 3**	**Grain 4**	**Grain 5**	**Grain 6**	**Grain 7**	**Grain 8**	**Grain 9**	**Grain 10**
	N= 11	***N= 19***	***N= 29***	***N= 41***	***N= 45***	***N=35***		***N=25***	***N=38***	***N=9***	***N=11***	***N=38***	***N=10***	***N=32***	***N=30***	***N=35***	***N=25***
SiO_2	35.61	39.3	40.71	44.52	41.01	44.92	**SiO_2**	38.41	36.78	43.81	39.42	39.01	31.6	38.35	39.17	45.19	43.82
TiO_2	0.02	0.02	0.02	0.02	0.02	0.02	**TiO_2**	0.09	0.06	0.06	0.06	0.06	0.07	0.04	0.05	0.04	0.06
Al_2O_3	5.42	5.32	2.92	6.3	5.9	3.05	**Al_2O_3**	3.8	4.38	3.39	2.7	3.47	8.43	3.78	2.53	2.56	2.68
FeO (T)	19.95	15.1	13.96	15.39	14.34	10.14	**FeO (T)**	30.28	29.61	29.38	31.64	28.81	35.65	26.79	27.15	29.07	28.38
MgO	14.94	14.6	15.1	16.3	17.3	18.42	**MgO**	4.8	6.36	6.92	3.43	3.99	7.18	4.63	3.95	4.41	4.95
MnO	0.08	0.09	0.05	0.05	0.05	0.04	**MnO**	0.34	0.28	0.3	0.28	0.25	0.2	0.21	0.24	0.27	0.28
CaO	1.47	2.11	1.57	0.95	1.35	1.06	**CaO**	2.42	2.33	2.03	2.52	2.64	0.96	2.51	2.1	1.65	1.7
Na_2O	0.15	0.25	0.14	0.06	0.18	0.11	**Na_2O**	0.21	0.14	0.2	0.18	0.18	0.1	0.17	0.02	0.08	0.08
K_2O	0.22	0.33	0.32	0.18	0.23	0.22	**K_2O**	0.51	0.45	0.45	0.48	0.43	0.18	0.36	0.31	0.29	0.18
P_2O_5	0	0	0	0	0	0	**P_2O_5**	b.dl	b.dl	b.dl	b.dl	b.dl	0.02	b.dl	b.dl	b.dl	b.dl
Cr_2O_3	b.dl	0.04	0.05	0.06	0.06	0.08	**Cr_2O_3**	b.dl	b.dl	b.dl	b.dl	b.dl	b.dl	b.dl	b.dl	0.03	b.dl
NiO	0.14	0.13	0.17	0.24	0.2	0.25	**NiO**	0.04	0.07	0.06	0.1	0.07	0.04	0.11	0.11	0.11	0.08
Total	**77.98**	**77.39**	**75.12**	**84.09**	**80.63**	**78.31**	**Total**	**80.91**	**80.48**	**86.61**	**80.82**	**78.92**	**84.44**	**76.96**	**75.65**	**83.7**	**82.22**
XMg	**0.57**	**0.63**	**0.66**	**0.64**	**0.68**	**0.76**	**XMg**	**0.22**	**0.25**	**0.27**	**0.15**	**0.19**	**0.27**	**0.22**	**0.2**	**0.21**	**0.23**
Fe/Si	**0.93**	**0.64**	**0.57**	**0.58**	**0.58**	**0.38**	**Fe/Si**	**1.33**	**1.35**	**1.12**	**1.34**	**1.24**	**1.95**	**1.17**	**1.16**	**1.07**	**1.09**
N	**No of Analysis**																
b.dl	**Below detection limit**																

The olivine grains from the picrites have high forsterite (high Fo) content (Mg-rich) whereas the olivine grains from tholeiites are compositionally more evolved. Both the olivine grains show normal compositional zoning. In picrites, the olivine phenocrysts composition ranges from core of Fo_{90} to rims of Fo_{83}, with an average forsterite content of ~Fo_{88}. And in tholeiites, the olivine core to rim composition ranges from Fo_{49} to Fo_{33}, with an average composition of ~Fo_{40} (Table 5.1).

Table 5.1 illustrates the chemical composition of the altered clay minerals found within the fractures of the olivine phenocryst in both basalt samples. The FeO and MgO content of the altered clay minerals also exhibits similar chemical behavior in picrite and tholeiite, respectively.

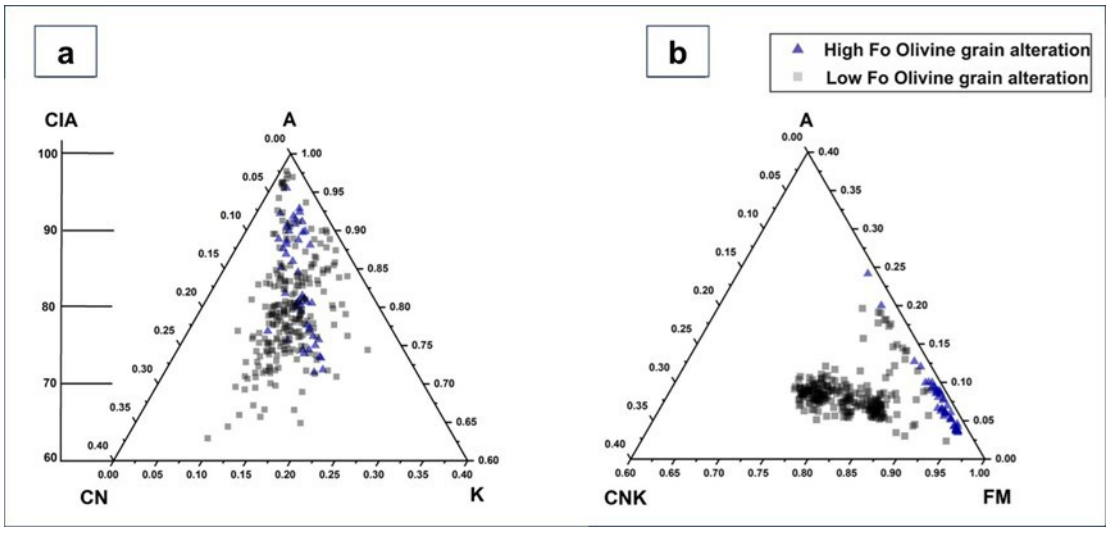

Fig. 5.4*: illustrates ternary diagrams used to examine the behaviour of altered products in both high Fo and low Fo basalt samples. In Fig. a, the Al_2O_3–(CaO^*+Na_2O)–K_2O (A–CN–K) ternary plot is shown, where a similar trend is observed for the altered products in both sample types. As the alteration progresses, continuous leaching of mobile cations, such as CaO^*, Na_2O,and K_2O, occurs, resulting in a relative enrichment of Al_2O_3. Fig. b presents the Al_2O_3– (CaO^*+Na_2O+K_2O)–(Fe_2O_3T+MgO) (A–CNK–FM) ternary diagram, where a comparable behaviour is again observed. The data points align along the A–FM line and cluster near the FM apex, indicating a consistent alteration pathway for both basalt types.*

To gain a better understanding of the extent to which olivine grains have been altered, it is essential to examine the gain or loss of both mobile and immobile cations throughout the alteration process. The elemental loss also serves as a reliable indicator

of the extent of alteration. The Al_2O_3–CaO*+Na_2O–K_2O (A-CN-K) ternary plot (Fig. 5.4a) indicates that the clay minerals in both samples exhibit a similar compositional scatter. In both cases, the clay minerals do not align along any A-CN or A-K axis (Fig. 6a) and have similarly high CIA values, with most samples clustering near the A apex. This indicates an increase in Al_2O_3, while concurrently experiencing leaching of CaO*, Na_2O, and K_2O as the reaction progresses. The Al_2O_3–CaO*+Na_2O+K_2O-$Fe_2O_3^T$+MgO (A-CNK-FM) ternary diagram (Fig. 5.4b) shows an interesting characteristic of the clay minerals. The clay minerals for the picritic basalt (high Fo) samples falls along the A-FM line, with data points concentrated near the FM apex, whereas the clay minerals for the tholeiitic basalt (low Fo) samples appear to be more enriched in CaO*- Na_2O- K_2O (CNK) than its picritic basalt counterpart and hence occupy a region not along the A-FM axis. However, in both scenarios we see an increase in the FM ($Fe_2O_3^T$- MgO) content which signifies substantial enrichment of $Fe_2O_3^T$ and MgO in the clay minerals relative to other components. Furthermore, the binary plots reveal that the iddingsite/clay minerals from both samples behave in a comparable manner.

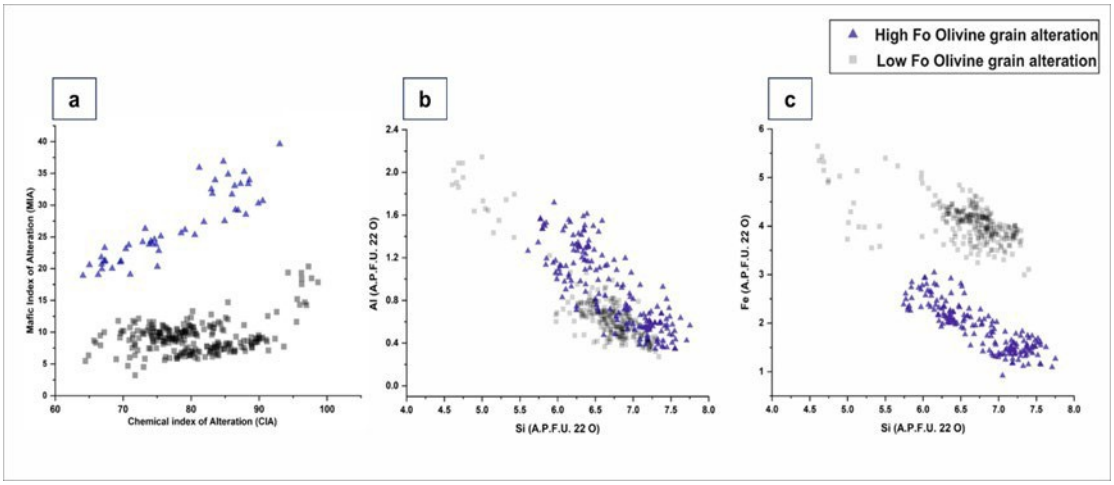

Fig. 5.5*: a represents the Mafic Index of Alteration (MIA) vs Chemical Index of Alteration (CIA) bi variant plot for the altered products in both basalt samples. The CIA for the altered products of both basalt samples remains nearly the same. Also, the altered products for high Fo basalt exhibit a linear correlation between the MIA and CIA, which is notseen for the low Fo counterpart. Fig. (b & c) exhibits a bivariate plot of Al and Fe (a.p.f.u.) versus Si (a.p.f.u.) of the altered products for both basalt samples. A similar trend in the behaviour of the altered products is also seen.*

The Mafic Index of Alteration (MIA: $100\times[(Al_2O_3+Fe_2O_3^T)/(Al_2O_3+Fe_2O_3^T+MgO+CaO^*+Na_2O+K_2O)]$, MIA under reducing condition for tholeiite and MIA under reducing condition for picrite, after (Babechuk et al. 2014) along with the Chemical Index of Alteration (CIA: $[100\times Al_2O_3/(Al_2O_3+CaO^*+Na_2O+K_2O)]$) (Fig. 5.5a) plot exhibit that the clays within the olivine of tholeiite is likely to have experienced a lower MIA as compared to thosein the picrite basalt, whereas the CIA of the clays remain relatively similar.Consequently, there are chemical differences between the clay minerals from tholeiiteand picrite, despite their exhibiting significant similarities. In the MIA versus CIAbivariant plot, the clay minerals from both picrite and tholeiite show consistentweathering patterns (Fig. 5.5a). The Al vs. Si and Fe vs. Si bivariant plots (Fig. 5.5b,&, c) suggest that the iddingsite of both the chemically distinct basalt samples have astrong correlation and follows a similar trend and exhibits a consistent Si enrichment.

X-ray maps provide essential insights into the mobility of cations, particularly when analyzing the altered clay minerals within the fractures of olivine grains. These analyses are vital for constraining the leaching and enrichment of clay minerals as the primary minerals undergo alteration. In both scenarios (see Fig. 5.6 and 5.7), the altered products exhibit a depletion of Mg and Fe, alongside an enrichment of Ca, Al, and Si, relative to the host phase (olivine).

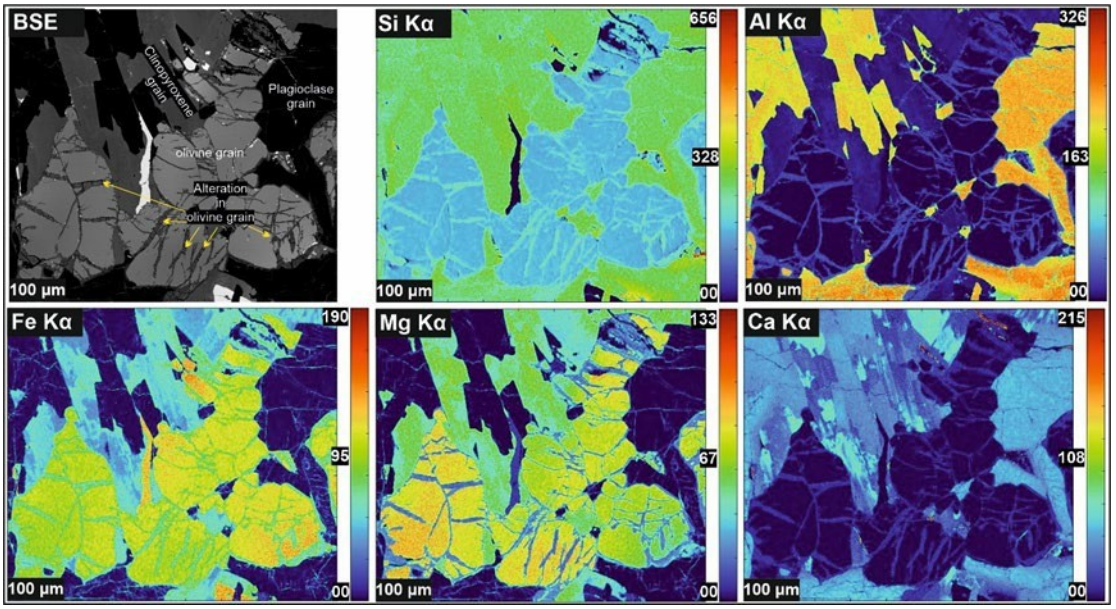

Fig. 5.6: *represents the X-ray map of the olivine. This figure represents the olivine grain in the tholeiitic basalt sample. We observe cation mobility where Ca, Al, and Si cations are mainly contributed from the nearby phases present within the groundmass, whereas Mg and Fe are leached from olivine grains and are incorporated into the altered phase mixture.*

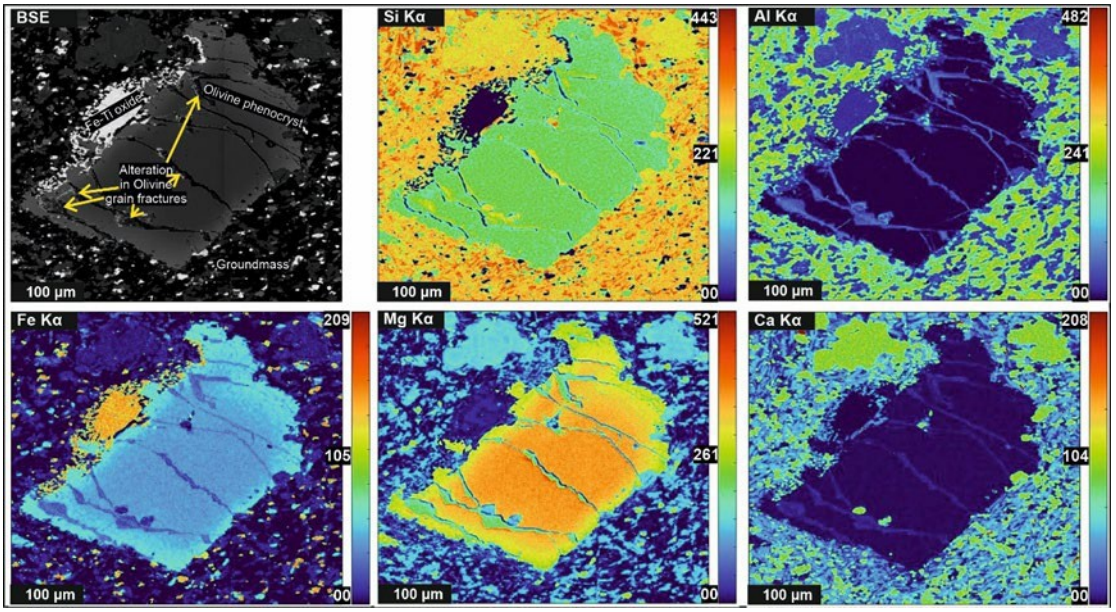

Fig. 5.7: represents the X-ray map of the olivine. This Fig. represents the olivine grain in the picritic basalt sample. Here just like the tholeiitic basalt counterpart we observe similar cationmobility, where Ca, Al, and Si cations are mainly contributed from the nearby phases present within the groundmass, whereas Mg and Fe are leached from olivine grains and are incorporated into the altered phase mixture

.

5.3. Discussions

5.3.1. Formation mechanism of veins

The majority of secondary minerals in olivine (either along fractures and the margin) suggest olivine is more reactive as compared to the adjacent pyroxene and plagioclase (Goldich, 1938). Likewise, when compared to other common orthosilicates, olivine is particularly susceptible to breakdown (Velbel, 1999). A crucial observation is that the alteration products are limited to the fractures within the host olivine grains, indicating that the alteration in these basalt samples is primarily fracture-controlled and that the alteration that happened in both the samples occurred in a rather limited water-rock ratio condition, owing to the high susceptibility of olivine to erode (Velbel, 1999).

The space for secondary mineral veins is inferred to have been produced either by the dissolution of olivine or the opening of fractures and filling up. The opening of fractures can't be fully discounted, especially when the fractures are relatively wide within the olivine grains from tholeiite. Nevertheless, the formation of fine serrations along the vein walls is primarily attributed to the dissolution-precipitation mechanism. However, a few veins show smooth outline walls and the absence of typical fine-scale serrations. Moreover, the formation of serrated veins in olivine does not always imply different conditions of aqueous alteration events. Additionally, serrations are also dependent on their crystallographic orientation. They are more prominent only on those veins that have been cut at low angles to (100), and the crystallographic orientation dictates the rate of reaction between vein walls and aqueous solution. Further, only those olivine-hosted veins whose walls were parallel to (001) are widened as alteration progresses (Lee et al., 2015a). Additionally, dissolution rates were often locally enhanced by elastically strained crystal structures associated with dislocations. Plumper et al. (2012) proposed that interface-coupled dissolution-precipitation at the walls of an

initial fracture or etch pit produces hydrous minerals whose volumetric expansion produces stress. These stresses are sufficient to fracture the olivine, thus enabling aqueous solutions to penetrate further into grain interiors. However, the formation of successive layered deposits of secondary minerals is also proposed by Changela and Bridges (2010). The typical layering structure is only noticed in low Fo olivine from tholeiite, likely suggesting multiple episodes of aqueous alteration events. The presence of etch-pits and dissolution grooves is also consistent with this finding. Furthermore, the formation of corrosion features on the retreating olivine surface is linked to prolonged interaction with aqueous fluids at relatively low thermal conditions (Velbel, 2009). The pits associated with iddingsite from tholeiite suggest the weathering of olivine occurred after, rather than during, the alteration process. The etch feature is produced by weathering, superimposed on previously iddingsitised olivine, and is morphologically identical to those formed through weathering in the absence of prior alteration products. The poorly crystalline nature of the alteration product, which forms at low-temperature conditions, also corroborates the other petrographic findings.

The alteration of low-Fo and high Fo olivine and formation of secondary mineral veins occurred through a fracture-controlled, low-temperature dissolution–precipitation mechanism under limited fluid conditions. Olivine's higher reactivity led to preferential alteration along fractures, influenced by crystallographic orientation and local strain. Layered vein structures and corrosion features indicate multiple episodes of aqueous alteration followed by weathering, consistent with interface-coupled dissolution–precipitation of olivine along initial microfractures led to volumetric expansion and further cracking. Both dissolution-driven and stress-assisted processes operated together, resulting in progressive, fracture-controlled alteration of olivine to iddingsite under low-temperature, fluid-rock interaction. It remains to be established

whether the distinct olivine surface textures formed by aqueous alteration at different temperatures are a consequence of the difference in temperature, of the presence of a product, or of different geochemical conditions associated with the product-forming conditions.

5.4.1. Temperature of Formation

Earlier views argued olivine alteration as a deuteric alteration, and the iddingsitisation was interpreted as a high-temperature, magmatic process (Sheppard, 1962). Later,Baker and Haggerty (1967) proposed that iddingsite actually represents a mixed mineralphase rather than a single phase, and the associated goethite and phyllosilicate correspond to low-temperature and oxidative hydrothermal alteration. Later, Eggleton(1984), using the TEM, further demonstrated the fine-scale mineralogy of the iddingsite.

To comment on the temperature of iddingsite formation, it is important to document the associated mineral first. The typical mineral association of saponite and goethite suggests a low-temperature alteration (<140ºC, Baker and Haggerty, 1967).The presence of goethite is further suggestive of an oxidative alteration. The coincidence of iron oxides and hydroxides with the degradation of the olivine doublet in Raman spectra reflects the concurrent oxidation of iron with alteration (Kuebler et al., 2013). However, in tholeiite, the iron oxides and hydroxides are absent, suggesting a mildly reduced environment (Baker & Neil, 2017).

In the A-CN-K plot, both low and high Fo olivine altered clay show similar behaviour where there is very little K-enrichment, suggesting leaching of K from nearby phases and incorporation within the clay as alteration progresses (Fig. 5.6a). Theclay mineral composition is also significantly Fe-Mg rich as understood in the A-CNK-FM plot (Fig. 5.4b). The low MIA values of altered clays in both picritic (high Fo) and

tholeiitic (low Fo) basalt samples signifies that the alteration that happened in both the basalt samples happened in a relatively closed-system with limited water-rock ratio (Fig. 5.5a). The resultant clay minerals in tholeiite is comparatively Fe-rich, and under a reducing condition, the rate of dissolution of fayalite is relatively higher as compared to forsterite (Hausrauth & Brantley, 2010). The gradual increase in Si with respect to Al and Fe suggests that alteration took place in a relatively acidic environment (Fig. 5.5b, c). This alteration may have resulted from cation migration, as evidenced by the X-ray maps (Fig. 5.6). Saponite, similar to nontronite, incorporates some Al^{3+} ions that substitute for Si^{4+} in the tetrahedral layer. Although the aluminium content may be minimal, it raises questions regarding its presence in a pseudomorph derived from a mineral that initially lacked aluminium. It is plausible that the aluminium found in these clay minerals is a result of hydrothermal alteration, facilitating the transfer of aluminium from surrounding minerals. This phenomenon is illustrated in the X-ray map of the Deccan olivine grain, which indicates that aluminium is likely concentrated in the fractures of the olivine, originating from the groundmass (Fig. 5.6 & 5.7).

5.4. Implications for Mars

Olivine is a common and geochemically important mineral on Mars. The olivine-bearing formations have been identified on the surface of Mars through various studies (Rogers et al., 2005; Ody et al., 2012 and references therein). McSween et al., (2006) determined that the rocks found in the Gusev crater, which exhibit a high olivine content (approximately 15–20%), are indicative of primitive mantle magmas that have erupted as picritic basalts. Additionally, olivine has been detected through *in situ* analyses conducted by the Curiosity rover at Gale Carter (Lane & Christensen, 2013). Recently, olivine-rich outcrops from the Seiteh Formation in Jezero Crater suggested moderate alteration by the aqueous fluid (Tice et al., 2022). Olivine is also abundant in Martian

meteorites (Shergottite-Nakhla-Chassignite). Mild aqueous alteration of olivine in Nakhla is evidenced by a suite of secondary minerals collectively termed as iddingsite (Changela & Bridges, 2010; Lee et al., 2015a; Daly et al., 2019).

Applying evidence from a terrestrial analogue to the Martian context is challenging, especially in the absence of a source area. Therefore, the well-documented terrestrial continental flood basalt, specifically the Deccan Traps in India, offers an opportunity to compare the mineralogical and geochemical characteristics of secondary minerals. Orbiter and meteoritic evidences indicate the presence of secondary minerals resulting from water-rock interaction within basaltic crusts. The infrared spectrometers CRISM (Compact Reconnaissance Imaging Spectrometer for Mars) and OMEGA (Observatoire pour la Minéralogie, l'Eau, les Glaces et l'Activité) have been employed to identify phyllosilicate and carbonate similar to those found in meteorites (Carter et al., 2013). The detection of smectite and associated clay minerals by the Mars 2020 Perseverance rover also aligns with previous discoveries of clay on Mars. The impact-induced hydrothermal activity at crater walls and ejecta produced conducive environment compatible with the conditions suggested formation of terrestrial iddingsite at surface and near-surface environments. Additionally, the microtextural similarities such as serrated fractures, dissolution pits, and vein-filling secondaryphases observed in both terrestrial and Martian olivine grains indicate that comparable alteration mechanisms likely operated on the two planets. In terrestrial basalts, such textures typically form through a dissolution–precipitation process driven by low-temperature interaction between basaltic rocks and percolating aqueous fluids under oxidising and mildly acidic conditions. The limited fluid flux and low water–rock (WR) ratios promote incomplete alteration, resulting in the formation of Fe–Mg smectite (iddingsite) assemblages along cracks and grain boundaries.

On Mars, similar alteration features identified in olivine-bearing meteorites (e.g., Nakhla) and surface basalts (e.g., Gusev and Jezero craters) suggest that transient aqueous activity under geochemically analogous conditions—oxidising, low pH, and low W/R ratios—could have driven partial hydration and oxidation of olivine. The mineral assemblages dominated by Fe-rich smectites, and oxides on Mars are consistent with such a process. In addition to the oxidizing fluid conditions observed on Mars (Hicks et al., 2014), experimental validations have been made regarding octahedral site substitutions of Fe^{2+} and Fe^{3+} in smectite solid solutions (Grauby et al., 1994), which may contribute to the elevated Fe content observed in the smectite found in both Fe-rich terrestrial and Martian iddingsite. Furthermore, a significant distinction between terrestrial and Martian assemblages is that the secondary alteration fluid has been reported to be predominantly composed of Fe-rich carbonate, especially in Lafayette and ALH84001 (Piercy et al., 2022) and formation of iddingsite in Nakhla occasionally linked to the mild shock metamorphism as compared to terrestrial counterpart (Treiman, 2005). Nevertheless, the preservation of hydrated minerals within veins and fractures further indicates that alteration occurred in localized, short-lived aqueous systems, possibly linked to some aqueous fluid or volcanic–hydrothermal events.

Establishing this correspondence between terrestrial and Martian alteration processes provides critical insight into Mars' past geochemical and hydrological evolution. It suggests that even though liquid water was not abundant or long-lived, it was active enough to mediate chemical weathering and secondary mineral formation. Moreover, these limited-aqueous environments would have been thermodynamically favourable for the preservation of organics and could have served as transient habitable niches, contributing to the long-term retention of life-related compounds on Mars.

5.5. Conclusion

Alteration of olivine to iddingsite is generally confined to the fractures of olivine grains from Deccan Trap basalt irrespective of their chemical composition (high and low Fo). The high Fo picritic basalt exhibits a typical serrated fracture (saw-tooth features), while the fractures in low Fo olivine are wide and relatively straight. In case of the low Fo olivine, the altered products, which are dominated by the smectite group at the initial phase of alteration when a minimal amount of rock is undergoing alteration of mineral (saponite-nontronite), remain stable for a wider array of WR conditions (1-50) as compared to the high Fo olivine alteration scenario (WR 10-50). However, the temperature of alteration remains low during the aqueous alteration. Multiple aqueous alteration events are also likely proposed for layered clay minerals in Low Fo olivine under a mildly reducing condition. On the other hand, the picritic basalts experienced comparatively a low pH, low water to rock ratio condition as compared to the tholeiitic basalts. The higher Si content in saponite is also indicative of low temperature, hydrothermal alteration under acidic conditions. The variability within the altered products, as illustrated in petrography (Fig.5.2b) for the low Fo basalt sample, has been validated by simulation, suggesting a more progressive type of alteration.

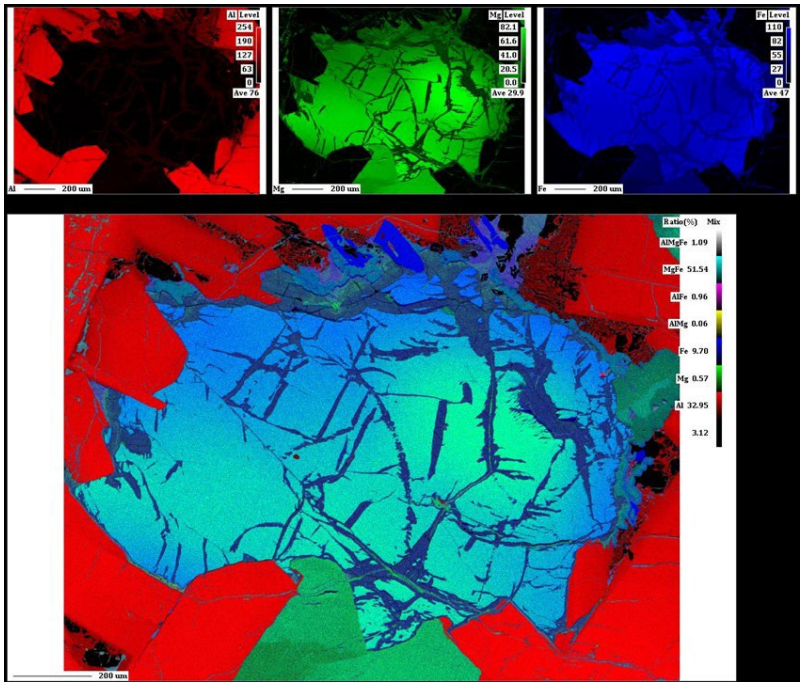

Fig. 5.8: *depicts an elemental X-ray map showing the distribution of Al, Mg, and Fe within an altered olivine phenocryst. The top row displays individual element maps for Al (red), Mg (green), and Fe (blue), highlighting elemental zoning and fracture-controlled alteration. The bottom composite map presents a quantitative phase map based on elemental ratios.*

This variability is further highlighted by the Mg Kα X-ray map of the low Fo sample (Fig. 5.8), where Mg-rich altered products are observed to form along the fracture axis, while the Mg-poor clay products encircle the Mg-rich clay that occupies the remainder of the fracture, confirming the idea of alteration product heterogeneity. These findings could have significant implications for comprehending alteration processes on Mars, as they may assist in defining the geochemical conditions and the characteristics of the fluid involved. Research on terrestrial analogues, although differing in their fundamental mineral composition (such as Fe and Mg levels), demonstrates alteration products and conditions that closely resemble those observed in Martian meteorites, thus helping in deciphering episodes of alteration during the water-crust interaction on Mars. Additionally, phyllosilicates/ clay significantly enhances the preservation potential of biosignatures on Mars, which continues to be the foremost priority of the ongoing and future Mars missions.

The detailed petrographic and mineral-chemical analyses presented in this chapter demonstrate how olivine in both picritic and tholeiitic Deccan basalts undergoes alteration when exposed to limited amounts of water at low temperature. Although the two basalt types differ in their Fo content, fracture morphology, and early dissolution pathways, the overall style of alteration remains remarkably similar: only a small portion of each olivine grain participates in the reaction, the secondary products are dominated by smectite clays with varying Mg and Fe proportions, and the extent of alteration remains low even where fluids penetrated the fractures. These findings reinforce the idea that water availability—not temperature alone—was the main control on alteration in these systems. Furthermore, the behaviour observed in these terrestrial samples mirrors many of the features documented in the nakhlite Yam-593, suggesting that similar physico-chemical constraints may have operated on Mars.

However, while petrography and mineral chemistry provide essential qualitative insights, they cannot by themselves quantify the fluid compositions, pH evolution, mineral stability fields, or precise water-to-rock ratios that drove these alterations. To move beyond descriptive observations, a more controlled and quantitative approach is required—one that can test how changes in olivine composition, water availability, and temperature influence the progression of alteration. The following chapter addresses this need by applying geochemical modelling to both Mg-rich and Fe-rich Deccan basalts, and then extending the same framework to the Martian nakhlite Yam-593. Through these simulations, the next chapter reconstructs the chemical conditions that best reproduce the natural alteration features observed in the previous chapters and provides a unified geochemical basis for understanding aqueous alteration under fluid-limited conditions on Earth and Mars.

Chapter 6: When Earth's Basalts Explain Mars: A Geochemical Modelling Approach

Understanding how basaltic rocks respond to small amounts of water is essential for interpreting alteration processes on both Earth and Mars. In the previous chapters, the petrography, mineral chemistry, and elemental mapping of Deccan basalts and the Martian nakhlite Yam-593 showed that alteration was extremely limited, restricted mainly to fractures in olivine, and produced only small quantities of smectite clays and iron-rich products. However, they could not fully explain the chemical conditions that made these transformations possible. To address this gap, this chapter uses geochemical modelling to recreate the alteration environment under controlled conditions and to test how different olivine compositions, water–rock ratios, and temperatures influence the formation of secondary minerals. In this chapter, this modelling approach is applied to Mg-rich picritic basalt, Fe-rich tholeiitic basalt, and the Fe-rich Martian olivine in Yam-593. By using natural thermal-spring water compositions and running simulations across 25–75°C under restricted water availability, the models capture the low-temperature to mild hydrothermal settings thought to have operated in the Amazonian on Mars. By comparing the terrestrial and Martian outcomes, the modelling provides a clearer understanding of the physico-chemical environment that may have existed onMars when the nakhlites altered, and demonstrates how terrestrial basalts can be usedas meaningful analogues

6.1. Introduction

Olivine is a common mineral in basaltic rocks on both Earth and Mars and is known for its sensitivity to chemical weathering (Goldich, 1938; Nesbitt & Wilson, 1992). Because olivine alters much faster than other major silicate minerals, it often records the earliest signs of water–rock interaction. These early alteration stages usually produce a mixture of smectite clays and iron oxides, commonly referred to as iddingsite (Baker & Haggerty, 1967; Smith, 1987). This mixture is important because it forms only when water is present, and its mineralogy can help identify the chemical conditions that existed when alteration took place.

Both Earth and Mars show evidence for such alteration in basaltic settings. On Earth, the Deccan Continental Flood Basalt (CFB) province in western India contains olivine-bearing basalts that display clear signs of fracture-controlled alteration. On Mars, olivine-bearing nakhlites including Yam-593—also contain fractures lined with clay minerals and iron oxides (Changela & Bridges, 2010; Lee et al., 2015a). Although the two planets have very different climates and water histories, the alteration features in these samples appear surprisingly similar.

The Deccan basalts provide an excellent terrestrial analogue for understanding olivine alteration under limited water availability. Picritic basalts from Botad, Gujarat, contain highly forsteritic olivine (Fo ~88), whereas tholeiitic basalts from the Konkan Plain contain more Fe-rich olivine (Fo ~33–49). In both cases, alteration is observed mainly within fractures of olivine grains, while neighbouring minerals remain mostly unaltered. This indicates that water–rock interaction occurred under very low water-to-

rock (W/R) ratios, where only small amounts of water interacted with the rock, as also inferred for the nakhlites (Lee et al., 2015b; Daly et al., 2019).

Clay minerals documented in these Deccan samples include smectite-group minerals such as saponite and nontronite, along with iron oxides like hematite and goethite (Veneranda et al., 2019; Hernanz et al., 2008). Similar mixtures of smectite and iron oxides define the iddingsite found in nakhlites (Smith, 1987; Changela & Bridges, 2010). Because the nakhlites formed under Martian conditions, their alteration provides rare evidence of past aqueous activity on Mars, particularly during the Amazonian period when water was limited.

To understand these alteration processes more clearly, geochemical modelling provides a controlled way to simulate fluid–rock interaction using measured rock compositions, fluid chemistry, and temperature conditions. In the Deccan basalts, alteration was found to be restricted to olivine fractures, suggesting the system behaved like a closed environment with limited fluid circulation. Raman spectroscopy confirmed that the altered products were mainly smectites and iron oxides formed under low-temperature conditions, generally below 200°C (Keubler et al., 2006; Kuebler et al., 2013). Because the same mineral groups appear in the nakhlites, the Deccan modelling results can be used to help interpret the geochemical setting in which alteration occurred on Mars.

This chapter combines the modelling components from the earlier work on Deccan basalts and the nakhlite Yam-593 to present a unified geochemical analysis. The aim is to compare alteration in Mg-rich picritic olivine, Fe-rich tholeiitic olivine, and Fe-rich Martian olivine, all under similar low-temperature and low-W/R conditions. The

combined modelling approach helps address several key querries expressed in previous chapters:

- Understanding how differences in olivine composition (high Fo versus low Fo) influence the specific clay minerals that form during alteration.
- Identifying the range of water-to-rock ratios and temperatures that best reproduce the alteration textures observed in both terrestrial and Martian samples.
- Using the Deccan modelling results to help constrain the possible geochemical conditions that existed on Mars when the nakhlites underwent alteration.
- Assessing whether the similarities between Deccan and Martian alteration are consistent with alteration occurring under conditions of limited water availability.

By exploring these questions, this chapter helps link terrestrial and Martian alteration pathways. The results from the modelling not only support petrographic observations but also provide quantitative constraints on water–rock ratios, fluid chemistry, pH evolution, and mineral stability. These details are important for interpreting the alteration history recorded in nakhlites, which represent one of the few ground-truth samples available from Mars.

6.2. Geological Framework and Sample Information

6.2.1. Deccan Basalts

The Deccan Flood Basalt province is one of the largest continental basalt provinces on Earth, with lava flows, dykes, and intrusions showing a variety of basaltic compositions (Krishnamurthy et al., 2020). Picritic basalts from Botad contain olivine with Fo values around 88–90, whereas tholeiitic basalts from the Konkan Plain contain evolved olivine with Fo values around 33–49. Weathering in this tropical basaltic terrain has produced

visible alteration, especially within olivine fractures, which are often filled with clay minerals and iron oxides. Petrographic work shows that the fractures in picritic basalts have a serrated morphology, while fractures in tholeiitic basalts are smoother. In both cases, alteration is confined to the olivine grains, supporting the interpretation of low W/R conditions (Velbel, 1999). Raman spectroscopy confirms the presence of saponite, nontronite, hematite, and goethite within these fractures. These minerals suggest low-temperature alteration in mildly acidic to mildly oxidizing fluids.

6.2.2. Martian Meteorite Yamato-593

Nakhlite Yam-593 also contains olivine grains fractured and filled with smectite and Fe-oxide phases (Changela & Bridges, 2010). The Fe-rich nature of its olivine resembles that of the Deccan tholeiites, making their comparison meaningful. The alteration in Yam-593 is thought to have occurred under low water availability and limited fluid circulation, similar to the conditions inferred for Deccan olivine fractures. X-ray element maps show similar patterns of enrichment (Si, Al, Ca) and depletion (Mg, Fe) in both terrestrial and Martian altered zones, suggesting that comparable geochemical processes operated in each setting.

6.3. Geochemical modelling

Geochemical modelling was carried out to better understand the chemical environment and conditions under which alteration occurred within the fractures of olivine grains in both the Deccan basalts and the Martian nakhlite Yam-593. Petrographic observations from previous chapters show that in all samples—whether terrestrial picritic basalt, terrestrial tholeiitic basalt, or Martian nakhlite—alteration was highly localized and restricted mainly to the internal fractures of olivine grains. These fractures contain secondary products composed of smectite clays mixed with iron oxides. Such compositions point toward low-temperature alteration under limited fluid availability,

making geochemical modelling an important tool for reconstructing the chemical pathways and conditions that produced these secondary phases. The overall objective of the modelling framework was therefore to simulate early-stage aqueous alteration under controlled conditions, using starting compositions directly derived from the rock samples. By comparing the outcomes for the magnesium-rich picritic basalt, the more iron-rich tholeiitic basalt, and the Fe-rich olivine in Yam-593, it becomes possible to identify shared chemical behaviours as well as differences related to olivine composition. This also helps in narrowing down the possible geochemical conditions that may have existed on Mars during the Amazonian period, when water availability was extremely limited.

Petrography shows that alteration products in all Martian as well as the terrestrial samples occur only within the fractures of olivine grains and do not extend into surrounding minerals such as pyroxene or plagioclase. This spatial confinement implies very restricted fluid movement. The fractures acted as narrow pathways through which small amounts of fluid interacted with olivine, without widespread circulation through the rest of the rock. Such a setting is consistent with a closed-system environment, where the fluid re-equilibrates with the host minerals but does not exchange with the external atmosphere or an open reservoir.

This behaviour is also reflected in Raman spectroscopy results, where smectite peaks and iron oxide (Keubler et al., 2006; Veneranda et al., 2019; Kuebler et al., 2013) features indicate low-temperature alteration in confined spaces. The same kind of fracture-focused alteration appears in nakhlites (Changela & Bridges, 2010; Lee et al., 2015a). Because of this, all simulations in this chapter were conducted assuming closed-system conditions, consistent with the natural observations.

The temperature range selected for the simulations—30°C, 50°C, and 75°C—was chosen to match the conditions suggested by mineralogical and Raman evidence. In both Deccan basalts and nakhlites, the altered products consist mainly of smectite-group clays with iron oxides or hydroxides. These mineral associations are characteristic of low-temperature alteration (Baker & Haggerty, 1967; Eggleton, 1984), typically below 200°C. In the Deccan samples, the presence of poorly crystalline clay minerals and serrated fractures further indicates low-temperature dissolution–precipitation processes (Velbel, 2009). Since the modelling aims to capture the earliest stages of olivine alteration rather than advanced hydrothermal alteration, this moderate temperature range is appropriate. It also reflects conditions thought to have existed during short-lived aqueous events on Mars, such as local hydrothermal activity or limited subsurface water (Changela & Bridges, 2010; Tice et al., 2022).

A key part of the modelling framework involved varying the water-to-rock (W/R) ratio to examine how different degrees of fluid availability influence clay mineral formation. Based on petrographic observations, the alteration is extremely limited, and only small amounts of clay minerals have formed within the fractures. This suggests low W/R ratios, since only a small fraction of the olivine reacted. For the Deccan basalt simulations, W/R ratios ranged from **1 to 100**, covering conditions from very restricted to moderately available water. The picritic basalt responded strongly within the range of 10 to 50, whereas the tholeiitic basalt required a broader range (1 to 50) to generate similar mineral assemblages. These variations reflect the influence of olivine chemistry on reaction pathways. The nakhlite Y-593 simulations followed a similar W/R range but were interpreted in light of the highly Fe-rich olivine compositions. These Fe-rich compositions allow easier formation of Fe-rich smectites such as nontronite, especially at low W/R values, consistent with petrographic findings

described in. These modelling choices reflect the natural conditions inferred for both the Deccan and Martian settings: alteration occurred in short-lived, localized events where water was scarce but capable of inducing limited mineralogical change.

To accurately simulate the aqueous alteration behaviour of the Deccan basalts and the Martian nakhlite Yam-593, it was essential to define both the initial rock composition and the composition of the interacting fluid in a way that reflects natural geological settings. Tables 8 and 9 summarise these starting conditions for theterrestrial basalts and Yam-593, respectively. These compositions were selected to replicate the low-temperature, limited-water environments inferred from petrography, mineral analyses, and previous modelling studies. For both the picritic and tholeiitic Deccan basalts, the simulations used a simplified whole-rock composition consisting of 70 wt% olivine, 20 wt% plagioclase, and 10 wt% pyroxene. This choice reflects thefact that, in the natural samples, alteration was restricted almost entirely to fractures within olivine grains, while the surrounding groundmass minerals remained largely unaltered. Including plagioclase and pyroxene in minor proportions ensured that the overall chemical environment of the simulations remained realistic, even though most of the reactive behaviour is governed by olivine dissolution. A parallel set of simulations was carried out for the Fe-rich Martian nakhlite Yam-593. As in the Deccancases, the whole-rock composition used for modelling consisted of 70 wt% olivine, 20wt% plagioclase, and 10 wt% pyroxene. This proportion reflects the fact that alterationin Yam-593, like in the Deccan basalts, is confined to fractures within olivine grains.

The chemical composition of the fluid used in the simulations was based on natural data related to basalt–water systems. For the Deccan basalt modelling, the fluid compositions were derived from Deccan Trap thermal springs (Minissale et al., 2000),

which provided concentrations of major ions such as SO_4^{2-}, Cl^-, SiO_2, and HCO_3^-, as well as log(pCO_2) values. These fluids represent diluted aqueous solutions interacting with basaltic crust, making them suitable analogues for early-stage alteration. For Mg^{2+} and Fe^{2+} concentrations, values from hydrothermal alteration studies by Bridges and Schwenzer (2012) were used. These data are also relevant for Martian conditions, since they are based on basaltic alteration models that aim to replicate processes occurring on Mars. No external CO_2 buffering was applied in the simulations. This reflects the closed-system conditions inferred from petrography, where the fluid interacts only with the host rock and is not in contact with an external atmospheric reservoir. The only CO_2 present in the model comes from the initial fluid composition.

All geochemical modelling was carried out using the **REACT** module of the Geochemist's Workbench (GWB) software suite. This platform allows simulation of fluid–rock equilibration and the evolution of mineral phases as reactions proceed. The thermodynamic data were taken from the **V8 R6+ database** maintained by the Lawrence Livermore National Laboratory (Bethke, 2007), which provides reliable thermodynamic parameters for low-temperature geochemical systems.

Table 6.1: represents the initial composition for the fluid as well as the rock composition, which has been used for the running geochemical simulations in a closed environment at low temperature under varying WR ratios (low to moderate). In here, for both case scenarios, we have taken 70 wt% olivine, 10 wt% plagioclase, and 20 wt% pyroxene since the alteration is limited to the fractures of the olivine grain.

Ion	**Tholeiitic basalt starting liquiud composition (Sativli T.S.) (mmol/kg)**	**Picritic basalt starting liquid composition (Unai T.S.) (mmol/kg)**		**High Fo initial rock composition**	**Low Fo initial rock composition**
				Rock composition for simulation: Olivine-70 wt%, Plagioclase- 20 wt%, pyroxene- 10wt%	
				Rock composition for geochemical alteration simulations	
Na^+	2.04	2.04	**SiO_2**	44.56%	41.82%
K^+	0.013	0.013	**TiO_2**	0.00%	0.00%
Ca^{2+}	0.923	0.923	**Al_2O_3**	5.99%	5.10%
Al^{3+}	0.09	0.09	**FeO (T)**	5.88%	29.40%
[a]Mg^{2+}	5.6	5.6	**MnO**	0.00%	0.00%
[a]Fe^{2+}	3.2	3.2	**MgO**	37.80%	18.18%
[b]HCO_3^-	0.311	0.311	**CaO**	4.85%	3.94%
[b]CO_3^{2-}	0.006	0.008	**Na_2O**	0.93%	1.46%
[b]SO_4^{2-}	2	1.93	**K_2O**	0.00%	0.00%
[b]Cl^-	23.24	15.1	**P_2O_5**	0.00%	0.00%
[b]SiO_2	0.999	1.232	**Cr_2O_3**	0.00%	0.00%
[b]pCO_2	-4.45	-4.32			
T.S.	**Thermal springs**				

[a]Bridges & Schwenzer, 2012; [b]Minissale et al., 2000

Table 6.2: represents the initial composition for the initial fluid as well as the rock composition for Yam-593, which has been used for the running geochemical simulations in a closed environment at low temperature under varying WR ratios (low to moderate). In here, we have taken 70 wt% olivine, 10 wt% plagioclase, and 20 wt% pyroxene since the alteration is limited to the fractures of the olivine grain. The fluid composition is derived from a thermal spring (Minissale et al., 2000) in the Deccan Traps, where the Fe, Mg are adapted from Bridges and Schwenzer, 2012.

Ion	**Yam-593 starting liquid composition (Unai T.S.) (mmol/kg)**		**Yam-593 initial rock composition**
			Rock composition for simulation: Olivine-70 wt%, Plagioclase- 20 wt%, pyroxene-10wt%
Na^+	2.04	**SiO_2**	40.34%
K^+	0.013	**TiO_2**	0.00%
Ca^{2+}	0.923	**Al_2O_3**	5.49%
Al^{3+}	0.09	**FeO (T)**	34.55%
[a]Mg^{2+}	5.6	**MnO**	0.00%
[a]Fe^{2+}	3.2	**MgO**	13.89%
HCO_3^-	1.68	**CaO**	4.46%
[b]CO_3^{2-}	0.008	**Na_2O**	1.26%
[b]SO_4^{2-}	1.93	**K_2O**	0.00%
[b]Cl^-	15.1	**P_2O_5**	0.00%
[b]SiO_2	1.232	**Cr_2O_3**	0.00%
[b]*pCO_2*	-4.32		
T.S.	**Thermal springs**		

[a]Minissale et al., 2000
[b]Bridges & Schwenzer, 2012

To maintain realistic results, several minerals that are unlikely to form under the simulated conditions were suppressed. This included minerals such as quartz, epidote, prehnite, rutile, various zeolites, muscovite, tremolite, wollastonite, and several iron sulphides (Mitra et al., 2018). These minerals form under either higher temperature conditions or specific geochemical conditions not supported by the petrographic evidence from the Deccan basalts or the nakhlites. Because the alteration in both samples was restricted to low-temperature clay minerals and iron oxides, suppressing high-temperature or kinetically slow minerals ensures that the modelling output stays consistent with natural observations.

6.4. Results

The results of the geochemical modelling provide a clearer picture of how olivine responds to water–rock interaction under low-temperature and restricted water conditions. These simulated conditions match the fracture-controlled alteration seen in both the terrestrial Deccan basalts and the Martian nakhlite Yam-593. By examininghow alteration progresses in magnesium-rich and iron-rich terrestrial basalts andcomparing this behaviour with Fe-rich Martian olivine, it becomes possible to link thechemical pathways observed in laboratory models with the natural textures and mineral assemblages documented in the previous chapters. The models also support the interpretation that all three rock types experienced aqueous alteration in environments with limited water availability and under conditions where the fluid remained chemically connected to the host rock, rather than circulating freely.

In the picritic basalt, which contains highly forsteritic olivine (Fo ~88), the modelling shows that even small volumes of water can produce smectite-group clays when interacting with the mineral. Across the temperature range of 30°C to 75°C, and particularly at water–rock ratios between 10 and 50, the simulations predict the

formation of saponite as the dominant clay mineral, with small but consistent amounts of nontronite and associated iron oxides such as hematite. These results match the mineralogical patterns seen in the natural picritic samples, where the fracture fillings were composed mainly of smectites and iron-rich phases (Fig. 6.1).

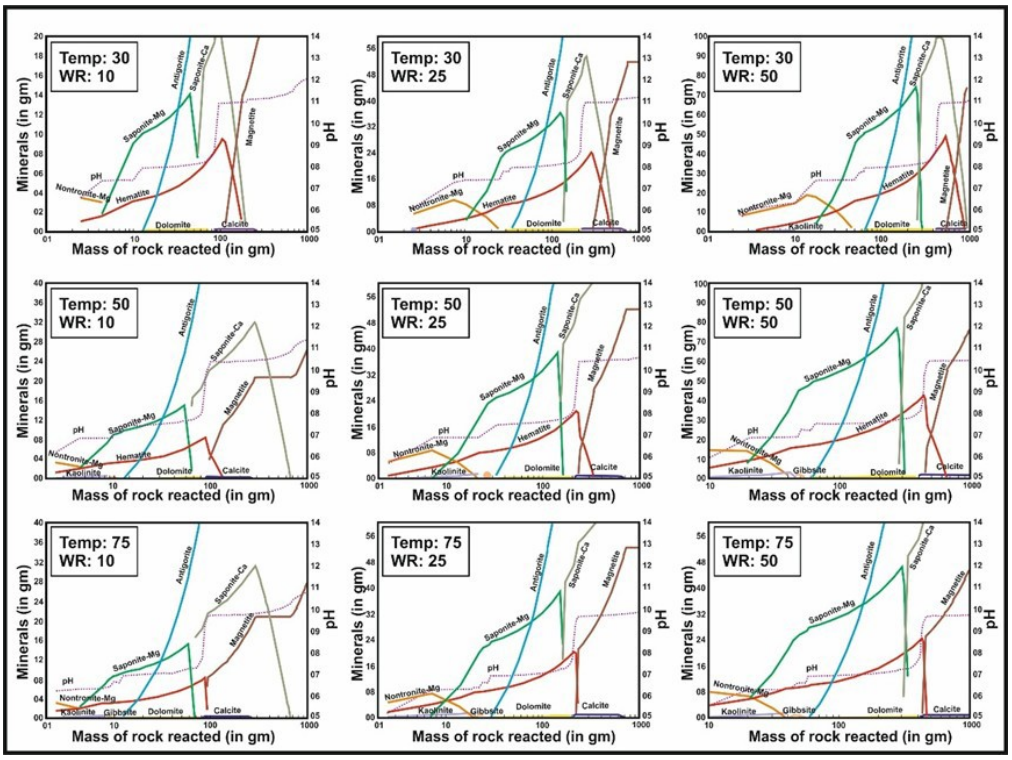

Fig. 6.1: These simulations represent the aqueous alteration scenario of picritic basalt, wherethe simulation has been performed at 30, 50, and 75 °C for WR ratios ranging from 10 to 50.

The extent of alteration remained low in all simulations, consistent with the petrographic evidence that most of the olivine grains were preserved, while only the fracture zones displayed mineralogical change. At very low water–rock ratios, the model showed a shift toward antigorite formation, indicating that extremely restricted fluid availability favours serpentine-type minerals over smectites. The modelling also showed that the reacting fluid gradually became less acidic as alteration progressed, reflecting the buffering effect of Mg-rich olivine dissolution in a closed system.

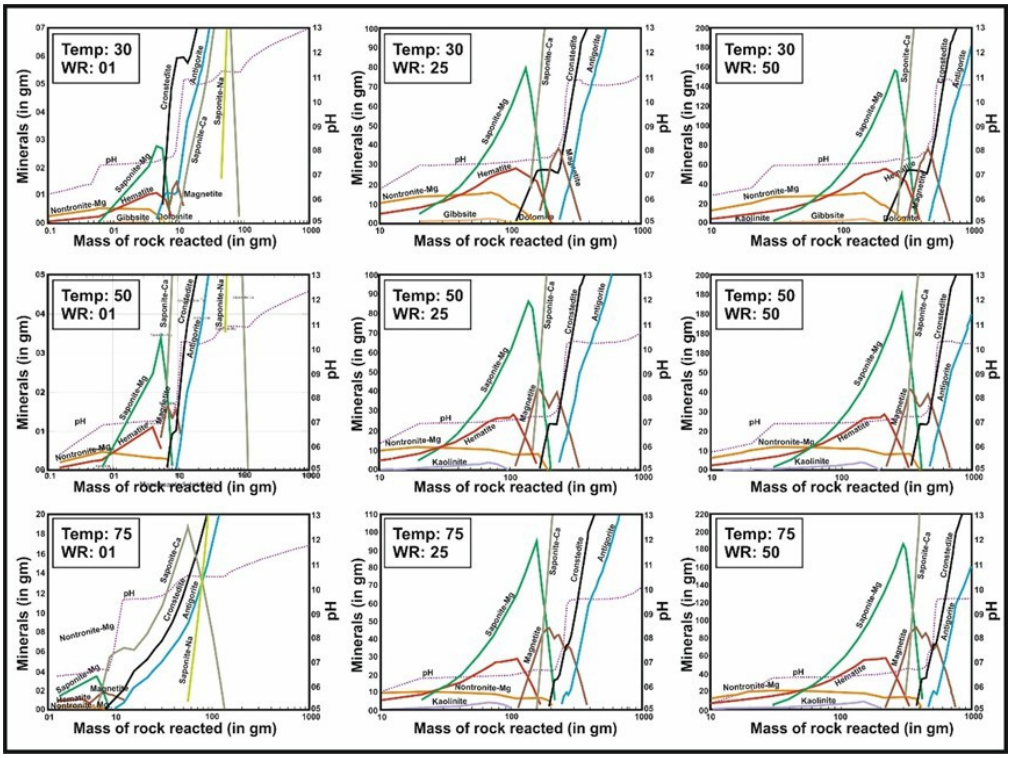

Fig. 6.2*: represents an alteration scenario for the tholeiitic basalt counterpart, where the simulations have been run for a wider range of WR ratios, ranging from 1 to 50.*

The behaviour of the tholeiitic basalt, which contains more Fe-rich olivine (Fo ~33–49), reveals differences that arise from the chemical composition of the olivine. In this case, the simulations showed that Fe-rich smectites such as nontronite formed more readily during the early stages of alteration, especially at lower water–rock ratios (Fig. 6.2). As alteration advanced and the fluid composition shifted, saponite eventually became stable, echoing the mixed Fe–Mg smectite assemblages seen petrographically. The modelling also reproduced the iron oxide components that accompany the smectites in the natural samples. The requirement of a broader range of water–rock ratios (1–50) to reproduce the natural mineral assemblages highlights the increased reactivity of Fe-rich olivine compared to its Mg-rich counterpart. The modelling results also reflect the smoother fracture morphologies and the presence of dissolution pits observed in the natural tholeiitic samples (Fig. 5.4a–b), which point to more extensive but still localized dissolution at the onset of alteration. Despite these differences, the

overall degree of alteration remained small, and only the fracture regions displayed significant changes, just as seen under the microscope. As in the picritic basalt, the reacting fluid became progressively less acidic, suggesting that the basalt acted as an efficient pH buffer.

A detailed comparison between the picritic and tholeiitic systems shows that the general pathway of alteration remains similar in both cases, although the mineralogy shifts according to olivine composition. Magnesium-rich olivine tends to favour the formation of Mg-saponite, while iron-rich olivine more readily produces Fe-rich nontronite before transitioning to saponite. In both systems, smectites and iron oxides dominate the secondary mineral assemblages, alteration is restricted to fractures, and only small portions of the olivine grains are affected. These similarities indicate that while the chemical composition of the host olivine affects the exact clay mineral that forms, the overall alteration behaviour is governed mainly by water availability and low-temperature conditions. The limited degree of alteration seen in the models reinforces the interpretation of closed-system processes, where the water–rock ratio remained low and the reacting fluid could not disperse widely.

When the modelling framework was applied to the Fe-rich nakhlite Yam-593 (Fig. 6.3), the results showed behaviour closely aligned with the Fe-rich tholeiitic basalt, as expected from their similar olivine chemistry. In the nakhlite simulations, alteration was explored across water–rock ratios of 25 to 75 and temperatures between 30°C and 50°C, reflecting the restricted fluid availability and low-temperature hydrothermal conditions proposed for the Amazonian-age alteration event. Under these conditions, the models consistently predicted the formation of Fe-rich smectite clays, particularly nontronite, during the early stages of alteration.

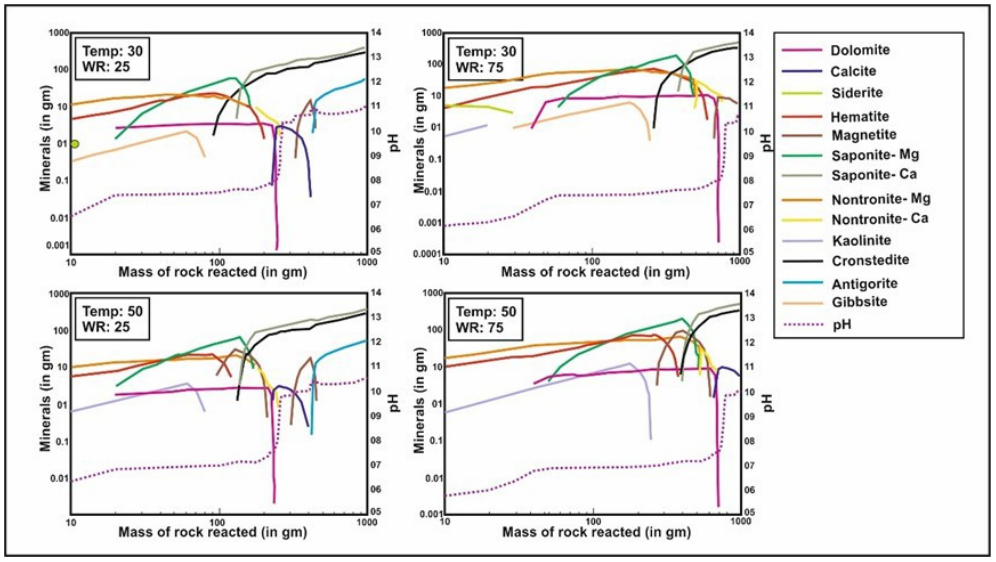

Fig. 6.3: *Geochemical simulations were also performed for the Fe-rich nakhlite Yam-593 (Fo_{26}) to understand how secondary minerals and pH evolve at temperatures of 30 °C and 50°C under higher WR ratios (25 and 75).*

Only minor quantities of clay were produced overall, and alteration remained confined to a small fraction of the original rock—mirroring the limited reaction progressobserved in analogous terrestrial systems when water availability is low. As the reactionproceeded, the model allowed for the stabilization of Mg-bearing smectites at later stages, similar to the gradual transition seen in the terrestrial Fe-rich basalt simulations.The nakhlite results demonstrate that even within a simulated hydrothermal regime, short-lived interaction with small volumes of fluid produces only limited alteration, supporting the interpretation that Yam-593 experienced aqueous modification under conditions of restricted water-rock interaction and modest temperatures. The close correspondence between the nakhlite simulations and those of the Deccan tholeiite (modelled across W/R ratios of 1 to 50 and temperatures of 30–75°C) highlights that Fe-rich olivine follows a similar geochemical pathway in both terrestrial and Martian environments when subjected to low-temperature alteration with limited water.

Element mobility patterns produced by the modelling also match the natural observations remarkably well. In both terrestrial and Martian samples, X-ray maps

show that Mg and Fe are leached from the olivine host and incorporated into the altered clay products, while elements such as Si, Al, and Ca become enriched within the fractures (Figs. 5.7, 5.8; Fig. 4.7, 4.8). The modelling reproduces this distribution by allowing olivine dissolution to release Mg and Fe into solution, while Al, Ca, and Si enter the system either from the initial fluid or from minor dissolution of neighbouring minerals. These similar geochemical trends across both planets reinforce the idea that alteration occurred under broadly comparable chemical conditions, even if the environmental settings were different.

The close parallels between the terrestrial basalts and Yam-593 indicate that the main factors controlling alteration—low temperature, limited water, and closed-system behaviour—were likely the same in both settings. The fracture-controlled nature of alteration in all samples suggests that water entered the rock in small amounts,interacted with olivine locally, and then either dried up or was no longer replenished. The predicted rise in pH during alteration provides further insight into the fluid conditions, suggesting that Martian fluids, like terrestrial ones, became less acidic as they reacted with olivine. The consistent formation of smectite clays and iron oxides across all three systems supports the conclusion that these minerals serve as reliable indicators of localized aqueous alteration in basaltic crusts.

Taken together, the modelling results show that both Mg-rich and Fe-rich olivine follow similar alteration pathways under low-temperature and low-water conditions, but the dominant clay mineral formed depends on olivine composition. Picritic basalt favours Mg-saponite, tholeiitic basalt favours Fe-rich nontronite at early stages, and the nakhlite behaves similarly to the tholeiite. In all cases, alteration remains minimal and restricted to fractures, reflecting the limited availability of water. These results support the broader interpretation that the conditions responsible for altering

nakhlite olivine on Mars were similar to those observed in the Deccan basalts, and that terrestrial modelling can be used as a meaningful guide for understanding Martian aqueous processes.

6.5. Discussions

The geochemical modelling carried out in this study provides a detailed and internally consistent picture of how olivine-bearing basalts respond to aqueous alteration when water is extremely limited. By modelling both the Mg-rich picritic basalt and the Fe-rich tholeiitic basalt under a wide range of water–rock (W/R) ratios and temperatures, it becomes possible to understand how such rocks behave in environments where only small volumes of fluid are available. This is an important constraint, because geological evidence suggests that the nakhlite meteorites from Mars, including Yam-593, experienced alteration during the Amazonian era—a period when liquid water on the Martian surface and near-surface was very restricted. Therefore, understanding how alteration progresses under low-water conditions on Earth provides a valuable analogue for reconstructing the geochemical environment on Mars during the time when the nakhlites interacted with aqueous fluids.

To capture a broad range of possible natural environments, the modelling was carried out at temperatures from 25°C to 75°C. This temperature interval serves two purposes. First, 25–50°C represents the typical range of low-temperature aqueous alteration on Earth, where smectite clays commonly form within fractures of primary minerals. Second, the upper part of this range—50–75°C—overlaps with a mild hydrothermal regime, still well below 100°C, but high enough to simulate the type of low-grade hydrothermal activity thought to have affected the nakhlites. Several studies have proposed that the nakhlites experienced short-lived heating and fluid flow after their crystallization, possibly triggered by impact-induced hydrothermal circulation.

Because the Amazonian period was marked by limited availability of liquid water, such hydrothermal events would have involved only small volumes of fluid interacting with the host rock for brief periods. Therefore, the modelling of terrestrial basalts at these temperatures allows us to simulate conditions broadly consistent with the geological context of the nakhlites, without introducing additional assumptions.

Across all simulations, whether picritic or tholeiitic basalt was used, andwhether the temperature was 25°C, 50°C, or 75°C, a consistent result was observed: For a very small amount of the rock that underwent alteration (~ 1 wt% of rock in caseof picrites or ~ 10wt % of rock in case of tholeiites), small quantities of clay minerals were produced. Even under the highest W/R ratios considered—although still within the low-to-moderate range—the amount of altered product did not significantly increase. This pattern is important because it indicates that the geochemical system quickly reached equilibrium with the available fluid. In other words, once the limited water interacted with the olivine and dissolved a small quantity of ions into solution, the fluid chemistry changed rapidly. As soon as the solution became buffered by ions released from the olivine, the alteration reactions slowed dramatically or stopped altogether. This behaviour, repeated across all model runs, shows that the duration of the alteration was brief, and that only a small fraction of the total rock could be alteredbefore the fluid lost its ability to continue reacting.

The modelling also shows that the same general behaviour occurs regardless of differences in olivine composition. Picritic basalt contains olivine that is richer in magnesium (high forsterite, Fo88), whereas tholeiitic basalt contains more iron-rich olivine (averaging Fo40). Despite this compositional contrast, both rock types responded similarly to low water–rock ratios: minor dissolution of olivine released Mg^{2+} and Fe^{2+} into the solution, and smectite-group clays formed as secondary phases

when only a small portion of the host rock was consumed. In picritic basalt, smectite minerals formed across W/R ratios of roughly 10–50, while in tholeiitic basalt the same minerals formed across a broader range (W/R 1–50). Although this difference reflects the chemical variability of the starting rock, the overall degree of alteration remained comparably low in both cases. This reinforces the conclusion that the availability of water, rather than the chemical composition of the rock, was the primary factor controlling how alteration proceeded. In other words, when water is limited, both Fe-rich and Mg-rich basalt behave in similar ways: alteration is mild, short-lived, and restricted to small volumes of the host rock. Another important trend emerging from the modelling is the progressive rise in fluid pH as alteration proceeds. This pH increase occurs because the dissolution of olivine releases divalent cations such as Mg^{2+} and Fe^{2+}, which neutralize the mildly acidic starting solution. As the pH rises, the fluid's ability to continue dissolving minerals decreases. This change in pH therefore acts as a natural brake on the alteration process. The modelling consistently demonstrates that the pH increases rapidly under low W/R conditions, reinforcing the interpretation that the system behaved as a closed environment, with little or no replenishment of fresh fluid. This is precisely the type of environment expected on Amazonian Mars, where water was neither abundant nor continuously available.

When the same geochemical modelling approach was extended to the Fe-rich nakhlite meteorite Yam-593, it allowed us to examine how an Amazonian-age Martian basalt might undergo aqueous alteration under conditions of restricted water availability, and to better understand the possible physico-chemical conditions that may have prevailed on Mars at the time these meteorites experienced alteration. As with the Deccan simulations, Yam-593 was modelled across temperatures of 25–75°C to reproduce a low-temperature to mild hydrothermal environment, which is consistent

with interpretations that nakhlites experienced short-lived, low-volume hydrothermal alteration on Mars. To maintain geochemical continuity, the starting fluid composition was taken from Deccan thermal springs (Minissale et al., 2000), because these fluids represent dilute, basalt-reactive waters suitable for simulating a comparable hydrothermal setting. Under these conditions, the Yam-593 simulations produced results that strongly resemble those obtained for the terrestrial basalts: alteration remained confined to a very small proportion of the total rock mass, only limited amounts of secondary smectite-group clays were generated, and the fluid's chemistry rapidly evolved toward equilibrium as Mg^{2+} and Fe^{2+} were released from the breakdown of olivine.

Because the modelling conditions successfully replicate low-temperature to mild hydrothermal environments, and because the simulated water–rock interactions are consistent with short-lived aqueous activity, the results can be meaningfully applied to the nakhlite meteorites. When the same modelling framework is used to simulate alteration of Fe-rich nakhlite-like compositions under limited water conditions, the results are remarkably similar to the terrestrial scenario. Smectite-group clays appear as the dominant secondary minerals when alteration remains confined to small amounts of the starting material. As in the terrestrial models, the fluid pH increases as alteration progresses, indicating that the Martian system would also have behaved as a closed environment. These parallels show that the physical and chemical constraints derived from the Deccan basalt simulations are directly relevant to understanding the alteration environment of the nakhlites.

A particularly important implication of these findings is that the nakhlites did not require large volumes of water or long-lived hydrothermal systems to produce the secondary minerals observed in them. Instead, the modelling suggests that the nakhlites

could have undergone alteration during a short-lived hydrothermal pulse involving minimal water, consistent with conditions expected during the Amazonian era. This interpretation aligns with geological models suggesting that Mars experienced only isolated and transient hydrological events during this period. The nakhlite alteration therefore records one such event—a brief episode of interaction between olivine and a small amount of slightly acidic water at low to moderate temperatures.

To reflect the likely conditions that affected the nakhlite during the Amazonian, the simulations were deliberately run over a temperature range of 25–75°C, chosen to capture both low-temperature aqueous alteration and the upper end of a mild, low-grade hydrothermal regime that may have influenced the meteorite. This range was selected not to imply that alteration is insensitive to temperature, but to reproduce the type of thermal environment proposed for the nakhlites: short-lived, low-intensity hydrothermal activity where water was scarce. To make the experiments realistic, the starting fluid chemistry for the terrestrial basalt samples was taken from thermal springs (Minissale et al., 2000), and similar fluid compositions were then used in the nakhlite simulations so as to mimic the hydrothermal fluids that likely reacted with Fe-rich olivine on Mars. Under these temperature and fluid conditions the models show that only small fractions of the host rock react and only minor amounts of clay are produced, consistent with a short-lived, limited-water hydrothermal event rather than a long-lasting, high-flux system.

Taken together, these results demonstrate that the style, extent, and products of alteration in both terrestrial and Martian systems can be understood primarily as a consequence of low water–rock ratios operating at low-to-moderate temperatures. Because both the Deccan basalts and the Martian nakhlites behave in nearly identical ways when subjected to limited aqueous interaction, the modelling confirms that they

share comparable alteration pathways despite their compositional differences. This makes the Deccan basalts—especially the Fe-rich tholeiitic samples—a useful terrestrial analogue for interpreting the geochemical environment of Amazonian Mars.

6.6. Conclusion

- The geochemical modelling demonstrates that basalt alteration under low water availability produces only minor secondary minerals, consistent with the limited fracture-controlled alteration observed in natural samples.
- Across the temperature range of 25–75°C, only a small fraction of the host rock reacts, showing that alteration was short-lived and occurred in closed-system conditions.
- Picritic basalt (high Fo, Mg-rich olivine) consistently forms Mg-saponite as the dominant smectite clay at water–rock ratios of 10–50 and temperatures of 30–75°C. Tholeiitic basalt (low Fo, Fe-rich olivine) first forms Fe-rich nontronite, later stabilising saponite as the fluid chemistry evolves, showing a clear control of olivine composition on clay mineralogy. Despite compositional differences between picritic and tholeiitic basalts, both systems follow similar alteration pathways when water availability is low.
- Modelling of nakhlite Yam-593, using water–rock ratios of 25–75 and temperatures of 30–50°C, reproduces Fe-rich smectite formation consistent with natural observations.
- In all cases, the fluid becomes progressively less acidic as it reacts with olivine, showing that basalt acts as an effective pH buffer in closed systems.
- The overall alteration remains minimal in terrestrial and Martian simulations, indicating that water–rock interaction was limited in duration and fluid volume.

- The modelling provides strong evidence that nakhlite alteration on Mars likely occurred during brief, low-temperature hydrothermal events under severely restricted water availability.
- Results from Deccan basalts and Yam-593 together establish the key physico-chemical conditions—low W/R ratios, mild temperatures, closed-system behaviour—that best explain their natural alteration textures.

These findings form a basis for understanding aqueous processes on Mars and support the broader interpretations summarised in the final chapter of the thesis.

Chapter 7: Summary and Conclusion

This thesis focuses on understanding aqueous alteration of basaltic materials under conditions where liquid water was limited, short-lived, and spatially restricted. The work combines observations from Martian nakhlite meteorites, terrestrial basaltic analogues from the Deccan Continental Flood Basalts, and geochemical modelling to reconstruct the physicochemical conditions under which such alteration occurred. By integrating petrography, mineral chemistry, elemental mapping, and thermodynamic simulations, the study provides a coherent framework for interpreting low-temperature aqueous processes on Mars, particularly during the Amazonian period. A central theme that emerges from this work is that aqueous alteration in basaltic systems does not necessarily require large volumes of water or prolonged interaction. Instead, the results consistently show that limited amounts of water, interacting locally with reactive minerals such as olivine, can produce distinct secondary mineral assemblages. This finding is significant for Mars, where geomorphological and mineralogical evidence increasingly suggests that water was present episodically and in restricted environments, rather than as long-lived surface bodies, during much of the planet's geological history.

7.1. Fracture-controlled alteration as a dominant process

One of the most consistent observations across all datasets examined in this thesis is the strongly localized nature of alteration. In the Martian nakhlite meteorites, secondary

minerals are overwhelmingly confined to fractures within olivine grains. The interiors of olivine crystals remain largely unaltered, and neighbouring phases, such as augite and plagioclase, show minimal direct replacement. This fracture-controlled pattern suggests that fluids accessed the rock through pre-existing weaknesses and interacted with only small volumes of material before becoming chemically exhausted or isolated.

Comparable textures were identified in terrestrial Deccan basalts, where olivine-hosted alteration is similarly restricted to fractures. Despite differences in geological setting, age, and environment, the similarity in textural relationships between Martian and terrestrial samples strongly suggests that fracture-controlled alteration is a fundamental response of olivine-rich basalts to low water availability. This observation supports the idea that fluid flow was limited, discontinuous, and short-lived in both systems. The localized nature of alteration further implies that these environments operated under low water–rock ratios. Fluids were likely consumed rapidly through reaction with olivine, preventing widespread alteration of the host rock. This interpretation is consistent with both petrographic evidence and modelling results presented in this thesis.

7.2. Behaviour of olivine during aqueous alteration

Olivine plays a central role in this study due to its high reactivity compared to other basaltic minerals. Across all nakhlite meteorites examined, olivine grains show little to no chemical zoning between core and rim, indicating that their primary magmatic compositions were preserved prior to alteration. This homogeneity suggests that aqueous alteration did not proceed through pervasive diffusion or bulk recrystallization, but rather through localized dissolution–precipitation processes along fractures.

During alteration, magnesium and iron were preferentially released from olivine and incorporated into secondary minerals. This behaviour was observed consistently in

elemental X-ray maps, where Mg and Fe concentrations increase within fracture-hosted alteration products relative to the host olivine. At the same time, elements such as aluminium and calcium are enriched in the altered zones compared to olivine, indicating that these components were introduced from external sources, likely through interaction with adjacent phases or the reacting fluid itself. In the terrestrial Deccan basalts, similar element mobility patterns were documented. Olivine served as the primary source of Mg and Fe, while Al and Ca were contributed by surrounding minerals, such as plagioclase and clinopyroxene. This consistent pattern across both Martian and terrestrial samples suggests that similar geochemical conditions may have been prevalent during the water-starved Amazonian Mars.

7.3. Nature and composition of alteration products

The alteration products identified in this study are primarily composed of smectite-group clay minerals, particularly saponite and nontronite, often associated with iron oxides. These assemblages are characteristic of low-temperature aqueous alteration and are commonly grouped under the term “iddingsite.” Raman spectroscopy, mineral chemistry, and geochemical modelling collectively support this interpretation. In most nakhlites, including Yam-593, MIL 03346, and Nakhla, the alteration products within olivine fractures appear chemically homogeneous. Elemental maps show relatively uniform distributions of major elements within the altered zones, with no strong internal zoning or compositional layering. This homogeneity suggests that alteration occurred under relatively stable chemical conditions, likely during a single dominant alteration episode.

In contrast, the Lafayette meteorite exhibits a more complex alteration record. Within olivine fractures, altered material shows subtle chemical variability, including unusually high aluminium enrichment that exceeds that of nearby Al-rich plagioclase.

This observation suggests that Lafayette interacted with a geochemically distinct fluid, possibly enriched in aluminium relative to those affecting the other nakhlites. Additionally, Lafayette uniquely preserves alteration within the mesostasis region, where Fe–Ca carbonate phases occur alongside phyllosilicate clays. The coexistence of carbonates and clays, along with their spatial relationships, suggests a changing fluid chemistry during alteration. In particular, the presence of carbonates enclosed by phyllosilicates suggests a shift in fluid conditions, likely involving changes in pH from acidic to more alkaline environments. Such features are absent in the other nakhlites, highlighting the exceptional nature of Lafayette's alteration history.

7.4. Chemical indices and constraints on alteration intensity

Chemical indices were used to quantify and compare the degree of alteration across the nakhlite meteorites. The Chemical Index of Alteration (CIA) and the Mafic Index of Alteration (MIA) provide complementary information on the redistribution of major elements during aqueous alteration. The CIA–MIA bivariate plots show that Yam-593 and MIL 03346 cluster tightly, indicating chemically consistent alteration under restricted conditions. Nakhla also forms a compact cluster, though at slightly lower CIA values, suggesting a more limited degree of alteration. In contrast, Lafayette shows a wide spread across the plot, extending to high CIA values. This broad range indicates substantial chemical variability and points to more extensive or multi-stage alteration. These trends are reinforced by A–CN–K ternary plots. Yam-593 and Nakhla display closely clustered compositions, reflecting uniform alteration chemistry. MIL 03346 shows a wider spread, indicating variable cation mobility and less uniform alteration behaviour than initially expected. Lafayette plots along the A–CN line, characterized by strong aluminium enrichment, consistent with high CIA values and significant aqueous alteration. Together, these compositional patterns indicate that while most

nakhlites experienced alteration under relatively closed-system conditions, Lafayette likely underwent more open-system alteration involving multiple fluid episodes.

7.5. Evidence for multiple alteration episodes

Bi-variant plots comparing Si with Fe, Fe+Mg, and Al provide further insight into alteration pathways. Yam-593, MIL 03346, and Nakhla show consistent inverse relationships between Si and Fe or Fe+Mg, indicating progressive silica enrichment accompanied by depletion of mafic components. These coherent trends suggest that alteration in these meteorites followed similar chemical pathways under stable conditions. Lafayette, however, displays multiple trends in all bi-variant plots. Two distinct trends are observed in Fe–Si and Fe+Mg–Si space, and three trends are evident in Al–Si space. This behaviour indicates that the alteration products in Lafayette did not form during a single event. Instead, the data support the interpretation that Lafayette experienced more than one pulse of alteration, each characterised by different fluid compositions or reaction conditions. The presence of carbonate phases within the mesostasis further supports this interpretation. Previous studies have suggested different sequences of carbonate and clay formation in Lafayette, and the observations in this thesis are consistent with a complex alteration history involving evolving fluid chemistry.

7.6. Insights from terrestrial analogues

A key strength of this thesis lies in the use of terrestrial Deccan basalts as analogues for Martian alteration processes. The Deccan samples exhibit olivine-hosted alteration textures and mineral assemblages that closely resemble those observed in nakhlites. Both picritic (Mg-rich) and tholeiitic (Fe-rich) basalts exhibit fracture-controlled alteration under low-temperature and limited water-rock ratio conditions, resulting in smectite clays with limited overall alteration. Differences between picritic and tholeiitic

basalts highlight the influence of olivine composition on alteration products. Mg-rich olivine favours the formation of Mg-saponite, whereas Fe-rich olivine more readily produces Fe-rich smectites such as nontronite. These trends closely mirror the behaviour observed in Fe-rich nakhlites, strengthening the link between terrestrial and Martian systems. Importantly, the terrestrial analogues demonstrate that such alteration can occur under Earth conditions without extensive water circulation, reinforcing the interpretation that similar processes could operate on Mars under limited hydrological regimes.

7.7. Constraints from geochemical modelling

Geochemical modelling provides important quantitative constraints on the conditions under which aqueous alteration occurred in both terrestrial basalts and Martian nakhlite meteorites. The modelling was designed to test whether the alteration features observed in olivine-rich rocks could be produced under conditions of limited water availability and low to moderately elevated temperatures. The results consistently show that alteration remains restricted when water–rock interaction occurs in a closed or near-closed system. Across all simulated scenarios, only a small fraction of the host rock undergoes chemical alteration. Even when reactions are allowed to proceed across a range of temperatures and water–rock ratios, the models predict the formation of only minor amounts of secondary minerals. This behaviour closely matches petrographic observations from both Deccan basalts and nakhlite meteorites, where alteration products are confined to fractures within olivine grains and do not affect the surrounding groundmass. The modelling, therefore, supports the interpretation that aqueous alteration was short-lived and spatially localized. When water availability is limited, the reacting fluid becomes rapidly modified by interaction with olivine, and chemical equilibrium is reached before extensive dissolution can occur. Under these

conditions, smectite-group clays are produced without leading to pervasive alteration of the rock. In contrast, higher water–rock ratios result in larger volumes of altered material that are inconsistent with the textures observed in natural samples. This indicates that the alteration recorded in both terrestrial and Martian materials took place under water-limited conditions. The temperature range explored in the models was selected to represent both low-temperature aqueous alteration and mild hydrothermal conditions. The modelling demonstrates that smectite formation can occur across this temperature range without requiring high-temperature processes. Importantly, even at the upper end of the simulated temperatures, alteration remains limited when water availability is restricted. This shows that temperature alone did not control the degree of alteration; instead, the amount of available water exerted the dominant influence. These results support the interpretation that alteration occurred under low-intensity hydrothermal or near-surface conditions rather than during prolonged, high-flux fluid circulation. Differences in olivine composition are also reflected in the modelling results. Magnesium-rich systems favour the formation of Mg-rich smectites, whereas iron-rich systems initially produce Fe-rich smectites before transitioning toward more Mg-bearing compositions as alteration progresses. Despite these differences, the overall alteration behaviour remains similar across all compositions, with limited reaction progress and fracture-controlled mineral formation. This consistency suggests that olivine chemistry influences the type of clay formed but does not fundamentally change the style of alteration under water-limited conditions. When applied to Fe-rich nakhlite compositions, the modelling results closely resemble those obtained for Fe-rich terrestrial basalts. Only small amounts of clay are produced at low to moderate water–rock ratios, and the alteration remains restricted. This similarity indicates that the same physicochemical principles governed alteration on Earth and Mars. In the Martian

context, the modelling supports a scenario in which olivine alteration occurred during brief, localized aqueous or hydrothermal events under limited water availability during the Amazonian period. Overall, the geochemical modelling places tight constraints on the alteration environment, indicating low water–rock ratios, modest temperatures, restricted fluid circulation, and short-lived reaction conditions. These constraints provide a coherent framework that links petrographic observations, mineral chemistry, and alteration textures in both terrestrial analogues and Martian meteorites.

7.8. Broader implications for Mars

The results of this thesis have important implications for understanding aqueous processes on Mars. The findings support a scenario in which alteration occurred under limited water availability, likely during short-lived events rather than prolonged periods of surface water. Such conditions are consistent with current models of Amazonian Mars, which suggest episodic hydrothermal activity driven by impacts, volcanism, or localized heat sources. The ability of small amounts of water to produce clay minerals and, in some cases, carbonates highlights the need for caution when interpreting the presence of alteration minerals as evidence for long-lived habitable environments. Instead, these minerals may record brief but geochemically significant interactions between water and basaltic crust.

7.9. Limitations & Future scope of work

- **Improved constraints on Martian fluid chemistry:** One of the main limitations of this study is that the exact chemical composition of the fluids responsible for alteration on Mars remains unknown. In future work, a wider range of fluid compositions could be tested through geochemical modelling. Variations in parameters such as pH, redox conditions, and dissolved carbonspecies could be explored to better constrain the types of fluids that are most capable of producing the alteration features observed in nakhlite meteorites.
- **Comparison with orbital and rover observations:** The results of this thesis can be directly compared with clay mineral detections made by orbiters and rovers on Mars. Such comparisons would help connect meteorite-scale observations with features observed on the Martian surface. This approach would improve our understanding of how the Martian crust has responded to aqueous alteration under different water availability conditions, ranging from water-rich environments in the Noachian period to more water-limited conditions during the Amazonian period.
- **Implications for localized habitability:** Although this thesis does not directly address biological processes, the identification of low-temperature, localized aqueous alteration raises questions about transient micro-environments that may have briefly supported habitable conditions. Future work could explore these environments cautiously, focusing on their physicochemical characteristicsrather than biological claims.

Bibliography

Abramov, O., & Kring, D. A. (2004). Numerical modeling of an impact-induced hydrothermal system at the Sudbury crater. Journal of Geophysical Research: Planets, 109(E10). https://doi.org/10.1029/2003JE002213

Abramov, O., & Mojzsis, S. J. (2016). Thermal effects of impact bombardments on Noachian Mars. Earth and Planetary Science Letters, 442, 108-120. https://doi.org/10.1016/j.epsl.2016.02.035

Agee, C. B., Wilson, N. V., McCubbin, F. M., Ziegler, K., Polyak, V. J., Sharp, Z. D., ... & Elardo, S. M. (2013). Unique meteorite from early Amazonian Mars: Water- rich basaltic breccia Northwest Africa 7034. Science, 339(6121), 780-785. https://doi.org/10.1126/science.1228858

Alexander, C. M. O. D., McKeegan, K. D., & Altwegg, K. (2018). Water reservoirs in small planetary bodies: meteorites, asteroids, and comets. Space science reviews, 214(1), 36. https://doi.org/10.1007/s11214-018-0474-9

Almuslet, N. A., Ahmed, M. M., & Hassen, S. M. (2017). Usage of laser Raman spectroscopy to indentify the unstable compounds of iron oxides. International Journal of Current Advanced Research, 6(4), 3470–3473.

Anand, M., Williams, C. T., Russell, S. S., Jones, G., James, S., & Grady, M. M. (2005). Petrology and geochemistry of nakhlite MIL 03346: A new Martian meteorite from Antarctica. http://www.lpi.usra.edu/meetings/lpsc2005/pdf/1639.pdf

Arndt, N. T. (1977). Ultrabasic magmas and high-degree melting of the mantle. Contributions to Mineralogy and Petrology, 64(2), 205–221. https://doi.org/10.1007/BF00371512

Baker, I., & Haggerty, S. E. (1967). The alteration of olivine in basaltic and associated lavas: Part II: Intermediate and low temperature alteration. Contributions to Mineralogy and Petrology, 16, 258–273. https://doi.org/10.1007/BF00371095

Baker, L. L., & Neill, O. K. (2017). Geochemistry and mineralogy of a saprolite developed on Columbia River Basalt: Secondary clay formation, element leaching, and mass balance during weathering. American Mineralogist, 102(8), 1632-1645. https://doi.org/10.2138/am-2017-5964

Bandfield, J. L. (2002). Global mineral distributions on Mars. Journal of Geophysical Research: Planets, 107(E6), 9-1. https://doi.org/10.1029/2001JE001510

Banham, S. G., Roberts, A. L., Gupta, S., Davis, J. M., Thompson, L. M., Rubin, D. M., & Vasavada, A. R. (2024). Ice? Salt? Pressure? Sediment deformation structures as evidence of late-stage shallow groundwater in Gale crater, Mars. Geology. https://doi.org/10.1130/G51849.1

Barnhisel, R. I. (1977). Chlorites and hydroxy interlayered vermiculite and smectite.

Basilevsky, A. T., Werner, S. C., Neukum, G., Head, J. W., Van Gasselt, S., Gwinner, K., & Ivanov, B. A. (2006). Geologically recent tectonic, volcanic and fluvial activity on the eastern flank of the Olympus Mons volcano, Mars. Geophysical Research Letters, 33(13). https://doi.org/10.1029/2006GL026396

Beane, J. E., & Hooper, P. R. (1988). A note on the picrite basalts of the Western Ghats, Deccan Trap, India. Memoir-Geological Society of India, (10), 117-133.

Beane, J. E., Turner, C. A., Hooper, P. R., Subbarao, K. V., & Walsh, J. N. (1986). Stratigraphy, composition and form of the Deccan basalts, Western Ghats, India. Bulletin of Volcanology, 48, 61-83. https://doi.org/10.1007/BF01073513

Beaty, D. W., Grady, M. M., McSween, H. Y., Sefton-Nash, E., Carrier, B. L., Altieri, F., ... & Zorzano, M. P. (2019). The potential science and engineering value of samples delivered to Earth by Mars sample return: International MSR Objectives and Samples Team (iMOST). Meteoritics & Planetary Science, 54, S3-S152. https://doi.org/10.1111/maps.13242

Bellucci, J. J., Herd, C. D. K., Whitehouse, M. J., Nemchin, A. A., Kenny, G. G., & Merle, R. E. (2020). Insights into the chemical diversity of the martian mantle from the Pb isotope systematics of shergottite Northwest Africa 8159. Chemical Geology, 545, 119638. https://doi.org/10.1016/j.chemgeo.2020.119638

Bethke, C. M. (2007). Geochemical and biogeochemical reaction modeling (2nd ed.). Cambridge University Press. https://doi.org/10.1017/CBO9780511619670

Beyssac, O., Forni, O., Cousin, A., Udry, A., Kah, L. C., Mandon, L. E. C. Y. L., ... & SuperCam Team. (2023). Petrological traverse of the olivine cumulate Séítah formation at Jezero crater, Mars: A perspective from SuperCam onboard Perseverance. Journal of Geophysical Research: Planets, 128(7), e2022JE007638. https://doi.org/10.1029/2022JE007638

Bibring, J. P., Langevin, Y., Gendrin, A., Gondet, B., Poulet, F., Berthé, M., ... & Omega Team. (2005). Mars surface diversity as revealed by the OMEGA/Mars Express observations. Science, 307(5715), 1576-1581. https://doi.org/10.1126/science.1108806

Bibring, J. P., Langevin, Y., Mustard, J. F., Poulet, F., Arvidson, R., Gendrin, A., ... & Neukum, G. (2006). Global mineralogical and aqueous Mars history derived from OMEGA/Mars Express data. science, 312(5772), 400-404. https://doi.org/10.1126/science.1122659

Bishop, J. L., & Rampe, E. B. (2016). Evidence for a changing Martian climate from the mineralogy at Mawrth Vallis. Earth and Planetary Science Letters, 448, 42- 48. https://doi.org/10.1016/j.epsl.2016.04.031

Bishop, J. L., Dobrea, E. Z. N., McKeown, N. K., Parente, M., Ehlmann, B. L., Michalski, J. R., ... & Bibring, J. P. (2008). Phyllosilicate diversity and past aqueous activity revealed at Mawrth Vallis, Mars. Science, 321(5890), 830-833. https://doi.org/10.1126/science.1159699

Bishop, J. L., Fairén, A. G., Michalski, J. R., Gago-Duport, L., Baker, L. L., Velbel, M. A., ... & Rampe, E. B. (2018). Surface clay formation during short-term warmer and wetter conditions on a largely cold ancient Mars. Nature Astronomy, 2(3), 206-213. https://doi.org/10.1038/s41550-017-0377-9

Bjoraker, G. L., Mumma, M. J., & Larson, H. P. (1989, June). Isotopic abundance ratios for hydrogen and oxygen in the martian atmosphere. In Bulletin of the American Astronomical Society, Vol. 21, p. 991 (Vol. 21, p. 991).

Borg, L. E., & Draper, D. S. (2003). A petrogenetic model for the origin and compositional variation of the Martian basaltic meteorites. Meteoritics & Planetary Science, 38(12), 1713-1731. https://doi.org/10.1111/j.1945-5100.2003.tb00011.x

Borg, L., & Drake, M. J. (2005). A review of meteorite evidence for the timing of magmatism and of surface or near-surface liquid water on Mars. Journal of Geophysical Research: Planets, 110(E12). https://doi.org/10.1029/2005JE002402

Bottke, W. F., & Andrews-Hanna, J. C. (2017). A post-accretionary lull in large impacts on early Mars. Nature Geoscience, 10(5), 344-348. https://doi.org/10.1038/ngeo2937

Bragg, W. H., & Bragg, W. L. (1913). The reflection of X-rays by crystals. Proceedings of the Royal Society of London. Series A, Containing Papers of a Mathematical and Physical Character, 88(605), 428–438. https://doi.org/10.1098/rspa.1913.0040

Bridges, J. C., & Schwenzer, S. P. (2012). The nakhlite hydrothermal brine on Mars. Earth and Planetary Science Letters, 359, 117-123. https://doi.org/10.1016/j.epsl.2012.09.044

Bridges, J. C., Catling, D. C., Saxton, J. M., Swindle, T. D., Lyon, I. C., & Grady, M. M. (2001). Alteration assemblages in Martian meteorites: Implications for near- surface processes. Space Science Reviews, 96(1), 365-392. https://doi.org/10.1023/A:1011965826553

Bristow, T. F., Bish, D. L., Vaniman, D. T., Morris, R. V., Blake, D. F., Grotzinger, J. P., ...& McAdam, A. C. (2015). The origin and implications of clay minerals from Yellowknife Bay, Gale crater, Mars. American Mineralogist, 100(4), 824-836. https://doi.org/10.2138/am-2015-5077CCBYNCND

Bristow, T. F., Rampe, E. B., Achilles, C. N., Blake, D. F., Chipera, S. J., Craig, P.,.....& Yen, A. S. (2018). Clay mineral diversity and abundance in sedimentary rocks of Gale crater, Mars. Science advances, 4(6), eaar3330. https://doi.org/10.1126/sciadv.aar3330

Broquet, A., & Andrews-Hanna, J. C. (2023). Geophysical evidence for an active mantle plume underneath Elysium Planitia on Mars. Nature Astronomy, 7(2), 160–169. https://doi.org/10.1038/s41550-022-01836-3

Brown, G., & Brindley, G. W. (1980). X-ray diffraction procedures for clay mineral identification. https://doi.org/10.1180/mono-5.5

Bultel, B., Viennet, J. C., Poulet, F., Carter, J., & Werner, S. C. (2019). Detection of carbonates in Martian weathering profiles. Journal of Geophysical Research: Planets, 124(4), 989-1007. https://doi.org/10.1029/2018JE005845

Bunch, T. E., & Reid, A. M. (1975). The nakhlites Part I: Petrography and mineral chemistry. Meteoritics, 10(4), 303-315. https://doi.org/10.1111/j.1945-5100.1975.tb01187.x

Calvès, G., Schwab, A. M., Huuse, M., Clift, P. D., Gaina, C., Jolley, D., ... & Inam, A. (2011). Seismic volcanostratigraphy of the western Indian rifted margin: The pre-Deccan igneous province. Journal of Geophysical Research: Solid Earth, 116(B1). https://doi.org/10.1029/2010JB000862

Caroff, M., Maury, R. C., Cotten, J., & Clément, J. P. (2000). Segregation structures in vapor-differentiated basaltic flows. Bulletin of Volcanology, 62(3), 171-187. https://doi.org/10.1007/s004450000077

Carr, M. H., & Head III, J. W. (2010). Geologic history of Mars. Earth and Planetary Science Letters, 294(3-4), 185-203. https://doi.org/10.1016/j.epsl.2009.06.042

Carter, J., Loizeau, D., Mangold, N., Poulet, F., & Bibring, J. P. (2015). Widespread surface weathering on early Mars: A case for a warmer and wetter climate. Icarus, 248, 373-382. https://doi.org/10.1016/j.icarus.2014.11.011

Carter, J., Poulet, F., Bibring, J. P., & Murchie, S. (2010). Detection of hydrated silicates in crustal outcrops in the northern plains of Mars. Science, 328(5986), 1682- 1686. https://doi.org/10.1126/science.1189013

Carter, J., Poulet, F., Bibring, J. P., Mangold, N., & Murchie, S. (2013). Hydrous minerals on Mars as seen by the CRISM and OMEGA imaging spectrometers: Updated global view.

Journal of Geophysical Research: Planets, 118(4), 831- 858. https://doi.org/10.1029/2012JE004145

Catling, D. C. (2014). Mars atmosphere: History and surface interactions. In Encyclopedia of the solar system (pp. 343-357). Elsevier. https://doi.org/10.1016/B978-0-12-415845-0.00016-5

Changela, H. G., & Bridges, J. C. (2010). Alteration assemblages in the nakhlites: Variation with depth on Mars. Meteoritics & Planetary Science, 45(12), 1847- 1867. https://doi.org/10.1111/j.1945-5100.2010.01123.x

Chatterjee, N. (2024). Petrogenesis of the Deccan high-Mg basalts and picrites. Contributions to Mineralogy and Petrology, 179(10), 90. https://doi.org/10.1007/s00410-024-021727

Chevrier, V., Poulet, F., & Bibring, J. P. (2007). Early geochemical environment of Mars as determined from thermodynamics of phyllosilicates. Nature, 448(7149), 60-63. https://doi.org/10.1038/nature05961

Chopelas, A. (1991). Thermal properties of β-Mg2SiO4 at mantle pressures derived from vibrational spectroscopy: Implications for the mantle at 400 km depth. Journal of Geophysical Research: Solid Earth, 96(B7), 11817–11829. https://doi.org/10.1029/91JB00898

Christensen, P. R., Bandfield, J. L., Bell III, J. F., Gorelick, N., Hamilton, V. E., Ivanov, A., ... & Wyatt, M. B. (2003). Morphology and composition of the surface of Mars: Mars Odyssey THEMIS results. science, 300(5628), 2056-2061. https://doi.org/10.1126/science.1080885

Christensen, P. R., Bandfield, J. L., Hamilton, V. E., Ruff, S. W., Kieffer, H. H., Titus, T. N., ... & Greenfield, M. (2001). Mars Global Surveyor Thermal Emission Spectrometer

experiment: investigation description and surface science results. Journal of Geophysical Research: Planets, 106(E10), 23823–23871. https://doi.org/10.1029/2000JE001370

Christensen, P. R., Bandfield, J. L., Smith, M. D., Hamilton, V. E., & Clark, R. N. (2000). Identification of a basaltic component on the Martian surface from Thermal Emission Spectrometer data. Journal of Geophysical Research: Planets, 105(E4), 9609-9621. https://doi.org/10.1029/1999JE001127

Christensen, P. R., McSween Jr, H. Y., Bandfield, J. L., Ruff, S. W., Rogers, A. D., Hamilton, V. E., ... & Moersch, J. E. (2005). Evidence for magmatic evolution and diversity on Mars from infrared observations. Nature, 436(7050), 504-509. https://doi.org/10.1038/nature03639

Clément, J. P., Caroff, M., Dudoignon, P., Launeau, P., Bohn, M., Cotten, J., ... & Guille,G. (2007). A possible link between gabbros bearing high temperature iddingsite alteration and huge pegmatoid intrusions: The Society Islands, French Polynesia. Lithos, 96(3-4), 524-542 https://doi.org/10.1016/j.lithos.2006.12.001

Cohen, B. E., Mark, D. F., Cassata, W. S., Lee, M. R., Tomkinson, T., & Smith, C. L. (2017). Taking the pulse of Mars via dating of a plume-fed volcano. Nature Communications, 8(1), 640. https://doi.org/10.1038/s41467-017-00513-8

Cucciniello, C., Avanzinelli, R., Sheth, H., & Casalini, M. (2022). Mantle and crustal contributions to the Mount Girnar alkaline plutonic complex and the circum- Girnar mafic-silicic intrusions of Saurashtra, northwestern Deccan Traps. Journal of Petrology, 63(3), egac007. https://doi.org/10.1093/petrology/egac007

Cucciniello, C., Demonterova, E. I., Sheth, H., Pande, K., & Vijayan, A. (2015). 40 Ar/39 Ar geochronology and geochemistry of the Central Saurashtra mafic dyke swarm: insights

into magmatic evolution, magma transport, and dyke-flow relationships in the northwestern Deccan Traps. Bulletin of Volcanology, 77, 1- 19. https://doi.org/10.1007/s00445-015-0932-0

Daly, L., Lee, M. R., Piazolo, S., Griffin, S., Bazargan, M., Campanale, F., ... & Benedix, G. K. (2019). Boom boom pow: Shock-facilitated aqueous alteration and evidence for two shock events in the Martian nakhlite meteorites. Science Advances, 5(9), eaaw5549. https://doi.org/10.1126/sciadv.aaw5549

Das, A., Sarkar, S., Ray, D., & Sirvi, R. (2025). The Columnar Jointing in the Deccan Continental Flood Basalt, India: Implications as a Martian Analogue. Earth and Planetary Science, 4(1), 26-38. https://doi.org/10.36956/eps.v4i1.1652

Day, J. M., Tait, K. T., Udry, A., Moynier, F., Liu, Y., & Neal, C. R. (2018). Martian magmatism from plume metasomatized mantle. Nature communications, 9(1), 4799. https://doi.org/10.1038/s41467-018-07191-0

Day, J. M., Taylor, L. A., Floss, C., & Mcsween Jr, H. Y. (2006). Petrology and chemistry of MIL 03346 and its significance in understanding the petrogenesis of nakhlites on Mars. Meteoritics & Planetary Science, 41(4), 581-606. https://doi.org/10.1111/j.1945-5100.2006.tb00484.x

De Blasio, F. V. (2011). Landslides in Valles Marineris (Mars): A possible role of basal lubrication by sub-surface ice. Planetary and Space Science, 59(13), 1384- 1392. https://doi.org/10.1016/j.pss.2011.04.015

Deer, W. A., Howie, R. A., & Zussman, J. (2013). An Introduction to the Rock-Forming Minerals. 3rd ed. The Mineralogical Society, London, 498 p

Deka, B., Ahmad, A., Patel, R. R., & Nair, A. M. (2019, December). Spectral Mapping of the Pavonis Mons of Mars using CRISM and THEMIS data. In AGU Fall Meeting Abstracts (Vol. 2019, pp. EP21E-2215).

Delvigne, J., Bisdom, E. B. A., Sleeman, J., & Stoops, G. (1979). Olivines, their pseudomorphs and secondary products.

Dessai, A. G., & Bertrand, H. (1995). The "Panvel Flexure" along the Western Indian continental margin: an extensional fault structure related to Deccan magmatism. Tectonophysics, 241(1-2), 165-178. https://doi.org/10.1016/00401951(94)00077-M

Donovan, J. J., & Tingle, T. N. (1996). An improved mean atomic number background correction for quantitative microanalysis. Microscopy and Microanalysis, 2(1), 1-7. https://doi.org/10.1017/S1431927696210013

Downs, R. T., & MSL Science Team. (2015). Determining mineralogy on Mars with the CheMin X-ray diffractometer. Elements, 11(1), 45-50. https://doi.org/10.2113/gselements.11.1.45

Duncan, R. A., & Richards, M. A. (1991). Hotspots, mantle plumes, flood basalts, and true polar wander. Reviews of Geophysics, 29(1), 31-50. https://doi.org/10.1029/90RG02372

Edwards, C. S., & Ehlmann, B. L. (2015). Carbon sequestration on Mars. Geology, 43(10), 863-866. https://doi.org/10.1130/G36983.1

Eggleton, R. A. (1984). Formation of iddingsite rims on olivine: a transmission electron microscope study. Clays and Clay Minerals, 32(1), 1-11.

Ehlmann, B. L., & Edwards, C. S. (2014). Mineralogy of the Martian surface. Annual Review of Earth and Planetary Sciences, 42(1), 291-315. https://doi.org/10.1146/annurev-earth-060313-055024

Ehlmann, B. L., Anderson, F. S., Andrews-Hanna, J., Catling, D. C., Christensen, P. R., Cohen, B. A., ... & Zahnle, K. J. (2016). The sustainability of habitability on terrestrial planets: Insights, questions, and needed measurements from Mars for understanding the evolution of Earth-like worlds. Journal of Geophysical Research: Planets, 121(10), 1927-1961. https://doi.org/10.1002/2016JE005134

Ehlmann, B. L., Berger, G., Mangold, N., Michalski, J. R., Catling, D. C., Ruff, S. W., ... & Poulet, F. (2013). Geochemical consequences of widespread clay mineral formation in Mars' ancient crust. Space Science Reviews, 174(1), 329-364. https://doi.org/10.1007/s11214-012-9930-0

Ehlmann, B. L., Mustard, J. F., Fassett, C. I., Schon, S. C., Head III, J. W., Des Marais, D. J., ... & Murchie, S. L. (2008). Clay minerals in delta deposits and organic preservation potential on Mars. Nature Geoscience, 1(6), 355-358. https://doi.org/10.1038/ngeo207

Ehlmann, B. L., Mustard, J. F., Murchie, S. L., Bibring, J. P., Meunier, A., Fraeman, A. A., & Langevin, Y. (2011). Subsurface water and clay mineral formation during the early history of Mars. Nature, 479(7371), 53-60. https://doi.org/10.1038/nature10582

Ehlmann, B. L., Mustard, J. F., Swayze, G. A., Clark, R. N., Bishop, J. L., Poulet, F., ... & Murchie, S. L. (2009). Identification of hydrated silicate minerals on Mars using MRO-CRISM: Geologic context near Nili Fossae and implications for aqueous alteration. Journal of Geophysical Research: Planets, 114(E2). https://doi.org/10.1029/2009JE003339

Eiler, J. M., Kitchen, N., Leshin, L., & Strausberg, M. (2002). Hosts of hydrogen in Allan Hills 84001: Evidence for hydrous martian salts in the oldest martian meteorite?. Meteoritics & Planetary Science, 37(3), 395-405. https://doi.org/10.1111/j.1945-5100.2002.tb00823.x

Ember, K. J., Hoeve, M. A., McAughtrie, S. L., Bergholt, M. S., Dwyer, B. J., Stevens, M. M., ... & Campbell, C. J. (2017). Raman spectroscopy and regenerative medicine: a review. NPJ Regenerative medicine, 2(1), 12. https://doi.org/10.1038/s41536-017-0014-3

Eugster, O., Busemann, H., Lorenzetti, S., & Terribilini, D. (2002). Ejection ages from krypton-81-krypton-83 dating and pre-atmospheric sizes of Martian meteorites. Meteoritics & Planetary Science, 37(10), 1345-1360. https://doi.org/10.1111/j.1945-5100.2002.tb01033.x

Fainstein, R., Richards, M., & Kalra, R. (2019). Seismic imaging of Deccan-related lava flows at the KT boundary, deepwater west India. The Leading Edge, 38(4), 286-290. https://doi.org/10.1190/tle38040286.1

Fairén, A. G., Chevrier, V., Abramov, O., Marzo, G. A., Gavin, P., Davila, A. F., ... & McKay, C. P. (2010). Noachian and more recent phyllosilicates in impact craters on Mars. Proceedings of the National Academy of Sciences, 107(27), 12095- 12100. https://doi.org/10.1073/pnas.1002889107

Fassett, C. I., & Head III, J. W. (2008). Valley network-fed, open-basin lakes on Mars: Distribution and implications for Noachian surface and subsurface hydrology. Icarus, 198(1), 37-56. https://doi.org/10.1016/j.icarus.2008.06.016

Fritz, J., Artemieva, N., & Greshake, A. (2005). Ejection of Martian meteorites. Meteoritics & Planetary Science, 40(9-10), 1393-1411. https://doi.org/10.1111/j.1945-5100.2005.tb00409.x

Fuentes-Carreón, C. A., Cruz-Castañeda, J. A., Mateo-Martí, E., & Negrón-Mendoza, A. (2022). Stability of DL-Glyceraldehyde under Simulated Hydrothermal Conditions: Synthesis of Sugar-like Compounds in an Iron (III)-Oxide- Hydroxide-Rich Environment under Acidic Conditions. Life, 12(11), 1818. https://doi.org/10.3390/life12111818

Gainey, S. R., Hausrath, E. M., Adcock, C. T., Tschauner, O., Hurowitz, J. A., Ehlmann, B. L., ... & Bartlett, C. L. (2017). Clay mineral formation under oxidized conditions and implications for paleoenvironments and organic preservation on Mars. Nature communications, 8(1), 1230. https://doi.org/10.1038/s41467-017-01235-7

Gates-Rector, S., & Blanton, T. (2019). The powder diffraction file: a quality materials characterization database. Powder diffraction, 34(4), 352–360. https://doi:10.1017/S0885715619000812

Georgiadis, A., Dietel, J., Dohrmann, R., & Rennert, T. (2019). What are the nature and formation conditions of hydroxy-interlayered minerals (HIMs) in soil?. Journal of Plant Nutrition and Soil Science, 183(1), 12-26. https://doi.org/10.1002/jpln.201900283

Gillet, P., Barrat, J. A., Deloule, E., Wadhwa, M., Jambon, A., Sautter, V., & Lesourd, M. (2002). Aqueous alteration in the Northwest Africa 817 (NWA 817) Martian meteorite. Earth and Planetary Science Letters, 203(1), 431-444. https://doi.org/10.1016/S0012-821X(02)00835-X

Goff, F. (1996). Vesicle cylinders in vapor-differentiated basalt flows. Journal of Volcanology and Geothermal Research, 71(2-4), 167-185. https://doi.org/10.1016/0377-0273(95)00073-9

Goldich, S. S. (1938). A study in rock-weathering. The Journal of Geology, 46(1), 17- 58. https://doi.org/10.1086/624619

Golombek, M. P., Grant, J. A., Crumpler, L. S., Greeley, R., Arvidson, R. E., Bell III, J. F., ... & Squyres, S. W. (2006). Erosion rates at the Mars Exploration Rover landing sites and long-term climate change on Mars. Journal of Geophysical Research: Planets, 111(E12). https://doi.org/10.1029/2006JE002754

Gooding, J. L. (1992). Soil mineralogy and chemistry on Mars: Possible clues from salts and clays in SNC meteorites. Icarus, 99(1), 28-41. https://doi.org/10.1016/0019-1035(92)90168-7

Goodrich, C. A. (2002). Olivine-phyric Martian basalts: A new type of shergottite. Meteoritics & Planetary Science, vol. 37, Supplement, p. 31-34, 37, 31-34.

Goudge, T. A., Head, J. W., Mustard, J. F., & Fassett, C. I. (2012). An analysis of open- basin lake deposits on Mars: Evidence for the nature of associated lacustrine deposits and post-lacustrine modification processes. Icarus, 219(1), 211-229. https://doi.org/10.1016/j.icarus.2012.02.027

Gourronc, M., Bourgeois, O., Mège, D., Pochat, S., Bultel, B., Massé, M., ...& Mercier, D. (2014). One million cubic kilometers of fossil ice in Valles Marineris: Relicts of a 3.5 Gy old glacial landsystem along the Martian equator. Geomorphology, 204, 235-255. https://doi.org/10.1016/j.geomorph.2013.08.009

Grauby, O., Petit, S., Decarreau, A., & Baronnet, A. (1994). The nontronite-saponite series; an experimental approach. European journal of mineralogy, 6(1), 99- 112.

Grim, R. E. (1953). Clay mineralogy (Vol. 76, No. 4, p. 317). LWW.

Gualtieri, A. F., Gemmi, M., & Dapiaggi, M. (2003). Phase transformations and reaction kinetics during the temperature-induced oxidation of natural olivine. American Mineralogist, 88(10), 1560-1574. https://doi.org/10.2138/am-2003-1019

Hagerty, J. J., & Newsom, H. E. (2001, March). New evidence for impact-induced hydrothermal alteration at the Lonar crater, India: Implications for the effect of small craters on the mineralogical and chemical composition of the Martian regolith. In Lunar and Planetary Science Conference (p. 1131). https://ui.adsabs.harvard.edu/abs/2001LPI32.1131H/abstract

Hagerty, J. J., & Newsom, H. E. (2003). Hydrothermal alteration at the Lonar Lake impact structure, India: Implications for impact cratering on Mars. Meteoritics & Planetary Science, 38(3), 365-381. https://doi.org/10.1111/j.1945-5100.2003.tb00272.x

Hallis, L. J., & Taylor, G. J. (2011). Comparisons of the four Miller Range nakhlites, MIL 03346, 090030, 090032 and 090136: Textural and compositional observations of primary and secondary mineral assemblages. Meteoritics & Planetary Science, 46(12), 1787-1803. https://doi.org/10.1111/j.1945-5100.2011.01293.x

Hallis, L. J., Ishii, H. A., Bradley, J. P., & Taylor, G. J. (2014). Transmission electron microscope analyses of alteration phases in Martian meteorite MIL 090032. Geochimica et Cosmochimica Acta, 134, 275-288. https://doi.org/10.1016/j.gca.2014.02.007

Hallis, L. J., Taylor, G. J., Nagashima, K., Huss, G. R., Needham, A. W., Grady, M. M., & Franchi, I. A. (2012). Hydrogen isotope analyses of alteration phases in the nakhlite martian meteorites. Geochimica et Cosmochimica Acta, 97, 105-119. https://doi.org/10.1016/j.gca.2012.08.017

Hartmann, W., Winterhalter, D., & Geiss, J. (2005). Chronology and physical evolution of planet Mars. The Solar System and Be-yond—Ten Years of ISSI, ISSI Bern SR-003, 211-228.

Hausrath, E. M., & Brantley, S. L. (2010). Basalt and olivine dissolution under cold, salty, and acidic conditions: What can we learn about recent aqueous weathering on Mars?. Journal of Geophysical Research: Planets, 115(E12). https://doi.org/10.1029/2010JE003610

Hawkesworth, C. J., Gallagher, K., Kirstein, L., Mantovani, M. S. M., Peate, D. W., & Turner, S. P. (2000). Tectonic controls on magmatism associated with continental break-up: an example from the Paraná–Etendeka Province. Earth and Planetary Science Letters, 179(2), 335-349. https://doi.org/10.1016/S0012-821X(00)00114-X

Hazen, R. M., Sverjensky, D. A., Azzolini, D., Bish, D. L., Elmore, S. C., Hinnov, L., & Milliken, R. E. (2013). Clay mineral evolution. American Mineralogist, 98(11-12), 2007-2029. https://doi.org/10.2138/am.2013.4425

Herd, C. D., Walton, E. L., Agee, C. B., Muttik, N., Ziegler, K., Shearer, C. K., ... & Caffee, M. W. (2017). The Northwest Africa 8159 martian meteorite: Expanding the martian sample suite to the early Amazonian. Geochimica et Cosmochimica Acta, 218, 1-26. https://doi.org/10.1016/j.gca.2017.08.037

Hernanz, A., Bratu, I., Marutoiu, O. F., Marutoiu, C., Gavira-Vallejo, J. M., & Edwards, H. G. M. (2008). Micro-Raman spectroscopic investigation of external wall paintings from

St. Dumitru's Church, Suceava, Romania. Analytical and Bioanalytical Chemistry, 392, 263-268. https://doi.org/10.1007/s00216-008-2262-y

Hewins, R. H., Humayun, M., Barrat, J. A., Zanda, B., Lorand, J. P., Pont, S., ... & Sautter, V. (2020). Northwest Africa 8694, a ferroan chassignite: Bridging the gap between nakhlites and chassignites. Geochimica et Cosmochimica Acta, 282, 201-226. https://doi.org/10.1016/j.gca.2020.05.021

Hewins, R. H., Zanda, B., Pont, S., & Zanetta, P. M. (2019). Northwest Africa 10414, a pigeonite cumulate shergottite. Meteoritics & Planetary Science, 54(9), 2132- 2148. https://doi.org/10.1111/maps.13374

Hicks, L. J., Bridges, J. C., & Gurman, S. J. (2014). Ferric saponite and serpentine in the nakhlite martian meteorites. Geochimica et Cosmochimica Acta, 136, 194- 210. https://doi.org/10.1016/j.gca.2014.04.010

Hobley, D. E., Howard, A. D., & Moore, J. M. (2014). Fresh shallow valleys in the Martian midlatitudes as features formed by meltwater flow beneath ice. Journal of Geophysical Research: Planets, 119(1), 128-153. https://doi.org/10.1002/2013JE004396

Hoefen, T. M., Clark, R. N., Bandfield, J. L., Smith, M. D., Pearl, J. C., & Christensen, P. R. (2003). Discovery of olivine in the Nili Fossae region of Mars. Science, 302(5645), 627-630. https://doi.org/10.1126/science.1089647

Horgan, B., & Bell III, J. F. (2012). Widespread weathered glass on the surface of Mars. Geology, 40(5), 391-394. https://doi.org/10.1130/G32755.1

Horvath, D. G., & Andrews-Hanna, J. C. (2017). Reconstructing the past climate at Gale crater, Mars, from hydrological modeling of late-stage lakes. Geophysical Research Letters, 44(16), 8196-8204. https://doi.org/10.1002/2017GL074654

Imae, N., & Ikeda, Y. (2010). High-pressure polymorphs of magnesian orthopyroxene from a shock vein in the Yamato-000047 lherzolitic shergottite. Meteoritics & Planetary Science, 45(1), 43-54. https://doi.org/10.1111/j.1945-5100.2009.01004.x

Ivanov, B. A. (2001). Mars/Moon cratering rate ratio estimates. Space Science Reviews, 96(1), 87-104. https://doi.org/10.1023/A:1011941121102

Ivanov, M. A., Slyuta, E. N., Grishakina, E. A., & Dmitrovskii, A. A. (2020). Geomorphological analysis of ExoMars candidate landing site Oxia Planum. Solar System Research, 54, 1-14. https://doi.org/10.1134/S0038094620010050

Jambon, A., Barrat, J. A., Sautter, V., Gillet, P., Göpel, C., Javoy, M., ... & Lesourd, M. (2002). The basaltic shergottite Northwest Africa 856: Petrology and chemistry. Meteoritics & Planetary Science, 37(9), 1147-1164. https://doi.org/10.1111/j.1945-5100.2002.tb00885.x

Jambon, A., Sautter, V., Barrat, J. A., Gattacceca, J., Rochette, P., Boudouma, O., ... & Devouard, B. (2016). Northwest Africa 5790: revisiting nakhlite petrogenesis. Geochimica et Cosmochimica Acta, 190, 191-212. https://doi.org/10.1016/j.gca.2016.06.032

Jay, A. E., & Widdowson, M. (2008). Stratigraphy, structure and volcanology of the SE Deccan continental flood basalt province: implications for eruptive extent and volumes. Journal of the Geological Society, 165(1), 177-188. https://doi.org/10.1144/0016-76492006-062

Johnson, M. C., Rutherford, M. J., & Hess, P. C. (1991). Chassigny petrogenesis: Melt compositions, intensive parameters and water contents of Martian (?) magmas. Geochimica et Cosmochimica Acta, 55(1), 349-366. https://doi.org/10.1016/0016-7037(91)90423-3

Kelley, D. S., Karson, J. A., Blackman, D. K., FruÈh-Green, G. L., Butterfield, D. A., Lilley, M. D., ... & AT3-60 Shipboard Party. (2001). An off-axis hydrothermal vent field near the Mid-Atlantic Ridge at 30 N. Nature, 412(6843), 145-149. https://doi.org/10.1038/35084000

Kerr PF (1977) Optical mineralogy. 4st edition, McGrawHill Book Company, p 492

Kerridge, J. F. (1985). Carbon, hydrogen and nitrogen in carbonaceous chondrites: Abundances and isotopic compositions in bulk samples. Geochimica et Cosmochimica Acta, 49(8), 1707-1714. https://doi.org/10.1016/0016-7037(85)90141-3

Khanna, T. C., Barbeau Jr, D. L., Arora, K., & Sariput, S. (2023). Petrogenesis of Neoarchean granitoids beneath the Koyna-Warna region, Deccan Volcanic Province, India. Journal of Asian Earth Sciences, 241, 105455. https://doi.org/10.1016/j.jseaes.2022.105455

Kizovski, T. V., Izawa, M. R. M., Tait, K. T., Moser, D. E., Day, J. M. D., Hyde, B. C.,... & Joy, B. R. (2020). Petrogenesis, alteration, and shock history of intermediate shergottite Northwest Africa 7042: Evidence for hydrous magmatism on Mars?. Geochimica et Cosmochimica Acta, 283, 103-123. https://doi.org/10.1016/j.gca.2020.05.030

Klingelhofer, G., Morris, R. V., Bernhardt, B., Schroder, C., Rodionov, D. S., de Souza Jr, P. A., ... & Arvidson, R. E. (2004). Jarosite and hematite at Meridiani Planum from Opportunity's Mossbauer spectrometer. Science, 306(5702), 1740-1745. https://doi.org/10.1126/science.1104653

Kloprogge, J. T., & Ponce, C. P. (2021). Spectroscopic studies of synthetic and natural saponites: a review. Minerals, 11(2), 112. https://doi.org/10.3390/min11020112

Krasnopolsky, V. A., Mumma, M. J., & Gladstone, G. R. (1998). Detection of atomic deuterium in the upper atmosphere of Mars. Science, 280(5369), 1576-1580. https://doi.org/10.1126/science.280.5369.1576

Krishnamurthy, P. (2020). The Deccan Volcanic Province (DVP), India: a review: Part 2: Geochemistry, petrological evolution, petrogenesis, mantle sources, age and erupted volume relations, Upper Cretaceous-Palaeogene (K-Pg) mass extinctions, economic aspects, summary and future studies in DVP. Journal of the Geological Society of India, 96(2), 111-147. https://doi.org/10.1007/s12594-020-1521-1

Krishnamurthy, P., & Cox, K. G. (1977). Picrite basalts and related lavas from the Deccan Traps of western India. Contributions to Mineralogy and Petrology, 62(1), 53-75. https://doi.org/10.1007/BF00371027

Krishnamurthy, P., Gopalan, K., & Macdougall, J. D. (2000). Olivine compositions in picrite basalts and the Deccan volcanic cycle. Journal of Petrology, 41(7), 1057- 1069. https://doi.org/10.1093/petrology/41.7.1057

Krämer Ruggiu, L., Devouard, B., Gattacceca, J., Bonal, L., Piani, L., Leroux, H., & Grauby, O. (2025). Multistage aqueous alteration in CeC 022 and other nakhlites. Meteoritics & Planetary Science, 60(2), 151-174. https://doi.org/10.1111/maps.14295

Kshirsagar, P. V., Sheth, H. C., Seaman, S. J., Shaikh, B., Mohite, P., Gurav, T., & Chandrasekharam, D. (2012). Spherulites and thundereggs from pitchstones of the Deccan Traps: geology, petrochemistry, and emplacement environments. Bulletin of Volcanology, 74, 559-577. https://doi.org/10.1007/s00445-011-0543-3

Kuebler, K. E. (2013). A combined electron microprobe (EMP) and Raman spectroscopic study of the alteration products in Martian meteorite MIL 03346. Journal of Geophysical Research: Planets, 118(3), 347-368. https://doi.org/10.1029/2012JE004244

Kuebler, K. E., Jolliff, B. L., Wang, A., & Haskin, L. A. (2006). Extracting olivine (Fo– Fa) compositions from Raman spectral peak positions. Geochimica et Cosmochimica Acta, 70(24), 6201-6222. https://doi.org/10.1016/j.gca.2006.07.035

Lane, M. D., & Christensen, P. R. (2013). Determining olivine composition of basaltic dunes in Gale Crater, Mars, from orbit: Awaiting ground truth from Curiosity. Geophysical Research Letters, 40(14), 3517-3521. https://doi.org/10.1002/grl.50621

Langlais, B., Thebault, E., & Milbury, C. (2011, October). A magnetic time line for Mars. In EPSC-DPS Joint Meeting 2011 (Vol. 2011, p. 773).

Lapen, T. J., Righter, M., Andreasen, R., Irving, A. J., Satkoski, A. M., Beard, B. L., ... & Caffee, M. W. (2017). Two billion years of magmatism recorded from a single Mars meteorite ejection site. Science advances, 3(2), e1600922. https://doi.org/10.1126/sciadv.1600922

Le Bas, M. J. (2000). IUGS reclassification of the high-Mg and picritic volcanic rocks. Journal of Petrology, 41(10), 1467-1470. https://doi.org/10.1093/petrology/41.10.1467

Lee, M. R., Daly, L., Cohen, B. E., Hallis, L. J., Griffin, S., Trimby, P., ... & Mark, D. F. (2018). Aqueous alteration of the Martian meteorite Northwest Africa 817: Probing fluid–rock interaction at the nakhlite launch site. Meteoritics & Planetary Science, 53(11), 2395-2412. https://doi.org/10.1111/maps.13136

Lee, M. R., MacLaren, I., Andersson, S. M. L., Kovacs, A., Tomkinson, T., Mark, D. F., & Smith, C. L. (2015). Opal-A in the Nakhla meteorite: A tracer of ephemeral liquid water

in the Amazonian crust of Mars. Meteoritics & Planetary Science, 50(8), 1362-1377. https://doi.org/10.1111/maps.12471

Lee, M. R., Tomkinson, T., Hallis, L. J., & Mark, D. F. (2015). Formation of iddingsite veins in the martian crust by centripetal replacement of olivine: Evidence from the nakhlite meteorite Lafayette. Geochimica et Cosmochimica Acta, 154, 49- 65. https://doi.org/10.1016/j.gca.2015.01.022

Leshin, L. A., Epstein, S., & Stolper, E. M. (1996). Hydrogen isotope geochemistry of SNC meteorites. Geochimica et Cosmochimica Acta, 60(14), 2635-2650. https://doi.org/10.1016/0016-7037(96)00122-6

Loretto, M. H. (1984). Interpretation of Analytical Data. In Electron Beam Analysis of Materials (pp. 153–178). Dordrecht: Springer Netherlands. https://doi.org/10.1007/978-94-009-5540-0_6

Lu, J. F., & Tsai, C. J. (2014). Hydrothermal phase transformation of hematite to magnetite. Nanoscale research letters, 9, 1-8. https://doi.org/10.1186/1556-276X-9-230

Mahoney, J. J., Duncan, R. A., Khan, W., Gnos, E., & McCormick, G. R. (2002). Cretaceous volcanic rocks of the South Tethyan suture zone, Pakistan: implications for the Réunion hotspot and Deccan Traps. Earth and Planetary Science Letters, 203(1), 295-310. https://doi.org/10.1016/S0012-821X(02)00840-3

Marguí, E., Queralt, I., & De Almeida, E. (2022). X-ray fluorescence spectrometry for environmental analysis: Basic principles, instrumentation, applications and recent trends. Chemosphere, 303, 135006. https://doi.org/10.1016/j.chemosphere.2022.135006

Marinova, M. M., Aharonson, O., & Asphaug, E. (2008). Mega-impact formation of the Mars hemispheric dichotomy. Nature, 453(7199), 1216-1219. https://doi.org/10.1038/nature07070

Marzo, G. A., Davila, A. F., Tornabene, L. L., Dohm, J. M., Fairén, A. G., Gross, C., & McKay, C. P. (2010). Evidence for Hesperian impact-induced hydrothermalism on Mars. Icarus, 208(2), 667-683. https://doi.org/10.1016/j.icarus.2010.03.013

Mateus, A. C. C., Varajão, A. F. D. C., Oliveira, F. S., & Schaefer, C. E. (2018). Alteration of olivine in volcanic rocks from Trindade Island, South Atlantic. Applied Clay Science, 160, 40-48. https://doi.org/10.1016/j.clay.2018.01.033

Matsubara, Y., Howard, A. D., & Gochenour, J. P. (2013). Hydrology of early Mars: Valley network incision. Journal of Geophysical Research: Planets, 118(6), 1365-1387. https://doi.org/10.1002/jgre.20081

McCollom, T. M., & Seewald, J. S. (2013). Serpentinites, hydrogen, and life. Elements, 9(2), 129-134. https://doi.org/10.2113/gselements.9.2.129

McCubbin, F. M., Elardo, S. M., Shearer Jr, C. K., Smirnov, A., Hauri, E. H., & Draper, D. S. (2013). A petrogenetic model for the comagmatic origin of chassignites and nakhlites: Inferences from chlorine-rich minerals, petrology, and geochemistry. Meteoritics & Planetary Science, 48(5), 819-853. https://doi.org/10.1111/maps.12095

McCubbin, F. M., Hauri, E. H., Elardo, S. M., Vander Kaaden, K. E., Wang, J., & Shearer Jr, C. K. (2012). Hydrous melting of the martian mantle produced both depleted and enriched shergottites. Geology, 40(8), 683-686. https://doi.org/10.1130/G33242.1

McCubbin, F. M., Tosca, N. J., Smirnov, A., Nekvasil, H., Steele, A., Fries, M., & Lindsley, D. H. (2009). Hydrothermal jarosite and hematite in a pyroxene- hosted melt inclusion in

martian meteorite Miller Range (MIL) 03346: Implications for magmatic-hydrothermal fluids on Mars. Geochimica et Cosmochimica Acta, 73(16), 4907-4917. https://doi.org/10.1016/j.gca.2009.05.031

McEwen, A. S., Ojha, L., Dundas, C. M., Mattson, S. S., Byrne, S., Wray, J. J., ... & Gulick, V. C. (2011). Seasonal flows on warm Martian slopes. science, 333(6043), 740-743. https://doi.org/10.1126/science.1204816

McEwen, A. S., Preblich, B. S., Turtle, E. P., Artemieva, N. A., Golombek, M. P., Hurst, M., ... & Christensen, P. R. (2005). The rayed crater Zunil and interpretations of small impact craters on Mars. Icarus, 176(2), 351-381. https://doi.org/10.1016/j.icarus.2005.02.009

McKeown, N. K., Bishop, J. L., Noe Dobrea, E. Z., Ehlmann, B. L., Parente, M., Mustard, J. F., ... & Silver, E. A. (2009). Characterization of phyllosilicates observed in the central Mawrth Vallis region, Mars, their potential formational processes, and implications for past climate. Journal of Geophysical Research: Planets, 114(E2). https://doi.org/10.1029/2008JE003301

McLennan, S. M., Anderson, R. B., Bell III, J. F., Bridges, J. C., Calef III, F., Campbell, J. L., ... & Harri, A. M. (2014). Elemental geochemistry of sedimentary rocks at Yellowknife Bay, Gale crater, Mars. Science, 343(6169), 1244734. https://doi.org/10.1126/science.1244734

McMahon, S., Bosak, T., Grotzinger, J. P., Milliken, R. E., Summons, R. E., Daye, M., & Briggs, D. E. G. (2018). A field guide to finding fossils on Mars. Journal of Geophysical Research: Planets, 123(5), 1012-1040. https://doi.org/10.1029/2017JE005478

McSween Jr, H. Y. (1984). SNC meteorites: Are they Martian rocks?. Geology, 12(1), 3-6. https://doi.org/10.1130/0091- 7613(1984)12%3C3:SMATMR%3E2.0.CO;2

McSween, H. Y., Wyatt, M. B., Gellert, R., Bell III, J. F., Morris, R. V., Herkenhoff, K. E., ... & Zipfel, J. (2006). Characterization and petrologic interpretation of olivine-rich basalts at Gusev Crater, Mars. Journal of Geophysical Research: Planets, 111(E2). https://doi.org/10.1029/2005JE002477

Meech, K., Raymond, S. N., Meadows, V., Arney, G., Schmidt, B., & Des Marais, D. G. (2020). Origin of Earth's water: sources and constraints. Planetary astrobiology, 325.

Melluso, L., Beccaluva, L., Brotzu, P., Gregnanin, A., Gupta, A. K., Morbidelli, L., & Traversa, G. (1995). Constraints on the mantle sources of the Deccan Traps from the petrology and geochemistry of the basalts of Gujarat State (Western India). Journal of Petrology, 36(5), 1393-1432. https://doi.org/10.1093/petrology/36.5.1393

Meunier, A., Petit, S., Ehlmann, B. L., Dudoignon, P., Westall, F., Mas, A., ... & Ferrage, E. (2012). Magmatic precipitation as a possible origin of Noachian clays on Mars. Nature Geoscience, 5(10), 739-743. https://doi.org/10.1038/ngeo1572

Mikouchi T., Makishima J., Kurihara T., Hoffmann V. H., and Miyamoto M. 2012. Relative burial depth of nakhlites revisited (abstract #2363). 43rd Lunar and Planetary Science Conference. CD-ROM.

Mikouchi, T. (2005). Northwest Africa 1950: Mineralogy and comparison with Antarctic lherzolitic shergottites. Meteoritics & Planetary Science, 40(11), 1621-1634. https://doi.org/10.1111/j.1945-5100.2005.tb00135.x

Milazzo, M. P., Keszthelyi, L. P., Jaeger, W. L., Rosiek, M., Mattson, S., Verba, C., ... & HiRISE Team. (2009). Discovery of columnar jointing on Mars. Geology, 37(2), 171-174. https://doi.org/10.1130/G25187A.1

Milliken, R. E., & Bish, D. L. (2010). Sources and sinks of clay minerals on Mars. Philosophical Magazine, 90(17-18), 2293-2308. https://doi.org/10.1080/14786430903575132

Ming, D. W., Mittlefehldt, D. W., Morris, R. V., Golden, D. C., Gellert, R., Yen, A., ... & Wang, A. (2006). Geochemical and mineralogical indicators for aqueous processes in the Columbia Hills of Gusev crater, Mars. Journal of Geophysical Research: Planets, 111(E2). https://doi.org/10.1029/2005JE002560

Minissale, A., Vaselli, O., Chandrasekharam, D., Magro, G., Tassi, F., & Casiglia, A. (2000). Origin and evolution of 'intracratonic'thermal fluids from central- western peninsular India. Earth and Planetary Science Letters, 181(3), 377-394. https://doi.org/10.1016/S0012-821X(00)00200-4

Misawa, K., Shih, C. Y., Reese, Y., Bogard, D. D., & Nyquist, L. E. (2006). Rb–Sr, Sm– Nd and Ar–Ar isotopic systematics of martian dunite chassigny. Earth and Planetary Science Letters, 246(1-2), 90-101. https://doi.org/10.1016/j.epsl.2006.03.044

Misawa, K., Shih, C. Y., Wiesmann, H., Garrison, D. H., Nyquist, L. E., & Bogard, D. D. (2005). Rb-Sr, Sm-Nd and Ar-Ar isotopic systematics of Antarctic nakhlite Yamato 000593. Antarctic meteorite research, 18, 133-151. https://doi.org/10.15094/00006069

Mitchell, K. L., & Wilson, L. (2003). Mars: a geologically active planet. Astronomy & Geophysics, 44(4), 4-16. https://doi.org/10.1046/j.1468-4004.2003.44416.x

Mitra, K., Mitra, S., Gupta, S., Bhattacharya, S., Chauhan, P., & Jain, N. (2018). Modelling basalt weathering at elevated CO2 concentrations: implications for terminal to post-magmatic rifting in the Deccan Traps, Kachchh, India. https://doi.org/10.1144/SP463.8

Mitrofanov, I., Malakhov, A., Djachkova, M., Golovin, D., Litvak, M., Mokrousov, M., .. & Zelenyi, L. (2022). The evidence for unusually high hydrogen abundances in the central part of Valles Marineris on Mars. Icarus, 374, 114805. https://doi.org/10.1016/j.icarus.2021.114805

Mittelholz, A., Morschhauser, A., Johnson, C. L., Langlais, B., Lillis, R. J., Vervelidou, F., & Weiss, B. P. (2018). The Mars 2020 candidate landing sites: A magnetic field perspective. Earth and Space Science, 5(9), 410-424. https://doi.org/10.1029/2018EA000420

Mojzsis, S. J., Arrhenius, G., McKeegan, K. D., Harrison, T. M., Nutman, A. P., & Friend, C. R. L. (1996). Evidence for life on Earth before 3,800 million years ago. Nature, 384(6604), 55-59. https://doi.org/10.1038/384055a0

Morbidelli, A. (2018). Accretion processes. arXiv preprint arXiv:1803.06708. https://doi.org/10.48550/arXiv.1803.06708

Morbidelli, A., Brasser, R., Gomes, R., Levison, H. F., & Tsiganis, K. (2010). Evidence from the asteroid belt for a violent past evolution of Jupiter's orbit. The Astronomical Journal, 140(5), 1391. https://doi.org/10.1088/0004- 6256/140/5/1391

Morrison, S. M., Downs, R. T., Blake, D. F., Vaniman, D. T., Ming, D. W., Hazen, R. M., & Craig, P. I. (2018). Crystal chemistry of martian minerals from Bradbury Landing through Naukluft Plateau, Gale crater, Mars. American Mineralogist: Journal of Earth and Planetary Materials, 103(6), 857-871. https://doi.org/10.2138/am-2018-6124

Moura, C. C., Tare, R. S., Oreffo, R. O., & Mahajan, S. (2016). Raman spectroscopy and coherent anti-Stokes Raman scattering imaging: prospective tools for monitoring skeletal cells and skeletal regeneration. Journal of The Royal Society Interface, 13(118), 20160182. https://doi.org/10.1098/rsif.2016.0182

Murchie, S. L., Mustard, J. F., Ehlmann, B. L., Milliken, R. E., Bishop, J. L., McKeown, N. K., ... & Bibring, J. P. (2009). A synthesis of Martian aqueous mineralogy after 1 Mars year of observations from the Mars Reconnaissance Orbiter. Journal of Geophysical Research: Planets, 114(E2). https://doi.org/10.1029/2009JE003342

Murchie, S. L., Mustard, J. F., Ehlmann, B. L., Milliken, R. E., Bishop, J. L., McKeown, N. K., ... & Bibring, J. P. (2009). A synthesis of Martian aqueous mineralogy after 1 Mars year of observations from the Mars Reconnaissance Orbiter. Journal of Geophysical Research: Planets, 114(E2). https://doi.org/10.1029/2009JE003342

Murray, J., & Jagoutz, O. (2024). Olivine alteration and the loss of Mars' early atmospheric carbon. Science Advances, 10(39), eadm8443. https://doi.org/10.1126/sciadv.adm8443

Mustard, J. F., Murchie, S. L., Pelkey, S. M., Ehlmann, B. L., Milliken, R. E., Grant, J. A., ... & Wolff, M. (2008). Hydrated silicate minerals on Mars observed by the Mars Reconnaissance Orbiter CRISM instrument. Nature, 454(7202), 305-309. https://doi.org/10.1038/nature07097

Mustard, J. F., Poulet, F., Gendrin, A., Bibring, J. P., Langevin, Y., Gondet, B., ... & Altieri, F. (2005). Olivine and pyroxene diversity in the crust of Mars. Science, 307(5715), 1594-1597. https://doi.org/10.1126/science.1109098

Nesbitt, H. W., & Wilson, R. E. (1992). Recent chemical weathering of basalts. American Journalof science, 292(10), 740-777. https://doi.org/10.2475/ajs.292.10.740

Nesbitt, H. W., & Young, G. M. (1984). Prediction of some weathering trends of plutonic and volcanic rocks based on thermodynamic and kinetic considerations. Geochimica et cosmochimica acta, 48(7), 1523-1534. https://doi.org/10.1016/0016-7037(84)90408-3

Nesbitt, H. W., 1992, Diagenesis and metasomatism of weathering profiles, with emphasis on Precambrian paleosols in Martini, I. P., and Chesworth, W., editors, Weathering, Soils and Paleosols; Amsterdam, Elsevier, Developments in Earth Surface Processes, v. 2, p. 127–153.

Nimmo, F., & Tanaka, K. (2005). Early crustal evolution of Mars. Annu. Rev. Earth Planet. Sci., 33(1), 133-161. https://doi.org/10.1146/annurev.earth.33.092203.122637

Noe Dobrea, E. Z., Bishop, J. L., McKeown, N. K., Fu, R., Rossi, C. M., Michalski, J. R., ... & Hash, C. (2010). Mineralogy and stratigraphy of phyllosilicate-bearing and dark mantling units in the greater Mawrth Vallis/west Arabia Terra area: Constraints on geological origin. Journal of Geophysical Research: Planets, 115(E7). https://doi.org/10.1029/2009JE003351

Noguchi, T., Nakamura, T., Misawa, K., Imae, N., Aoki, T., & Toh, S. (2009). Laihunite and jarosite in the Yamato 00 nakhlites: Alteration products on Mars?. Journal of Geophysical Research: Planets, 114(E10). https://doi.org/10.1029/2009JE003364

Nyquist, L. E., Bogard, D. D., Shih, C. Y., Greshake, A., Stöffler, D., & Eugster, O. (2001). Ages and geologic histories of Martian meteorites. Space Science Reviews, 96(1), 105-164. https://doi.org/10.1023/A:1011993105172

O'Brien, D. P., Walsh, K. J., Morbidelli, A., Raymond, S. N., & Mandell, A. M. (2014). Water delivery and giant impacts in the 'Grand Tack'scenario. Icarus, 239, 74- 84. https://doi.org/10.1016/j.icarus.2014.05.009

O'Brien, Á. C., Hallis, L. J., Regnault, C., Morrison, D., Blackburn, G., Steele, A., ... & Lee, M. (2022). Using Organic Contaminants to Constrain the Terrestrial Journey of the Martian Meteorite Lafayette. Astrobiology, 22(11), 1351-1362. https://doi.org/10.1089/ast.2021.0180

Ody, A., Poulet, F., Bibring, J. P., Loizeau, D., Carter, J., Gondet, B., & Langevin, Y. (2013). Global investigation of olivine on Mars: Insights into crust and mantle compositions. Journal of Geophysical Research: Planets, 118(2), 234-262. https://doi.org/10.1029/2012JE004149

Ody, A., Poulet, F., Langevin, Y., Bibring, J. P., Bellucci, G., Altieri, F.,.....& Manaud, N. C. E. J. (2012). Global maps of anhydrous minerals at the surface of Mars from OMEGA/MEx. Journal of Geophysical Research: Planets, 117(E11). https://doi.org/10.1029/2012JE004117 Ojha, L., Wilhelm, M. B., Murchie, S. L., McEwen, A. S., Wray, J. J., Hanley, J., ... & Chojnacki, M. (2015). Spectral evidence for hydrated salts in recurring slope lineae on Mars. Nature Geoscience, 8(11), 829-832.https://doi.org/10.1038/ngeo2546

Owen, T., Maillard, J. P., De Bergh, C., & Lutz, B. L. (1988). Deuterium on Mars: The abundance of HDO and the value of D/H. Science, 240(4860), 1767-1767. https://doi.org/10.1126/science.240.4860.1767

Palandri, J. L., & Kharaka, Y. K. (2004). A compilation of rate parameters of water- mineral interaction kinetics for application to geochemical modeling (No. 2004- 1068). US Geological Survey. https://doi.org/10.3133/ofr20041068

Pan, L., Ehlmann, B. L., Carter, J., & Ernst, C. M. (2017). The stratigraphy and history of Mars' northern lowlands through mineralogy of impact craters: A comprehensive survey. Journal of Geophysical Research: Planets, 122(9), 1824-1854. https://doi.org/10.1002/2017JE005276

Pande, K., Yatheesh, V., & Sheth, H. (2017). 40Ar/39Ar dating of the Mumbai tholeiites and Panvel flexure: intense 62.5 Ma onshore–offshore Deccan magmatism during India-

Laxmi Ridge–Seychelles breakup. Geophysical Journal International, 210(2), 1160-1170. https://doi.org/10.1093/gji/ggx205

Peng, Z. X., & Mahoney, J. J. (1995). Drillhole lavas from the northwestern Deccan Traps, and the evolution of Réunion hotspot mantle. Earth and Planetary Science Letters, 134(1-2), 169-185. https://doi.org/10.1016/0012-821X(95)00110-X.

Phua, Y. Y., Ehlmann, B. L., Siljeström, S., Czaja, A. D., Beck, P., Connell, S., ... & Yanchilina, A. G. (2024). Characterizing hydrated sulfates and altered phases inJezero Crater fan and floor geologic units with SHERLOC on Mars 2020. Journal of Geophysical Research: Planets, 129(7), e2023JE008251. https://doi.org/10.1029/2023JE008251

Piercy, J. D., Bridges, J. C., & Hicks, L. J. (2022). Carbonate dissolution and replacement by odinite and saponite in the Lafayette nakhlite: Part of the CO2- CH4 cycle on Mars?. Geochimica et Cosmochimica Acta, 326, 97-118. https://doi.org/10.1016/j.gca.2022.02.003

Plümper, O., Røyne, A., Magrasó, A., & Jamtveit, B. (2012). The interface-scale mechanism of reaction-induced fracturing during serpentinization. Geology, 40(12), 1103–1106. https://doi.org/10.1130/G33390.1

Poulet, F., Bibring, J. P., Mustard, J. F., Gendrin, A., Mangold, N., Langevin, Y., & Gomez, C. (2005). Phyllosilicates on Mars and implications for early Martian climate. Nature, 438(7068), 623-627. https://doi.org/10.1038/nature04274

Poulet, F., Mangold, N., Platevoet, B., Bardintzeff, J. M., Sautter, V., Mustard, J. F., & Aléon-Toppani, A. (2009). Quantitative compositional analysis of Martian mafic regions using the MEx/OMEGA reflectance data: 2. Petrological implications. Icarus, 201(1), 84-101. https://doi.org/10.1016/j.icarus.2008.12.042

Ramirez, R. M., Kopparapu, R., Zugger, M. E., Robinson, T. D., Freedman, R., & Kasting, J. F. (2014). Warming early Mars with CO2 and H2. Nature Geoscience, 7(1), 59-63. https://doi.org/10.1038/ngeo2000r

Rampe, E. B., Kraft, M. D., Sharp, T. G., Golden, D. C., Ming, D. W., & Christensen, P. R. (2012). Allophane detection on Mars with Thermal Emission Spectrometer data and implications for regional-scale chemical weathering processes. Geology, 40(11), 995-998. https://doi.org/10.1130/G33215.1

Rampe, E. B., Lapotre, M. G. A., Bristow, T. F., Arvidson, R. E., Morris, R. V., Achilles, C. N., ... & Treiman, A. H. (2018). Sand mineralogy within the Bagnold Dunes, Gale crater, as observed in situ and from orbit. Geophysical Research Letters, 45(18), 9488-9497. https://doi.org/10.1029/2018GL079073

Raymond, S. N., & Izidoro, A. (2017). Origin of water in the inner Solar System: Planetesimals scattered inward during Jupiter and Saturn's rapid gas accretion. Icarus, 297, 134-148. https://doi.org/10.1016/j.icarus.2017.06.030

Robbins, S. J., Hynek, B. M., Lillis, R. J., & Bottke, W. F. (2013). Large impact crater histories of Mars: The effect of different model crater age techniques. Icarus, 225(1),173-184. https://doi.org/10.1016/j.icarus.2013.03.019

Robert, F., Gautier, D., & Dubrulle, B. (2000). The solar system D/H ratio: observations and theories. Space Science Reviews, 92(1), 201-224. https://doi.org/10.1023/A:1005291127595

Rogers, A. D., Christensen, P. R., & Bandfield, J. L. (2005). Compositional heterogeneity of the ancient Martian crust: Analysis of Ares Vallis bedrock with THEMIS and TES data. Journal of Geophysical Research: Planets, 110(E5). https://doi.org/10.1029/2005JE002399

Schmidt, S.T. (2023). The Petrographic Microscope: A Polarized Light Microscope. In: Transmitted Light Microscopy of Rock-Forming Minerals . Springer Textbooks in Earth Sciences, Geography and Environment. Springer, Cham. https://doi.org/10.1007/978-3-031-19612-6_3

Self, S., Mittal, T., Dole, G., & Vanderkluysen, L. (2022). Toward understanding Deccan volcanism. Annual Review of Earth and Planetary Sciences, 50(1), 477- 506. https://doi.org/10.1146/annurev-earth-012721-051416

Settle, F. A. (1997). Handbook of instrumental techniques for analytical chemistry. prentice Hall PTR.

Seybold, H. J., Kite, E., & Kirchner, J. W. (2018). Branching geometry of valley networks on Mars and Earth and its implications for early Martian climate. Science advances, 4(6), eaar6692. https://doi.org/10.1126/sciadv.aar6692

Sharma, S., Roppel, R. D., Murphy, A. E., Beegle, L. W., Bhartia, R., Steele, A., ... & Yanchilina, A. (2023). Diverse organic-mineral associations in Jezero crater, Mars. Nature, 619(7971), 724-732. https://doi.org/10.1038/s41586-023-06143-z

Sharma, V., & Bhardwaj, A. (2019). Scanning electron microscopy (SEM) in food quality evaluation. In Evaluation technologies for food quality (pp. 743-761). Woodhead Publishing. https://doi.org/10.1016/B978-0-12-814217-2.00029-9

Shellnutt, J. G., Yeh, M. W., Suga, K., Lee, T. Y., Lee, H. Y., & Lin, T. H. (2017). Temporal and structural evolution of the Early Palaeogene rocks of the Seychelles microcontinent. Scientific Reports, 7(1), 179. https://doi.org/10.1038/s41598-017-00248-y

Shen, J., Chen, Y., Sun, Y., Liu, L., Pan, Y., & Lin, W. (2022). Detection of biosignatures in Terrestrial analogs of Martian regions: Strategical and technical assessments. Earth and Planetary Physics, 6(5), 431-450. http://dx.doi.org/10.26464/epp2022042

Sheppard, R. A. (1962). Iddingsitization and recurrent crystallization of olivine in basalts from the Simcoe Mountains, Washington. American Journal of Science, 260(1), 67-74.

Sheth, H. C. (2005). The great plume debate. Current Science, 89(10), 1659-1661. http://www.jstor.org/stable/24111200

Sheth, H. C., & Melluso, L. (2008). The Mount Pavagadh volcanic suite, Deccan Traps: geochemical stratigraphy and magmatic evolution. Journal of Asian Earth Sciences, 32(1), 5-21. https://doi.org/10.1016/j.jseaes.2007.10.001

Sheth, H. C., Choudhary, A. K., Cucciniello, C., Bhattacharyya, S., Laishram, R., & Gurav, T. (2012). Geology, petrochemistry, and genesis of the bimodal lavas of Osham Hill, Saurashtra, northwestern Deccan Traps. Journal of Asian Earth Sciences, 43(1), 176-192. https://doi.org/10.1016/j.jseaes.2011.09.008

Sheth, H., Naik, A., Shekhar, A., Astha, B., & Samant, H. (2024). Lava squeeze-ups and volcanic resurfacing: a review. Journal of Volcanology and Geothermal Research, 108085. https://doi.org/10.1016/j.jvolgeores.2024.108085

Shih, C. Y., Nyquist, L. E., & Wiesmann, H. (1999). Samarium-neodymium and rubidium-strontium systematics of nakhlite Governador Valadares. Meteoritics & Planetary Science, 34(4), 647-655. https://doi.org/10.1111/j.1945- 5100.1999.tb01370.x

Sleep NH (2012) Maintenance of permeable habitable subsurface environments by earthquakes and tidal stresses. Int J Astrobiol 11:257–268. https://doi.org/10.1017/S1473550412000122

Smith, K. L., Milnes, A. R., & Eggleton, R. A. (1987). Weathering of basalt: formation of iddingsite. Clays and Clay Minerals, 35(6), 418-428. https://doi.org/10.1346/CCMN.1987.0350602

Squyres, S. W., Grotzinger, J. P., Arvidson, R. E., Bell III, J. F., Calvin, W., Christensen, P. R., ... & Soderblom, L. A. (2004). In situ evidence for an ancient aqueous environment at Meridiani Planum, Mars. Science, 306(5702), 1709-1714. https://doi.org/10.1126/science.1104559

Steele, A., Benning, L. G., Wirth, R., Schreiber, A., Araki, T., McCubbin, F. M.,.... & Rogers, K. (2022). Organic synthesis associated with serpentinization and carbonation on early Mars. Science, 375(6577), 172-177. https://doi.org/10.1126/science.abg7905

Stopar, J. D., Lawrence, S. J., Lentz, R. C. F., & Taylor, G. J. (2005, March). Preliminary analysis of nakhlite MIL 03346, with a focus on secondary alteration. In 36th Annual Lunar and Planetary Science Conference (p. 1547).

Sugiura, N., & Hoshino, H. (2000). Hydrogen-isotopic compositions in Allan Hills 84001 and the evolution of the Martian atmosphere. Meteoritics & Planetary Science, 35(2), 373-380. https://doi.org/10.1111/j.1945-5100.2000.tb01783.x

Sun, M. S. (1957). The nature of iddingsite in some basaltic rocks of New Mexico. American Mineralogist: Journal of Earth and Planetary Materials, 42(7-8), 525-533.

Sun, V. Z., & Milliken, R. E. (2014). The geology and mineralogy of Ritchey crater, Mars: Evidence for post-Noachian clay formation. Journal of Geophysical Research: Planets, 119(4), 810-836. https://doi.org/10.1002/2013JE004602

Sun, V. Z., & Milliken, R. E. (2015). Ancient and recent clay formation on Mars as revealed from a global survey of hydrous minerals in crater central peaks. Journal of Geophysical Research: Planets, 120(12), 2293-2332. https://doi.org/10.1002/2015JE004918

Tait, K. T., & Day, J. M. (2018). Chondritic late accretion to Mars and the nature of shergottite reservoirs. Earth and Planetary Science Letters, 494, 99-108. https://doi.org/10.1016/j.epsl.2018.04.040

Talbi, E. H., & Honnorez, J. (2003). Low-temperature alteration of mesozoic oceanic crust, Ocean Drilling Program Leg 185. Geochemistry, Geophysics, Geosystems, 4(5). https://doi.org/10.1029/2002GC000405

Tanaka, K. L., Skinner, J. A., & Hare, T. M. (2005). Geologic map of the northern plains of Mars (Vol. 2888). US Department of the Interior, US Geological Survey.

Tanaka, K. L., Robbins, S. J., Fortezzo, C. M., Skinner Jr, J. A., & Hare, T. M. (2014). The digital global geologic map of Mars: Chronostratigraphic ages, topographic and crater morphologic characteristics, and updated resurfacing history. Planetary and Space Science, 95, 11-24. https://doi.org/10.1016/j.pss.2013.03.006

Tardy, Y., Duplay, J., & Fritz, B. (1987). Stability fields of smectites and illites as a function of temperature and chemical composition (No. SKB-TR--87-20). Swedish Nuclear Fuel and Waste Management Co., Stockholm.

Tice, M. M., Hurowitz, J. A., Allwood, A. C., Jones, M. W., Orenstein, B. J., Davidoff, S & PIXL team. (2022). Alteration history of Séítah formation rocks inferred by PIXL x-ray

fluorescence, x-ray diffraction, and multispectral imaging on Mars. Science Advances, 8(47), eabp9084. https://doi.org/10.1126/sciadv.abp9084

Tomkinson, T., Lee, M. R., Mark, D. F., & Smith, C. L. (2013). Sequestration of Martian CO2 by mineral carbonation. Nature Communications, 4(1), 2662. https://doi.org/10.1038/ncomms3662

Treiman, A. H. (2005). The nakhlite meteorites: Augite-rich igneous rocks from Mars. Geochemistry, 65(3), 203-270. https://doi.org/10.1016/j.chemer.2005.01.004

Treiman, A. H. (2005). The nakhlite meteorites: Augite-rich igneous rocks from Mars. Geochemistry, 65(3), 203-270. https://doi.org/10.1016/j.chemer.2005.01.004

Treiman, A. H., & Gooding, J. L. (1991). Iddingsite in the Nakhla meteorite: TEM study of mineralogy and texture of pre-terrestrial (Martian?) alterations. Meteoritics, vol. 26, p. 402-402 (1991)., 26, 402-402.

Treiman, A. H., Drake, M. J., Janssens, M. J., Wolf, R., & Ebihara, M. (1986). Core formation in the Earth and shergottite parent body (SPB): Chemical evidence from basalts. Geochimica et Cosmochimica Acta, 50(6), 1071-1091. https://doi.org/10.1016/0016-7037(86)90389-3

Treiman, A. H., Dyar, M. D., McCanta, M., Noble, S. K., & Pieters, C. M. (2007). Martian Dunite NWA 2737: Petrographic constraints on geological history, shock events, and olivine color. Journal of Geophysical Research: Planets, 112(E4). https://doi.org/10.1029/2006JE002777

Treiman, A. H., Gleason, J. D., & Bogard, D. D. (2000). The SNC meteorites are from Mars. Planetary and Space Science, 48(12-14), 1213-1230.

https://doi.org/10.1016/S0032-0633(00)00105-7

Treiman, A. H., McKay, G. A., Bogard, D. D., Mittlefehldt, D. W., Wang, M. S., Keller, L., ... & Garrison, D. (1994). Comparison of the LEW88516 and ALHA77005 martian meteorites: Similar but distinct. Meteoritics, 29(5), 581-592.. https://doi.org/10.1111/j.1945-5100.1994.tb00771.x

Tremblay, M. M., Mark, D. F., Barfod, D. N., Cohen, B. E., Ickert, R. B., Lee, M. R.,. & Smith, C. L. (2024). Dating recent aqueous activity on Mars. Geochemical Perspectives Letters. https://doi.org/10.7185/geochemlet.2443

Tschegg, C., Ntaflos, T., Kiraly, F., & Harangi, S. (2010). HIGH TEMPERATURE CORROSION OF OLIVINE PHENOCRYSTS IN PLIOCENE BASALTS FROM BANAT, ROMANIA. Austrian Journal of Earth Sciences, 103(1).

Tsiganis, K., Gomes, R., Morbidelli, A., & Levison, H. F. (2005). Origin of the orbital architecture of the giant planets of the Solar System. Nature, 435(7041), 459-

461. https://doi.org/10.1038/nature03539

TuSmith, K. L., Milnes, A. R., & Eggleton, R. A. (1987). Weathering of basalt: formation of iddingsite. Clays and Clay Minerals, 35(6), 418-428. https://doi.org/10.1346/CCMN.1987.0350602

Udry, A., & Day, J. M. (2018). 1.34 billion-year-old magmatism on Mars evaluated from the co-genetic nakhlite and chassignite meteorites. Geochimica et Cosmochimica Acta, 238, 292-315. https://doi.org/10.1016/j.gca.2018.07.006

Udry, A., Howarth, G. H., Herd, C. D. K., Day, J. M., Lapen, T. J., & Filiberto, J. (2020). What Martian meteorites reveal about the interior and surface of Mars. https://doi.org/10.1029/2020JE006523

Udry, A., Ostwald, A. M., Day, J. M., & Hallis, L. J. (2025). Fundamental constraints and questions from the study of martian meteorites and the need for returned samples. Proceedings of the National Academy of Sciences, 122(2), e2404254121. https://doi.org/10.1073/pnas.2404254121

Vaniman, D. T., Bish, D. L., Ming, D. W., Bristow, T. F., Morris, R. V., Blake, D. F., ... & Freissinet, C. (2014). Mineralogy of a mudstone at Yellowknife Bay, Gale crater, Mars. Science,343(6169), 1243480.https://doi.org/10.1126/science.1243480

Velbel, M. A. (1999). Bond strength and the relative weathering rates of simple orthosilicates. American Journal of Science, 299(7-9), 679-696.

Velbel, M. A. (2009). Dissolution of olivine during natural weathering. Geochimica et CosmochimicaActa, 73(20), 6098-6113.https://doi.org/10.1016/j.gca.2009.07.024

Veneranda, M., Manrique-Martinez, J. A., Lopez-Reyes, G., Medina, J., Torre-Fdez, I., Castro, K., ... & Rull, F. (2019). Spectroscopic study of olivine-bearing rocks and its relevance to the ExoMars rover mission. Spectrochimica Acta Part A: Molecular and Biomolecular Spectroscopy, 223, 117360.https://doi.org/10.1016/j.saa.2019.117360

Viennet, J. C., Bernard, S., Le Guillou, C., Sautter, V., Grégoire, B., Jambon, A., ... & Remusat, L. (2021). Martian magmatic clay minerals forming vesicles: perfect niches for emerging life?. Astrobiology, 21(5), 605-612. https://doi.org/10.1089/ast.2020.2345

Viennet, J. C., Bernard, S., Le Guillou, C., Sautter, V., Schmitt-Kopplin, P., Beyssac, O., & Remusat, L. (2020). Tardi-magmatic precipitation of Martian Fe/Mg- rich clay minerals via igneous differentiation. https://doi: 10.7185/geochemlet.2023

Viviano, C. E., Murchie, S. L., Daubar, I. J., Morgan, M. F., Seelos, F. P., & Plescia, J.B. (2019). Composition of Amazonian volcanic materials in Tharsis andElysium, Mars, from

MRO/CRISM reflectance spectra. Icarus, 328, 274-286. https://doi.org/10.1016/j.icarus.2019.03.001

Wade, J., Dyck, B., Palin, R. M., Moore, J. D., & Smye, A. J. (2017). The divergent fates of primitive hydrospheric water on Earth and Mars. Nature, 552(7685), 391-394. https://doi.org/10.1038/nature25031

Walsh, K. J., Morbidelli, A., Raymond, S. N., O'brien, D. P., & Mandell, A. M. (2012). Populating the asteroid belt from two parent source regions due to the migration of giant planets—"The Grand Tack". Meteoritics & Planetary Science, 47(12), 1941-1947. https://doi.org/10.1111/j.1945-5100.2012.01418.x

Werner, S. C. (2009). The global martian volcanic evolutionary history. Icarus, 201(1), 44-68. https://doi.org/10.1016/j.icarus.2008.12.019

Werner, S. C., & Tanaka, K. L. (2011). Redefinition of the crater-density and absolute-age boundaries for the chronostratigraphic system of Mars. Icarus, 215(2), 603-607. https://doi.org/10.1016/j.icarus.2011.07.024

Werner, S. C., Ody, A., & Poulet, F. (2014). The source crater of martian shergottite meteorites. Science, 343(6177), 1343-1346.https://doi.org/10.1126/science.1247282

Wernicke, L. J., & Jakosky, B. M. (2021). Martian hydrated minerals: A significant water sink. Journal of Geophysical Research: Planets, 126(3), e2019JE006351. https://doi.org/10.1029/2019JE006351

Wiens, R. C., Udry, A., Beyssac, O., Quantin-Nataf, C., Mangold, N., Cousin, A., & SuperCam Team. (2022). Compositionally and density stratified igneous terrain in Jezero crater, Mars. Science Advances, 8(34), eabo3399. https://doi.org/10.1126/sciadv.abo3399

Wilson, M. J. (2004). Weathering of the primary rock-forming minerals: processes, products and rates. Clay Minerals, 39(3), 233-266. https://doi:10.1180/0009855043930133

Wimpenny, J., 2018, Clay minerals, in Encyclopedia of Earth Sciences Series, https://doi.org/10.1346/ccmn.1982.0300513

Wittmann, A., Korotev, R. L., Jolliff, B. L., Irving, A. J., Moser, D. E., Barker, I., & Rumble III, D. (2015). Petrography and composition of Martian regolith breccia meteorite Northwest Africa 7475. Meteoritics & Planetary Science, 50(2), 326- 352. https://doi.org/10.1111/maps.12425

Wordsworth, R. D. (2016). The climate of early Mars. Annual Review of Earth and Planetary Sciences, 44(1), 381-408. https://doi.org/10.1146/annurev-earth-060115-012355

Wordsworth, R., Kalugina, Y., Lokshtanov, S., Vigasin, A., Ehlmann, B., Head, J., ... & Wang, H. (2017). Transient reducing greenhouse warming on early Mars. Geophysical Research Letters, 44(2), 665-671. https://doi.org/10.1002/2016GL071766

Wright, S. P., Christensen, P. R., & Sharp, T. G. (2011). Laboratory thermal emission spectroscopy of shocked basalt from Lonar Crater, India, and implications for Mars orbital and sample data. Journal of Geophysical Research: Planets, 116(E9). https://doi.org/10.1029/2010JE003785

Wright, T. L., & Peck, D. L. (1978). Crystallization and differentiation of the Alae magma, Alae lava lake, Hawaii (No. 935-C). US Govt. Print. Off.,.Yatheesh, V. (2020). Structure and tectonics of the continental margins of India and the adjacent deep ocean basins: current status of knowledge and some unresolved problems. Episodes Journal of International Geoscience, 43(1), 586-608.

Ye, B., & Michalski, J. R. (2021). Precipitation-driven pedogenic weathering of volcaniclastics on early Mars. Geophysical Research Letters, 48(5), e2020GL091551. https://doi.org/10.1029/2020GL091551

Ye, B., & Michalski, J. R. (2022). Chemical weathering over hundreds of millions of years of greenhouse conditions on Mars. Communications Earth & Environment, 3(1), 266. https://doi.org/10.1038/s43247-022-00602-7

Zellmer, G. F., Sheth, H. C., Iizuka, Y., & Lai, Y. J. (2012). Remobilization of granitoid rocks through mafic recharge: evidence from basalt-trachyte mingling and hybridization in the Manori–Gorai area, Mumbai, Deccan Traps. Bulletin of Volcanology, 74, 47-66. https://doi.org/10.1007/s00445-011-0498-4.